Development of low-cost sensing and separation devices based on macro, micro and nano technology for health applications

by

Una Bernadette Crowley B.S.c.

A thesis submitted to the National University of Ireland

for the degree of Doctor of Philosophy

August 2014

Under the supervision of Dr. Eric Moore and Professor Jeremy Glennon

Department of Chemistry

Tyndall National Institute,

National University of Ireland,

Cork.

Acknowledgements

I would like to extend my sincere thanks to all those people who helped me during the course of this thesis. I would like to express my gratitude in particular to Professor Jeremy Glennon and Dr. Eric Moore for giving me the opportunity to work under you both and for all your guidance and support. I would like to thank Dr. Miloslav Pravda for his help and advice over the last 4 years. I would also like to thank the staff of the Chemistry department, especially Eileen, Mary, Christine, Tina and Matthias, whose help and time I greatly appreciated.

To all my friends and colleagues both in LSI in Tyndall and ABCRF in UCC, without you guys I would never have successfully completed this study. A special thanks to Eileen Hurley who is always willing to lend a helping hand. Walter, Michelle, Niall, Lisa, Gerard, Shauna, David, Rachel, Victor, Amy and Elaine thank you all for always listening to my many, many complaints and helping me through the tough times.

To my family, especially Mam and Dad, who have supported me and given me nothing but encouragement throughout my thesis. It has been a very long road but I am finally at the end of it. They always knew that I could do whatever I wanted to do with my life and their faith in me and my abilities have now been realised. Last but not least I would like to express my sincere gratitude to my boyfriend, Kenneth for being the driving force behind me over the past few years and in particular over the past few months in achieving completion of this thesis. Thank you all from the bottom of my heart.

Declaration

I hereby declare that this thesis is my own work, in partial fulfilment of the requirements of the Doctor of Philosophy degree. It is based on research carried out in the Department of Chemistry and the Tyndall National Institute, University College Cork, Ireland between October 2010 and July 2014.

_____

Una Crowley

Abstract

The work presented in this thesis described the development of low-cost sensing and separation devices with electrochemical detections for health applications. This research employs macro, micro and nano technology. The first sensing device developed was a toner-based micro-device. The initial development of microfluidic devices was based on glass or quartz devices that are often expensive to fabricate; however, the introduction of new types of materials, such as plastics, offered a new way for fast prototyping and the development of disposable devices. One such microfluidic device is based on the lamination of laser-printed polyester films using a computer, printer and laminator. The resulting toner-based microchips demonstrated a potential viability for chemical assays, coupled with several detection methods, particularly Chip-Electrophoresis-Chemiluminescence (CE-CL) detection which has never been reported in the literature.

Following on from the toner-based microchip, a three-electrode micro-configuration was developed on acetate substrate. This is the first time that a micro-electrode configuration made from gold; silver and platinum have been fabricated onto acetate by means of patterning and deposition techniques using the central fabrication facilities in Tyndall National Institute. These electrodes have been designed to facilitate the integration of a 3-electrode configuration as part of the fabrication process. Since the electrodes are on acetate the dicing step can automatically be eliminated. The stability of these sensors has been investigated using electrochemical techniques with excellent outcomes. Following on from the generalised testing of the electrodes these sensors were then coupled with capillary electrophoresis.

The final sensing devices were on a macro scale and involved the modifications of screen-printed electrodes. Screen-printed electrodes (SPE) are generally seen to be far less sensitive than the more expensive electrodes including the gold, boron-doped diamond and glassy carbon electrodes. To enhance the sensitivity of these electrodes they were treated with metal nano-particles, gold and palladium. Following on from this, another modification was introduced. The carbonaceous material carbon monolith was drop-cast onto the SPE and then the metal nano-particles were electrodeposited onto the monolith material.

Table of Contents

Acknowledgements i

Declaration ii

Abstract iii

Table of Contents iv

List of Figures xii

List of Tables xxi

List of Abbreviations xxiii

Objectives and Thesis Overview xxv

1 General Introduction 1

1.1 Sensors and Separation 2

1.2 An Introduction to Electro-Analytical Principles 6

1.2.1 General Introduction 6

1.3 Fundamentals of Electroanalytical Chemistry 8

1.3.1 Introduction 8

1.3.2 Electrochemical Cell 8

1.3.3 Electrochemical Measurements 12

1.3.4 Electrochemical Measurement Techniques 24

1.3.4.1 Linear Sweep Voltammetry (LSV) 25

1.3.4.2 Cyclic Voltammetry 29

1.3.4.3 Square Wave Voltammetry 32

1.3.4.4 Differential Pulse Voltammetry 33

1.3.4.5 Electrical Impedance Spectroscopy (EIS) 34

1.4 Transducers 37

1.4.1 Introduction 37

1.4.2 Potentiometric Transducers 37

1.4.3 Conductometric Transducers 38

1.4.4 Amperometric Transducers 38

1.4.5 Optical Transducers 39

1.4.6 Piezoelectric Transducers 40

1.4.7 Acoustical Transducers 41

1.4.8 Calorimetric Transducers 42

1.5 Working Electrode Material 43
1.5.1 Macroelectrodes 43
1.5.1.1 Introduction 43
1.5.1.2 Metal Working Electrodes 43
1.5.1.3 Mercury Electrodes 44
1.5.1.4 Carbon Electrodes 45
1.5.1.5 Screen-Printed Electrodes 45
` 1.5.2 Microelectrodes 46
1.5.2.1 Introduction 46
1.5.2.2 Fabrication, Shapes and Responses 52

1.6 Chemically Modified Electrodes 55
1.6.1 Introduction 55
1.6.2 Approaches to Chemically Modify Electrodes 58

1.7 Other Measurement Techniques used in the work in this Thesis 60
1.7.1 Capillary Electrophoresis 60
1.7.1.1 Introduction 60
1.7.1.2 Electrophoresis 62
1.7.1.3 Electro-osmotic flow (EOF) 63
1.7.2 Chemiluminescence 68
1.7.2.1 Introduction 68
1.7.2.2 Luminol Chemiluminescence Reaction 71

1.8 Statistical Information 72
1.8.1 Introduction 72
1.8.2 Validation 72
1.8.2.1 Calibration Range 73
1.8.2.2 Limit of detection 73
1.8.2.3 Selectivity 74
1.8.2.4 Sensitivity 74
1.8.2.5 Accuracy and Precision 75
1.8.3 Repeatability and Reproducibility 75
1.8.4 Percentage Recovery 76
1.8.5 Correlation 76

1.9 Buffers 77
1.9.1 Introduction 77
1.9.2 pH 77

1.10 Electrochemical Instrumentation 78
1.10.1 Introduction 78
1.10.2 Chi 1040A Electrochemical Workstation 78
1.10.3 Palmsens Electrochemical Workstation 79

1.11 References 80

2 Toner-Based Microchips 86

2.1 Objectives 87

2.2 Introduction 88

2.3 Experimental Details 91
2.3.1 Reagents 91
2.3.2 Apparatus 91

2.4 Procedures 92
2.4.1 Fabrication of Toner-based microchip 92
2.4.2 Preparation of Reagents 93
2.4.2.1 Amino Acids 93
2.4.2.2 Chiral Compounds 93
2.4.3 Experimental Protocol 93

2.5 Results 95
2.5.1 Amino Acids 97
2.5.1.1 Optimisation of the CL detection of amino acids using toner-based microchips 97
2.5.1.2 ME separation of Amino acids on toner-based microchips 97
2.5.1.3 Preparation of calibration curve of amino acids using CL detection in Toner-chip 98
2.5.1.4 Analysis of plasma sample 99
2.5.2 Chiral Separation 101
2.5.2.1 Optimisation of the CL detection of D,L-phenylalanine using toner-based microchips 101
2.5.2.2 ME separation of D,L-phenylalanine on toner-based microchips 101
2.5.2.3 Preparation of calibration curve of D,L-phenylalanine using CL detection in Toner-chip 103

2.6 Limitations of toner-based microchips 104

2.7 Conclusions and Future Work 105

2.8 Highlights 106

2.9 References 107

3 Acetate Microelectrode 109

3.1 Objectives 110

3.2 Introduction 110

3.2.1 Technical Background 111

3.2.2Substrate Cleaning 111

3.2.3Metallisation 112

3.2.4 Photolithography 113

3.2.5 Capillary Electrophoresis 113

3.2.6 Analytes used in this work 114

3.2.6.1 Uric Acid used for initial testing of microelectrodes 114

3.2.6.2 Neurotransmitters used in CE 114

3.3 Experimental Details 116

3.3.1 Reagents 116

3.3.2 Apparatus 116

3.3.2.1 Initial electrochemical testing 116

3.3.2.2 CE work 117

3.4 Procedures 117

3.4.1 Fabrication of the Three Electrode System 117

3.4.1.1 Designing the Electrodes 117

3.5.1.2 Steps involved in the fabrication of the electrodes 118

3.4.2 Preparing electrode for CE 121

3.4.2.1 Acetate microelectrode with CE 121

3.4.2.2 Conventional 3-electrode system with CE 121

3.4.3 Electrode system setup with Capillary Electrophoresis 121

3.4.3.1 Conventional 3-electrode system 121

3.4.3.2 Acetate microelectrode 123

3.5 Results 124

3.5.1 Initial Testing of microelectrodes 124

3.5.1.1 Electrochemical behaviour of UA at the microelectrode 124

3.5.1.2 Effect of scan rate 125

3.5.1.3 Effect of solution pH 127
3.5.1.4 Determination of UA by Cyclic Voltammetry 128
3.5.1.5 Real sample analysis: determination of UA in human plasma serum 130
3.5.2 Coupling microelectrode with CE 131
3.5.2.1 $Na_2B_4O_7 \cdot 10H_2O$ solution, pH 9.5 131
3.5.2.2 Determination of analytes individually with the acetate microelectrode using Cyclic Voltammetry 132
3.5.2.3 Optimising conditions for acetate microelectrode coupled with CE 133
3.5.2.3.1 Effect of Injection time 133
3.5.2.3.2 Effect of buffer pH 134
3.5.2.3.3 Effect of buffer concentration 135
3.5.2.4 Preparation of calibration curve of neurotransmitters using acetate microelectrode configuration 136
3.5.2.5 Stability and Repeatability of the acetate microelectrode 137
3.5.2.6 Real sample analysis: determination of neurotransmitters in human plasma serum 137
3.5.2.7 Comparison of optimum microelectrode results with the conventional 3-electrode system 138
3.6 Conclusions and Future Work 140
3.7 Highlights 141
3.8 References 142
4 Modification of Macro electrodes using metal nanoparticles and carbon monolith 145
4.1 Objectives 146
4.2 Introduction 146
4.3 Experimental 149
4.3.1 Reagents 149
4.3.2 Apparatus 149
4.3.3 Procedures 150
4.3.3.1 Fabrication of the Screen-Printed Electrode 150
4.3.3.2 Protocol for modifying the SPE with gold and palladium nanoparticles 151
4.3.3.3 Protocol for modifying the SPE with CM 151

4.3.3.4 Protocol for drop angle measurement 152
4.3.3.5 Protocol for Electrochemical Impedance Spectroscopy (EIS) 153
4.3.3.6 Studies on the influence of Scan Rate 153
4.3.3.7 Cyclic Voltammetry (CV) 153

4.4 Results 153
4.4.1 SPE/Au nanoparticles 154
4.4.1.1 Characterisation using SEM of the SPE with gold nanoparticles 154
4.4.1.2 Contact-angle measurement of SPE and SPE/Au 155
4.4.1.3 Electrochemical behaviour of SPE and SPE/ Au 155
4.4.1.3.1 Comparison of Cyclic Voltammogramms 155
4.4.1.3.2 Vary Scan Rate 156
4.4.1.4 EIS measurements 160
4.4.1.5 Effect of pH on the oxidation of DA and UA 161
4.4.1.6 Effect of deposition time on the oxidation of DA and UA 162
4.4.1.7 Simultaneous determination of DA and UA 162
4.4.1.8 Characterisation of the SPE/Au using amperometric (I-t) curve 164
4.4.1.9 Stability and repeatability of the SPE/Au 164
4.4.1.10 Real sample analysis: determination of DA and UA in human serum 165
4.4.2 SPE/ Pd nanoparticles 166
4.4.2.1 Characterisation using SEM of the SPE with palladium nanoparticles 166
4.4.2.2 Contact-angle measurement of SPE and SPE/Pd 167
4.4.2.3 Electrochemical behaviour of SPE and SPE/Pd 168
4.4.2.3.1 Comparison of Cyclic Voltammogramms 168
4.4.2.3.2 Vary Scan Rate 169
4.4.2.3.3 EIS measurements 170
4.4.2.3.4 Effect of pH on the oxidation of AA and UA 171
4.4.2.3.5 Effect of deposition time on the oxidation of AA and UA 173
4.4.2.3.6 Simultaneous determination of AA and UA 173
4.4.2.3.7 Characterisation of the SPE/Pd usin using amperometric (I-t) curve 175
4.4.2.3.8 Stability and repeatability of the SPE/Pd 176
4.4.2.3.9 Real sample analysis: determination of AA

and UA in human serum 176
4.4.3 SPE/ CM/Au nanoparticles 177
4.4.3.1 Characterisation using SEM of the SPE/CM with gold nanoparticles 177
4.4.3.2 Contact-angle measurement of SPE, SPE/CM and SPE/CM/Au 179
4.4.3.3 Electrochemical behaviour of SPE/CM and SPE/CM/Au 180
4.4.3.3.1 Comparison of Cyclic Voltammogramms 180
4.4.3.3.2 Vary Scan Rate 181
4.4.3.3.3 EIS measurements 182
4.4.3.3.4 Effect of pH on the oxidation of DA and UA 184
4.4.3.3.5 Effect of deposition time on the oxidation of DA and UA 186
4.4.3.3.6 Simultaneous determination of DA and UA 186
4.4.3.3.7 Characterisation of the SPE/CM/Au using using amperometric (I-t) curve 188
4.4.3.3.8 Stability and Repeatability of the SPE/CM/Au 188
4.4.3.3.9 Real sample analysis: determination of DA and UA in human serum 189
4.4.4 SPE/CM/ Pd nanoparticles 190
4.4.4.1 Characterisation using SEM of the SPE with palladium nanoparticles 190
4.4.4.2 Contact-angle measurement of SPE, SPE/CM and SPE/CM/Pd 191
4.4.4.3 Electrochemical behaviour of SPE and SPE/CM/Pd 192
4.4.4.3.1 Comparison of Cyclic Voltammogramms 192
4.4.4.3.2 Vary Scan Rate 193
4.4.4.3.3 EIS measurements 194
4.4.4.3.4 Effect of pH on the oxidation of AA and UA 195
4.4.4.3.5 Effect of deposition time on the oxidation of AA and UA 197
4.4.4.3.6 Simultaneous determination of AA and UA 197
4.4.4.3.7 Characterisation of the SPE/CM/Pd using using amperometric (I-t) curve 199
4.4.4.3.8 Stability and repeatability of the SPE/CM/Pd 199

4.4.4.3.9 Real sample analysis: determination of AA and UA in human serum 200

4.5 Discussion and Future Work 201

4.6 Highlights 202

4.7 References 205

5 Conclusions & Future Work 206

5.1 Introduction 207

5.2 Chapter 2 208

5.3 Chapter 3 208

5.4 Chapter 4 209

5.5 Conclusions 210

6 Appendix 211

6.1 List of Journal Publications, Oral and Poster Presentations 212

6.1.1 List of Journal Publications 212

6.1.2 List of Oral Presentations 213

6.1.3 List of Poster Presentations 214

6.1.4 List of Awards 215

List of Figures

Figure 1.1	Schematic layout of a sensor	3
Figure 1.2	Simple schematic of a three-electrode electrochemical cell	10
Figure 1.3	Schematic representation of the electrical double layer put forward by Helmholtz	15
Figure 1.4	Schematic representation of the electrical double layer put forward by Stern	16
Figure 1.5	Schematic representation of diffusion	20
Figure 1.6	Schematic representation of migration	21
Figure 1.7	Schematic representation of convection	21
Figure 1.8	Schematic representation of Fick's First Law of Diffusion	23
Figure 1.9	Representation of a typical LSV graph	25
Figure 1.10	(A) Typical potential-time excitation signal for voltammetry and (B) Typical voltammogram for a reversible process	31
Figure 1.11	(A) Typical voltammogram for an irreversible process and (B) Typical voltammogram for a quasi-reversible process	32
Figure 1.12	Potential wave form for square wave voltammetry	33
Figure 1.13	Potential wave form for differential pulse voltammetry	34
Figure 1.14	Impedance circuit (Randles model) for characterisation of modified electrodes	35
Figure 1.15	Nyquist plot for oxidation/reduction reaction of 5 mM $[Fe(CN)_6]^{3-/4-}$ in 0.1 M KCl (imaginary impedance versus real impedance). Frequency from 1 to 100 kHz	36
Figure 1.16	Position transducers, contactless and potentiometric	38
Figure 1.17	Simple three electrode cell	39

Figure 1.18	Optical fiber sensor	40
Figure 1.19	Quartz crystal microbalance	41
Figure 1.20	Example of an acoustic sensor for grinders	42
Figure 1.21	Working SPE design	46
Figure 1.22	Highlighting the unique differences between a micro electrode and a conventional sized electrode where (A) shows the quasi steady-state behaviour observed at a disk micro-electrode where convergent diffusion is predominantly observed and (B) shows the typical peak-shaped voltammogram obtained under the same conditions at a conventional sized electrode where planar diffusion is predominantly observed.	49
Figure 1.23	Illustrations of the most common microelectrode geometries and their diffusion fields	52
Figure 1.24	Scheme of Capillary Electrophoresis	60
Figure 1.25	Flow profiles in HPLC and CZE	62
Figure 1.26	The double layer at the capillary wall	63
Figure 1.27	Illustration of CZE separation	66
Figure 1.28	Basic Chemiluminescence Reaction	69
Figure 1.29	Overall luminol chemiluminescence reaction in aqueous medium	71
Figure 1.30	Chi 1040A Electrochemical Workstation	78
Figure 1.31	PalmsensElectrochemical Workstation	79
Figure 2.1	Representation of steps involved in fabrication process	92
Figure 2.2	Layout and dimensions of the toner-based microchip used in this work	94

Figure 2.3	Scheme of MCE-CL System	94
Figure 2.4	View of MCE-CL System	95
Figure 2.5	Fluorescein migrating through cross-channel of toner chip	96
Figure 2.6	Electropherogram obtained from the separation of a standard sample. MCE conditions: the running buffer was 50 mM phosphate buffer (pH 9.6) containing 2.5mM luminol, 0.45 mM Cu^{2+} and 4.5 mM tartrate. The oxidiser solution was 50mM phosphate buffer (pH 9.6) containing 50 mM H_2O_2. All analyte concentrations are 1.0×10^{-5} M. Peaks: 1. Glycine; 2. Cysteine; 3. Histidine; 4. Tryptophan.	98
Figure 2.7	Electropherogram obtained from the plasma sample spiked with 25 µM Gly, Cys, His and Trp. MCE conditions are as in Fig. 2.6. Peaks: 1. Gly; 2. Cys; 3. His; 4. Trp.	100
Figure 2.8	Electropherogram obtained from the separation of a standard sample. MCE conditions: the running buffer was 25 mM phosphate buffer (pH 9.4) containing 2.5 mM luminol, 0.45 mM Cu^{2+} and 0.9 mM D-penicillamine. The oxidiser solution was 25 mM phosphate buffer (pH 9.4) containing 50mM H_2O_2. All analyte concentrations are 1.0×10^{-5} M. Peaks: 1. L- phenylalanine 2. D- phenylalanine.	102
Figure 2.9	Electropherogram obtained from the separation of a standard sample. MCE conditions are as in Fig. 2.8. Analyte concentrations are 2.0×10^{-5} M L- phenylalanine and 1.0×10^{-5} M .D- phenylalanine . Peaks: 1. L- phenylalanine 2. D- phenylalanine.	103
Figure 3.1	(A) Close-up view of microelectrode configuration connected to Chi 1040A. (B) View of experimental apparatus including Chi, monitor, microelectrode and connections.	117
Figure 3.2	(A) Designs for the three electrode system and (B) dimensions of the electrodes (images are not in scale).	118
Figure 3.3	Schematic diagram of the different layers of the microchip	120
Figure 3.4	Acetate wafer and a close up view of an individual microelectrode	120
Figure 3.5	Scheme of the conventional 3-electrode system	122
Figure 3.6	Setup of the conventional 3-electrode system which includes a Au working electrode, Ag/AgCl reference electrode and Pt wire for the counter electrode.	123

Figure 3.7 Setup of the microelectrode system 124

Figure 3.8 Cyclic voltammograms of an acetate microelectrode using a) 50 mM Phosphate buffer solution pH4 and b) 50 mM Phosphate buffer solution pH 4 with 1.7 mM UA. Scan rate: 50 mV/s. 125

Figure 3.9 Cyclic voltammograms of acetate electrode in 5 mM $Fe(CN)_6^{3-/4-}$ containing 0.1 M KCl solution at scan rate from 50 to 400 mV/s. 126

Figure 3.10 The plot of the anodic peak current versus square root of the scan rate. 126

Figure 3.11 The plot of anodic current of UA versus pH values on cyclic voltammograms. 127

Figure 3.12 The linear relationship between the peak potential and solution pH of UA. 128

Figure 3.13 CVs of various UA concentrations (a-f); 1.7 x 10^{-3}, 2.22 x 10^{-3} M, 2.73 x 10^{-3} M, 3.21 x 10^{-3} M, 3.68 x 10^{-3} M and 4.14 x 10^{-3} M at the acetate electrode in 50 mM PB solution in pH 4.0. 129

Figure 3.14 Calibration plot obtained from the CVs shown above. 129

Figure 3.15 Cyclic voltammogram obtained at (a) the conventional 3-electrode system and (b) the acetate microelectrode in 50 mM PB solution pH 9.5. Scan rate 100 mV/s. 131

Figure 3.16 CVs obtained from the individual analytes using the acetate microelectrode in 50 mM $Na_2B_4O_7 \cdot 10H_2O$ solution, pH9.5. All analyte concentrations are 100μM. 132

Figure 3.17 Electropherograms obtained from varying the injection time. Injection buffer: 50 mM $Na_2B_4O_7 \cdot 10H_2O$ solution, pH 9.5. The running buffer was similar to the injection buffer. Concentration of analytes: 100 μM each. Separation voltage: 10 kV. 133

Figure 3.18 Electropherograms obtained from varying the buffer pH. Injection buffer: 50 mM$Na_2B_4O_7 \cdot 10H_2O$ solution. The running buffer was similar to the injection buffer with an injection time of 5 s. Concentration of analytes: 600 μM each. Separation voltage: 10 kV. 134

Figure 3.19 Electropherograms obtained from varying the buffer concentration. Injection buffer: varied concentration $Na_2B_4O_7 \cdot 10H_2O$ solution, pH 9.5, and the running buffer was similar to the injection buffer with an injection time of 5 s. Concentration of analytes: 600μM each. Separation voltage: 10kV. 135

Figure 3.20 Electropherograms obtained from the plasma sample spiked with 1 mM TA, DA, Ep and NEP Injection buffer: 25 mM $Na_2B_4O_7 \cdot 10H_2O$ solution, pH 9.5, and the running buffer was similar to the injection buffer with an injection time of 5 s. Separation voltage: 10 kV. Order of elution; TA, DA, Ep and NEP. 138

Figure 3.21 Electropherograms obtained from the separation of a standard sample (A) using the conventional 3-electrode system and (B) using the acetate microelectrode. Analyte concentrations are 500 μM TA and 200 μM DA, Ep and NEP. Injection buffer: 50 mM $Na_2B_4O_7 \cdot 10H_2O$ solution, pH 9.5, and the running buffer was similar to the injection buffer with an injection time of 5 s. Separation voltage: 10 kV. Order of elution; TA, DA, Ep and NEP. 139

Figure 4.1 Experimental Apparatus which includes the Chi1040A with monitor attached to a 3-electrode system, SPE, Ag/AgCl electrode and platinum wire. 150

Figure 4.2 SPE design and layer development 151

Figure 4.3 The SEM images (A) of the SPE, (B) of the bare surface with Au nanoparticles, (C) of the bare surface with Au nanoparticles magnified. 154

Figure 4.4 Images of water droplet on surface of (A) SPE (CA = 118.7º) and (B) SPE/Au (CA = 95º) 155

Figure 4.5 Cyclic Voltammograms obtained at the (A) SPE/Au and (B) SPE in 0.1 M PB solution pH 5 at scan rate 100 mV/s. 156

Figure 4.6 Cyclic Voltammograms obtained at the (A) SPE and (B) the SPE/Au in 5 mM $[Fe(CN)_6]^{3-/4-}$ in 0.1 M KCl solution at scan rate 50 to 400 mV/s. Below the scan rates: the plot of the redox peak currents versus square root of the scan rate. 158

Figure 4.7 (A) Nyquist plots of $[Fe(CN)^6]^{3-/4-}$ in 0.1 M KCl solution with (A) a SPE, and (B) a SPE/Au. The frequency range is from 1 Hz to 100 kHz. 160

Figure 4.8 Effect of buffer pH on the peak current for the oxidation of (A) DA and (B) UA. Concentrations: DA, 0.08 mM; UA, 0.2 mM. Scan rate 50 mV/s. 161

Figure 4.9 Effect of buffer pH on the peak oxidation potential for the oxidation of AA and UA. Concentrations: DA, 0.08 mM; UA, 0.2 mM. Scan rate 50 mV/s. 161

Figure 4.10 Effect of deposition time on the peak current for the oxidation of DA and UA. Concentrations: DA, 0.08 mM; UA 0.2 mM. Scan rate 50 mV/s. 162

Figure 4.11 (A) CV of DA 0.17 mM and UA 0.3 mM at the (a) SPE and (b) SPE/Au in 0.1 M PB solution pH 5.0. (B) CVs of various DA and UA concentrations at the SPE/CM/Au in 0.1 M PB solution pH 5.0. Concentrations of analytes (a-g); 0.05, 0.07, 0.09, 0.11, 0.13, 0.15 and 0.17 mM for DA and 0.12, 0.15, 0.18, 0.21, 0.24, 0.27 and 0.3 mM for UA. (C) Calibration plot for DA obtained from the CV's shown in (B). (D) Calibration plot for UA obtained from the CV's shown in (B). Scan rate: 50 mV/s. 163

Figure 4.12 A typical current-time response of the SPE/CM/Au upon the successive additions of (A) 8 µM DA and (B) 40 µM UA in 0.1 M PB solution pH 5,E=0.2 V. 164

Figure 4.13 The SEM images (A) of the SPE and (B) of the SPE surface with Pd nanoparticles. 166

Figure 4.14 Images of water droplet on surface of (A) SPE (CA = 118.7º) and (B) SPE/Pd (CA = 79º) 167

Figure 4.15 Cyclic voltammograms obtained at the (A) SPE and (B) SPE/Pd in 0.1 M PB solution pH 4 at scan rate 50 mV/s. 168

Figure 4.16 Cyclic voltammogram and the plot of the redox peak currents versus square root of the scan rate obtained at the SPE/Pd in 5 mM $[Fe(CN)_6]^{3-/4-}$ in 0.1 M KCl solution at scan rate 50 to 400 mV/s. 169

Figure 4.17 Nyquist plots of $[Fe(CN)^6]^{3-/4-}$ in 0.1 M KCl solution with (A) a SPE, and (B) a SPE/Pd. The frequency range is from 1 Hz to 100 kHz. 171

Figure 4.18 Effect of buffer pH on the peak current for the oxidation of (A) AA and (B) UA. Concentrations: AA, 0.5 mM; UA, 0.5 mM. Scan rate 50 mV/s. 172

Figure 4.19 Effect of buffer pH on the peak oxidation potential for the oxidation of AA and UA. Concentrations: AA, 0.5 mM; UA, 0.5 mM. Scan rate 50 mV/s 172

Figure 4.20 Effect of deposition time on the peak current for the oxidation of (A) AA and (B) UA. Concentrations: AA, 0.5 mM; UA, 0.5 mM. Scan rate 50 mV/s. 173

Figure 4.21 (A) CVs of various AA and UA concentrations at the SPE/Pd in 0.1 M PB solution pH 4.0. Concentration of analytes; 0.03, 0.06, 0.09, 0.12, 0.15, 0.18 and 0.21 mM for both AA and UA. (B) Calibration plot for AA obtained from the CV's shown in (A). (C) Calibration plot for UA obtained from the CV's shown in (A). Scan rate: 50 mV/s. 174

Figure 4.22 A typical current-time response of the SPE/Pd upon the successive additions of (A) 20 µM AA and (B) 30 µM UA in 0.1M PB solution pH 4, E= 0.2V. 175

Figure 4.23 The SEM images (A) of the SPE, (B) of the CM surface, (C) of the magnified CM surface and (D) of the magnified CM with Au nanoparticles. 178

Figure 4.24 Images of water droplet on surface of (A) SPE (CA = 118.7º), (B) SPE/CM (CA = 132.8º) and (C) SPE/CM/Au (CA = 106.5º). 179

Figure 4.25 Cyclic voltammograms obtained at the (A) SPE, and (B) SPE/CM/Au in 0.1 M PB solution pH 5 at scan rate 50 mV/s. 180

Figure 4.26 Cyclic voltammograms and the plot of the redox peak currents versus square root of the scan rate obtained at the (A) SPE and (B) SPE/CM/Au in 5 mM $[Fe(CN)_6]^{3-/4-}$ in 0.1 M KCl solution at scan rate 50 to 400 mV/s. 181

Figure 4.27 (A) Nyquist plots of $[Fe(CN)^6]^{3-/4-}$ in 0.1 M KCl solution with (a) a SPE, (b) a SPE/CM, and (c) a SPE/CM/Au. The frequency range is from 1 Hz to 100 kHz. (B) Nyquist plot of $[Fe(CN)^6]^{3-/4-}$ in 0.1 M KCl solution with a SPE/CM/Au. 183

Figure 4.28 Effect of buffer pH on the peak current for the oxidation of (A) DA and (B) UA. Concentrations: DA, 0.128 mM; UA, 0.64 mM. Scan rate 50 mV/s. 184

Figure 4.29 Effect of buffer pH on the peak oxidation potential for the oxidation of (A) DA and (B) UA. Concentrations: DA, 0.128 mM; UA, 0.64 mM. Scan rate 50 mV/s. 185

Figure 4.30 Effect of deposition time on the peak current for the oxidation of (a) UA and (b) DA. Concentrations: UA, 0.64 mM; DA, 0.128 mM. Scan rate 50 mV/s. 186

Figure 4.31 (A) CV of DA 0.06 mM and UA 0.593 mM at the (a) SPE and (b) SPE/CM/Au in 0.1 M PB solution pH 5.0. (B) CVs of various DA and UA concentrations at the SPE/CM/Au in 0.1 M PB solution pH 5.0. Concentrations of analytes (a-e); 0.03, 0.06, 0.09, 0.12, 0.15 and 0.18 mM for DA and 0.298, 0.446, 0.593, 0.739, 0.884 and 1.028 mM for UA. (C) Calibration plot for DA obtained from the CV's shown in (B). (D) Calibration plot for UA obtained from the CV's shown in (B). Scan rate: 50 mV/s. 187

Figure 4.31 A typical current-time response of the SPE/CM/Au upon the successive additions of (A) 6 µM DA and (B) 30 µM UA in 0.1 M PBS solution pH 5, E= 0.2V. 188

Figure 4.33 The SEM images (A) of the SPE, (B) of the CM surface, (C) of the CM surface with Pd nanoparticles and (D) of the magnified CM with Pd nanoparticles. 190

Figure 4.34 Images of water droplet on surface of (A) SPE (CA = 118.7º), (B) SPE/CM (CA = 132.8º) and (C) SPE/CM/Au (CA = 116.7º). 191

Figure 4.35 Cyclic Voltammogram obtained at the (A) SPE and (B) SPE/CM/Pd in 0.1 mol L^{-1} PB solution pH 4 at scan rate 50 mV/s. 192

Figure 4.36 Cyclic Voltammogram and the plot of the redox peak currents versus square root of the scan rate obtained at the SPE/CM/Pd in 5 mM $[Fe(CN)_6]^{3-/4-}$ in 0.1M KCl solution at scan rate 10 to 100 mV/s. 193

Figure 4.37 Nyquist plots of $[Fe(CN)^6]^{3-/4-}$ in 0.1 M KCl solution with a SPE, a SPE/CM, and a SPE/CM/Pd. The frequency range is from 1 Hz to 100 kHz. 195

Figure 4.38 Effect of buffer pH on the peak oxidation potential for the oxidation of AA and UA. Concentrations: AA, 0.787 mM; UA, 1.27 mM. Scan rate 50 mV/s. 196

Figure 4.39 Effect of buffer pH on the peak current for the oxidation of AA and UA. Concentrations: AA, 0.787 mM; UA, 1.27 mM. Scan rate 50 mV/s. 196

Figure 4.40 Effect of deposition time on the peak current for the oxidation of AA and UA. Concentrations: AA, 0.787 mM; UA, 1.27 mM. Scan rate 50 mV/s. 197

Figure 4.41 (A) CV of AA 0.787 mM and UA 1.27 mM at the (a) SPE/CM/Pd and (b) SPE in 0.1 M PB solution pH 4.0. (B) CVs of various AA and UA concentrations at the SPE/CM/Pd in 0.1 M PB solution pH 4.0. Concentrations of analytes (a-e); 0.495, 0.787, 1.076, 1.362, 1.644, 1.923 and 2.199 mM for AA and 0.98, 1.267, 1.456, 1.737, 2.015, 2.29 and 12.562 mM for UA. (C) Calibration plot for AA obtained from the CV's shown in (B). (D) Calibration plot for UA obtained from the CV's shown in (B). Scan rate: 50 mV/s. 198

Figure 4.42 A typical current-time response of the SPE/CM/Pd upon the successive additions of (A) 50 µM AA and (B) 70 µM UA in 0.1 M PB solution pH 4, E= 0.2V. 199

List of Tables

Table 1.1	Examples of different types of transducers	37
Table 1.2	Types of microelectrodes and their diffusion field geometry	52
Table 1.3	Different modes of CE available	65
Table 1.4	Different modes of luminescence available	70
Table 1.5	Table of validation characteristics	72
Table 1.6	Table of validation characteristics	75
Table 2.1	Linear ranges and detection limits of the amino acids using PT microchips	99
Table 2.2	Linear ranges and detection limits of the chiral compounds using PT microchips	104
Table 2.3	Comparison of PT microchip with glass chip and other polymeric microchips	105
Table 3.1	The recovery of UA in real-sample for the proposed method using the acetate microelectrode configuration	130
Table 3.2	Linear ranges and detection limits of the analytes using acetate microelectrode	136
Table 4.1	The anodic (Ipa) and catodic (Ipc) peak currents versus the square root of the scan rate ($V^{1/2}$) for SPE and SPE/Au	159
Table 4.2	The recovery of DA and UA for the proposed method using SPE/Au	165
Table 4.3	The anodic (Ipa) and catodic (Ipc) peak currents versus the square root of the scan rate ($V^{1/2}$) for SPE and SPE/Pd	170
Table 4.4	The recovery of AA and UA for the proposed method using SPE/Pd	176
Table 4.5	The anodic (Ipa) and catodic (Ipc) peak currents versus the square root of the scan rate ($V^{1/2}$) for SPE and SPE/CM/Au	182
Table 4.6	The recovery of DA and UA for the proposed method using the SPE/CM/Au	189
Table 4.7	The anodic (Ipa) and catodic (Ipc) peak currents versus the square root of the scan rate ($V^{1/2}$) for SPE and SPE/CM/Pd	194

Table 4.8 The recovery of AA and UA for the proposed method using SPE/CM/Pd 200

List of Abbreviations

AA	ascorbic acid
AC	alternating current
AD	amperometric detection
Ag	silver
Ag/AgCl	silver/silver chloride
Au	gold
AuNPs	gold nanoparticles
BGE	background electrolyte
CE	capillary electrophoresis
CL	chemiluminescence
CM	carbon monolith
Cys	L-cysteine
CV	cyclic voltammetry
CZE	capillary zone electrophoresis
DA	dopamine
DMF	dimethylformamide
DPV	differential pulse voltammetry
EC	electrochemical
EIS	electrochemical impedance spectroscopy
EOF	electroosmotic flow
EP	epinephrine
EtOH	ethanol
$FeCl_3$	ferric chloride
FET	field effect transistor
FI	flow injection
Gly	glycine
H_2O	water
H_2O_2	hydrogen peroxide
H_2SO_4	sulphuric acid
H_3PO_4	phosphoric acid
HCl	hydrochloric acid

His	histidine
HPLC	high performance liquid chromatography
Hz	hertz
IUPAC	International Union of Pure and Applied Chemistry
$K_3Fe(CN)_6$	potassium ferricyanide
$K_4Fe(CN)_6$	potassium ferrocyanide
KCl	potassium chloride
LOD	limit of detection
LSV	linear sweep voltammetry
M	molar
ME	microchip electrophoresis
MEKC	micellar electrokinetic capillary chromatography
MeOH	methanol
mM	milli Molar
MS	mass spectrometry
NaCl	sodium chloride
NaH_2PO_4	monosodium phosphate
Na_2HPO_4	disodium phosphate
NaOH	sodium hydroxide
NEP	norepinephrine
OFN	oxygen free nitrogen
PDDA	Poly (diallyl dimethylammonium) Chloride
PDMS	Polydimethylsiloxane
PdNPs	palladium nanoparticles
Pt	platinum
PT	polyester-toner
TA	tryptamine
Trp	Tryptophan
UA	uric acid
UV	ultra-violet
ΔEp	Peak-to-peak separation

Objectives and Thesis Overview

The work described in this thesis focuses on the development of inexpensive sensors for health applications. Chapter one is an introduction into the principles of electrochemistry, and an introduction to the work outlined involved in this thesis. Chapter 2 investigates the use of toner-based microchips for the separation and determination of amino acids and chiral compounds. This microfluidic device is based on the lamination of laser-printed polyester films using a computer, printer and laminator. The advantages of these microchips are numerous and include fast analysis times, minute consumption of samples and reagents, as well as the low-cost and rapid fabrication. The resulting toner-based microchips demonstrated a potential viability for chemical assays, coupled with several detection methods, particularly Chip-Electrophoresis-Chemiluminescence (CE-CL) detection.

Chapter 3 involves the fabrication of micro-electrodes which are made of gold, silver and platinum by means of patterning and deposition techniques onto acetate using the central fabrication facilities in Tyndall National Institute. These electrodes have been designed to facilitate the integration of a 3-electrode configuration as part of the fabrication process. Since the electrodes are on acetate the dicing step can automatically be eliminated. This gives more control and flexibility to tailor the size and shape of the acetate electrode depending on what detection method you are coupling them with. The stability of these sensors has been investigated using cyclic voltammetry and potentiometry with excellent outcomes. Following on from the generalised testing of the electrodes coupling these sensors was performed with capillary electrophoresis.

Chapter 4 involves working and modifying in-house fabricated screen-printed electrodes (SPE) and is divided into two parts. These electrodes are generally seen to be far less sensitive than the more expensive electrodes including the gold, boron-doped diamond and glassy carbon electrodes. The first part of this work involved electro-depositing metal nanoparticles directly onto the SPE. The second part involved first modifying the SPE with carbon monolith material and then to electrodeposit metal nano-particles onto the carbonaceous material. Both of these types of modification allowed for simultaneous determination of multiple analytes

which was not possible using the bare electrode initially. Chapter 5 discusses the general conclusions of the work in this thesis and possible future work. Chapter 6 represents the lists of published papers, awards, oral and poster presentations achieved during the period of study.

Chapter 1

General Introduction

1 General Introduction

1.1 Sensors and Separation

Separation science involves using the physical properties and molecular interactions of chemical and biological compounds to move them between gaseous, liquid or solid phases. The ultimate aim of separation science often involves separating out the chemical and/or biological components in mixtures such as pharmaceuticals, wastewater, blood or food ingredients. Separation science is typically coupled with sensitive detection methods to measure the amounts or concentrations of chemical or biological compounds present. The work presented in this thesis develops new platforms and sensor technologies to help address the separation and measurement needs of global industry and wider society at a relatively low-cost.

A sensor is a converter that measures a physical quantity and converts it into a signal which can be read by an observer or by an (today mostly electronic) instrument [1]. We can divide sensors into three types, namely;

- Physical sensors -for measuring distance, mass, temperature, pressure etc.
- Chemical sensors – which measure chemical substances by chemical or physical responses and
- Biosensors which measure chemical substances by using a biological sensing element.

All of these devices have to be connected to a transducer of some sort, so that a visibly observable response occurs. I will further discuss transducers in section 1.4. Chemical sensors and biosensors are generally concerned with sensing and measuring particular chemicals which may or may not be biological themselves [2]. These chemicals are usually given the general term analyte. Figure 1.1 shows the general schematic arrangement of a sensor.

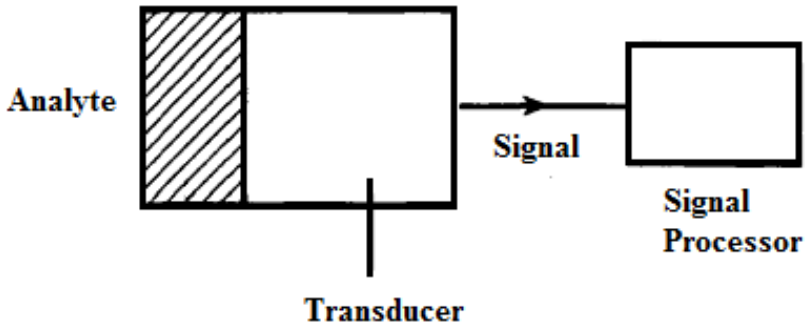

Figure 1.1: Schematic layout of a sensor

The development of instrumentation, microelectronics and computers makes it possible to design sensors utilizing most of the known chemical, physical and biological principles that have been used in chemistry.

The work in this thesis focuses on chemical sensors. Chemical sensors may be classified according to the operating principle of the transducer:

1. Optical devices transform changes of optical phenomena, which are the result of an interaction of the analyte with the receptor part. This group may be further subdivided according to the type of optical properties which have been applied in chemical sensors:

- *Absorbance*, measured in a transparent medium, caused by the absorptivity of the analyte itself or by a reaction with some suitable indicator.
- *Reflectance*, is measured in non-transparent media, usually using an immobilized indicator.
- *Luminescence*, based on the measurement of the intensity of light emitted by a chemical reaction in the receptor system.
- *Fluorescence*, measured as the positive emission effect caused by irradiation. Also, selective quenching of fluorescence may be the basis of such devices.

- *Refractive Index*, measured as the result of a change in solution composition. This may also include a surface plasmon resonance effect.
- *Optothermal Effect*, based on a measurement of the thermal effect caused by light absorption.
- *Light Scattering*, based on effects caused by particles of definite size present in the sample.

2. Thermometric devices are based on the measurement of the heat effects of a specific chemical reaction or adsorption which involve the analyte. In this group the heat effects may be measured in various ways, for example in the so called catalytic sensors, the heat of a combustion reaction or an enzymatic reaction is measured by use of a thermistor.

3. Magnetic devices are based on the change of paramagnetic properties of a gas being analysed. These are represented by certain types of oxygen monitors.

4. Mass sensitive devices transform the mass change at a specially modified surface into a change of a property of the support material. The mass change is caused by accumulation of the analyte.

a) Piezoelectric devices used mainly in gaseous phase, but also in solutions, are based on the measurement the frequency change of the quartz oscillator plate caused by adsorption of a mass of the analyte at the oscillator.

b) Surface acoustic wave devices depend on the modification of the propagation velocity of a generated acoustical wave affected by the deposition of a definite mass of the analyte.

5. Electrical devices are based on measurements, where no electrochemical processes take place, but the signal arises from the change of electrical properties caused by the interaction of the analyte.

a) Metal oxide semiconductor sensors used principally as gas phase detectors, based on reversible redox processes of analyte gas components.

b) Organic semiconductor sensors are based on the formation of charge transfer complexes, which modify the charge carrier density.

c) Electrolytic conductivity sensors.

d) Electric permittivity sensors.

6. Electrochemical devices transform the effect of the electrochemical interaction analyte - electrode into a useful signal. Such effects may be stimulated electrically or may result in a spontaneous interaction at the zero-current condition. The following subgroups may be distinguished:

a) Voltammetric sensors, including amperometric devices, in which current is measured in the D.C. or A.C. mode. This subgroup may include sensors based on chemically inert electrodes, chemically active electrodes and modified electrodes. In this group sensors are included with and without (galvanic sensors) external current source.

b) Potentiometric sensors, in which the potential of the indicator electrode (ion-selective electrode, redox electrode, metal/meta1 oxide electrode) is measured against a reference electrode.

c) Chemically sensitised field effect transistor (CHEMFET) in which the effect of the interaction between the analyte and the active coating is transformed into a change of the source-drain current. The interactions between the analyte and the coating are, from the chemical point of view, similar to those found in potentiometric ion-selective sensors.

d) Potentiometric solid electrolyte gas sensors work in high temperature solid electrolytes and are usually applied for gas sensing measurements.

The work in this thesis focuses on electrochemical devices, in particular voltammetric sensors. Before the principles behind these sensors can be explained, the basic fundamentals of electrochemistry must first be discussed.

1.2 **An Introduction to Electro-Analytical Principles**

1.2.1 **General Introduction**

Electrochemistry is the area of chemistry dealing with the interconversion of electrical energy and chemical energy. It may be defined as the branch of chemistry that is concerned with electrolysis and other similar phenomena that occurs when a current is passed through a solution of an electrolyte, or with the behaviour of ions in solution and the properties shown by these solutions [3].

Electrochemistry was discovered in the mid-1780s by anatomist Luigi Galvani (Bologna, Italy) whilst he was studying the effects of atmospheric electrical discharge. One day, he fastened brass hooks between the spinal cord of a dissected frog and an iron railing. To his amazement the frog's legs began twitching wildly, not only when lightning flashed, but also when the sky was calm. The most significant consequence of Galvani's discovery was the concept of Galvanism which refers to the production of electrical current from the contact of two metals in a moist environment [4].

Alessandro Giuseppe Volta (Como, Italy), made another important discovery following on from Galvani's work. According to Volta's interpretation, the muscle twitches were induced by current flowing between two dissimilar metals connected by the moist flesh of the frog's leg. This led him to develop the first device which demonstrated chemical production of electric current [5]. Other particular early events in the development of electrochemistry included Humphrey Davy (1778-1829), who utilised the recently discovered voltaic pile to lay the qualitative foundations of electrochemistry. Davy isolated elemental potassium which was soon followed by sodium, barium, calcium, strontium, magnesium and later isolated boron and silicon [6].

Michael Faraday (1791-1867), who began his career as Davy's laboratory assistant, achieved scientific prominence of his own for the First Law of Electrochemistry, developed in 1834: 'The chemical power of a current of electricity is in direct proportion to the absolute quantity of electricity which

passes'. The Second Law of Electrochemistry, also defined by Faraday, states: 'Electrochemical equivalents coincide, and are the same, with ordinary chemical equivalents'. The work that led to these two laws also resulted in many of the modern electrochemical terms such as electrode, electrolyte, and ion [7].

In 1905 Julius Tafel discovered that electric current passing across metal-solution interfaces could be made to increase exponentially by changing the electric potential of the electrode across the surface of which they passed. He is now known for the Tafel equation which is an equation in electrochemical kinetics relating the rate of an electrochemical reaction to the overpotential, $\Delta V = A \times \ln (i / i_0)$, where ΔV is the overpotential, A is the so-called "Tafel slope", I is the current density and i_0 is the so-called exchange current density [8].

Other more recent advances in the last century include the introduction of cyclic voltammetry by Hickling (1940's) and the invention of the operational amplifier (1950's). During the 1960's and 70's quantum electrochemistry was developed by Revaz Dogonadze and his pupils. Other advances include chemically modified electrodes and photoelectrochemistry in the 70's and the introduction of microelectrodes in the 90's [7]. This has allowed electrochemistry to become an extremely broad subject encompassing such various areas as batteries, fuel cells, corrosion studies, hydrogen energy conversion, and bioelectricity [9].

Electroanalysis has many advantages including selectivity and sensitivity as well as its inexpensive equipment, ample choice of working electrode materials and direct accessibility, especially to electronic and hence automatic control, automated data treatment and simple insertion. Although there may be circumstances in which an electroanalytical method, as a consequence of the additional chemicals required, has disadvantages in comparison with instrumental techniques of analysis, the above-mentioned advantages often make electroanalysis the preferred approach for chemical control in industrial and environmental studies. Without a doubt electroanalysis has generated a vast range of applications including; environmental monitoring, biomedical analysis and industrial quality control [10]. This chapter will focus on the basic electrochemical principles in relation to electroanalytical chemistry, as well as a

range of commercially available electrodes with particular emphasis on screen-printed electrodes. The chapter will also target the possibilities for chemical modification of these screen-printed electrodes and finally some insight into microelectrode configurations.

1.3 **Fundamentals of Electroanalytical Chemistry**

1.3.1 **Introduction**

Electrochemical processes take place at the electrode-solution interface. The type of electrical signal used for quantitation differentiates the various electroanalytical techniques. In principle there are two types of electroanalytical measurements: potentiometric and potentiostatic [10]. Both require at least two electrodes and an electrolyte solution which make up the electrochemical (voltammetric) cell. The electrochemical cell and the processes involved with the electrode reactions will be further discussed in the forthcoming sections.

1.3.2 **Electrochemical Cell**

Electrochemical cells are categorised as either galvanic or electrolyte cells. Both cells have faradaic currents flowing through them, however a galvanic cell experiences spontaneous reactions at the electrodes by an oxidation-reduction couple and are often used in converting chemical energy into electrical energy. It is for this reason that galvanic cells are commonly used as batteries [11]. An electrolyte cell is one where the reactions are non-spontaneous and are induced by an external voltage greater than the open circuit potential of the cell. The electrolyte cells are regularly used to carry out desired chemical reactions by burning up electrical energy.

The term electrolysis is defined as: the passage of a direct electric current through an ion-containing solution, which produces chemical changes at the electrodes [4]. It can also be broadly classified as chemical changes that accompany faradaic reactions at electrodes in contact with an electrolyte solution. The electrode at

which oxidations occur is called the anode whilst the electrode where reductions exist is termed a cathode. A cathodic current occurs when a current in which electrons move across the interface from the electrode to a species in solutions, while electron flow from the species in solution into the electrode is termed anodic current.

The electrochemical cell can be defined as a device that generates a potential difference between electrodes using chemical reactions. In general, there is a measureable difference in potential between the two electrodes whether a current is present in the cell or not. The overall chemical reaction taking place in a cell is made up of two half reactions which are independent to each other [12]. Most of the time only one of these reactions is of interest, and the electrode at which it occurs is termed the working electrode. The purpose of this electrode, which is in contact with the species in solution, is to execute the required amount of potential in an orderly manner and promote the two-way electron transmission to and from the species. In order to focus on the working electrode, it is necessary to standardise the other half of the cell by using an electrode made up of phases of constant composition, the reference electrode. As the reference electrode is of stable composition its potential value is fixed and hence can be employed for the measurement of the potential of the working electrode. Thus one can state that one observes the potential of the working electrode with respect to the reference electrode. Equalising the current measured at the working electrode is the duty of the counter (or auxiliary) electrode. To achieve this task, the counter electrode may frequently move back and forth between the severe potentials found at the boundaries of the solvent window, where it undergoes oxidation while forcing the solvent or counter electrolyte to suffer reduction [13]. A typical three-electrode electrochemical cell is shown in Figure 1.2.

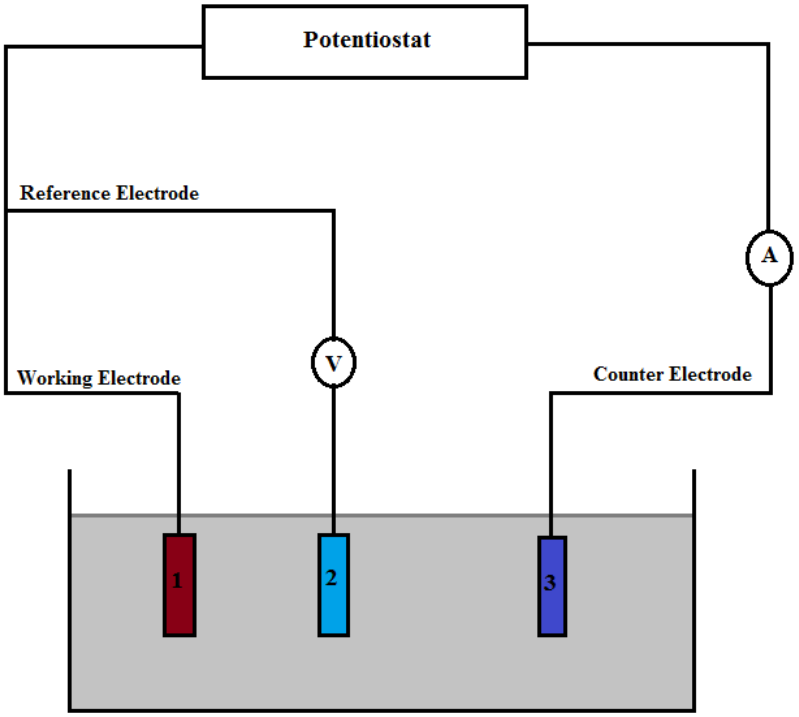

Figure 1.2: Simple schematic of a three-electrode electrochemical cell, showing the working electrode, reference electrode and counter electrode immersed in solution. The electrodes are all connected to a potentiostat so that the potential differences between the electrodes can be measured.

Working electrodes come in a range of designs and sizes but in general it is a small sphere, a wire or a small disk with an area of $< 0.25\ cm^2$, although microelectrodes which will be discussed later are substantially smaller than this [13]. The electrode surface needs to be clean and smooth to ensure the geometry and mass transport are well defined [13]. It is also important that the working electrode should not react chemically with the solvent or the species in solution. There are multiple types of working electrodes including gold, silver, boron doped diamond, mercury, platinum, glassy carbon, carbon paste and screen printed. The screen printed electrodes will be discussed in more detail in Section 1.5.1.5. There are also several types of reference electrodes such as the mercury-mercurous chloride, also known as the calomel electrode which were widely used up until about 1960. However, a big problem with this type of reference electrode presents

itself when the electrode is exposed to temperatures greater than 50 degrees Celsius. The mercurous chloride element of the electrode breaks down under this kind of heat, which will cause unreliable readings [14]. Another common type of reference electrode is the silver/silver chloride electrode which is the most common type of reference electrode. They are very easy to manufacture and are able to function in a wide variety of ambient temperatures. The maximum temperature at which this type of electrode can function is about 130 degrees Celsius [14]. The most common counter electrode material is platinum, usually a wire or a coil [13].

An electrolyte is a compound which produces an ionic solution when dissolved in an aqueous solution; this ionic solution is called the electrolyte solution. The electrolyte solution is the medium between the electrodes in the cell. This solution which also incorporates the species of interest may also contain other compounds such as buffer or complexing agents. The choice of the solvent depends on a number of factors which include the solubility of the species in solution, its redox activity and on solvent properties such electrochemical and chemical activities as well as electrical conductivity [10]. It is important that the solution does not react with the species in solution and should be stable over a wide potential range, see typical three-electrode electrochemical cell in Figure 1.2. In certain electrochemical experiments a Faraday cage is used. A Faraday cage is a metallic enclosure that prevents the entry or escape of an electromagnetic field (EM field). An ideal Faraday cage consists of an unbroken, perfectly conducting shell. This ideal cannot be achieved in practice, but can be approached by using fine-mesh copper screening. For best performance, the cage should be directly connected to an earth ground and it forms an extended electrical field which reduces noise currents in the cell from nearby electromagnetic sources in the laboratory. This cage should be used when working with microelectrodes or electrodes with very weak current measurements (<1 pA).

1.3.3 **Electrochemical Measurements**

Any process measured in electroanalytical chemistry occurs at the surface of the electrode. Therefore electrochemical measurements reflect a surface process rather than a solution process. Thus the surface of the electrode itself, the distance of the analyte from the surface, the rate at which the analyte reaches the surface and interactions of analyte with the surface will all affect the measurement. The type and scale of the effect depends on the type of measurement performed.

The measurement types are:

I. Conductimetric: is the measure of a material's ability to carry electrical current. It is expressed as the conductance between opposite faces of a one-meter cube of material. The measurement unit of the conductance is the Siemens/m. Also called "specific conductance". The concentration of charge is obtained through measurement of the solutions resistance.

II. Amperometric: is where a constant potential is applied to the working electrode and the current is measured as a function of time.

III. Voltammetric: is a time-dependent potential to an electrochemical cell and measures the resulting current as a function of that potential.

IV. Potentiometric: is where a potentiometer is used to determine the difference between the potential of two electrodes. The potential of one electrode, the working or indicator electrode, responds to the analyte’s activity, and the other electrode - the counter or reference electrode, has a known, fixed potential [15].

Electrochemical methods can be classified as ‘bulk’ or ‘interfacial’. Interfacial techniques are the ones that consider the occurrences at the interface of electrode and solution, whereas bulk techniques are concerned with the occurrences at the solution level only. Interfacial techniques are further classified as potentiometric or voltammetric processes. Voltammetric processes are also sub-divided into

controlled-potential and controlled-current techniques. Controlled-potential techniques are deemed effective due to their high sensitivity, selectivity, transportability and economical installation. Examples include methods like voltammetry and chronoamperometry. In such techniques the current is quantified while potential is regulated.

The principle behind controlled potential electrolysis (CPE) experiments involves controlled-potential electroanalytical tests to receive a current reading that corresponds with the presence of the analyte under consideration. In order to achieve this, the electron transmission that takes place during the redox reaction of the analyte is observed:

$$\mathbf{O + ne^- \longleftrightarrow R}$$

Equation 1.1: Representation of oxidised and reduced entities that make up redox pair

Where, O and R represent the oxidised and the reduced entities that make up the redox pair, respectively [10]. These reactions are known as faradaic processes, since they involve the transfer of electrons across the electrode-solution interface. If only the oxidised species is initially present, then the potential is set at a constant value sufficiently negative to cause rapid reduction and is maintained at this value until only the reduced species is present in solution. The total charge passed during the CPE experiment (Q) is calculated by integrating the current and is related to the number of electrons transferred per molecule (n) and the number of moles of the oxidised species initially present (N) through Faraday's law:

$$\mathbf{Q = nFN}$$

Equation 1.2: Faraday’s Law

Where; F is Faraday's constant (96500 C mol^{-1}). Therefore, if one of n or N is known, the other can be calculated.

The current which results from a change in oxidation state of the analyte is termed the ‘faradaic current’ because it obeys Faraday’s law. This current is a direct measure of the rate of the redox reaction and the resulting current-potential plot is called a voltammogram. The shape of the voltammogram depends on the processes involved in the electrode reaction, and the total current is the sum of the faradaic currents for the analyte and blank solutions, and the non-faradaic charging background current which is the current that results from the electrical double-layer. The non-Faradaic process refers to the process in which no electron transfer takes place across the electrode-solution interface. When phenomena like adsorption and desorption takes place, the structure of the electrode-solution interface experiences a change that corresponds with the variation in potential or in the composition of the solution. To direct the non-Faradaic process, ‘transient current’ needs to be controlled while varying the potential, solution composition or electrode area.

The model which gave rise to the term 'electrical double layer' was first put forward in the 1850's by Helmholtz [16]. In this model he assumed that no electron transfer reactions occur at the electrode and the solution is composed only of electrolyte. The interactions between the ions in solution and the electrode surface were assumed to be electrostatic in nature and resulted from the fact that the electrode holds a charge density (q^m) which arises from either an excess or deficiency of electrons at the electrode surface. In order for the interface to remain neutral the charge held on the electrode is balanced by the redistribution of ions close to the electrode surface. Helmholtz's view of this region is shown in Figure 1.3 below:

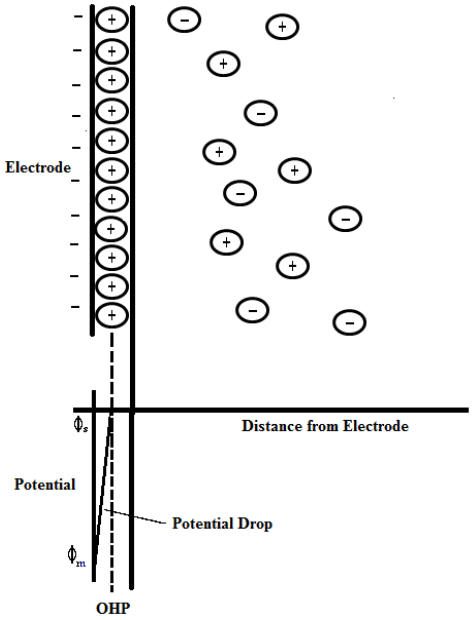

Figure 1.3: Schematic representation of the electrical double layer put forward by Helmholtz.

The attracted ions are assumed to approach the electrode surface and form a layer balancing the electrode charge; the distance of approach is assumed to be limited to the radius of the ion and a single sphere of solvation round each ion. The overall result is two layers of charge (the double layer) and a potential drop which is confined to only this region (termed the outer Helmholtz Plane, OHP) in solution. The result is absolutely analogous to an electrical capacitor which has two plates of charge separated by some distance (d) with the potential drop occurring in a linear manner between the two plates.

The model of Helmholtz while providing a basis for rationalising the behaviour of this region does not account for many factors such as diffusion/mixing in solution, the possibility of absorption on to the surface and the interaction between solvent dipole moments and the electrode. A later model put forward by Stern begins to address some of these limitations now the ions are assumed to be able to move in solution and so the electrostatic interactions are in competition with Brownian motion. This model can be seen in Figure 1.4. The result is still a region close to

the electrode surface ($100x10^{-10}$ m) containing an excess of one type of ion but now the potential drop occurs over the region called the diffuse layer.

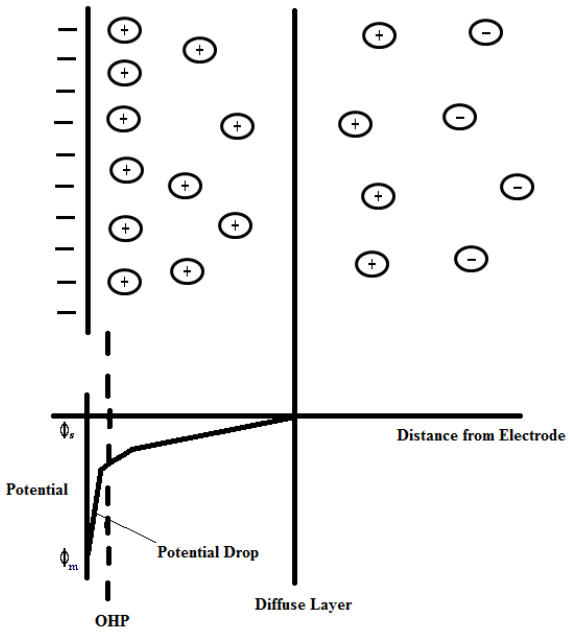

Figure 1.4: Schematic representation of the electrical double layer put forward by Stern.

Many modifications and improvements have been made to these early models with the latest approaches using numerical modelling to follow the redistribution effects as the electrode potential is varied [17-19].

When the overall reaction is controlled only by the rate at which the electroactive species reach the surface, the current is deemed mass transport limited, and is known as a Nernstian or reversible reaction because it obeys thermodynamic conditions. In potentiometry, information on the species in solution can be obtained by the potential appearing between two electrodes. This potential can be used to calculate the concentration of the electroactive species at the surface [C_o and C_r] using the Nernst equation:

$$\mathbf{E_{cell} = E^{0}_{cell} - (RT/nF)ln[C_o/C_r]}$$

Equation 1.3: The Nernst Equation

Where;

E_{cell} = cell potential under nonstandard conditions (V)

E^0_{cell} = cell potential under standard conditions

R = gas constant, which is 8.31 (volt-coulomb)/(mol-K)

T = temperature (K)

n = number of moles of electrons exchanged in the electrochemical reaction (mol)

F = Faraday's constant, 96485 C mol^{-1}

$[C_o/C_r]$ = concentration of electroactive species

The logarithmic term in the Nernst equation is the reaction quotient, Q.

$$\mathbf{Q = [C_o/C_r]}$$

Equation 1.4: Reaction Quotient, Q

Thus the equation can also be written as:

$$\mathbf{E_{cell} = E^0_{cell} - (RT/nF)lnQ}$$

Equation 1.5: Alternative Nernst Equation using reaction quotient, Q

Where;

Q = reaction quotient, which is the equilibrium expression with initial concentrations rather than equilibrium concentrations.

All other terms are previously described in Equation 1.3.

Q has the same form as the equilibrium constant, but the activities need not have their equilibrium values. Pure solids, pure liquids and solvents are omitted from Q because their activities are unity (or close to unity); concentrations of solutes are expressed as moles per litre and concentrations of gases are expressed as pressures in atmospheres.

When all activities are unity, Q = 1 and lnQ = 0, thus giving E = E^0.

Sometimes it is helpful to express the Nernst equation differently, converting the natural logarithm in Equation 1.5 to the base 10 logarithm gives:

$$\mathbf{E_{cell} = E^0_{cell} - (2.303*RT/nF)logQ}$$

Equation 1.6: Alternative Nernst Equation using reaction quotient, Q and converting the natural logarithm in Equation 1.5 to the base 10 logarithm.

and inserting T = 298.15 K (25.00 ºC) gives the most useful form of the Nernst equation:

$$\mathbf{E_{cell} = E^0_{cell} - (0.05916\ V/n)log\ Q}$$

Equation 1.7: Alternative Nernst Equation using reaction quotient, Q and converting the natural logarithm in Equation 1.5 to the base 10 logarithm and inserting T = 298.15 K (25.00 ºC).

By expressing the Nernst Equation in this form the potential changes by 59.16/n mV for each factor of 10 change in the value of Q.

These descriptions of the electrode reaction are in fact quite simplified, as the pathway can actually be quite complicated and take place in several steps. The simplest reactions involve only mass transfer of the electroactive species to the electrode surface, electron transfer across the interface, and transfer of the product back to the bulk solution [10]. In more complex reactions, additional chemical and surface reactions may occur either before or after the actual electron transfer. The slower process will then, obviously, be the rate-determining step. Mass transport to the electrode proceeds by three different processes:

(a) Diffusion

Diffusion is a process in which a body travels from a region of higher concentration to a region of lower concentration in order to reduce the concentration gradient [20]. In other words, it is an impulsive motion instigated by the concentration differences. When the electrode is oxidised while reducing the analyte, it will result in a reduced concentration of the analyte at the area of the electrode. To compensate for this reduction in the concentration, more analyte travels towards the electrode from the solution phase. This makes it the most substantial current-controlling feature in voltammetric method. During the electrochemical reaction, although the current is transmitted to the bulk solution by movement, still one should not overlook the possibility of diffusion because the concentration difference near the electrodes and the electroactive entities increase when the product is formed at the electrode, at the expense of the reagent. Also, in certain cases, diffusion is the only phenomenon that drives the electroactive species towards the electrode. This movement of a chemical species under the influence of a concentration gradient is described by Fick's first law [20]. A particle i will diffuse through a cross-sectional area as a function of the concentration gradient across the selected area. Flux, as particles per unit time across the given segment, is expressed as J_i according to:

$$J_i = -D_i\left(\frac{\partial C_i}{\partial x}\right)$$

Equation 1.8: Fick's First Law

Where; $\partial C_i / \partial x$ expresses the concentration gradient and D_i is the diffusion coefficient for particle i.

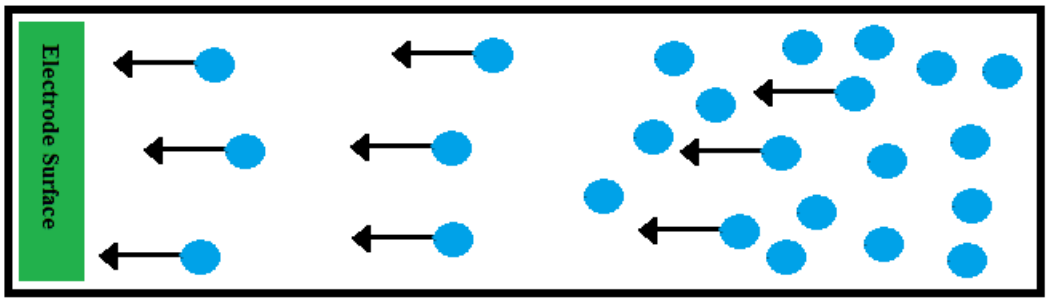

Figure 1.5: Schematic representation of diffusion where a body travels from a region of higher concentration to a region of lower concentration in order to reduce the concentration gradient.

(b) Migration

The process of transmission of charges in which charged particles move along an electrical field (the ions transmit the charge through the solution on the basis of their transference number) is known as migration [10].

An auxiliary electrolyte is required during controlled-potential tests for the reduction of the solution resistance and eradication of electromigration effects. This helps sustain a stable ionic strength. In the present study, a large quantity of inert salt, like KCl was added to eradicate or restrain electromigration. When it comes to investigative purposes, the existence of auxiliary electrolyte with a concentration that is hundred times higher than the concentration of electroactive ions implies that the role of the studied ions is below one percent in the migration transport. In such a case, it will be appropriate to believe that the analytes under study are transmitted to the electrode only because of diffusion.

When cations undergo oxidation or reduction, the current flux near the electrode can be controlled by the migration of electroactive entities. It facilitates the minimisation of the electrical field by amplifying the conductivity of the solution. Moreover, it causes the decrement or removal of sample matrix effects. The thinness of the double layer with regard to the diffusion layer is maintained with the help of the auxiliary electrolyte. In addition, a constant ionic strength is instigated all through the solution. Nevertheless, the gauging of the current flow

during merged migration may be benefited by the phenomenon of diffusion, especially in electrochemical and electroanalytical processes.

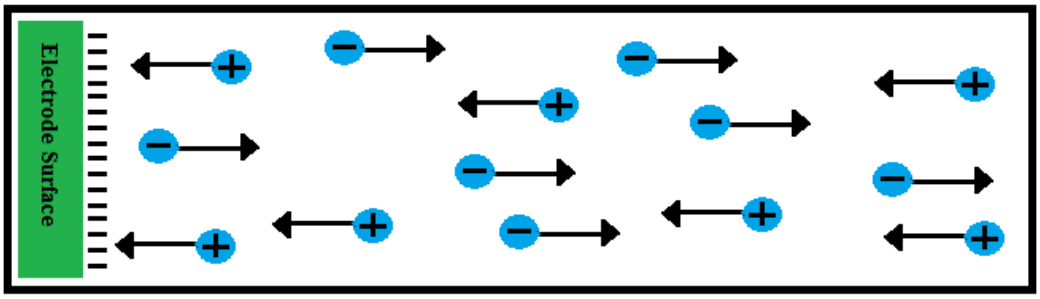

Figure 1.6: Schematic representation of migration, in which charged particles move along an electrical field (the ions transmit the charge through the solution on the basis of their transference number).

(c) Convection

The phenomenon in which an apparent physical motion causes the electrons to flow to the electrode is known as convection. The physical motion may include the flow of a fluid which can be caused by agitation or flow of the solution or due to the density gradient (i.e. natural convection) or by replacement or trembling of the electrode (i.e. forced convection) [10,15]. However, in the work involved in this thesis the cell was preserved in a calm and steady environment while conducting the Voltammetry experiment; hence no convection occurred.

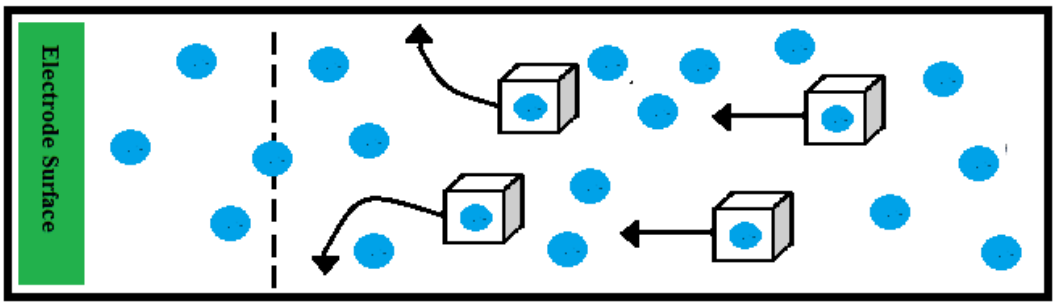

Figure 1.7: Schematic representation of convection, in which an apparent physical motion causes the electrons to flow to the electrode.

The total mass transport of material, or flux, to an electrode is described for one dimension by the Nernst-Planck equation:

$$J(x,t) = - [D (\partial C(x,t)/ \partial x)] - [(zF/ RT) D C(x,t)](\partial \varphi(x,t)/ \partial x) + C(x,t) \nu x (x,t)$$

Equation 1.9: Nernst-Planck Equation

Where;

J is the flux (mol $cm^{-2}s^{-1}$),

D is the diffusion coefficient of the solution species (cm^2/s),

C is the concentration of the species (mol/cm^3),

Φ is the electrostatic potential, and

νx is the hydrodynamic velocity.

The Nernst-Planck equation combines the individual contributions from diffusion (concentration gradient), migration (electric field), and convection (hydrodynamic velocity). Contributions from migration can be effectively eliminated by adding an inert electrolyte to the solution at a 10 – 100 fold excess with respect to the redox couple of interest. The electric field between the two electrodes involved in the measurement is dissipated over all of the ions in solution and not just the electroactive material. Under these conditions, the contribution of migration to the observed current is < 1% [21]. Contributions from convection can be reduced or eliminated by working in quiet (*unstirred*) solutions. With careful control of external vibration and temperature, diffusion controlled measurements for up to 20 seconds or so can be made without significant convective effects [22].

The flux can then be related to the observed current at the working electrode by:

$$It = n F A D (\partial Ci/ \partial x) \mid x = 0$$

Equation 1.10: Nernst-Planck Equation without migration and convection contributions

Where; A is the electrode area (cm^2), and all other symbols are described in equation 1.9.

As previously discussed, diffusion is the process whereby a solute moves from a region of high concentration to one of low concentration and the flow of solute is called the flux, J. In the schematic shown below the flux, J, will flow towards the right.

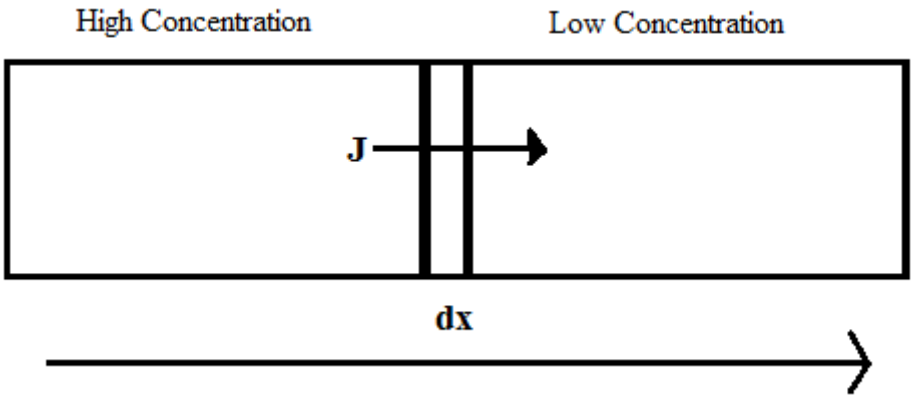

Figure 1.8: Schematic representation of Fick's First Law of Diffusion where the flux, J, moves from a region of high concentration to one of low concentration.

Fick's First Law of Diffusion sums up this process in the following mathematical expression:

$$J = -D(dc/dx)$$

Equation 1.11: Fick's First Law of Diffusion

Where: dc/dx is the concentration gradient per unit length and D is the diffusion constant.

While J is predominantly from left to right in this image there is flow from right to left. Diffusion occurs in both directions. The flow to the right in this case is greater than that to the left. The central region in the diagram experiences the following change; material flows in from the left side and flows out from the right side.

The diffusional flux is time dependent and this is described by Fick's second law:

$$\partial C/\partial t = D(\partial^2 C/(\partial x^2)$$

Equation 1.12: Fick's Second Law

This equation reflects the rate of change of concentration between parallel planes at points x and (x + dx) with time and is valid for planes parallel to one another and perpendicular to the direction of diffusion. In cases where diffusion is towards a spherical electrode, i.e. the lines of flux are not parallel but are perpendicular to segments of the sphere, Ficks second law takes the form

$$\partial C/\partial t = D((\partial^2 C/(\partial r^2) + 2/r(\partial C/(\partial r)) \qquad (1.13)$$

Equation 1.13: Fick's Second Law where diffusion is towards a spherical electrode.

Where, r is the distance from the centre of the electrode. Overall Fick's law describes the flux and the concentration of the electroactive species as functions of position and time [10].

1.3.4 **Electrochemical Measurement Techniques**

The electrochemical procedures used during this research are briefly outlined in this section. They do not represent the entire range of techniques currently available with modern instrumentation only the relevant techniques to this work.
Electrochemistry is based on the computation of both potential (potentiometry) and current response (Voltammetry). In order to fully comprehend the underlying

principles, it is essential to elaborate on the various electrochemical techniques that were used.

1.3.4.1 **Linear Sweep Voltammetry (LSV)**

Linear sweep voltammetry (LSV) employs a fixed potential range with the voltage being scanned from a lower limit to an upper limit as shown in Figure 1.9 below [16].

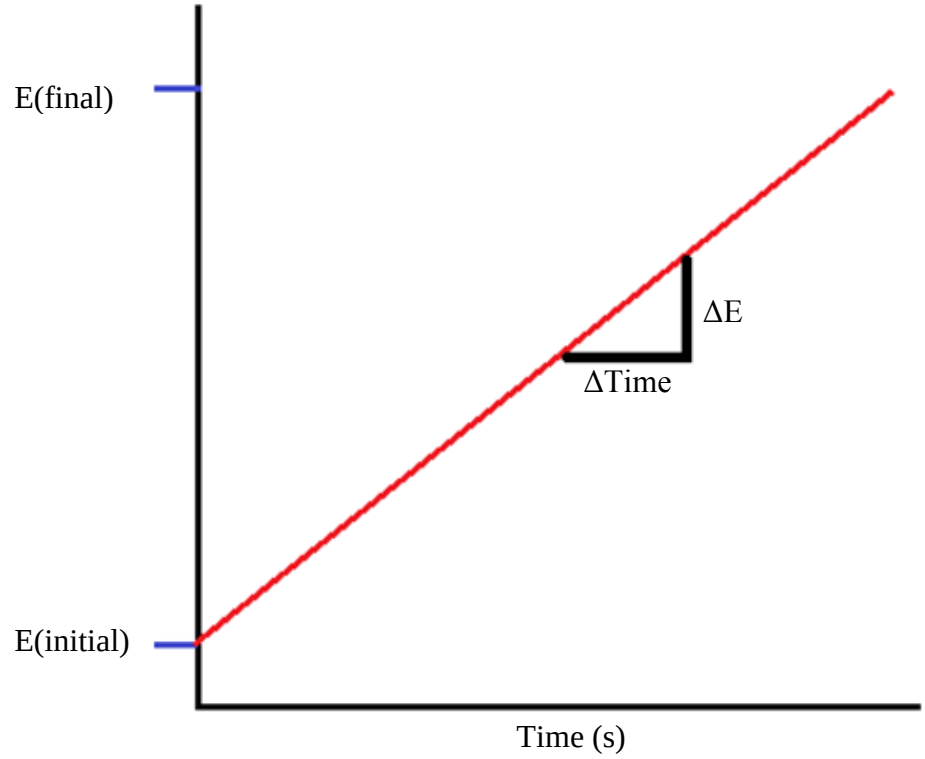

Figure 1.9: Representation of a typical LSV graph where the potential applied across the electrode-solution interface is scanned linearly from an initial value E_i to a final value E_f at a constant rate v.

LSV is the simplest of the potential-time waveforms, in which the potential applied across the electrode-solution interface is scanned linearly from an initial value E_i to a final value E_f at a constant rate v.

The voltage scan is calculated from the slope of the line. Clearly by changing the time taken to sweep the range one can alter the scan rate. When the potential

moves in the positive direction, i.e becoming increasingly positive, it is termed as a positive scan.

The characteristics of the linear sweep voltammogram recorded depend on a number of factors including [16]:

I. The rate of the electron transfer reaction(s)

II. The chemical reactivity of the electroactive species

III. The voltage scan rate

In LSV the initial potential scan E_i would generally cause no reaction and then scan through the standard electrode potential(s) of the species in solution, thus the composition of the reaction layer should not be altered at the beginning by the application of potential. The potential where the peak current is observed is called the peak potential, represented as Ep. When peak potential is reached, all the redox species have been consumed at the surface of the electrode and diffusion is the limiting factor for the current. The rate of electron transfer between the redox species and the electrode is signified by the intensity of the Faradaic current, Ipa (anodic peak current) or Ipc (cathodic peak current). During LSV experiments, the mechanisms of electron transmission can be categorised as a:

I. Reversible process

II. Irreversible process

III. Quasi-reversible process

The half-wave potential ($E^{1/2}$) for a reversible process is equal to the formal potential (Eó) and their relation with the standard potential (Eo) which is described below in equation 1.14:

$$\mathbf{E^{1/2} = Eo' = Eo + RT/2F \ln [O]/[R]}$$

Equation 1.14: The half-wave potential ($E^{1/2}$) for a reversible process is equal to the formal potential (Eo′) and their relation with the standard potential (Eo).

Where; R is the gas constant, T stands for temperature (in Kelvin), F is the Faraday's constant (96485 C mol^{-1}), [**O**] represents concentration of oxidized species (mol L^{-1}) and [**R**] denotes concentration of reduced species (mol L^{-1}).

In order to compute the formal redox potential,

$$\mathbf{Eo' = Epa + Epc / 2}$$

Equation 1.15: To compute the formal redox potential

Where; Epa stands for anodic peak potential and Epc symbolises cathodic peak potential.

Equation 1.16 can be used to calculate the number of electrons transmitted during a reversible process:

$$\mathbf{\Delta E = Epc - Epa = RT / nF}$$

Equation 1.16: To calculate the number of electrons transmitted during a reversible process

At 25º C, $\Delta E = 0.059V/n$

Where n represents number of electrons transferred. The remaining symbols have the same definition as given in Equations 1.14 and 1.15.

The peak current value of a reversible process at 2 5ºC, is calculated by the Randles-Sevcik Equation 1.17:

$$i_p = 2.69 \text{ X } 10^5 n^{3/2} A D^{1/2} C v^{1/2}$$

Equation 1.17: The Randles-Sevcik Equation

Where; i_p = peak current, n = number of electrons transferred, A = electrode area (cm^2), D = diffusion coefficient (cm^2/s), C = concentration of the species in the bulk solution (mol/cm^3), v = scan rate (V/s).

With the aid of the Randles-Sevcik Equation; Equation 1.17, a linear plot of Ip vs. $v^{1/2}$ is achieved for a planar diffusion [23] [24] at the surface of the electrode. When the plot diverges from linearity, it implies that either oxidized, reduced or both species have participated in the chemical reaction. The observations for **an irreversible process** may include only forward oxidation or reduction peak; but sometimes with a weak reverse peak

An irreversible process generally involves slow-moving electron transfer or sluggish chemical reactions at the electrode's end [25]. This process does not obey the Nernst equation because of the fact that electron transfer is not fast enough to achieve equilibrium.

For an irreversible process, the peak current, Ip can be calculated with the help of the following equation:

$$i_p = (2.99x10^5) n (\alpha n_a)^{1/2} A C D^{1/2} v^{1/2}$$

Equation 1.18: To calculate peak current, i_p, for an irreversible process.

Where; α is the transfer coefficient, n_a is the number of electrons transferred and the rest of the symbols have been described in Equation 1.17.

The peak current is still related to the bulk concentration, but will be lower in height depending on the value of α.

When the system is completely irreversible, Equation 1.19 is employed to calculate ΔEp:

$$E_p = E° - (RT/\alpha n_a F)[0.78 - \ln(k^o/(D)^{1/2}) + \ln (\alpha n_a F v/RT)^{1/2}]$$

Equation 1.19: To calculate ΔEp for an irreversible process

Where; k^o symbolizes heterogeneous electron transfer constant (cms^{-1}), while all the other symbols hold the previously mentioned meanings.

In Quasi-reversible processes, both charge transfer kinetics and mass transport play their parts in handling the current [10] [26]. Such a process lies in between the reversible and irreversible systems. A quasi-reversible process takes place when the relative rate of electron transfer with reference to that of mass transport is incapable of achieving Nernst equilibrium at the surface of the electrode. During a quasi-reversible process, as $\upsilon^{1/2}$ increases, Ip also increases but not linearly and an increase is observed in $\Delta E > 59/n$ mV when υ increases.

1.3.4.2 **Cyclic Voltammetry**

Cyclic voltammetry is a method for investigating the electrochemical behaviour of a system. It was first reported in 1948 and described theoretically by Randles [27]. Cyclic voltammetry (CV) is arguably the most widely used electrochemical technique for the characterisation of redox systems. It is an effective approach for the evaluation of the systems electron transfer in reactions, such as provision of data regarding kinetics and formal reduction, reversibility, stability and oxidation potentials of a system [28]. As CV is a logical extension of LSV, the theory and equations expressed in the previous section also apply to this method.

CV is often the first experiment performed in electrochemical analysis, offering a quick and convenient evaluation of the redox potentials, of the redox species and a determination of the effect of media upon the redox process. In this technique current flowing between the electrode of interest (whose potential is monitored

with respect to a reference electrode) and a counter electrode is measured under the control of a potentiostat. The voltammogram determines the potentials at which different electrochemical processes occur. The working electrode is subjected to a triangular potential sweep, whereby the potential rises from a start value Ei to a final value Ef then returns back to the start potential at a constant potential sweep rate. Single or multiple cycles can be performed depending on the information required. The sweep rate applied can vary from a few millivolts per second to a hundred volts per second. The current measured during this process is often normalised to the electrode surface area and referred to as the current density. The current density is then plotted against the applied potential, and the result is referred to as a cyclic voltammogram [29]. A peak in the measured current is seen at a potential that is characteristic of any electrode reaction taking place. The peak width and height for a particular process may depend on the sweep rate, electrolyte concentration and the electrode material [12,30].

Cyclic voltammetry makes possible the clarification of the kinetics of electrochemical reactions taking place at electrode surfaces [31]. In a typical voltammogram, there can be several peaks. It is possible to investigate the role of diffusion, adsorption and coupled homogeneous chemical reaction mechanisms from the sweep-rate dependence of the peak amplitudes, widths and potentials of the peaks observed in the voltammogram [7,32]. As in LSV the important parameters of CV include the magnitude of the peak currents i_{pa} (anodic peak current) and i_{pc} (cathodic peak current) and the potentials at which the peaks occur E_{pa} and E_{pc}.

A reversible system will contain all of these parameters thus CV can be an important method in determining whether a system is reversible or not. A redox couple in which both the oxidative and reductive species rapidly exchange electrons with the working electrode is known as an electrochemically reversible couple, and can be identified from a cyclic voltammogram by the presence of two peaks, an oxidation peak and a reduction peak, and by measurement of the potential difference between the potentials of these two peaks:

$$\Delta E = E_{pa} - E_{pc} \approx 0.058/n$$

Equation 1.20: Electrochemically reversible couple

Where; n is the number of electrons transferred. This 0.058/n V separation of peak potentials is independent of scan rate for a reversible couple but is slightly dependent on the cycle number and switching potential. When the scan rate is increased the anodic and cathodic peak potentials both increase in proportion to the scan rate. For an irreversible couple, plots of the anodic and cathodic peak potentials versus the scan rate should be linear with intercepts at the origin. The values of i_{pa} and i_{pc} should be similar in magnitude for a reversible couple with no kinetic complications, i.e., $i_{pa}/\boldsymbol{i}_{pc} \approx 1$.

Electrochemical irreversibility is caused by slow electron exchange of the redox species with the working electrode and is characterised by a separation peak potential that is greater than 0.059/n V and is dependent on the scan rate (see Equation 1.20). In CV the presence of only one peak ($\boldsymbol{i}_{pa}$ or $\boldsymbol{i}_{pc}$) can be an indication of irreversibility. For quasi-reversible systems, the current is controlled by both the mass transport and charge transfer. Voltammograms of a quasi-reversible system are more extended and exhibit a larger separation in peak potentials compared to the separation peaks in a reversible system [10]. Figure 1.10 shows a typical potential-time excitation signal for voltammetry and a cyclic voltammogram for a reversible process while Figure 1.11 shows cyclic voltammograms for irreversible and quasi-reversible redox processes.

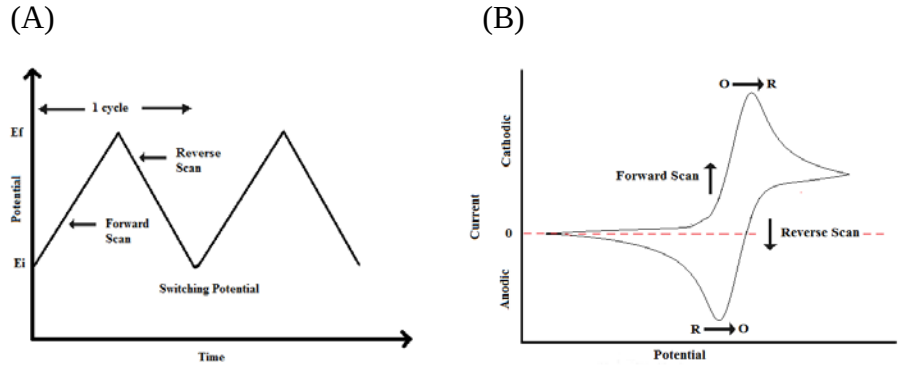

Figure 1.10: (A) Typical potential-time excitation signal for voltammetry, where Ei is the initial potential and Ef is the final potential, and (B) is a typical voltammogram for a reversible process.

(A) (B)

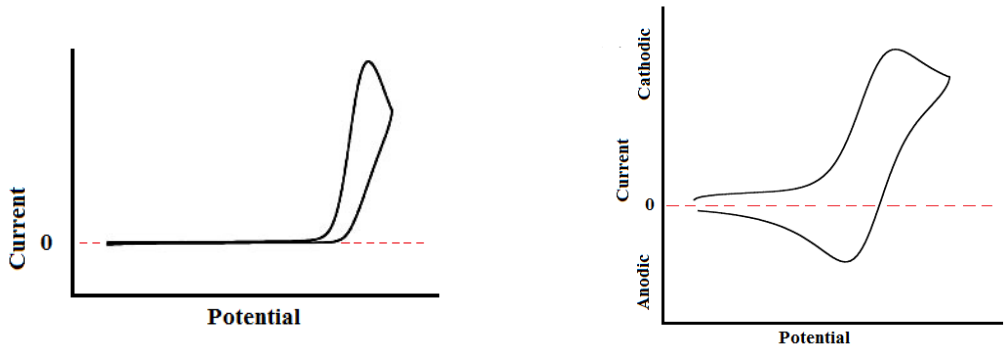

Figure 1.11: (A) Typical voltammogram for an irreversible process and (B) is a typical voltammogram for a quasi-reversible process.

1.3.4.3 **Square Wave Voltammetry**

Square wave voltammetry (SWV) is among the most sensitive means for the direct evaluation of concentrations. It can have direct detection limits as low as 10^{-8} M [33]. The excitation signal in SWV consists of a symmetrical square-wave pulse of amplitude E_{sw} superimposed on a staircase waveform of step height, ΔE, where the forward pulse of the square wave coincides with the staircase step as shown in Figure 1.12. The net current, i_{net}, is obtained by taking the difference between the forward and reverse currents ($i_{for} - i_{rev}$) and is centered on the redox potential. The peak height is directly proportional to the concentration of the electroactive species. The theory for a reversible system predicts that the resulting current-time behaviour should be symmetrical and almost bell-shaped with a peak at $E_{1/2}$. The peak current is a linear function of concentration and the square root of the square wave frequency. SWV has several advantages including its excellent sensitivity, the rejection of background currents, and its speed. This method also has several applications including the study of electrode kinetics, determination of some species at trace levels, and its use with electrochemical detection in HPLC [33].

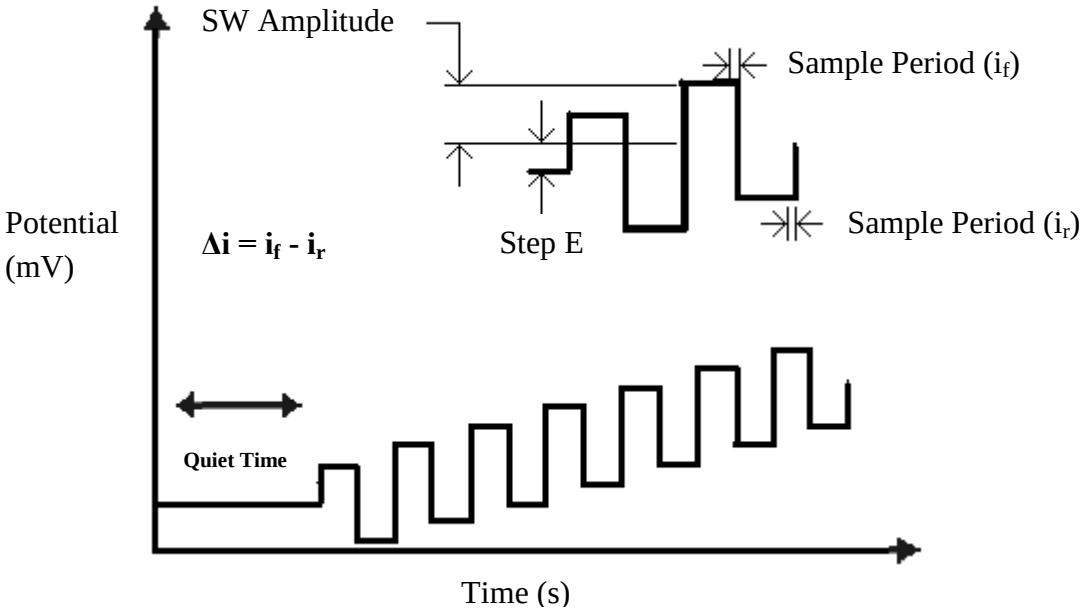

Figure 1.12: Potential wave form for square wave voltammetry

1.3.4.4 **Differential Pulse Voltammetry**

Differential pulse voltammetry (DPV) involves the application of small constant pulses (of the same amplitude) superimposed upon a staircase waveform [34]. The current is sampled twice in each pulse period, just before the pulse application and again late in the pulse life, when the charging current has decayed. The first current is subtracted from the second, and this current difference plotted versus the applied potential as shown in Figure 1.13. The resulting voltammogram consists of current peaks, the height of which is directly proportional to the concentration of the corresponding analytes.

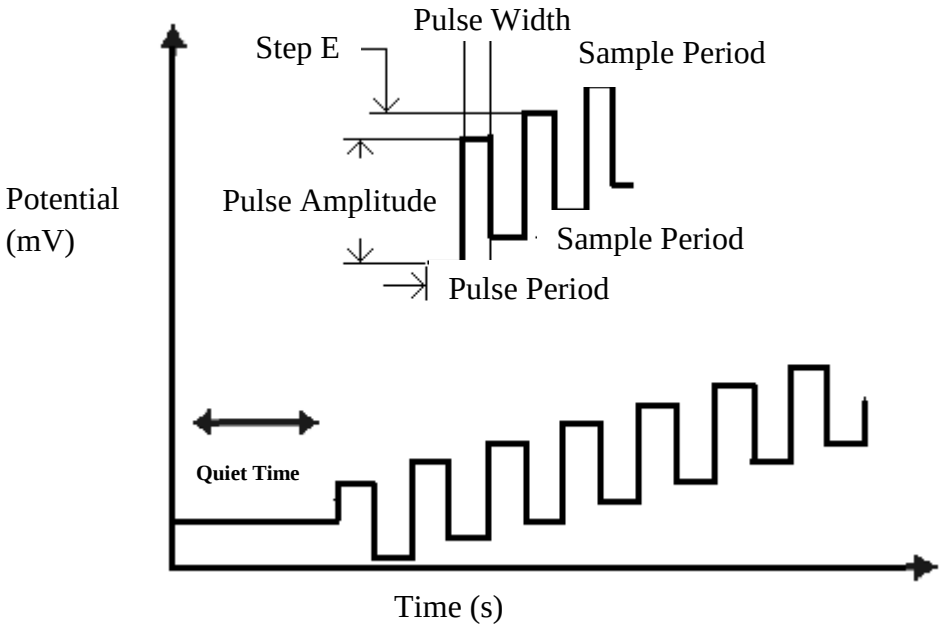

Figure 1.13: Potential wave form for differential pulse voltammetry

1.3.4.5 **Electrical Impedance Spectroscopy (EIS)**

Electrochemical impedance spectroscopy (EIS) is a sensitive technique, which monitors the electrical response of the system studied after the application of periodic small amplitude of AC signal. Analysis on the system provides information concerning the interface and reactions occurring at it.

EIS data is commonly analysed by fitting the data to an equivalent electrical circuit model. Common electrical elements such as resistors, capacitors and inducers are the most used in the circuit model. A Randles circuit is an equivalent electrical circuit that consists of an active electrolyte resistance R_s in series with the parallel combination of the double-layer capacitance D_{dl} and an impedance of a faradaic reaction. Figure 1.14 shows the typical Randles Model for EIS characterisation on modified electrodes used in Chapter 4.

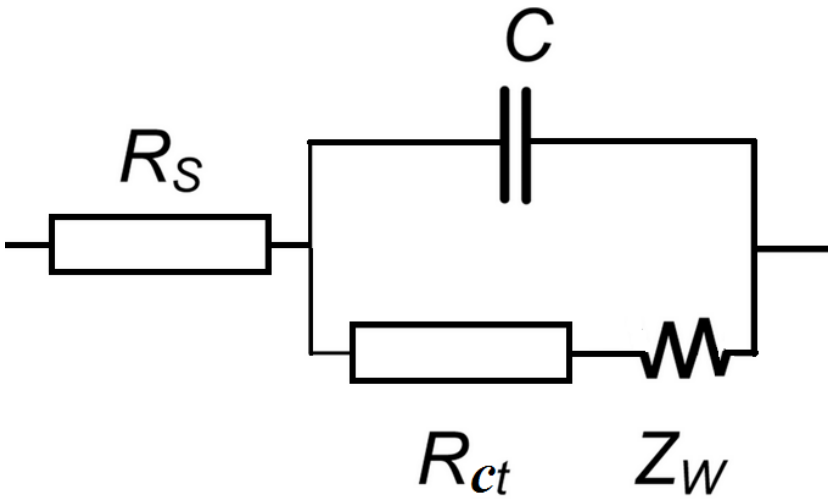

Figure 1.14: Impedance circuit (Randles model) for characterisation of modified electrodes

In Randles model circuit, R_s represents the dynamic solution resistance, C_{dl} represents the double layer capacitance measured between the electrode and the electrolyte solution, R_{ct} is the charge transfer resistance and Z_w is the Warburg element describing the time (frequency) dependence of mass transport.

The impedance data could also be presented using the Nyquist plot, as the results in this thesis were plotted, where the imaginary (Z") versus (Z') components of the impedance is plotted. Figure 1.15 represents an example of a Nyquist plot of the Randles impedance with the semi-circle at higher frequencies and the straight line at an angle to the real axis at lower frequencies.

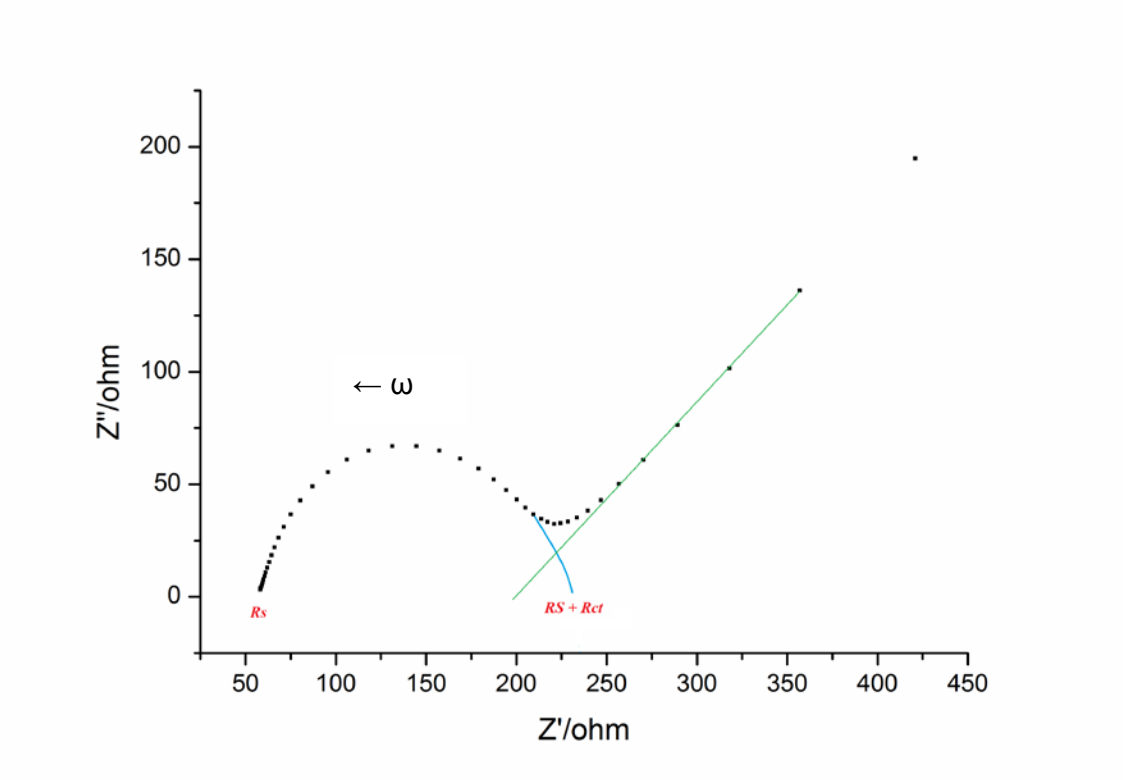

Figure 1.15: Nyquist plot for oxidation/reduction reaction of 5 mM $[Fe(CN)_6]^{3-/4-}$ in 0.1 M KCl (imaginary impedance versus real impedance). Frequency measured from 1Hz to 100 kHz.

Using the model circuit that was previously mentioned in Figure 1.14, the C_{dl} value could only be calculated after the frequency information is provided. The Warburg impedance could be calculated as shown in Equation 1.21.

$$\omega_Z^{Im}{}_{max} = 1 / (C_{dl} R_{ct})$$

Equation 1.21: Equation to calculate Warburg impedance

1.4 Transducers

1.4.1 Introduction

A transducer is a device that converts a signal in one form of energy to another form of energy [35]. While the term transducer commonly implies the use of a sensor/detector, any device which converts energy can be considered a transducer. There are several types of transducer from which to choose and these are outlined in table 1.1. Electrochemical and optical transducers are among the most popular ones used.

Table of Transducers

Electrochemical	Optical	Other
Potentiometric	Luminescence	Colorimetric
Amperometric	UV/Visible	Piezoelectric
Conductometric	Fiber optic	Acoustical (SAW)
	SPR	Thermal

Table 1.1: Examples of different types of transducers

1.4.2 Potentiometric Transducers

Potentiometric transducers are based on the principle that the potential of an electrolytic cell (E_{cell}) varies according to the Nernst equation, which was discussed previously in section 1.2.3, see equation 1.5.

Therefore since the potential of the cell is proportional to the log concentration, the Nernst equation provides a means for quantitation. An example of a potentiometric transducer is shown in Figure 1.16.

Figure 1.16: Position transducers, contactless and potentiometric

1.4.3 **Conductometric Transducers**

The principle behind the conductometric transducers is that a change in the number, charge or molarity of ions results in a change of the conductivity [36]. Therefore the overall conductance of an analyte is thus measured. Ionic species can either be consumed or produced depending on the reaction involved. This method is not very specific but can become selective if an enzyme for example is introduced to the detector.

1.4.4 **Amperometric Transducers**

Amperometric transducers function on the principle that the current produced is proportional to the concentration of analyte present [37-38]. When a constant potential is applied at the working electrode of the cell, the current measured from the redox process is proportional to the concentration of the analyte. Figure 1.17 below outlines a simple three-electrode cell.

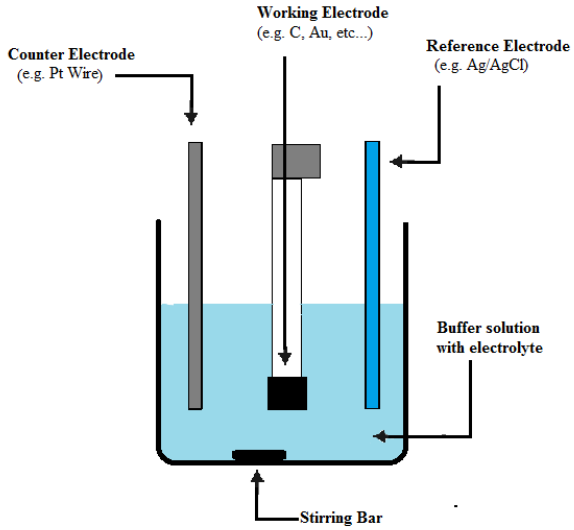

Figure 1.17: Simple three electrode cell

1.4.5 **Optical Transducers**

The optical transducers came about due to the development of optic fibers and work on the principle of total internal reflection and is shown in Figure 1.18 [39]. The basic type of optoelectronic transducer couples light conducting fibers with spectrophotometry, fluorimetry or reflectrometry. It is capable of inducing changes of optical parameters such as, light absorption, wavelength and refractive index. These devices incorporate either a single or dual optical fibre bundle for the incident light and for the light beam to be measured. They offer a number of advantages including; the sample remains chemically unchanged, they are suited to continuous monitoring, they are not susceptible to disturbances by electric field and they are easier to make mobile than electrochemical transducers.

Figure 1.18: Optical fiber sensor

1.4.6 **Piezoelectric Transducers**

Piezoelectric transducers rely on the principle of there being a linear relationship between the change in the oscillating frequency of a piezoelectric (PZ) crystal and the mass variation on its surface [40]. In 1959, Sauerbrey discovered that the change in mass is inversely proportional to the change in frequency of the resonating crystal, equation 1.21 [41].

$$\Delta f = -\frac{2\Delta m(n)(f_o^2)}{\mu_q(\rho_q)}$$

Equation 1.21: Sauerbrey equation

Where; Δf is the change frequency, Δm is the change in mass, μ_q is the viscosity of the quartz, ρ_q is the density of the quartz, n is the overtone number and f_o is the basic oscillator frequency.

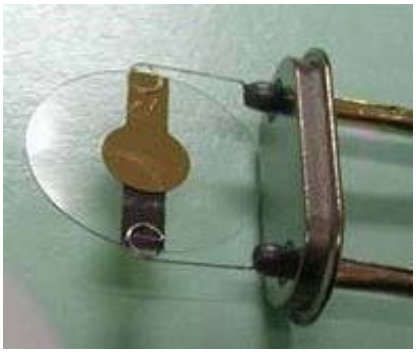

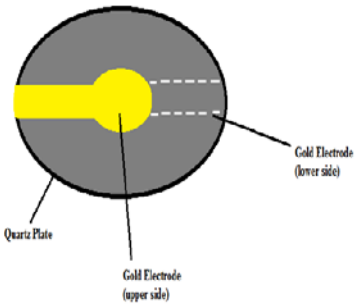

Figure 1.19: Quartz crystal microbalance

1.4.7 **Acoustical Transducers**

A surface acoustic wave (SAW) is an acoustic wave travelling along the surface of a material exhibiting elasticity, with amplitude that typically decays exponentially with depth into the substrate. SAWs were first explained in 1885 by Lord Rayleigh, who described the surface acoustic mode of propagation and predicted its properties in his classic paper [42]. The SAW devices operate by the generation of acoustoelectric waves either along the surface of the crystal or through a combination of bulk and surface. The oscillation of the crystal in SAW devices is more than 10 times greater than the oscillation of the crystal used in piezoelectric (PZ) devices as well as vibrating at much higher frequencies giving it the potential for tighter control of particles. It is less sensitive than PZ devices and works best with larger molecules [43].

Figure 1.20: Example of an acoustic sensor for grinders

1.4.8 **Calorimetric Transducers**

Calorimetric transducers are only useful with enzyme-catalysed reactions. These reactions exhibit the same enthalpy changes as spontaneous chemical reactions and considerable heat is evolved, ranging from 5 – 100 kJ/mol. Therefore, calorimetric transducers are universally applicable in enzyme sensors [44].

1.5 **Working Electrode Material**

1.5.1 **Macroelectrodes**

1.5.1.1 **Introduction**

The working electrode (WE) represents the most important component of an electrochemical cell. It is at this interface between the WE and the solution that electron transfers of greatest interest occur. The selection of a working electrode material is critical to the experiments success. So far a variety of electrode substrates have been exploited. Noble metals, mercury, carbon and semi-conductor materials are commonly used electrode materials. Some composite materials with excellent characteristics have also been employed for electrode substrates, such as tantalum and niobium [45-46]. Several important factors need to be considered before choosing which electrode material would best suit any given experiment. The first factor is that the material used must exhibit favourable redox behaviour with the analyte you intend to test and ideally fast with reproducible electron transfer without fouling. Another factor to be considered is the potential window over which the electrode performs in a given electrolyte. This potential window should be as wide as possible to allow for the highest degree of analyte characterisation. Additional considerations include the cost of the electrode material, its ability to be fabricated or formed into useful geometries, toxicity and the ease of surface renewal following a measurement [47].

1.5.1.2 **Metal Working Electrodes**

Noble metals such as platinum, gold and silver have all been widely used as electrode substrates. These metal electrodes can offer very favourable electron transfer kinetics and a wide potential range. The cathodic potential window of these electrodes is usually restricted due to the low hydrogen overvoltage. However, the formation of surface oxide or adsorbed hydrogen layers may lead to

high background currents, which can strongly affect the kinetics of the electrode reaction. To rectify this issue, a pulse potential cycle should be carried out before electrochemical experiments [48]. Several typical metal electrodes will now be discussed briefly.

The chemical properties of gold and platinum electrodes are both very stable and can be easily manufactured thus allowing them to become the most popular metal electrodes. Silver is also a valuable electrode substrate, which is usually used for the preparation of chemically modified electrodes (CMEs) in various electrochemical experiments [49-50]. Moreover, some proteins such as cytochrome c may exhibit the capability of direct electron transfer on silver electrode material, so silver substrate has also been used for protein analysis [51].

Besides noble metal electrodes, some other metals have also been employed as electrode substrates. For example, copper electrodes and nickel electrodes have been used for the detection of carbohydrates or amino acids in alkaline media. In comparison to gold or silver electrodes, these two kinds of electrodes possess a stable response for carbohydrates at constant potentials [52]. In addition alloy electrodes like platinum-ruthenium and nickel-titanium electrodes have also been reported, and these are often used for the preparation of fuel cells, owing to their bi functional catalytic mechanism [53].

1.5.1.3 **Mercury Electrodes**

Mercury is a classic electrode material. It displays an excellent potential window in the cathodic direction, but is severely limited in the anodic direction due to its ease of oxidation. Mercury electrodes possess highly reproducible, renewable and smooth surfaces, which are very beneficial in electrochemical analysis. A variety of mercury electrodes including the dropping mercury electrode, hanging mercury drop electrode and mercury film electrode have all been developed [54-56]. Among these mercury electrodes, the dropping mercury electrode (DME) is the most commonly used. A dropping mercury electrode is one in which drops are formed and fall off repeatedly during a potential scan, being replaced by a ‘fresh’ electrode every second or so. The main advantage of this is that the electrode is

self-renewing, so it does not need to be cleaned or polished before each experiment. Moreover, each drop of mercury has an uncontaminated and uniform surface. This was commonly used in past years however the toxicity of mercury has lead to a limited use in the present day experiments. Instead mercury films are formed on the surface of solid electrodes rather than the pure mercury metal [57-58].

1.5.1.4 **Carbon Electrodes**

A family of carbon materials have been widely used as electrode substrates to make various electrodes. The surface of these electrodes can be easily renewable for electron exchange due to the soft properties of carbon. This material allows for a broad potential window, low background current, rich surface chemistry and comparative chemical inertness. Carbon also has the advantage of having a very low cost in comparison to other substrate materials and therefore these electrodes are currently widely used. The most commonly used carbon electrodes include pyrolytic graphite electrode (PGE), glassy carbon electrode, carbon paste electrode, carbon fiber electrode and screen-printed electrode [59-63]. The work in this thesis uses the latter of these, the screen-printed electrode which will now be discussed in more detail.

1.5.1.5 **Screen-Printed Electrodes**

Production of screen-printed electrodes (SPE) involves several steps, including placement of an ink (both conducting and insulating) onto a patterned screen or stencil followed by forcing it through the screen with the aid of a squeegee onto a planar substrate (plastic or ceramic), and then drying/curing the printed patterns. Such a process yields mass-producible (uniform and disposable) electrodes of different shapes or sizes. The electrochemical reactivity and overall performance of screen-printed electrodes are dependent on the composition of the ink employed and on the printing and curing conditions (temperature, pressure, etc.).

The composition of the SPE is very important as it defines the general characteristic of the sensor. If the SPE are not uniform and reproducible then they are useless for analytical purposes. Vigorous quality control must be maintained and a batch system operated if error and defective electrodes are kept to a minimum. Figure 1.21 shows the shape of the working SPE used in this work. The fabrication method of this electrode will be further discussed in Chapter 4.

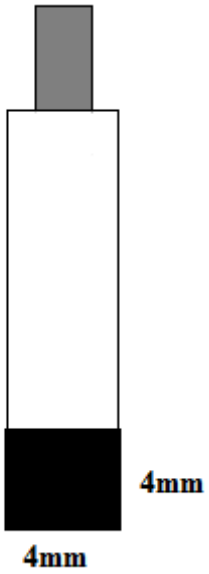

Figure 1.21: Working SPE design

1.5.2 **Microelectrodes**

1.5.2.1 **Introduction**

Microelectrodes have become increasingly popular since the 1970's. The earliest application of a true microelectrode was in Davies and Brink's work on the measurement of oxygen concentrations in biological tissues in 1942 [59]. In the years that followed, little attention was given to the use of microelectrodes due to the lack of technology available that is necessary to produce commercial devices and tools for measuring the small currents generated by these devices. In 1980, Fleischmann's group established the theory for a semi-infinite linear (non-planar)

diffusion profile more suitable to microelectrodes than the planar diffusion model of conventional electrodes (of mm dimension) [61]. A year later, microelectrodes were introduced in several new areas that were inaccessible to conventional size electrodes [63]. According to IUPAC in 2000, if the geometric dimensions of a voltammetric working electrode become progressively smaller than the behaviour of the electrode begins to depart from that of a large electrode which can be approximated by an electrode of infinite dimension [62]. These differences are caused by changing conditions of the mass transport from the bulk solution toward the electrode and have several important practical implications such as decreased ohmic drop of potential, IR, fast establishment of a steady state signal, a current increase due to enhanced mass transport at the electrode boundary and increased signal to noise ratio [64]. These effects make sufficiently small electrodes advantageous in many areas of electroanalytical chemistry. These small-size electrodes have been called “microelectrodes”. It is now conventionally assumed that a microelectrode has dimensions of tens of micrometers or less, down to submicrometer range [62]. Microelectrodes of various geometries have been prepared mechanically or lithographically. Numerous advantages arise from the physically small size of microelectrodes.

These include:

(a) Fast Mass Transport

(b) Decreased Capacitance and Enhanced Signal to Noise Ratio

(c) Increased Current Density

(d) Reduced Ohmic Effects

Each of these advantages will now be discussed in more detail.

(a) Fast Mass Transport

At minute electrode surfaces, the diffusion process in the diffusion layers is dependent on the size and geometry of the electrode. In a stationary state, diffusion is primarily perpendicular to the surface of a conventional electrode (planar diffusion), whereas radial diffusion to the surface of a microelectrode becomes important and its contribution to the overall diffusion subsequently greater. Hence, under identical conditions, the diffusion rate of electrochemically active species is significantly larger at a microelectrode than at a conventional electrode [65]. A steady-state response arises when the electrolysis rate is equal to the rate at which molecules diffuse to the surface and a steady-state voltammogram (sigmoidal voltammetric curve) results [65]. Equilibrium is more easily established at a microelectrode than at a conventional sized electrode and hence a sigmoidal voltammetric curve will result at the microelectrode, while a peak-shaped voltammogram is obtained at a conventional sized electrode. Figure 1.22 shows the near or quasi steady-state behaviour observed at a disk microelectrode where convergent diffusion is predominantly observed and the typical peak-shaped cyclic voltammogram obtained under the same conditions at a conventional sized electrode where planar diffusion is predominantly observed.

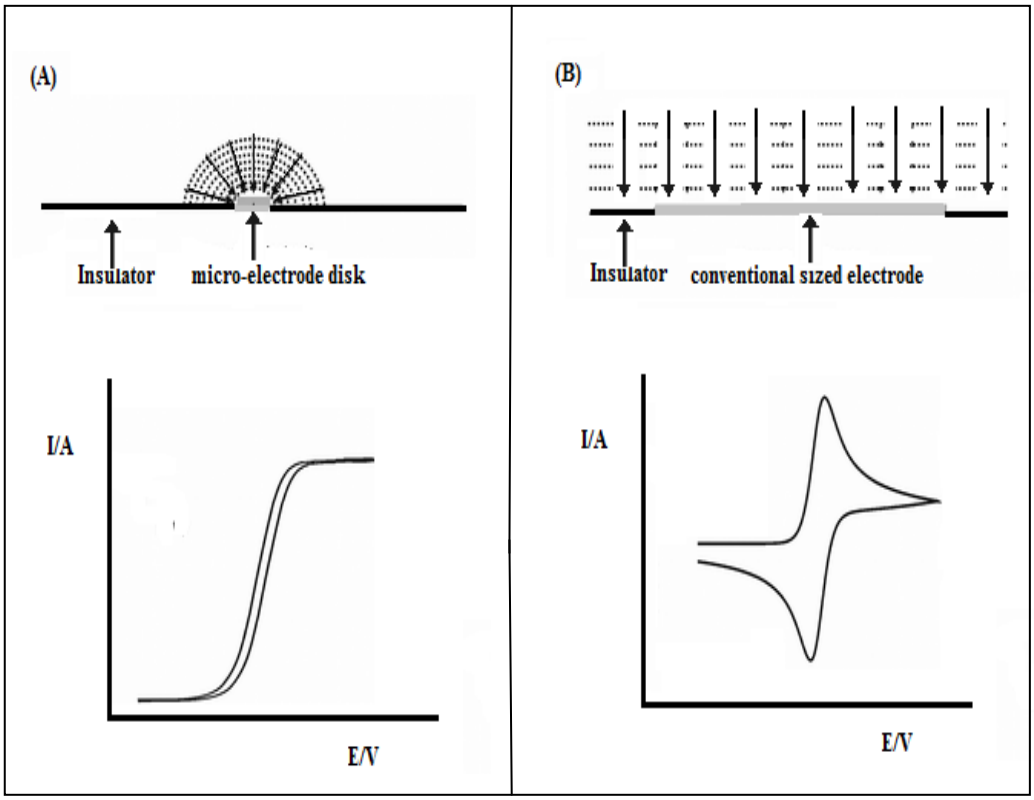

Figure 1.22: Highlighting the unique differences between a micro electrode and a conventional sized electrode where (A) shows the quasi steady-state behaviour observed at a disk microelectrode where convergent diffusion is predominantly observed and (B) shows the typical peak-shaped voltammogram obtained under the same conditions at a conventional sized electrode where planar diffusion is predominantly observed.

(b) Decreased Capacitance and Enhanced Signal to Noise Ratio

When an electrode comes into contact with an electrolytic solution, a double layer is formed at the interface, in which the charge present on the metal electrode is compensated for by a layer of oppositely charged ions in solution. In many respects, this electrochemical double layer behaves like an electrolytic capacitor. This process complicates the electrochemical measurement in two respects;

1. The potential at the interface does not reach the applied potential until this charging process is completed and,

2. The charging and faradaic currents are convolved at short times.

These two effects make it highly desirable to minimise both the magnitude of the charging current and the time it takes to charge the double layer [65].

$$\frac{i_f}{i_c} \approx \frac{1}{rC_dv}$$

Equation 1.22: representation of a double layer formed at the interface, in which the charge present on the metal electrode is compensated for by a layer of oppositely charged ions in solution.

Where; r is the electrode radius, C_d is the double layer capacitance and v is the scan rate. It is evident from the equation that reducing the electrode's radius and/or lowering the scan rate will result in an enhanced signal-to-noise ratio [65].

(c) Increased Current Density

For steady-state diffusion to a flat-plate electrode:

$$i_L = DCF/\delta$$

Equation 1.23: Steady-state diffusion to a flat-plate electrode

Where; i_L is the maximum current density allowed by diffusion, D is the diffusion coefficient, C is the reactant concentration, F is Faraday's constant, and δ is the steady state diffusion layer thickness (cm).

This quantity becomes constant after about 1 second of electrolysis due to the intervention of convection superimposed on diffusion, and has a value in a solution that is not artificially stirred of about 0.05 cm [66]. It was found in 1961 by Barton and Bockris, that for a spherical electrode of radius less than the diffusion layer thickness (i.e less than 0.05 cm), the maximum diffusion-controlled current is no longer DCF/r but rather controlled by DC_iF/r. This opens the possibility of obtaining increased limiting diffusion currents (for hemispherical electrodes with $r < \delta$) and increasing the range of current densities at which reaction rates can be measured without disturbance by interfering diffusion reactants to or from the electrode. Hence, by using a microelectrode, the maximum current density that remains free from transport control can be increased by up to several thousand times [66]. In addition, the contribution to steady-state current by convection is not apparent at microelectrodes, thus making them particularly applicable for use in free-flowing systems [67].

(d) Reduced Ohmic Effects

When faradaic and charging currents flow through a solution, they generate a potential that acts to weaken the applied potential by an amount IR, where I is the total current and R is the cell resistance [63]. This can lead to distortions of the experimental responses. Microelectrodes reduce these ohmic effects considerably as the faradaic currents observed are typically six orders of magnitude smaller than those at conventional size electrodes and these small currents may completely eliminate IR problems.

1.5.2.2 **Fabrication, Shapes and Responses**

Microelectrodes with several geometries are commonly found in the literature and they are listed in Table 1.2 and sketched in Figure 1.23. The most popular materials include platinum, gold and carbon fibres, although mercury, nickel, silver and superconducting ceramics have also been reported [68-71].

Type of microelectrode	Geometry of Diffusion Field
sphere	spherical
hemisphere	spherical
disc	spherical
wire	cylindrical
line	cylindrical
ring	spherical
normal size electrode	linear

Table 1.2: Types of microelectrodes and their diffusion field geometry.

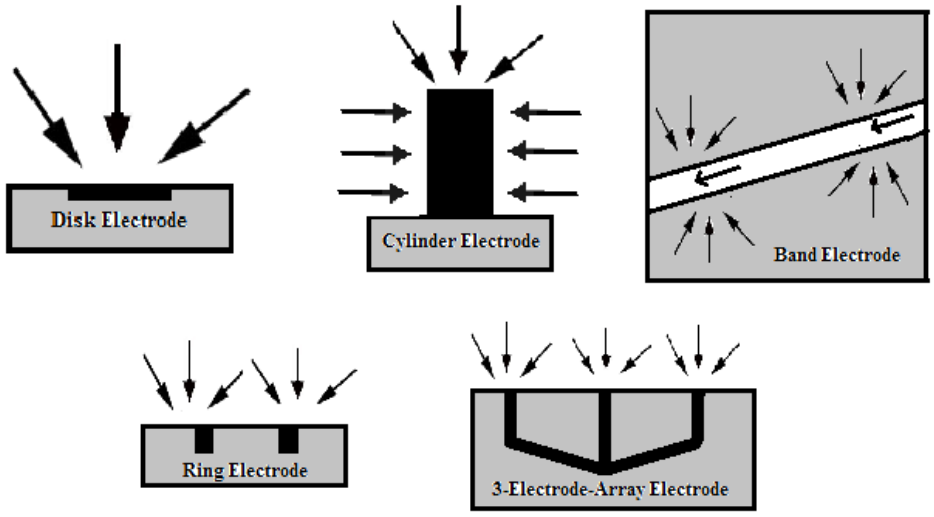

Figure 1.23: Illustrations of the most common microelectrode geometries and their diffusion fields.

Of the geometries mentioned in table 1.2 the disc and cylinder based microelectrodes are the most commonly used. The surface of a disc electrode is not uniformly accessible, nor are all points equivalent as electroactive species are primarily depleted by electrolysis at the disc electrode boundary, thus inducing non-uniform diffusion and varying current densities. The total diffusion-limited current composed of the planar flux and radial flux diffusion components are shown in equation 1.24;

$$\mathbf{i_{total} = i_{planar} + i_{radial}}$$

Equation 1.24: The total diffusion-limited current composed of the planar flux and radial flux diffusion components.

Where; for a disc microelectrode, the general expression for the radial component is

$$\mathbf{i_{radial} = \alpha rnFDC}$$

Equation 1.25: The general expression for the radial component of a disk microelectrode.

Where; r is the radius of the electrode, α is a function of the electrode geometry, D is the diffusion coefficient and C is the concentration [6].

For discs, spheres and hemispheres, the α values are equal to 4, 4π and 2π respectively. Such radial diffusion leads to a larger flux at the perimeter of the electrode (than at the centre), and hence to a non-uniform current density. Diffusion behaviour at spherical and ring electrodes is similar to this. The extent to which either predominates depends on the dimensions of the electrode and the diffusion layer.

When the diffusion layer is larger than the electrode;

$$\mathbf{Dt/r_o^2}$$

Equation 1.26: Equation used when diffusion layer is larger than the electrode.

Where *t* is the electrolysis time and r_o is the smallest dimension of the electrode [6].

For large values of Dt/r_o^2, $Dt/r_o^2 > 1$, (i.e. diffusion-layer thickness exceeds the size of the electrode), the current approaches steady state and sigmoidal voltammogramms are observed.

Conversely, at small values of Dt/r_o^2 planar diffusion predominates and peak-shaped behaviour is observed [6]. The case for radial diffusion to a cylinder shaped microelectrode differs slightly. Here, diffusion is identical at any cross-section plane perpendicular to the cylinder axis except at the end of a cylinder, which can be ignored.

There are several techniques available for constructing microelectrodes of the previously mentioned geometries [22]. To create a cylinder electrode, the protruding microwire need only be trimmed to the desired length. This microelectrode is the most common form due to the advantage of having a micro-sized radius and thus exhibits the beneficial features of a microelectrode, its length gives rise to easily measured currents so that high-sensitivity potentiostats are not required. It is fabricated by attaching a thin metal wire (e.g. platinum) or a carbon fibre to a copper wire and sealing this in a glassy capillary with the wire or fibre left protruding [22]. The drawbacks of cylinder microelectrodes are that they cannot be mechanically polished to refurbish their surfaces and they are physically unstable if their length is too great. Microdisk electrodes also predominate because of their ease of construction, and because the sensing surface of the electrode can be mechanically polished. These can be made by first grinding the sealed end of the glass tube with coarse sandpaper and subsequently polishing to a mirror finish with consecutively finer grades of abrasive [22]. Cone

microelectrodes can be produced by etching a carbon fibre or metal wire using flame, chemical vapour deposition or ion-beam techniques. Band array electrodes have been constructed using lithography [72]. The microelectrode used in this work was a three-electrode configuration fabricated onto acetate substrate. The fabrication procedure and electrodes performance will be discussed in further detail in Chapter Three.

1.6 **Chemically Modified Electrodes**

1.6.1 **Introduction**

With demands for accuracy and versatility of analysis increasing, research and development in the field of analytical chemistry is on the rise targeting highly specific, sensitive and efficient analytical methods with the ability to analyse trace components in complex samples. Modern analytical instrumentation is a powerful tool however the selective detection and/or separation of analytes are important to avoid errors due to matrix effects. A deliberate modification of the analytical sensor can improve its capabilities according to the needs of an analytical problem. This has allowed chemically modified electrodes (CMEs) to gain considerable interest in recent decades as researchers have sought to exert more direct control over the chemical nature of an electrode [73].

According to IUPACs recommendations published in 1997 a chemically modified electrode (CME) can be defined as an electrode made of a conducting or semi-conducting material that is coated with a selected monomolecular, multimolecular, ionic, or polymeric film of a chemical modifier and that by means of faradaic reactions or interfacial differences exhibits chemical, electrochemical, and/or optical properties of the film [74].

Chemically modified electrodes (CMEs) comprise a relatively modern approach to electrode systems that find utility in 1. a wide spectrum of basic electrochemical investigations, including the relationship of heterogeneous electron transfer and chemical reactivity to electrode surface chemistry,

electrostatic phenomena at electrode surfaces, and electron and ionic transport phenomena in polymers, and 2. the design of electrochemical devices and systems for applications in chemical sensing, energy conversion and storage, molecular electronics, electrochromic displays, corrosion protection, and electro-organic synthesis [74].

Compared with other electrode concepts in electrochemistry, the distinguishing feature of a CME is that a generally quite thin film of a selected chemical is bonded to or coated on the electrode surface to endow the electrode with the chemical, electrochemical, optical, electrical, transport and or other desirable properties of the film in a rational, chemically designed manner. While CMEs can operate both amperometrically (or voltammetrically) and potentiometrically, they are generally used amperometrically, a faradaic (charge transfer) reaction being the basis of experimental measurement. The modification of a voltammetric working electrode is performed by fixing reagents on the electrode surface thus the CME consists of two parts – the substrate electrode and a layer of chemical modifier. The choice of the parts is determined by the desired analytical features of the sensor. The methods employed for the introduction of a modifier onto the surface of the substrate electrode are based on only a few approaches;

- Direct irreversible adsorption,
- Covalent attachment to specific surface sites,
- Coating with a polymer film, and
- Mixing of the electrode substrate with a slightly soluble modifier and any further component.

While glass, platinum, gold and carbon have all been used as the base electrode material, in voltammetric applications the base electrode that is modified is usually carbon. In order to achieve satisfactory attachment of the modifier to the electrode, the bare substrate material must exhibit certain necessary electrochemical parameters. Generally the electrode substrate must be activated before modification. This can be done in a number of ways including physical, chemical and electrochemical cleaning. Chemical modifications to the bare

electrode can enhance the sensitivity and/or the selectivity of the device towards a particular analyte(s) by exploiting several phenomena that occur at chemically modified electrodes including:

- *Electrocatalysis*: for electroanalytical purposes, electrocatalysis at CMEs is used to amplify the detection signal. It consists in acceleration of heterogeneous electron transfer of the target analyte, which is slow at the same potential at a bare electrode, induced by an immobilized charge mediator, i.e., catalyst to mediate electron transfer between the analyte and the electrode, which otherwise would undergo very slow electrochemical reaction at the bare electrode [74].

- *Permeability*: is a general term describing discriminative transport through a membrane coating that controls the access of analyte and interfering substances to the electrode surface. An electrode coated with the permeable membrane is accessible to the target analyte while interfering substances are rejected or prevented from reaching the electrode surface. Thus, the electrode selectivity is improved [75].

- *Accumulation*: from dilute solutions, accumulation (preconcentration, collection, ingress, or preferential uptake) of a substance in solution can be performed at the electrode modified with a suitable receptor. For analytical purpose, either reagent or a target trace analyte is accumulated. By analogy to the protein-type biological cell-surface receptors, the CME receptors are the electrode-confined compounds which can interact selectively with target analytes or reagents [76].

- *Chemical Transformation*: in which an electo-inactive analyte can be reacted with the appropriate reagent immobilised at the chemically modified electrode to yield an electroactive product suitable for electrochemical determination. Electrode selectivity and sensitivity towards certain functional groups can be improved in this way. For

instance, Pt electrodes were modified by adsorption of an allylamine layer for determination of ferrocenecarboxaldehyde [77].

- *Ionic Equilibria*: whereby an electrolyte solution containing an analyte ion is on one side of a selective ion-exchange membrane and a solid electrode on the other. A review of ion-exchange voltammetry at polymer coated electrodes is given in [78].

- *Controlled Release*: in which an analyte accumulated at the chemically modified electrode can undergo quantitative release in the test solution, under electrochemical or chemical control. Different mechanisms are involved in controlled release from the CME. These depend on the nature of the analyte or reagent and the method of accumulation [79].

1.6.2 **Approaches to Chemically Modify Electrodes**

There are four main methods used to chemically modify electrodes and these include:

- Adsorption (Chemisorption)
- Covalent bonding
- Polymer film coating
- Composite

Adsorption: is an interaction between a molecule and a surface in which electron density is shared by the adsorbed molecule and the surface [22]. This interaction requires direct contact between the chemisorbed molecule and the electrode surface, as a result a monomolecular layer is usually the highest coverage achieved. A second limitation of this technique is that it is rarely completely irreversible due to the chemisorbed molecules slowly leaching into the contacting solution phase during the duration of the experiment.

Covalent Bonding: Stronger attachment to the substrate surfaces can be accomplished by covalent linking of the desired component to surface groups present on, or formed on, the substrate to form a monolayer. The surface functional group of base electrodes can be derivatised either by synthetic route or by controlling the oxidation/reduction potentials in a suitable medium.

Polymer Film Coating: Coating of an electrode with polymer films has proved to be one of the simplest and versatile approaches for surface modification. A huge number of polymers have been used to prepare chemically modified electrodes. These can be divided into three general categories; *redox polymers*, which contain electroactive functionalities either within the main polymer chain or in side groups to this chain; *ion-exchange and coordination polymers*, which are not electroactive themselves but can incorporate electroactive guest molecules; and *electronically conductive polymers*, where the polymer chains are themselves electroactive. Several methods exist for the application of polymer films to the electrode surface. The simplest is dip-coating, which involves dipping the electrode surface into a solution of polymer, removing it and allowing it to dry. A second approach involves the application of a measured amount of solution to the surface, which allows more accurate control of the amount of solution deposited. Spin-coating is widely used in the semi-conductor industry and yields very uniform film thickness. Another approach is that the polymer films can be electropolymerised directly onto the electrode surface [22].

Composite: Zeolites, clays and other microcrystalline-structured materials are of interest in electrode modification due to their ion-exchange properties as well as exhibiting well-defined microstructures that can withstand high temperatures and highly oxidizing solution environments [22].

The work involved in this thesis focuses on screen-printed carbon electrodes and their modifications using carbon monolith material and multi-walled carbon nanotubes. The carbonaceous material was then further modified using metal nanoparticles. This will be discussed in further detail in Chapter Four.

1.7 **Other Measurement Techniques used in the work in this Thesis**

1.7.1 **Capillary Electrophoresis**

1.7.1.1 **Introduction**

Another electrochemical procedure used during this research is capillary electrophoresis which was employed in the work carried out in Chapter 3.

Capillary electrophoresis (CE) is a modern analytical technique which allows rapid and efficient separations of charged components present in small sample volumes. Separations are based on the differences in electrophoretic mobilities of ions in electrophoretic media inside small diameter capillaries. The technique of CE was designed to separate species based on their size to charge ratio in the interior of a capillary filled with an electrolyte. Hjerten provided the earliest demonstration of the use of high electric field strength in free solution electrophoresis in 3 mm inner diameter (i.d.) capillaries in 1967 [80]. The most widely accepted initial demonstration of the power of CE was by Jorgenson and Lukacs [81-83].

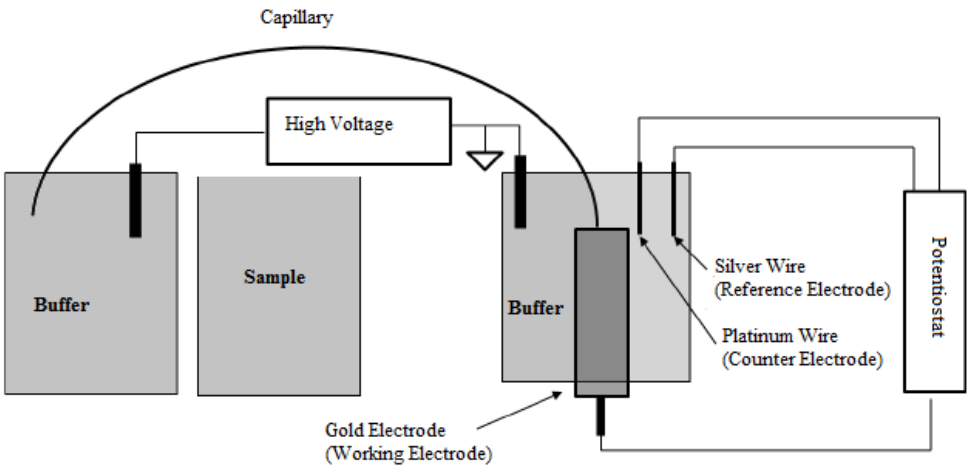

Figure 1.24: Scheme of Capillary Electrophoresis which includes the systems main components of a sample vial, source and destination vials, a capillary,

electrodes, a high-voltage power-supply, a detector and a data output and handling device.

A basic schematic of the CE system used in this work is shown in Figure 1.24. The system's main components are a sample vial, source and destination vials, a capillary, electrodes, a high-voltage power-supply, a detector and a data output and handling device. The source vial, destination vial and capillary are filled with an electrolyte such as an aqueous buffer solution. To introduce the sample, the capillary inlet is placed into a vial containing the sample and then returned to the source vial. The sample is introduced to the capillary via capillary action, pressure, or siphoning. This is accomplished by immersing the end of the capillary into a sample vial and applying pressure, vacuum or voltage. The migration of the analytes is then initiated by an electric field that is applied between the source and destination vials and is supplied to the electrodes by the high-voltage power supply. High electric field strengths are used to separate molecules based on differences in charge, size and hydrophobicity. The analytes separate as they migrate due to their electrophoretic mobility, and are detected near the outlet end of the capillary. The output of the detector is sent to a data output and handling device such as a computer. Separated chemical compounds appear as peaks with different migration times in an electropherogram which reports detector response as a function of time.

Capillary electrophoresis (CE) has attracted considerable attention in recent years due to its potential to achieve very high efficiency. The main reason for the extraordinary high efficiency in CE is attributable to its characteristically flat flow profile [80]. The flow of mobile phase in HPLC is maintained by a pump and therefore under normal operating conditions, a parabolic flow profile is observed. As this profile contributes to peak broadening, the flow profile inherently limits the separation efficiency theoretically achievable in HPLC separations. For CE, charged species migrate under the influence of an applied voltage, resulting in a practically flat flow profile (Figure 1.25). This fundamental difference in flow profile is the main reason for the extremely high efficiencies achievable using CE, where narrower peaks and potentially better resolution can be readily obtained, especially when selectivity is also optimized for the separation.

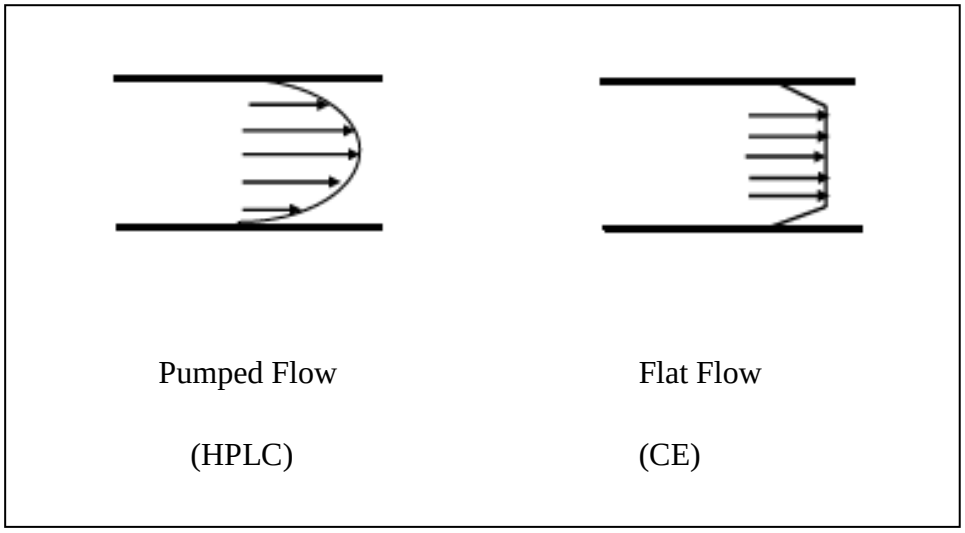

Figure 1.25: Flow profiles in HPLC and CZE.

1.7.1.2 **Electrophoresis**

The separation is based on the differences in the electrophoretic mobilities resulting in different velocities of migration of ionic species in the electrophoretic buffer contained in the capillary, see equation 1.26. The separation is mainly based on differences in solute size and charge at a given pH.

$$v = \mu_e E$$

Equation 1.27: The separation is mainly based on differences in solute size and charge at a given pH.

Where; v is ion velocity, μ_e is electrophoretic mobility and E is the applied electric field.

The electric field is simply a function of the applied voltage and capillary length in volts/cm. The mobility for a given ion and medium is a constant which is characteristic of that ion. The mobility is determined by the electric force that the molecule experiences, balanced by its frictional drag through the medium.

$$\mu_e = \frac{q}{6\pi\eta r}$$

Equation 1.28: The mobility is determined by the electric force that the molecule experiences, balanced by its frictional drag through the medium.

Where; q is the ion charge, η is solution viscosity and r is ion radius.

From equation 1.28, it is clear that small, highly charged species have high mobilities whereas large, minimally charged species have low mobilities.

1.7.1.3 **Electro-osmotic flow (EOF)**

Electroosmosis is an important phenomenon in CE and it refers to the flow of solvent in an applied potential field. Electroosmotic flow (EOF) originates from the negative charges on the inner wall of the capillary tube, which caused the formation of a double layer at the interface adjacent to the stagnant double layer; a diffuse layer consisting of mobile cations exists in the diffuse region of the double layer as shown in Figure 1.26. The EOF controls the amount of time analytes remain in the capillary by superposition of flow onto solute mobility. This can have an effect of altering the required capillary length, but does not affect selectivity.

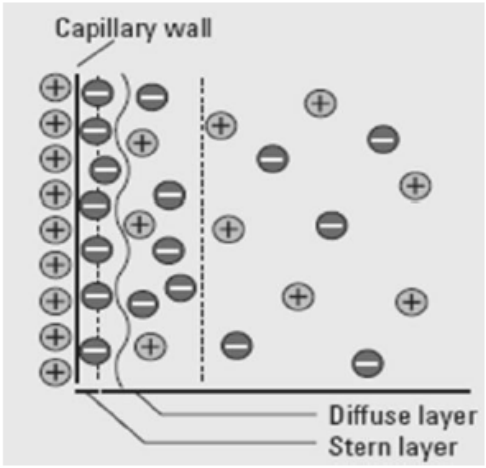

Figure 1.26: The double layer at the capillary wall.

Most capillaries used for CE today including the capillary used in this work are made of fused silica, which contain surface silanol groups. These silanol groups may become ionised in the presence of the electrophoretic medium. The interface between the fused silica tube wall and the electrophoretic buffer consists of three layers as in Figure 1.26; the negatively charged silica surface (at pH >2), the immobilised layer (inner Helmholtz plane), and the diffuse layer of cations adjacent to the surface of the silica, which tend to migrate towards the cathode. This flow of liquid through the capillary is called electroosmotic flow. The work in this thesis uses an uncoated fused silica capillary which has significant EOF with most commonly used buffers and both anions and cations can be separated in the same run. Cations are attracted towards the cathode and their speed is augmented by the EOF. Anions, although electrophoretically attracted towards the anode, are swept towards the cathode with the bulk flow of the electrophoretic medium. Under these conditions, cations with the highest charge/mass ratio migrate first, followed by cations with reduced ratios. All the neutral components are then migrated as their charge/mass ratio is zero and finally the anions migrate, with the lower charge/ mass ratio migrating earlier than the anions with greater charge/mass ratio. An important point to note is that it is possible to change the charge/mass ratio of many ions by adjusting the pH of the buffer medium to affect their ionisation and hence electrophoretic mobility [84]. There are also several methods to control the EOF which fundamentally requires alteration of the capillary surface or buffer viscosity as well as various analytical parameters that can affect CE. There are also different modes of CE available which can be accessed by altering the buffer composition. These are listed in Table 1.3.

Mode	Basis of Separation
Capillary Zone Electrophoresis	Free solution mobility
Micellar electrokinetic chromatography	Hydrophobic/ionic interactions with micelle
Capillary gel electrophoresis	Size and Charge
Isoelectric focusing	Isoelectric point
Isotachophoresis	Moving boundaries

Table 1.3: Different modes of CE available

- **Capillary Zone Electrophoresis (CZE);** is the most commonly used technique in CE and was the mode used in this work. Many compounds can be separated rapidly and easily. The separation mechanism in CZE is based on the differences in the electrophoretic mobilities resulting in different velocities of migration of ionic species in the electrophoretic buffer contained in the capillary [81,85-86]. Separation of both anionic and cationic solutes is possible by CZE due to electro-osmotic flow (EOF). Neutral solutes do not migrate and all coelute with the EOF. Fundamental to CZE are homogeneity of the buffer solution and constant field strength throughout the length of the capillary. The separation relies principally on the pH controlled dissociation of acidic groups on the solute or the protonation of basic functions on the solute. A significant feature of the electroosmotic flow (EOF) is that instead of showing parabolic flow profiles as in pressure-driven flows, such as high performance liquid chromatography, it tends to flow in a plug shape as shown in Figure 1.25. This increases the resolution in separations by reducing the band broadening of the analyte peak during its passage along the capillary.

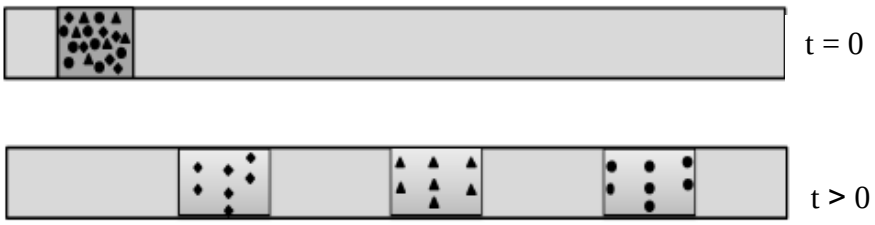

Figure 1.27: Illustration of CZE separation.

Briefly I will discuss the other modes listed in table 1.3:

- **Micellar Electrokinetic Capillary Chromatography (MEKC)**; Terabe and co-workers introduced micellar electrokinetic capillary chromatography (MEKC) in 1984 [87-89]. In MEKC, the main separation mechanism is based on solute partitioning between the micellar phase and the solution phase. The technique provides a way to resolve neutral molecules. Micelles form in solution when a surfactant is added to water in concentration above its critical micelle concentration (CMC). The most commonly used surfactant in MEKC is sodium dodecyl sulphate (SDS) (CMC=0.008 M), which is an anionic surfactant.
- **Microemulsion Electrokinetic Chromatography (MEEKC);** is a CE technique in which solutes partition with moving oil droplets in buffer. The microemulsion droplets are usually formed by sonicating immiscible heptanes with water. SDS is the most widely used emulsifier surfactant in MEEKC and is added at relatively high concentrations to stabilise the emulsion. This allows the separation of both aqueous and water-insoluble compounds.
- **Capillary Gel Electrophoresis (CGE);** The main separation mechanism in capillary gel electrophoresis (CGE) is based on differences in solute size as analytes migrate through the pores of the gel-filled column [[90-92]. Gels are potentially useful for electrophoretic separations mainly because they permit separation based on ‘molecule sieving’. Futhermore, they serve as anti-convective media, they minimize solute diffusion, which contributes to zone broadening, they prevent solute adsorption to the capillary walls and they help to eliminate electroosmosis. However, the gel must possess certain characteristics, such as temperature stability and the

appropriate range of pore size, for it to be a suitable electrophoretic medium. The technique is subjected to the limitation that neutral molecules would not migrate through the gel, since electroosmotic flow is suppressed in this mode of operation. This technique is commonly employed in SDS-gel molecular weight analysis of proteins and sizing of applications of DNA sequencing, genotyping and quality control of therapeutic recombinant monoclonal antibodies (rMAbs) [93-96].

- **Capillary Isoelectric Focusing (CIEF)**; the substances are separated on the basis of their isoelectric points or pI values [97]. The protein samples and a solution are forming a pH gradient inside the capillary. The anodic end of the column is placed into an acidic solution (anolyte), and the cathodic end is in a basic solution (catholyte). Under the influence of an applied electric field, charged proteins migrate through the medium until they reside in a region of pH where they become electrically netural and therefore stop migrating. Consequently, zones are focused until a steady state condition is reached. After focusing, the zones can migrate from the capillary by a pressurised flow, e.g. simply lifting the height of one end of the capillary and permitting the sample flow through the detection cell. By the principle of electroneutrality, sodium ions can exchange for protons in the tube, generating a pH imbalance gradient which causes the migration of the components [98]. Sharp peaks are obtained with good resolution, and a large peak capacity is observed mainly because the whole tube is simultaneously used for focusing. This technique is commonly employed in protein characterization as a mechanism to determine a protein's isoelectric point.
- **Capillary Isotachophoresis (CITP);** the main feature of CITP is that it is performed in a discontinuous buffer system. Sample components condense between leading and terminating constituents, providing a steady-state migrating configuration composed of consecutive sample zone [99]. In CITP, the isotachopherogram obtained contains a series of steps, with each step representing an analyte zone. Unlike in other CE modes, where the amount of sample present can be determined from the area under the peak as in chromatography, quantitation in CITP is mainly based on the

measured zone length which is proportional to the amount of sample present [100]. Although it is used as a mode of separation, transient ITP has been used primarily as a sample concentration technique.

- **Capillary Electrochromatography (CEC);** In capillary electrochromatography (CEC), the separation column is packed with a chromatographic packing which can retain analytes by the normal distribution equilibria upon which chromatography depends and is therefore an exceptional case of electrophoresis [101-102]. In CEC, the liquid is in contact with the silica wall, as well as the particle surfaces. Consequently, electroosmosis occurs in a similar way as in a capillary due to the presence of the fixed charges on the various surfaces. CEC offers a number of benefits over HPLC including; the flow in CEC is close to plug flow and is substantially more uniform than a pressure-driven system; the independence of the flow velocity along the capillary diameter, the capillary length, and also the particle size of the packing allows the use of small-bore capillaries and microparticulate chromatographic packing without the limitation of increased back pressure as occurs in HPLC and finally the CEC method successfully combines the selectivity of HPLC and efficiency of CE, allowing the separation of charged, as well as neutral analytes. In general, separation of charged analytes using CEC is based on combined differences in electrophoretic mobility and partitioning into the stationary phase. In contrast, neutral analytes are separated solely through interactions with the stationary phase coating on the capillary wall [103].

1.7.2 **Chemiluminescence**

1.7.2.1 Introduction

Chemiluminescence (CL) is another detection method used in the work in Chapter 2 of this thesis. The term of luminescence was introduced in 1888 by E. Wiedemann. He stated that certain compounds are capable of emitting light without previous heating. Wawilow generalised this definition and stated that luminescence is the excess of the molecule light radiation over thermal radiation

of the same molecule in the given spectral region and temperature. The current classification of luminescence phenomena is based on the categorisation proposed by Wiedemann and depends on excitation mechanisms of molecule [104]. Luminescence phenomena are classified as follows in Table 1.4. However the type of luminescence used in this work was chemiluminescence (CL), which will be discussed in more detail.

CL can be defined as the emission of light from a molecule or atom in an electronically excited state produced by a chemical reaction (Figure 1.28). CL reactions are currently exploited mainly either for analyte concentration measurements or for nucleic acid probes. In the former case, the analyte of interest directly participates in a chemiluminescence reaction or undergoes a chemical or an enzymatic transformation in such a way that one of the reaction products is a co-reactant of a chemiluminescence reaction. CL systems that require hydrogen peroxide for the light emission are of particular interest in biochemical analysis. Hydrogen peroxide is a product of several enzymatic reactions, which can be then coupled to chemiluminescence detection. Among the different synthetic compounds used for hydrogen peroxide determination, only luminol, which was used in this work, and oxalate esters have found widespread use.

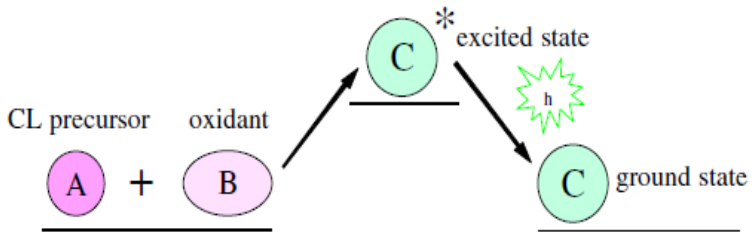

Figure 1.28: Basic Chemiluminescence Reaction

Table 1.4: Different modes of luminescence available

Mode	Basis of Emission
Photoluminescence	Emission produced by the absorption of UV, visible or IR radiation. Based on duration between absorption and emission of photons, fluorescence and phosphorescence are distinguished.
Thermoluminescence	Emission from solids induced by heating
Candoluminescence	Emission from incandescent solids
Triboluminescence	Emission induced by shaking, rubbing or crushing substance
Crystalloluminescence	Emission from crystallisation
Electroluminescence	Emission from electrical discharges
Sonoluminescence	Emission from exposure to ultrasonic waves in solution
Bioluminescence	Emission from living organisms or biological systems
Electroluminescence	Emission from electrical discharges
Oxyluminescence	Emission from polymers induced by oxidation
Chemiluminescence	Emission of the UV, visible or near IR radiation by molecules or atoms resulting from chemical reactions

1.7.2.2 Luminol Chemiluminescence Reaction

The chemiluminescent properties of lumiol (5-amino-2,3-dihydrophthalazine-1,4-dione) were first reported in 1928 by Albrecht [105]. Since that time, the chemiluminescence of luminol and related hydrazides has been studied extensively. In aprotic media, the chemiluminescent oxidation of luminol requires only oxygen and a strong base. In protic solvents, an oxidation system and an oxidative catalyst are required in addition to alkaline conditions. Hydrogen peroxide is the most frequently used oxidising agent. Transition metal cations (Cr^{3+}, Fe^{3+}, Co^{2+}, Ni^{2+}, Cu^{2+}, Hg^{2+}), either free or complexed to organic or inorganic ligands, catalyse the luminol chemiluminescence oxidation.

Dissolving luminol (3-aminophthalhydrazide or 5-amino-2,3-dihydro-1,4-phthalazinedione) in a base abstracts the protons from the two cyclic nitrogen atoms, resulting in an intermediate which is readily oxidised by hydrogen peroxide to an excited intermediate, the decay of which to a lower energy level is responsible for the emission of a photon of light. This reaction can be seen in Figure 1.29 [106]. The presence of a catalyst is paramount to this chemiluminescent method as an analytical tool. Many metal cations catalyse the reaction of luminol, H_2O_2, and OH^- in aqueous solution to increase light emission or at least to increase the speed of the oxidation to produce the emitter and therefore the onset/intensity of light production.

Figure 1.29: Overall luminol chemiluminescence reaction in aqueous medium

Chemiluminescence takes its place among other spectroscopic techniques because of its inherent sensitivity and selectivity. CL detection is one of the less developed

detection systems despite its many advantages including its low cost, simplicity minimal instrumentation and high sensitivity. In fact all CL detection systems require is a single light detector such as a photomultiplier tube. It does not need an excitation source (as does fluorescence and phosphorescence) or a monochromator and often not even a filter.

1.8 **Statistical Information**

1.8.1 **Introduction**

To establish criteria for statistical analysis a validation processes must be highly detailed. The objective of this validation process is to identify the performance of the analytical procedure and to demonstrate that the analytical system is operating in a state of statistical control. This 'state of statistical control' means that all causes of error remain constant and that they have been characterised statistically [107].

1.8.2 **Validation**

Validation of an analytical method is the process by which it is established, by laboratory studies, that the performance characteristics of the method meet the requirements for the intended analytical applications. These performance characteristics are outlined in Table 1.5.

Table 1.5: Table of validation characteristics

Calibration Range
Limit of Detection
Sensitivity
Selectivity
Accuracy and Precision

When outlining the results these characteristics should be clearly identified in the method description so that the suitability of the method for the specific application can be assessed.

1.8.2.1 **Calibration Range**

The calibration range of an analytical procedure is the interval between the upper and lower concentrations of analyte in the sample for which it has been demonstrated that the analytical procedure has a suitable level of precision, accuracy and linearity. The specified range is normally derived from linearity studies and depends on the intended application of the procedure.

1.8.2.2 **Limit of detection**

The detection limit of an individual analytical procedure is the lowest amount of analyte in a sample which can be detected but not necessarily quantitated under the stated experimental conditions. Although, when it is estimated by an appropriate means, it is perhaps the most valuable characteristic of an analytical system. The detection limit of an analytical method is the smallest concentration that the analyst can expect to detect with a given degree of confidence. The IUPAC (1978) has recommended that the limit of detection, defined in terms of either concentration (C_L) or amount (q_L), be related to the smallest measure of response (x_L) that can be detected with reasonable certainty in a given analytical method. According to this definition, the detection limit is given by Equation 1.29,

$$\mathbf{C_L \text{ (or } q_L) = ks_B/b}$$

Equation 1.29: Limit of detection; where s_B is the standard deviation of the blank of the method and b is the sensitivity of the method (expressed as the slope of the calibration curve). A value of k = 3 is recommended by IUPAC (based on confidence interval)

1.8.2.3 **Selectivity**

The selectivity refers to the extent in which a particular component in a material can be determined without interference from other components in the material. A method which is unquestionably selective for a variable is regarded as specific, however very few analytical methods are completely specific for a particular variable and hence cross-react with other analytes. This is because both the variable and other substances contribute to the analytical signal and cannot be differentiated. The effect of this interference on the signal may be positive or negative depending upon the type of interaction between the variable and interfering species.

1.8.2.4 **Sensitivity**

The sensitivity is the difference in variable concentration corresponding to the smallest difference in the response by the method that can be detected at a certain probability level. It can be calculated from the slope of a calibration curve. Most analytical methods require the establishment of a calibration curve for the determination of the variable or "unknown" concentration. Such a curve is achieved by plotting the instrumental response, y, versus the variable concentration, x. The relationship between y and x can be formulated by performing a linear regression analysis on the data in the linear range. The calibration function can be expressed by equation 1.30.

$$y = mx + c$$

Equation 1.30: Equation of a straight line

where c is the y intercept and m is the slope. As long as the calibration curve is within the linear response range of the method, the more points obtained to construct the calibration curve the better defined the slope will be. An important factor in defining the slope is that the measurement matrix must be physically and

chemically identical both for the samples to be analysed and the standards used to establish the calibration curve.

1.8.2.5 **Accuracy and Precision**

The term ‘accuracy’ is used to describe the difference between actual value obtained and the expected or true value. Generally, accuracy represents the sum of random error and systematic error or bias. Random errors arise from uncontrolled and unpredictable variations in the conditions of the analytical system during different analyses. Fluctuations in instrumental conditions, variations of the physical and chemical properties of sample or reagent taken on different occasions and analyst-dependent variations in reading results/scales are typical sources causing random errors. The origins for systematic or biases are detailed in Table 1.6.

Table 1.6: Table of validation characteristics

Instability of samples between sample collection and analysis
Deficiencies in the ability to determine all relevant forms of the variable
Biased calibration
Incorrect estimation of the blank

The term ‘precision’ should be used when speaking generally of the degree of agreement among repeated analyses. For numerical definition of this degree of agreement, the parameter standard deviation or relative standard deviation should be used.

1.8.3 **Repeatability and Reproducibility**

One of the most important aspects of developing an analytical device is the guarantee that it will produce the same result within an acceptable error over many tests. Repeating experiments several times ($n>3$) and reproducing the same results removes any doubt about the results obtained. It is a measure of how good

the device is when other operators in other laboratories can achieve the same result when running the same tests which also leads to the validation of the device.

1.8.4 **Percentage Recovery**

The percentage recovery is more often than not referred to in organic and inorganic chemistry where a yield is calculated after the completion of a reaction or purification. It shows how well the experiment was conducted and how accurate you were in your procedures. The percentage recovery can be calculated using equation 1.31.

$$\textbf{\% Recovery} = \frac{\textbf{Amount recovered}}{\textbf{Initial amount}} \times \frac{\textbf{100}}{\textbf{1}}$$

Equation 1.31: % Recovery:

1.8.5 **Correlation**

The correlation coefficient is a measure of the degree of fitness for a curve,or line in any given plot. The closer the value is to one the more accurate the fit and vice versa. The correlation coefficient is usually expressed as R^2.

1.9 **Buffers**

1.9.1 **Introduction**

A buffer solution is one which resists changes in pH when small quantities of an acid or alkali are added to it or when dilution occurs. You can adjust the pH of the buffer solution by changing the ratio of acid/base to salt, or by choosing a different acid/base and one of its salts. A buffer solution has to contain things which will remove any hydrogen ions or hydroxide ions that you might add to it, otherwise the pH will change. Acidic and alkaline solutions achieve this in different ways. The central equation dealing with buffers is the Henderson-Hasslebach equation, Equation 1.32.

$$pH = pK_a - \log \frac{[Acid]}{[Base]}$$

Equation 1.32: Henderson-Hasselbalch equation

1.9.2 **pH**

The pH of a solution is the negative of the logarithm of the hydronium ion concentration and is defined by equation 1.33. Using the pH scale is a convenient way to represent very small concentrations of hydronium ions in solution and to show changes in very small concentrations.

$$pH = - \log [H_3O^+]$$

Equation 1.33: pH equation

1.10 Electrochemical Instrumentation

1.10.1 **Introduction**

The use of instruments in analytical chemistry is vital as they determine the extent and scope of analysis that can be achieved. They therefore play a very important role in the advancement of analytical sensors especially in the areas of detection and validation. Two types of electrochemical workstations are described in this section; the *Chi 1040A* workstation and the *Palmsen*s workstation.

1.10.2 **Chi 1040A Electrochemical Workstation**

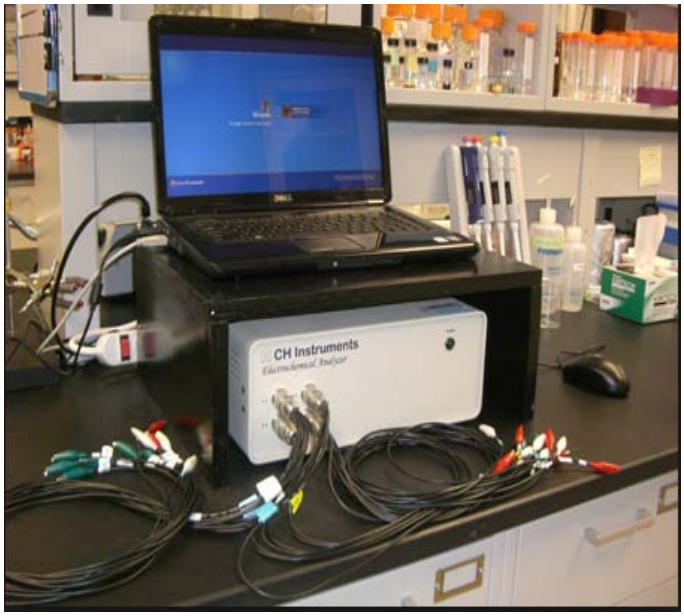

Figure 1.30: Chi 1040A Electrochemical Workstation

The CHI1040A electrochemical workstation, Figure 1.30, is a computerised 8 channel potentiostat. The system contains a digital function generator, a multiplexed data acquisition circuitry, a multi-potentiostat and can work with eight working electrodes in the same solution with a common reference electrode

and a common counter electrode. This workstation is bulky and is best suited for laboratory based sensors where mobility is not important.

1.10.3 **Palmsens Electrochemical Workstation**

The Palmsens instrument, Figure 1.31, is used for sensors with two or more electrodes. The wide dynamic range allows application of micro as well as macro electrodes. The response time of the instrument is short enough to apply fast techniques such as square wave voltammetry and its noise level is low enough to measure dc-currents with a resolution of a pico amp. The measured curves as well as the calibration plots are graphically displayed. The software allows determination by means of standard addition or using a calibration curve. The Pocket PC software also allows for easy control of Palmsens. The Palmsens workstation is also a more compact and highly mobile set-up than its Chi counterpart and can be used in field analysis.

Figure 1.31: PalmsensElectrochemical Workstation

1.11 References

[1] B.K. Sharma, Electro Chemistry, Krishna Prakashan, (1995).

[2] P.H. Rieger, Electrochemistry, Chapman & Hall, 1994.

[3] L. Wood, Evolution and the Future of Mankind, iUniverse, 2010.

[4] J. Wang, Analytical Electrochemistry, John Wiley & Sons, New York, (2006).

[5] A.J. Bard, G. Inzelt, F. Scholz, Electrochemical Dictionary, Springer, 2012.

[6] C.T. Reviews, e-Study Guide for: Fuel Cell Fundamentals by Fritz B. Prinz, ISBN 9780470258439, Cram101, 2012.

[7] M. Nuñez, Electrochemical studies of batteries, Nova Science Publishers, 2005.

[8] J. Wang, Analytical Electrochemistry, John Wiley & Sons, New York, 2006.

[9] R.J.D. Tilley, Understanding Solids: The Science of Materials, Wiley, 2005.

[10] Bard, A.J, Faulkner, LR (Bard, A.J, Faulkner, LR(Bard, A.J, Faulkner, LRs), Electrochemical Methods, Fundamentals and Applications, John Wiley & Sons, Inc., 1980.

[11] Southampton, Electrochemistry, Group, Instrumental Methods in Electrochemistry, Ellis Horwood, New York, 1990.

[12] Metrohm, Autolab, in.

[13] C.M.A. Brett, A.M.O. Brett, Electroanalysis, Oxford University Press, Oxford 1998.

[14] A. Tuteja, Fundamentals of Physical Chemistry, Discovery Publishing Pvt. Ltd., 2010.

[15] A.C. Michael, L. Borland, Electrochemical Methods for Neuroscience, CRC Press Taylor & Francis Group, Florida, 2010.

[16] J.O.M. Bockris, A.K.N. Reddy, Volume 1: Modern Electrochemistry: Ionics, Springer, 1998.

[17] P. Kissinger, W.R. Heineman, Laboratory Techniques in Electroanalytical Chemistry, Marcel Dekker, Inc., New York, (1996).

[18] Randles, J.E.B, Trans. Faraday Soc 44 (1948) p. 327.

[19] Nicholson, R.S., Shain, I., Anal. Chem. 36 (1964) 1351.

[20] P. Kissinger, W.R. Heineman, Laboratory Techniques in Electroanalytical Chemistry, Marcel Dekker, Inc., New York, 1996.

[21] Zoski, C.G. (Zoski, C.G.(Zoski, C.G.s), Handbook of Electrochemistry, Elsevier Science, 2007.

[22] Randles, J., Trans. Faraday Soc. 44 (1948) 327.

[23] Compton, R. G., Banks, C. E. (Compton, R. G., Banks, C. E.(Compton, R. G., Banks, C. E.s), Understanding Voltammetry, Imperial College Press, London, 2011.

[24] Heinz, J., "Cyclic Voltammetry-Electrochemical Spectroscopy" New Analytical Methods vol. 23 no. 11 (1984) p. 831.

[25] Gileadi, E., Kirowa-Eisner, E., Penciner, J. (Gileadi, E., Kirowa-Eisner, E., Penciner, J.(Gileadi, E., Kirowa-Eisner, E., Penciner, J.s), Interfacial Chemistry: An Experimental Approach, Addison-Wesley, USA, 1975.

[26] Brett, C.M.A, Brett, A.M.O, Electrochemistry: Principles, Methods and Applications, Oxford University Press (1993).

[27] Parsons, R., Chem. Rev. 90 (1990) 813.

[28] Kounaves, S.P. (Kounaves, S.P.(Kounaves, S.P.s), 'Voltammetric Techniques', in *Handbook of instrumental techniques for analytical chemistry* (ed.) Prentice Hall Publishers, Seattle, F.A., 1997.

[29] Bartlett, P.N., in, John Wiley & Sons, West Sussex, (2008) p 387-390.

[30] Sinclair, Ian (Sinclair, Ian(Sinclair, Ians), Sensors and Transducers, Newnes, Oxford, (2001), 13-14.

[31] Grundler, P. (Grundler, P.(Grundler, P.s), 'Chemical Sensors' *An Introduction for Scientists and Engineers*, Springer Berlin Heidelberg, (2007), 123-132.

[32] D. Grieshaber, R. MacKenzie, J. Vörös, E. Reimhult, Sensors 8 (2008) 1400.

[33] L.D. Mello, L.T. Kubota, Food Chemistry 77 (2002) 237.

[34] Mendelson, Y., in, CRC Press LLC, 2000.

[35] G.G. Guilbault, Analytical Chemistry 55 (1983) 1682.

[36] Sauerbrey, G. (Sauerbrey, G.(Sauerbrey, G.s), Z. Phys., 155, (1959) p. 206.

[37] L. Rayleigh, Proceedings of the London Mathematical Society s1-17 (1885) 4.

[38] Wolfbeis, O.S. (Wolfbeis, O.S.(Wolfbeis, O.S.s), Piezoelectric Sensors, Springer, (2007) p. 206.

[39] Kress-Rogers, E. (Kress-Rogers, E.(Kress-Rogers, E.s), Handbook of Biosensors and Electronic Noses, CRC Press, (1996) p. 261-264.

[40] C. D'Alkaine, L. De Souza, F. Nart, Corrosion science 34 (1993) 117.

[41] R.A. Bull, F.R.F. Fan, A.J. Bard, Journal of the Electrochemical Society 129 (1982) 1009.

[42] G. Li, P. Miao, Electrochemical analysis of proteins and cells, Springer, (2013), 5-8.

[43] D.C. Johnson, W.R. LaCourse, Analytical Chemistry 62 (1990) 589A.

[44] A. Gutés, C. Carraro, R. Maboudian, Electrochimica Acta 56 (2011) 5855.

[45] B. Baś, M. Jakubowska, Z. Kowalski, Electroanalysis 18 (2006) 1710.

[46] M.J. Eddowes, H.A.O. Hill, Journal of the Chemical Society, Chemical Communications (1977) 771b.

[47] L.A. Colon, R. Dadoo, R.N. Zare, Analytical Chemistry 65 (1993) 476.

[48] S. Wasmus, A. Küver, Journal of Electroanalytical Chemistry 461 (1999) 14.

[49] W. De Vries, E. Van Dalen, Journal of Electroanalytical Chemistry and Interfacial Electrochemistry 14 (1967) 315.

[50] J.W. Ross, R.D. DeMars, I. Shain, Analytical Chemistry 28 (1956) 1768.

[51] G. Kahan, Industrial & Engineering Chemistry Analytical Edition 14 (1942) 549.

[52] F. Fertonani, A. Benedetti, J. Servat, J. Portillo, F. Sanz, Thin Solid Films 349 (1999) 147.

[53] Z. Stojek, Z. Kublik, Journal of Electroanalytical Chemistry and Interfacial Electrochemistry 60 (1975) 349.

[54] H. Kuramitz, Y. Nakata, M. Kawasaki, S. Tanaka, Chemosphere 45 (2001) 37.

[55] M. Gattrell, D. Kirk, The Canadian Journal of Chemical Engineering 68 (1990) 997.

[56] R.R. Moore, C.E. Banks, R.G. Compton, Analyst 129 (2004) 755.

[57] T.M. O'Regan, M. Pravda, C.K. O'Sullivan, G.G. Guilbault, Talanta 57 (2002) 501.

[58] R. Adams, Analytical Chemistry 30 (1958) 1576.

[59] P. Davies, F. Brink Jr, in Fed. Proc, 1942, p. 19.

[60] A.M. Bond, Analyst 119 (1994) 1R.

[61] R.M. Wightman, Anal. Chem. 53 (1981) 1125.

[62] Stulik K., Amatore C., Holub K., Maracek V., K. W., Pure Appl. Chem., 72, (2000) 1483.

[63] R.J. Forster, Chemical Society Reviews 23 (1994) 289.

[64] J.O'M., A.K.N. Reddy (J.O'M., A.K.N. Reddy(J.O'M., A.K.N. Reddys), Modern Electrochemistry 2A: Fundamentals of Electrodics, Plenum Press, New York, (1998) Chapter 7.

[65] R.C. Matos, L. Angnes, M.C. Araújo, T.C. Saldanha, Analyst 125 (2000) 2011.

[66] R.J. Forster, Chemical Society Reviews 23 ((1994)) 289.

[67] X.-s. Zhu, C. Gao, J.-W. Choi, P.L. Bishop, C.H. Ahn, Lab on a Chip 5 (2005) 212.

[68] R.O. Gollmar, J.T. McDevitt, R.W. Murray, J.P. Collman, G.T. Yee, W.A. Little, Journal of the Electrochemical Society 136 (1989) 3696.

[69] G. Li, Y. Long, H. Chen, D. Zhu, Fresenius' journal of analytical chemistry 356 (1996) 359.

[70] A.M. Fermier, L.A. Colón, Journal of High Resolution Chromatography 19 (1996) 613.

[71] X.J. Huang, A.M. O'Mahony, R.G. Compton, Small 5 (2009) 776.

[72] IUPAC, Pure & Appl. Chem. 70 (1988) 1301.

[73] R.A. Durst, A.J. Baumner, R.W. Murray, R.P. Buck, C.P. Andrieux, Pure & Appl. Chem. 69 (1997) 1317.

[74] R.P. Buck, E. Lindner, Pure Appl. Chem 66 (1994) 2527.

[75] D.W. Arrigan, 119 (1994) 1953.

[76] J.F. Price, R.P. Baldwin, Analytical Chemistry 52 (1980) 1940.

[77] P. Ugo, L.M. Moretto, Electroanalysis 7 (1995) 1105.

[78] Kutner, W., Wang, J., L'her, M., Buck, R.P., Pure & Appl. Chem. 70 (1998) 1301.

[79] S. Hjertén, Chromatographic Reviews 9 (1967) 122.

[80] J.W. Jorgenson, K.D. Lukacs, Journal of Chromatography A 218 (1981) 209.

[81] J.W. Jorgenson, K.D. Lukacs, Clinical chemistry 27 (1981) 1551.

[82] J.W. Jorgenson, K.D. Lukacs, Anal. Chem. 53 (1981) 1298.

[83] L. S.F.Y. (L. S.F.Y.),L. S.F.Y.s), Capillary electrophoresis-principles, practice and applications, Elsevier Science, Amsterdam, the Netherlands, 1992.

[84] T. Tsuda, Journal of High Resolution Chromatography 10 (1987) 622.

[85] J.W. Jorgenson, K. Lukacs, Science 222 (1983) 266.

[86] S. Terabe, K. Otsuka, K. Ichikawa, A. Tsuchiya, T. Ando, Analytical Chemistry 56 (1984) 111.

[87] K. Otsuka, S. Terabe, Journal of Microcolumn Separations 1 (1989) 150.

[88] S. Terabe, K. Otsuka, T. Ando, Analytical Chemistry 61 (1989) 251.

[89] S. Hjertén, M.-D. Zhu, Journal of Chromatography A 327 (1985) 157.

[90] A. Cohen, B. Karger, Journal of Chromatography A 397 (1987) 409.

[91] S. Hjertén, K. Elenbring, F. Kilár, J.-L. Liao, A.J.C. Chen, C.J. Siebert, M.-D. Zhu, Journal of Chromatography A 403 (1987) 47.

[92] H.G. Lee, S. Chang, E. Fritsche, Journal of Chromatography A 947 (2002) 143.

[93] O. Salas-Solano, B. Tomlinson, S. Du, M. Parker, A. Strahan, S. Ma, Analytical Chemistry 78 (2006) 6583.

[94] G. Hunt, W. Nashabeh, Analytical Chemistry 71 (1999) 2390.

[95] J.P. Liu, S. Abid, M.S. Lee, Analytical Biochemistry 229 (1995) 221.

[96] S. Hjertén, M.-d. Zhu, Journal of Chromatography A 346 (1985) 265.

[97] S. Hjertén, J.-L. Liao, K. Yao, Journal of Chromatography A 387 (1987) 127.

[98] A. Martin, F. Everaerts, Proceedings of the Royal Society of London. A. Mathematical and Physical Sciences 316 (1970) 493.

[99] P. Gebauer, Z. Malá, P. Boček, Electrophoresis 32 (2011) 83.

[100] J. Knox, Chromatographia 26 (1988) 329.

[101] J. Knox, I. Grant, Chromatographia 24 (1987) 135.

[102] M.G. Cikalo, K.D. Bartle, M.M. Robson, P. Myers, M.R. Euerby, Analyst 123 (1998) 87R.

[103] E. Wiedemann, Annalen der Physik 270 (1888) 446.

[104] H.O. Albert, Z. Physik. Chem 136 (1928) 321.

[105] F. Baldini, N.A.T. Organization, Optical Chemical Sensors, Springer, 2006.

[106] Karlberg, B., in Inventory of Definitions in Analytical Chemistry, 2002.

Chapter 2

Toner-Based Microchips

2. Toner-based Microchips

2.1 Objectives

In this chapter a method based on micro-electrophoresis (ME) coupled with chemiluminescence (CL) detection was developed using polyester-toner (PT) microfluidic devices for the determination of amino acids, neurotransmitters and chiral compounds. Advantages of using chemiluminescence detection over other detection methods such as fluorescence, mass spectrometry or electrochemical include low costs and compact instrumentation as well as CL having a large linear range, and the presence of many well-characterised systems allowing CL to be uniquely suited to on-line detection for μ-TAS. CL detection is complementary to the other detection methods in that there are compounds that can be detected and quantified more sensitively by CL than by any of the other detection methods. Injection, electrophoretic separation and CL detection were integrated onto a simple toner-based microfluidic chip. The CL detection was based on the enhancement effects of the amino acids on the CL reaction of luminol with Cu^{2+} and H_2O_2. This work demonstrates that ME coupled with CL detection when applied to toner-based microchips is a simple and inexpensive method for the separation of biological samples and chiral compounds.

2.2 Introduction

The interest in low-cost, fast prototyping, disposable devices has increased dramatically since the introduction of micro-total analytical systems (μTAS) [1] and lab-on-a-chip technology. These microdevices have many advantages over conventional CE instruments, including portability, lower reagent and sample consumption, faster analysis times and higher sample throughput. Microanalytical devices were initially made using glass, silicon, and quartz substrates [2-3]. However, the cost of producing glass microchip devices has driven researchers and producers to seek alternative materials. Recent efforts in the last decade have thus led to increasing use of polymeric materials in the preparation of chip-based devices [4]. Techniques used for making polymer microfluidic devices include hot embossing, laser ablation, injection moulding and replica moulding [5-8]. These devices have demonstrated successfully their analytical capability yet to fabricate these devices is time-consuming and relatively expensive for use as a disposable device. This led the way for the development of toner- and paper-based devices.

Toner was first used in microfabrication science in 2001, when Tan *et al.* [9] proposed a simple method for the fabrication of PDMS microchips by using a photocopying machine to make a master on polyester film. This master was used to produce PDMS channels by a replica molding process in less than 1.5 hours. In 2003 Lucio do Lago *et al.* first described the technique of producing microfluidic devices based on the lamination of laser-printed polyester films [10]. Instead of a photocopying machine, a laser printer is used to transfer a toner layer onto a transparency film. The microfluidic channels are defined by the white regions of the image, for which the printer does not deposit any toner particles. The sealing of the channels is provided by a lamination step. This direct process allows tens of microchips to be prepared on a single transparency sheet in a matter of minutes. The advantages of these toner-based microchips are numerous and include fast analysis times, minute consumption of samples and reagents, as well as the obvious low-cost and rapid fabrication. Other advantages include greater flexibility in chip design, allows for multiple channels of different sizes and designs for a variety of CL reactions than either glass or polymeric micro-chips. These toner-chips coupled with chemiluminescence detection offers a very cheap, fast and flexible separation method for detecting biomarkers as well as the unique advantage of single-use

which avoids the need to regenerate the channel as is required when using glass or PDMS microchips. It also removes the possibility of contamination between samples.

Since do Lago's pioneering work, He *et al.* have demonstrated the electrokinetic control of fluid in these polyester-toner (PT) chips [11], while in 2008 Coltro *et al.* compared the analytical performance of electrophoresis microchannels fabricated in PDMS, glass, and PT microchips [12]. When compared with other popular microfluidic platforms such as glass and PDMS, PT electrophoresis devices exhibit the lowest electro-osmotic flow (EOF) magnitude. The low EOF observed is caused by the polyester film which is coated with a thin layer of a neutral polymeric base containing silica (~6%) [6]. Recently, Gabriela R.M. Buarte *et al.* used polyester toner-based microchips to perform DNA extraction and PCR amplification showing the growing interest in these simple microchips [13]. Despite the noticeable differences such as the EOF, PT chips offer many advantages over the classical materials in terms of fabrication time, cost, and perhaps most importantly, the required instrumentation for fabrication.

The toner-based microchip is based on the lamination of laser-printed toner on polyester films. In this work, a laser printer is used to selectively deposit toner onto polyester film, which is then laminated against another printed polyester film. The toner melts and binds the two polyester films and allows the blank regions to become channels for microfluidics [14].

Chemiluminescence (CL) detection is one of the less developed detection systems for CE despite its many advantages. Due to its simplicity, low cost, minimal instrumentation and high sensitivity, CL detection has become a useful detecting tool in flow injection (FI) and in CE systems [15]. CL can be defined as the emission of light from a molecule or atom in an electronically excited state produced by a chemical reaction [16]. There is no external light source needed, so the optical system is quite simple and strong background light levels from the source are eliminated. Potentially, with the background signal greatly reduced, detection limits can be significantly improved. In spite of its advantages, the requirement of suitable CL reagents for this detection mode may still limit its broad use; however, the significant increase in recent related publications may suggest an increasing interest in this area. The trends in the development of the field have been well-documented in several reviews since 1994. Baeyens *et al.* [17] were the first to review this area and discuss its many potentials and limitations. Staller and Sepaniak [18] and Garcia Campaña *et al.*[19] reviewed the principles

and applications of CL detection in CE. Further developments have been made recently with a growing interest in CL detection in microchip electrophoresis (ME-CL). Liu et al. [20], Tsukagosgi et al. [21], Huang *et al.* [22], and Ye *et al.* [23] have all published papers on ME-CL using either glass or polymeric micro-chips.

ME-CL using toner chips gives greater flexibility in chip design, allows for multiple channels of different sizes and designs for a variety of CL reactions than either glass or polymeric micro-chips. CL detection does not require as much instrumentation as fluorescence or electrochemical detection, since it does not need a light source like fluorescence, and it does not require an electrochemical detection cell (working, counter, and reference electrode) which can be complicated by the high voltages required for CE. Also, CL detection is complementary to the others in that there are some compounds that can be detected and quantified more sensitively by CL than by either of the other methods.

The analytes used for this work included amino acids, neurotransmitters and chiral compounds. The amino acids used in this work were glycine (Gly), cysteine (Cys), histidine (His) and tryptophan (Trp). Glycine is a non-essential amino acid that is required to build protein in the body and is used in the treatment of manic depression and hyperactivity [24]. Cysteine (Cys) is a sulphur containing non-essential amino acid that is necessary in the detoxification of the body from harmful xenobiotics [25]. Cysteine helps protect the liver and brain from damage. Histidine (His) is an essential amino acid that is required for the proper growth and repair of tissues. It is needed for the production of both red blood cells and white blood cells however histidine levels that are too high may lead to stress [26]. Tryptophan (Trp) is an essential amino acid required to produce vitamin B3 (niacin) and is also necessary for the production of the neurotransmitter serotonin [27]. Ye *et al.* [23] separated taurine and several amino acids on a PDMS microchip with CL detection using luminol, oxidizer (H_2O_2) and catalyst (Cu^{2+}). The impact of the buffer pH and the concentrations of luminol, H_2O_2 and Cu^{2+} on the CL intensity were investigated. The limit of detection of the amino acids was as low as 0.1 fmol.

The chiral compounds used in this work include D- and L- phenylanaline. D-Phenylalanine is a form of the essential amino acid, L-Phenylalanine, that, when taken as a supplement, protects the body's production of naturally occurring "painkillers" (endorphins), with no side-effects. D-Phenylalanine is the dextrorotatory form of the amino acid

Phenylalanine. The L-Forms (Levorotatory) of amino acids are ones that are bioavailable and are for protein synthesis and regulatory function. The L and D forms are mirror images of one another; however D-Phenylalanine is not absorbed into the body, but acts as an inhibiting agent to the enzymes that are responsible for the breakdown of endorphins, which control pain perception.

This is the first work based on ME-CL detection using PT microchips to the best of my knowledge. In the present study, the CL system used to detect the analytes is the luminol-H_2O_2-Cu^{2+} combination. The analytes form complexes with Cu^{2+}, and consequently either inhibit or enhance the CL emission [28]. The tartrate was included in the alkaline running buffer to complex the Cu^{2+} and prevent it from precipitating or polymerizing [29-30].

2.3 Experimental Details

2.3.1 **Reagents**

NaH_2PO_4, Na_2HPO_4, NaOH, 5-Amino-2,3-dihydro-1,4-phthalazinedione (luminol), potassium sodium tartrate tetrahydrate, copper (II) sulfate anhydrous , hydrogen peroxide, (30 wt % sol. in water), L-phenylalanine, D-phenylalanine, and DL-phenylalanine, D-penicillamine, L-histidine, L-tryptophan, L-cysteine and glycine were purchased from Sigma - Aldrich (Dublin, Ireland). Deionised water (18.2 MΩcm) was obtained fro m a Milli-Q (Millipore, Bedford, MA) water purification system. All reagents were of analytical grade with highest purity.

2.3.2 **Apparatus**

The CL photons were detected by a photomultiplier (PMT, Hamamatsu R928). The PMT was mounted in an integrated detection module including HV power supply, voltage divider and amplifier. The output signal of PMT was recorded and processed with a computer using Palmsens software (Palm Instruments BV, Houten, The Netherlands). A Labsmith HVS448 computer-controlled high-voltage sequencer, variable in the range 0-3000 V (Virum, Denmark) was used for sample injection and ME separation.

2.4 Procedures

2.4.1 **Fabrication of Toner-based microchip**

The PT microchips were fabricated by hand according to the procedure described elsewhere [10].The main steps of the microfabrication process are schematized in Figure 2.1. Briefly, the layout of the device and its mirror image, made in Microsoft Paint, were printed on a single 3M black & white laser transparency film CG3300, using a 600-dpi-resolution HP color laser jet CP1515n laser printer. The ink cartridge was a HP color laser jet black cartridge CB540A. An adapted paper punch was used to create holes on the mirrored layout. The layout and its perforated mirror image were folder over each other, aligned by hand, and sealed using a standard office laminator (no laminating pouch was used) at 120 °C at a rate of 30 cm/min. This lamination step sealed both PT films as a result of the toner layers melting onto each other. After the sealing step, the bases of 50 µL pipette tips were glued using UV glue over the holes to form solution reservoirs.

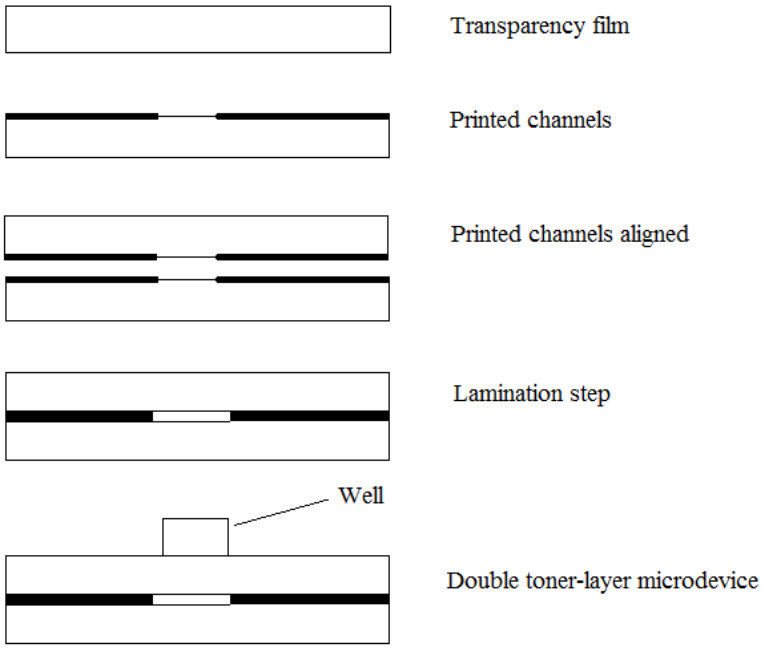

Figure 2.1: Representation of steps involved in fabrication process

2.4.2 **Preparation of Reagents**

2.4.2.1 **Amino Acids**

The electrophoresis and CL reaction buffers both contained 50 mM Phosphate solution, adjusted to pH9.6 with 1M NaOH. The electrophoresis buffer also contained 2.5 mM luminol, 0.45 mM Cu^{2+} and 4.5mM potassium sodium tartrate. The CL reaction buffer contained 50 mM H_2O_2. Human plasma from Sigma – Aldrich (Dublin, Ireland), was diluted 1:1 (*v*/*v*) in 50 mM phosphate buffer pH 9.6. All samples were filtered through 0.45 mM syringe filters (Millipore, Bedford, MA). The toner-chip was changed after each run.

2.4.2.2 **Chiral Compounds**

The electrophoresis and CL reaction buffers both contained 25 mM Na_2HPO_4 solution, adjusted to pH 9.3 with 1 M NaOH. The electrophoresis buffer also contained 2.5 mM luminol, 0.45 mM Cu^{2+} and 0.6 mM D-penicillamine. The CL reaction buffer contained 50 mM H_2O_2. The toner-chip was changed again after each run.

2.4.3 **Experimental Protocol**

The layout and dimensions of the toner-based microchip used in this work are shown in Figure 2.2. Platinum wires were placed into the reservoirs of the microchip as electrical contacts to the high-voltage power supply. The channels were allowed to fill with the electrophoresis buffer via capillary action from BW (buffer waste reservoir). Once channels were filled, reservoir S (sample reservoir) was filled with a solution containing the analytes, R (oxidation solution reservoir) was filled with CL reaction buffer and reservoirs B (buffer reservoir), SW (sample waste reservoir) and BW were filled with electrophoresis buffer. For electrokinetic injection, a set of electrical potentials were applied to five reservoirs for 25 seconds: reservoir S at -600 V, reservoir SW at 600 V, reservoir B at 200 V, reservoir R at 200 V and reservoir BW grounded. After 6 s the potentials were switched to -1600 V, -200 V, -200 V and -600 V at reservoir B, S, SW and R, respectively, while reservoir BW remained grounded for separation and detection. The same conditions were used both for the separation of the amino acids and the chiral compounds.

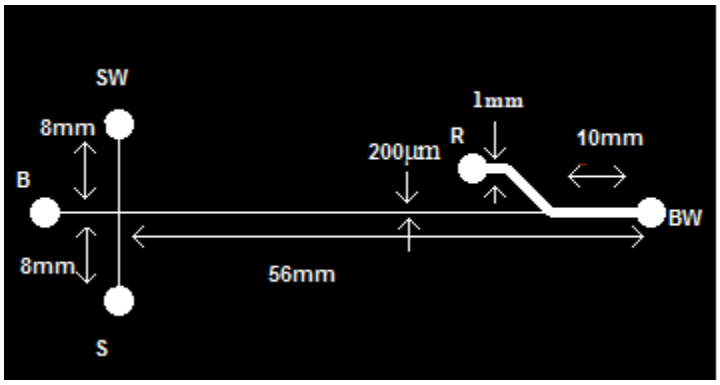

Figure 2.2: Layout and dimensions of the toner-based microchip used in this work. S, sample reservoir; B, buffer reservoir; SW, sample waste reservoir; BW, buffer waste reservoir and R, oxidiser solution reservoir.

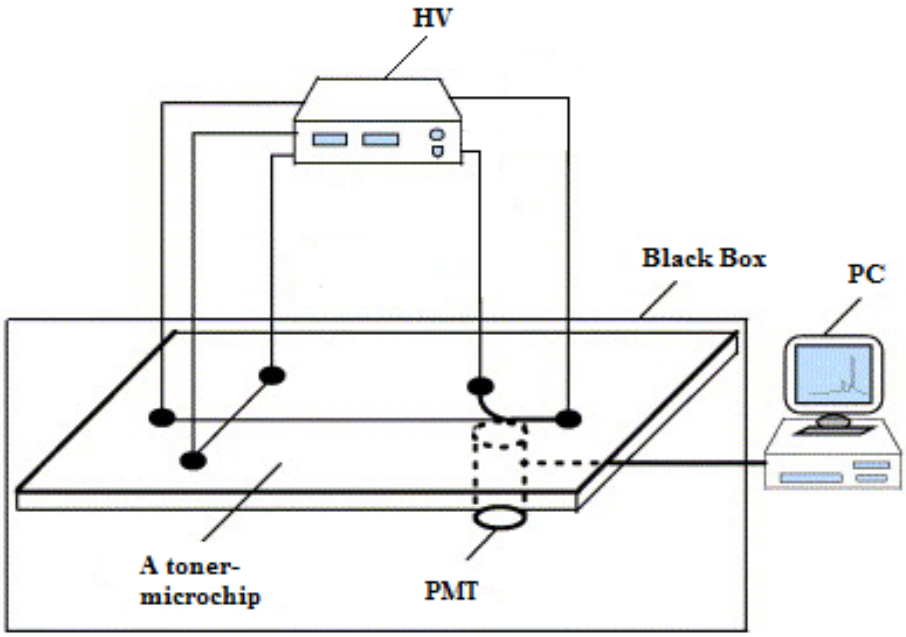

Figure 2.3: Scheme of MCE-CL System

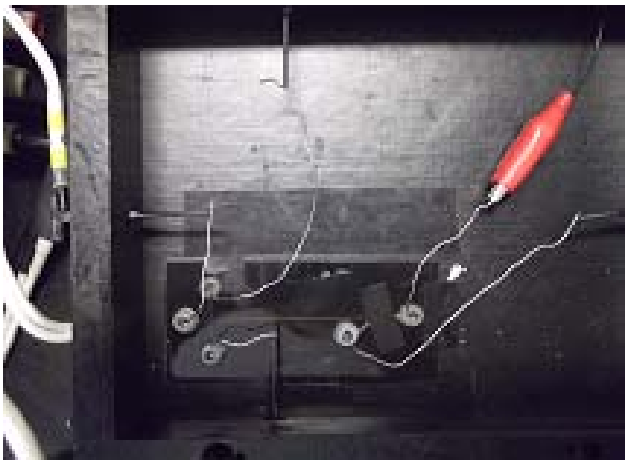

Figure 2.4: View of MCE-CL System

2.5 Results

Once the microdevice was fabricated, fluorescein was migrated through the cross-channel of the device via electro-osmotic flow shown in Figure 2.4. It is difficult to get a good visualization of the fluorescein due to the black ink and reflective acetate under a fluorescent microscope. However it is still clear that the fluorescein fills the channel and once the voltages switch the fluorescein which was at the cross channel migrates down the separation channel while the rest of the fluorescein flows back towards their wells. In Figure 2.4; A shows the empty PT chip, B shows the fluorescein migrating across the cross-channel , C shows the cross-channel filled with fluorescein, this occurred during the 25 sec injection time. Once the voltages changed; D shows the fluorescein in the centre of the cross channel begin to move down the separation channel, E shows the fluorescein migrating down the separation channel while the fluorescein in the cross-channel migrates back to their initial wells (B and A). F shows the cross channel empty again with the fluorescein moving down the separation channel and finally G shows the PT cross-channel empty again.

A B C

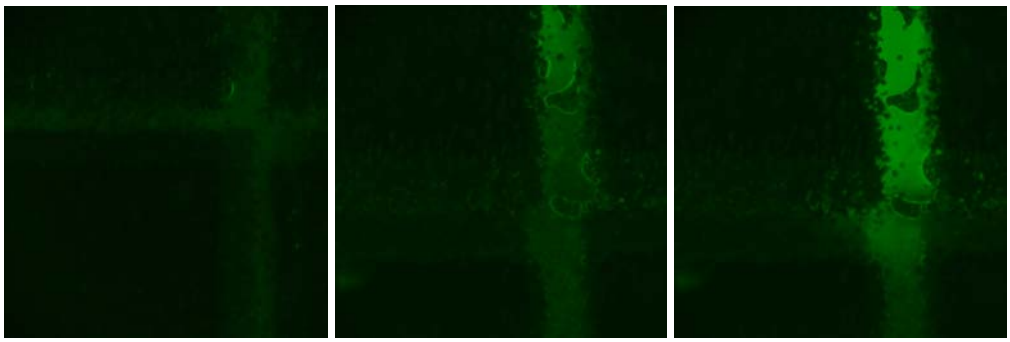

D **E** **F**

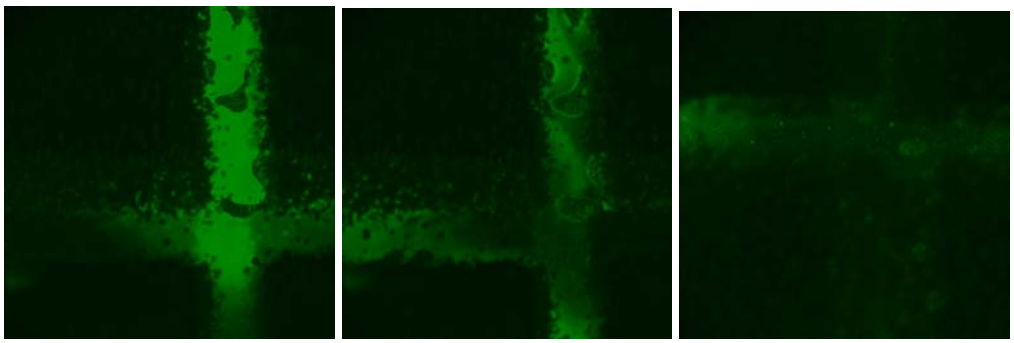

G

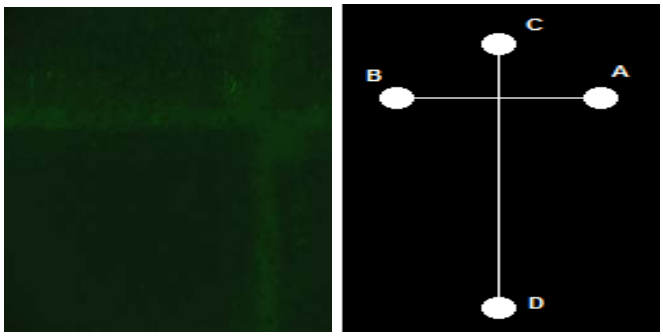

Figure 2.5: Fluorescein migrating through cross-channel of toner chip. Injection: for 25 seconds A = 200 V, B = -200 V, C = -100 V and D = -300 V. Running for 30 seconds A = 100 V, B = 100 V, C = -400 V and D = 800

The results from here will be discussed in two sections. The first part will be on the separation and detection of the amino acids while the second results section will focus on the chiral separation.

2.5.1 **Amino Acids**

2.5.1.1 **Optimisation of the CL detection of amino acids using toner-based microchips**

The concentrations of the CL reagent (luminol), oxidiser (H_2O_2) and catalyst (Cu^{2+}) were investigated in order to achieve maximum detection sensitivity. The luminol concentration was varied from 1.0 to 5.0 mM, the H_2O_2 was varied from 10 to 60 mM, and the Cu^{2+} concentration was varied from 0.2 mM to 0.6 mM. The maximum CL signal was obtained with luminol at 2.5 mM, H_2O_2 at 50 mM and Cu^{2+} at 0.45 mM. The effect of CL reaction buffer pH on the CL intensity was also investigated in a pH range of 8-11.5. The results suggested that the CL intensity increases with increasing pH; however, the baseline noise also increases with increasing pH. The CL reaction buffer gave a steady low-noise baseline at pH 9.6.

2.5.1.2 **ME separation of Amino acids on toner-based microchips**

To separate the amino acids, the ME conditions such as separation voltage, injection time and running buffer pH were investigated to achieve maximal separation. The effects of running buffer pH values from 8 to 11 were examined using the same background electrolyte composition. Effective separation was achieved at a pH value of 9.6. Separation voltage was examined over the range of -2300 V to -1200 V and the injection time was varied from 40 seconds to 15 seconds. As expected, increasing the separation voltage decreased migration times; however, the resolution of the amino acids decreased at high separation voltages. Taking into account both the analysis time and resolution, -1600V was chosen as the separation voltage giving an approximate electric current of 51 µA while the injection time chosen was 25 seconds. Figure 2.5 shows a typical electropherogram obtained from the separation of a mixture of the four amino acids examined under the optimized ME conditions.

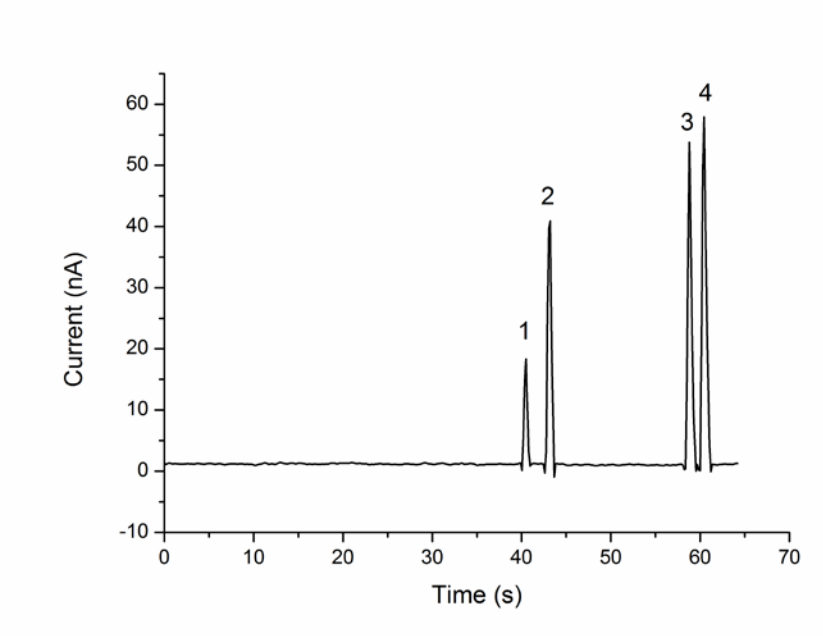

Figure 2.6: Electropherogram obtained from the separation of a standard sample. MCE conditions: the running buffer was 50 mM phosphate buffer (pH 9.6) containing 2.5 mM luminol, 0.45 mM Cu^{2+} and 4.5 mM tartrate. The oxidiser solution was 50 mM phosphate buffer (pH 9.6) containing 50 mM H_2O_2. All analyte concentrations are 1.0 x 10^{-5} M. Peaks: 1. Glycine; 2. Cysteine; 3. Histidine; 4. Tryptophan.

2.5.1.3 **Preparation of calibration curve of amino acids using CL detection in Toner-chip**

A calibration was carried out with aqueous standard solutions of 1, 2, 5, 10, 20, 40, 60, 100 and 200 µM (7 points). The curve of peak area versus concentration was found to be linear for this range, which covers the concentrations expected in the diluted samples. The following regression equations were obtained; Gly: I(nA) = 1.34 C(µM) + 7.98; Cys: I(nA) = 1.32 C(µM) + 4.31; His: I(nA) = 1.47 C(µM) + 3.73 and Trp: I(nA) = 2.09 C(µM) + 3.95. The corresponding correlation coefficient, r, was determined as 0.9952 for glycine, 0.995 for cysteine, 0.9957 for histidine and 0.998 for tryptophan (n=3). The limits of detection (LOD, 3 x signal-to-noise) were; Gly 0.81 µM; Cys 1.33 µM; His 0.93 µM and Trp 0.87 µM (n=10). The results are summarized in Table 2.1. It must also be stated that for each run the

microchip was replaced as the toner absorbs the buffer and analyte and to re-use the same chip would affect the results dramatically, thus, the reproducibility is based on different microchips.

Table 2.1 Linear ranges and detection limits of the amino acids using PT microchips:

Analytes	Linear Range (µM)	Calibration Equation	R^2	Detection Limit (µM)	Recovery % 25 µM	Recovery % 40 µM
Gly	1.00-200	I(nA) = 1.34 C(µM) + 7.98	0.995	0.32	82.4	91.9
Cys	1.00-200	I(nA) = 1.32 C(µM) + 4.31	0.995	0.29	90.0	95.2
His	1.00-200	I(nA) = 1.47 C(µM) + 3.73	0.996	0.22	87.1	94.4
Trp	1.00-200	I(nA) = 2.09 C(µM) + 3.95	0.998	0.21	84.3	97.7

2.5.1.4 **Analysis of plasma sample**

A typical electropherogram of the half diluted plasma sample spiked with the same four amino acids with a concentration of 25 µM each is shown in Figure 2.6. The % recovery of each of the amino acids in the plasma was as follows; glycine 82%; cysteine 90%; histidine 87% and tryptophan 84%. This clearly shows that the four amino acids were easily separated and detected within the human plasma. Further experimental work showed an increase in % recovery of the amino acids in the plasma when spiked with a concentration of 40 µM each. The % recovery of each of the amino acids in the plasma at a concentration of 40 µM was as follows; glycine 92%, cysteine 95%, histidine 94% and tryptophan 98%. Standard glycine, cysteine, histidine and tryptophan were spiked into the plasma sample for peak identification.

Dilution of the plasma sample also improved peak to peak separation and peak identification. All peaks were identified and the sequence was assigned as glycine, cysteine, histidine and tryptophan [31]. According to Armstrong *et al.* in human plasma the concentration of glycine is about 400 to 1000 µM, cysteine is about 40 to 200 µM, histidine is about 100 to 300 µM and tryptophan is about 30 to 150 µM [32]. Our detection limit is much lower than these values, so that our ME-CL system is suitable for real human plasma sample analysis. The blank sample gave a relatively stable baseline (Figure 2.6). Since most of the salts and proteins in the human plasma will not complex with luminol and copper, they will not give much signal thus the matrix in the human plasma will not interfere with the detection of amino acids.

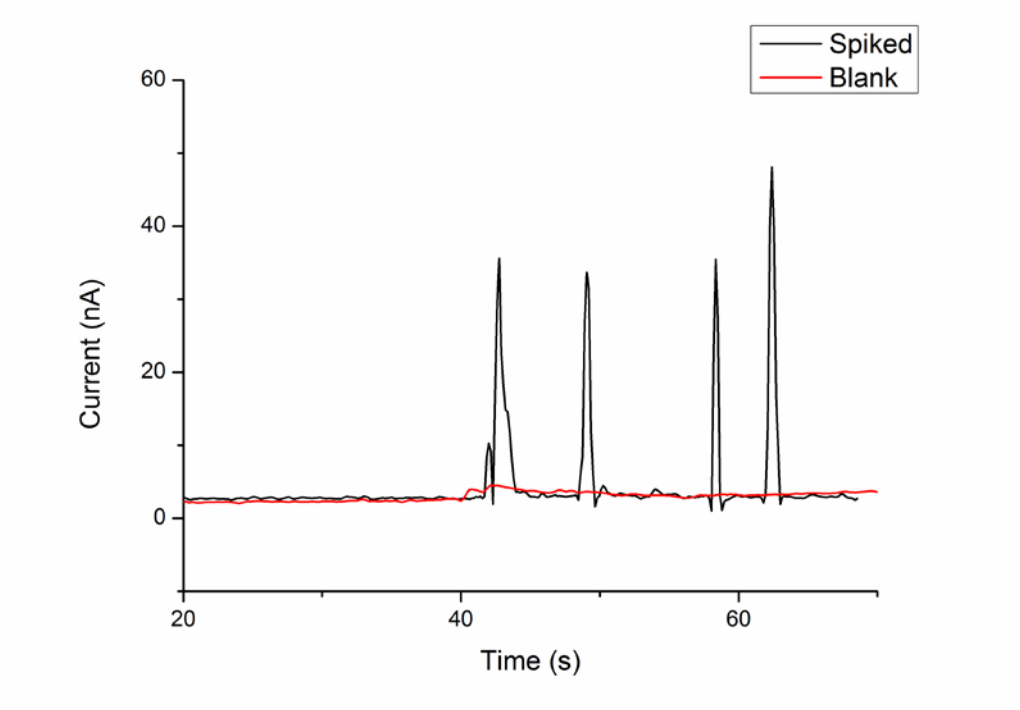

Figure 2.7: Electropherogram obtained from the plasma sample spiked with 25 µM Gly, Cys, His and Trp. MCE conditions are as in Fig. 2.5. Peaks: 1. Gly; 2. Cys; 3. His; 4. Trp.

2.5.2 **Chiral Separation**

2.5.2.1 **Optimisation of the CL detection of D,L-phenylalanine using toner-based microchips**

The concentrations of the CL reagent (luminol), oxidiser (H_2O_2), D-Penicillamine and catalyst (Cu^{2+}) were investigated in order to achieve maximum detection sensitivity. The luminol concentration was varied from 1.0 to 5.0 mM, the H_2O_2 was varied from 10 to 60 mM, the D-penicillamine was varied from 0.4 to 1.4 mM and the Cu^{2+} concentration was varied from 0.2mM to 0.6 mM. The maximum CL signal was obtained with luminol at 2.5 mM, H_2O_2 at 50 mM, D-penicillamine at 0.9 mM and Cu^{2+} at 0.45 mM. The effect of CL reaction buffer pH on the CL intensity was also investigated in a pH range of 8-11.5. The results suggested that the CL intensity increases with increasing pH; however, the baseline noise also increases with increasing pH. The CL reaction buffer gave a steady low-noise baseline at pH 9.3.

2.5.2.2 **ME separation of D,L-phenylalanine on toner-based microchips**

To separate the enantiomers, the ME conditions such as separation voltage, injection time and running buffer pH were investigated to achieve maximal separation. The effects of running buffer pH values from 8 to 11 were examined using the same background electrolyte composition. Effective separation was achieved at a pH value of 9.4 while separation could not be achieved below a pH of 9.2. Separation voltage was examined over the range of -2300 V to -1200 V and the injection time was varied from 15 seconds to 40 seconds. As expected, increasing the separation voltage decreased migration times; however, the resolution of the enantiomers decreased at high separation voltages. Taking into account both the analysis time and resolution, -1600 V was chosen as the separation voltage giving an approximate electric current of 51 µA while the injection time chosen was 20 seconds. Figure 2.7 shows a typical electropherogram obtained from the separation of a mixture of the enantiomers examined under the optimised ME conditions.

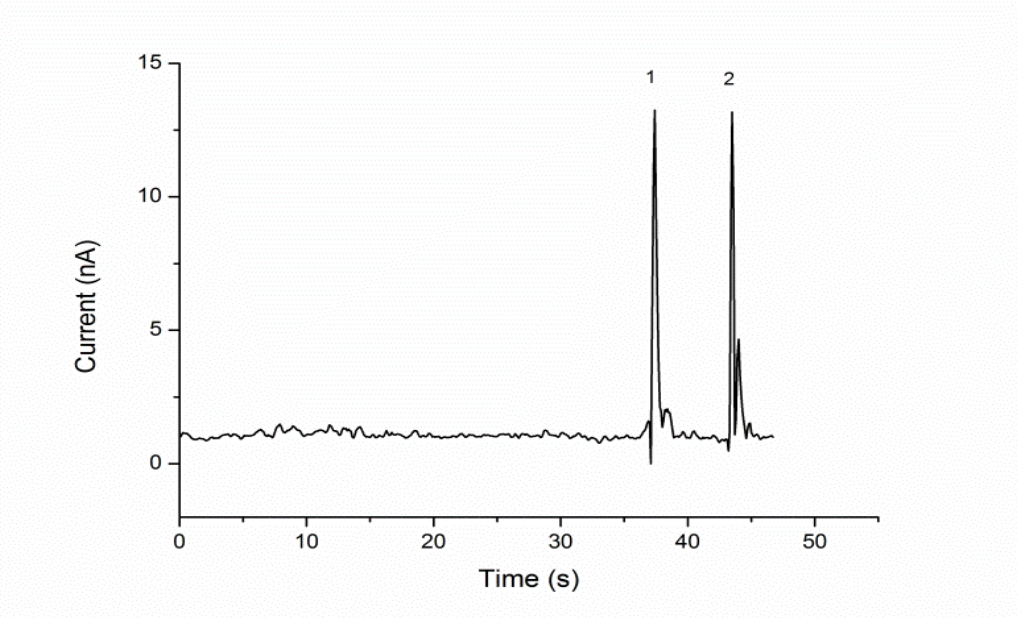

Figure 2.8: Electropherogram obtained from the separation of a standard sample. MCE conditions: the running buffer was 25 mM phosphate buffer (pH 9.4) containing 2.5 mM luminol, 0.45 mM Cu^{2+} and 0.9 mM D-penicillamine. The oxidiser solution was 25 mM phosphate buffer (pH 9.4) containing 50 mM H_2O_2. All analyte concentrations are 1.0 x 10^{-5} M. Peaks: 1. L-phenylalanine 2. D-phenylalanine.

Once both enantiomers were separated, the order of the peaks needed to be assigned. This was carried out by separating the enantiomers with L-phenylalanine having twice the concentration of D-phenylalanine.

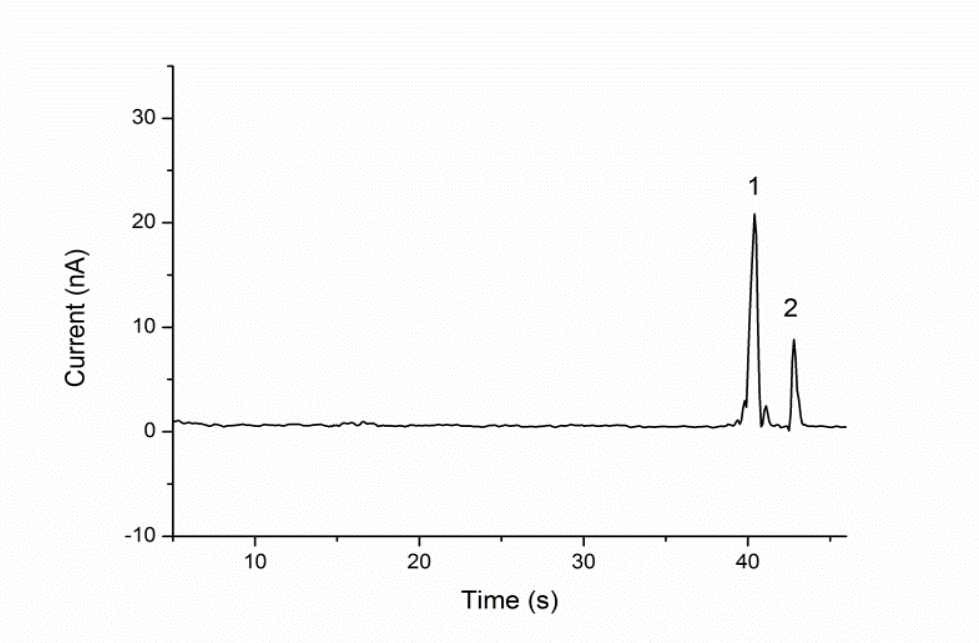

Figure 2.9: Electropherogram obtained from the separation of a standard sample. MCE conditions: the running buffer was 25 mM phosphate buffer (pH 9.4) containing 2.5 mM luminol, 0.45 mM Cu^{2+} and 0.9 mM D-penicillamine. The oxidiser solution was 25 mM phosphate buffer (pH 9.4) containing 50 mM H_2O_2. Analyte concentrations are 2.0 x 10^{-5} M L-phenylalanine and 1.0 x 10^{-5} M D-phenylalanine. Peaks: 1. L-phenylalanine 2. D-phenylalanine.

2.5.2.3 **Preparation of calibration curve of D,L-phenylalanine using CL detection in Toner-chip**

A calibration was carried out with aqueous standard solutions of 10, 20, 40, 60, 80, 100 and 120 µmol (7 points). The curve of peak area versus concentration was found to be linear for this range, which covers the concentrations expected in the diluted samples. The following regression equations were obtained; L-phenylalanine: I(nA) = 2.06 C(µM) + 3.98 and D-phenylalanine: I(nA) = 2.82 C(µM) + 3.71. The corresponding correlation coefficient, r, was determined as 0.989 for L-phenylalanine and 0.991 for D-phenylalanine (n=3). The limits of detection (LOD, 3 x signal-to-noise) were; L-phenylalanine: 0.93 µM and D-phenylalanine: 0.98 µM (n=10). The results are summarized in Table 2.2. It must also be stated that for each run the microchip was replaced as the toner absorbs the buffer and analyte.

Table 2.2 Linear ranges and detection limits of the chiral compounds using PT microchips:

Analytes	Linear Range (μM)	Calibration Equation	R^2	Detection Limit (μM)
L-	1.00-180	I(nA) = 2.06 C(μM) + 3.98	0.989	0.42
D-	1.00-180	I(nA) = 2.82 C(μM) + 3.71	0.991	0.54

2.6 Limitations of toner-based microchips

The advantages of these microchips are significant with regards to the instrumentation required for fabrication. Currently these chips are being prepared by hand which hinders the reproducibility of these microchips to a poor %RSD of 34% based on migration times and hence every electropherogram produced will have such an associated error. Since the chips are individually made by hand, no two microchips are exactly the same. This issue can be addressed with the development of masks and alignment markers ensuring much greater chip-to-chip reproducibility. Other limitations include the issue of air-bubble formation, which occurs if the microchip is re-used or if the running buffer is not sufficiently sonicated. Nonetheless, the fact remains that these PT chips, which are readily made from a computer, printer and laminator, can be successfully used for CE separations coupled with CL detection. This implies that future work on the fabrication of these chips will provide readily-designed, inexpensive, portable, and reliable micro-chip devices. Table 2.3 compares the PT microchip to other common microchip devices and the advantages of the PT chip clearly outweigh any disadvantages they may have. It is also important to note that these microdevices should be used more for qualitative determination rather than quantitative determination.

Table 2.3 Comparison of PT microchip with glass chip and other polymeric microchips

Comparison of PT microchip with glass chip and other polymeric microchips:

	PT Chip	**Glass Chip**	**PDMS Chip**	**PMMA Chip**
Cost per chip	$0.15	$40	$25	$510
Time to Fabricate	<10 mins	24 hrs	34 hrs	45 hrs
Reproducibility	Moderate	Excellent	Excellent	Excellent
Durabillity	Single-use	Reusable	Semi-reusable	Reusable

2.7 Conclusions and Future Work

A simple ME-CL detection method has been developed using toner-based micro-chips for the successful separation and determination of both amino acids and chiral compounds. Moreover, these inexpensive, versatile microchips demonstrated that the amino acids could be separated and detected using a real biological matrix. Although there is vast room for improvement particularly with the %RSD which will be addressed in future work this chapter demonstrates that it is possible to use ME-CL detection successfully and achieve results using these easily fabricated toner-based microchips with the usual ME advantages of fast analysis times and minute consumption of electrolyte. To the best of our knowledge, this is the first report that uses CL detection with toner-based microchips.

Future work will look at lowering the %RSD between microdevices.

2.8 Highlights

This chapter focused on the fabrication of toner-based microdevices. Once the devices were fabricated, fluorescein was then migrated through the channels via electro-osmotic flow.

The toner-chips were then coupled with chemiluminescence detection for the separation and detection of multiple amino acids. The conditions were optimised and the amino acids were then spiked into a real-biological sample, human serum. The microchip gave good % recoveries however the % RSD was a disappointing 34%. It's important to note that this is due to the microdevice being changed after each run and all devices are made by hand so no two devices are identical. Although the % RSD is poor it is crucial to acknowledge these micro-devices should only be used for qualitative measurements not for quantitative purposes.

The toner-chip was then once again coupled with CL to separate and detect chiral compounds D- and L-phenylalanine. The microdevice was able to separate these and also indicate which peak belonged to each enantiomer.

2.9 References

[1] A. Manz, N. Graber, H.á. Widmer, Sensors and actuators B: Chemical 1 (1990) 244.

[2] P.-A. Auroux, D. Iossifidis, D.R. Reyes, A. Manz, Analytical Chemistry 74 (2002) 2637.

[3] D.R. Reyes, D. Iossifidis, P.-A. Auroux, A. Manz, Analytical Chemistry 74 (2002) 2623.

[4] S.A. Soper, S.M. Ford, S. Qi, R.L. McCarley, K. Kelly, M.C. Murphy, Analytical Chemistry 72 (2000) 642 A.

[5] V. Dolník, S. Liu, S. Jovanovich, ELECTROPHORESIS 21 (2000) 41.

[6] C.D. García, C.S. Henry, Analytical Chemistry 75 (2003) 4778.

[7] S.K. Sia, G.M. Whitesides, ELECTROPHORESIS 24 (2003) 3563.

[8] J. Wang, M. Pumera, M.P. Chatrathi, A. Escarpa, R. Konrad, A. Griebel, W. Dörner, H. Löwe, ELECTROPHORESIS 23 (2002) 596.

[9] A. Tan, K. Rodgers, J.P. Murrihy, C. O'Mathuna, J.D. Glennon, Lab on a Chip 1 (2001) 7.

[10] C. Lucio do Lago, H.D. Torres da Silva, C.A. Neves, J.G. Alves Brito-Neto, J.A. Fracassi da Silva, Analytical Chemistry 75 (2003) 3853.

[11] F.-Y. He, A.-L. Liu, J.-H. Yuan, W.K.T. Coltro, E. Carrilho, X.-H. Xia, Analytical and Bioanalytical Chemistry 382 (2005) 192.

[12] W.K.T. Coltro, S.M. Lunte, E. Carrilho, Electrophoresis 29 (2008) 4928.

[13] G.R.M. Duarte, C.W. Price, B.H. Augustine, E. Carrilho, J.P. Landers, Analytical Chemistry 83 (2011) 5182.

[14] W.K.T. Coltro, D.P. de Jesus, J.A.F. da Silva, C.L. do Lago, E. Carrilho, Electrophoresis 31 (2010) 2487.

[15] F.J. Lara, A.M. García-Campaña, A.I. Velasco, ELECTROPHORESIS 31 (2010) 1998.

[16] R. Su, J.-M. Lin, K. Uchiyama, M. Yamada, Talanta 64 (2004) 1024.

[17] W.R.G. Baeyens, B.L. Ling, K. Imai, A.C. Calokerinos, S.G. Schulman, Journal of Microcolumn Separations 6 (1994) 195.

[18] T.D. Staller, M.J. Sepaniak, Electrophoresis 18 (1997) 2291.

[19] W.R.G. Baeyens, S.G. Schulman, A.C. Calokerinos, Y. Zhao, A.M. García Campaña, K. Nakashima, D. De Keukeleire, Journal of Pharmaceutical and Biomedical Analysis 17 (1998) 941.

[20] B.-F. Liu, M. Ozaki, Y. Utsumi, T. Hattori, S. Terabe, Analytical Chemistry 75 (2002) 36.

[21] K. Tsukagoshi, N. Jinno, R. Nakajima, Analytical Chemistry 77 (2005) 1684.

[22] X. Huang, J. Ren, Trends in Analytical Chemistry 25 (2006) 155.

[23] F. Ye, Y. Huang, Q. Xu, M. Shi, S. Zhao, Electrophoresis 31 (2010) 1630.

[24] D. Shemin, Journal of Biological Chemistry 162 (1946) 297.

[25] M.T. Heafield, S. Fearn, G.B. Steventon, R.H. Waring, A.C. Williams, S.G. Sturman, Neuroscience Letters 110 (1990) 216.

[26] W. Kriengsinyos, M. Rafii, L.J. Wykes, R.O. Ball, P.B. Pencharz, The Journal of Nutrition 132 (2002) 3340.

[27] J.D. Fernstrom, R.J. Wurtman, Science 174 (1971) 1023.

[28] Z. Lin, Z. Xie, Journal of Separation Science 31 (2008) 2852.

[29] K. Tsukagoshi, K. Nakahama, R. Nakajima, Analytical Chemistry 76 (2004) 4410.

[30] S.R. BENEDICT, Journal of the American Medical Association LVII (1911) 1193.

[31] L. Zhou, J.D. Glennon, J.H.T. Luong, Analytical Chemistry 82 (2010) 6895.

[32] M. Armstrong, K. Jonscher, N.A. Reisdorph, Rapid Communications in Mass Spectrometry 21 (2007) 2717.

Chapter 3

Acetate Microelectrode

3. Acetate Microelectrode

3.1 Objectives

There were two aims to this chapter. The first was to develop a microelectrode configuration onto acetate substrate which could perform electrochemical detection with good stability and reproducibility. The second was to use this microelectrode and couple it with capillary electrophoresis for the separation and detection of multiple analytes. This work also involved a comparison using the conventional 3-electrode system. To date this is the first time to the best of my knowledge that a microelectrode configuration of gold, platinum and silver/silver chloride has been fabricated onto acetate substrate.

3.2 Introduction

Electrochemical detectors have proven themselves as highly sensitive and selective systems for the determination of many electroactive species in a variety of samples. Over the past two decades, much research in this field has focused on the development of new electrode materials, new detection schemes, or new applications. Recent research has seen the development of electrochemical detection systems based on microelectrodes and chemically modified electrodes, both of which hold dominant positions in modern electrochemistry and have resulted in many interesting advances in electroanalytical techniques. One of the main challenges facing the analytical chemist is the development of methods that respond to the growing need to perform rapid ‘in situ’ analysis but at a relatively low-cost. These methods must be sensitive and accurate, and be able to determine various substances with different properties in ‘real-life’ samples. In recent years, many methods were developed with this end in sight and have been based on the use of electrochemical techniques due to their high sensitivity, selectivity, portable field-based size and of course low-cost.

This chapter introduces a novel microelectrode configuration which can be fabricated at a low cost due to the substrate being acetate material. The most common technique used in the manufacturing of microelectrodes and microfluidic devices is photolithography. This procedure consists of processing photoresist material to transfer the desired electrode pattern from a mask to the surface of a substrate [1-3]. When the surface for patterning is a metal

layer, the fabrication involves metallisation. The metallisation technique used for this work was electron-beam (e-beam) evaporation. Once the microelectrodes were fabricated they underwent several characterisation before being coupled with capillary electrophoresis to separate and detect a number of neurotransmitters.

3.2.1 **Technical Background**

Microtechnology can be defined as a technique involving dimensions comprised between the micron and the millimeter scale. The most common technique to process the thin layers and manufacture microelectrodes and microfluidic devices is photolithography [3]. Photolithography consists of processing photoresist material to transfer a pattern from a mask to the surface of a substrate. The process involves substrate cleaning, surface insulation, photoresist application, soft baking, mask alignment, UV-light exposure, photoresist development and hard-baking. It requires the fabrication to take place in a cleanroom environment with filters to remove ultraviolet light. Details of the fabrication of the microelectrodes used in this work will be further discussed in section 3.3.3.

The fabrication of a three dimensional microstructure consists of numerous different stages. These can be broadly summarized as:

- Substrate preparation- cleaning and metallisation
- Photolithography
- Bonding

3.2.2 **Substrate Cleaning**

The electrode configuration is microscale, and therefore it is vital that the substrate to work on is clean, i.e. that it is contamination and dust free. The substrate used in this work is an acetate wafer. Various cleaning methods exist for microfabrication. Mechanical cleaning such as ultrasonic agitation, manual polishing and supercritical cleaning are efficient ways to remove particles but they are less effective at removing surface residue. Other treatments

such as vapour cleaning, thermal treatments and plasma etching are also commonly used. Chemical cleaning can be used to remove organic contaminants or metal ions. Common methods use mixtures of hydrogen peroxide and various acids or bases in which the substrates are immersed [4].

3.2.3 **Metallisation**

When the process involves patterning metal, the fabrication starts with the metallisation of the substrate. The deposition process influences the film microstructure, and therefore its properties (e.g. coating density, surface roughness). For the study of electrochemistry at the surface of the electrode these parameters must be well defined and the material structure homogeneous. The three most common techniques used to cover a substrate with a thin metallic film are evaporation, sputtering and electroplating. The technique employed in this work was e-beam evaporation which will be further discussed.

- *Electron-Beam Evaporation*

Frequently called "e-beam", the electron-beam metallisation uses a focused beam of electrons, in a high vacuum chamber, to heat the metal for deposition. The metal source is kept in a water-cooled crucible and exposed to a beam of high energy electrons. As these come to rest in the metal, the heat released warms up the metal to create first a liquid and then a vapour. At this latter point the metal can evaporate and condense on the substrate. E-beam evaporation not only results in higher quality films with less contaminations, it also provides a higher deposition rate. There are two main disadvantages that come with this technique and these include that the process might induce x-ray damage and that the deposition equipment is more complex and costly [3]. For a given vacuum chamber, the deposition rate is determined by the thermal conductivity, specific heat capacity and melting point of the metal, and the current density of the electron beam.

3.2.4 **Photolithography**

Photolithography is the process of patterning a radiation-sensitive polymer (photoresist) [5].The photoresist is usually applied to the substrate by spin coating and its wet thickness depends on its viscosity and the speed and time of the spin. The polymer is then prebaked to remove the excess solvent. It is exposed to UV-light through the mask designed with the desired pattern. This exposure changes the photoresist's chemical resistance to the developer solution. Finally the photoresist is developed in wet chemicals in order to remove the soluble parts and form the desired pattern. Once the photoresist processing is finished, its pattern can be transferred into underlying layers using etching techniques.

3.2.5 **Capillary Electrophoresis**

Capillary electrophoresis (CE) in its modern form was first described by Jorgenson and Lukacs in 1981 [6-7]. Since that time, its use for the separation of a variety of samples has become increasingly widespread. Ultraviolet, fluorimetric (FL), mass spectrometric and electrochemical (EC) detection methods have all been used in conjunction with CE. The use of EC detectors with CE (CEEC) has grown steadily since the first report of such a system by Wallingford and Ewing in 1987 [8]. Free zone CE yields highly efficient separations based on size-to-charge ratios, which are typically completed in a minute to an hour, depending upon the conditions employed. Capillary electrophoresis is particularly suited to low volume sampling because the total volume of the separation capillary is of the order of a microliter. Electrochemical detection is well suited to capillary electrophoresis because the detection cell can be miniaturized with little or no loss in sensitivity. CEEC is typically operated in the amperometric mode, in which a constant potential is applied and the resulting current is measured. The major drawbacks to combining CE and EC are the need to isolate the electrochemical detector from the potential used in the separation and the difficulty encountered in aligning the working electrode with the end of the capillary. Fortunately, these problems can be overcome through the use of a decoupler, capillaries of very small diameter and electrode holders. Microelectrodes are employed in most CEEC systems, primarily because their size is compatible with the small diameters of the capillaries used for the CE separation. Using microelectrodes, the detection cell can easily be miniaturized, usually without a loss of sensitivity. This is because the noise at a microelectrode decreases more

rapidly than the signal when the size of the electrode is decreased. Over the years, working electrodes used for CEEC have been fabricated from a number of materials, including carbon [9-10], platinum [11-15], gold [15-19], copper [[20-22] and nickel [23-24]. Microelectrode configurations have been fabricated on numerous different substrates including glass, PDMS and polyimide to name just a few.

3.2.6 **Analytes used in this work**

3.2.6.1 **Uric Acid used for initial testing of microelectrodes**

Uric acid (UA) is the primary product of purine metabolism in the human body [25]. The concentration levels of UA in men is 200-430 μM and for women is 140-360 μM in serum for normal, healthy humans [26]. Monitoring UA continuously is necessary as it has been shown that extreme abnormalities of UA levels are symptoms of several diseases such as gout and Lesch-Nyhan syndrome [27-28]. It is therefore essential to develop rapid methods, preferably simple and inexpensive, for the determination of UA in routine analysis. UA exists as an anion beyond pH 5.4 in the alkaline range (pKa of UA is 5.4). Although there are several techniques available for the determination of UA including spectrophotometry [29-32] and chromatography [33-35], electrochemical detection of UA has received much interest due to its biological importance and easy oxidation property [36-40].

3.2.6.2 **Neurotransmitters used in CE**

Dopamine (DA), epinephrine (Ep), norepinephrine (NEP) and tryptamine (TA) occur naturally in the human body and serve as neurotransmitters or hormones in the sympathetic nervous system [41]. The measurement of these neurotransmitters in biological fluids has an essential role in the diagnostics of hypertension, multiple sclerosis, Parkinson's disease and various mental diseases [42]. As a consequence, simple, sensitive and accurate analytical methods in the quantitation of these neurotransmitters would be useful for physiological investigations and disease diagnosis. This has prompted the development of methods for the

determination of these catecholamines in human plasma, urine and pharmaceutical preparations. In the past decade, a number of methods have been reported for the quantitative analysis of catecholamine, such as high performance liquid chromatography (HPLC) with electrochemical [43], fluorescence [44-45] and chemiluminescence (CL) detection [46], the capillary electrophoresis (CE) with laser-induced fluorescence (LIF) [47], electrochemiluminescence (ECL) [48], mass spectrometry [49] and electrochemical detection [50-51], and flow-injection analysis [52].

This chapter discusses the novel approach to using electrodes by applying a 3-electode configuration onto acetate substrate. These microelectrodes are based on a Au working electrode, Ag/AgCl reference electrode and Pt counter electrode and are fabricated by means of patterning and deposition techniques using the central fabrication facilities in Tyndall National Institute. The main advantages of these microelectrodes include the fact that they are based on cheaper substrate material than the more conventional PDMS and pyrex substrates and since the electrodes are on acetate the dicing step can automatically be eliminated. This gives more control and flexibility to tailor the size and shape of the acetate electrode depending on what detection method you are coupling them with. The stability of these sensors has been investigated and has also been used in real samples determination using cyclic voltammetry with satisfactory results.

This work also involves CEEC with the microelectrode configuration. This is the first time to the best of our knowledge that such a microelectrode configuration on acetate has been fabricated and also coupled with capillary electrophoresis. This type of microelectrode has numerous advantages including the low fabrication cost, the ability to fabricate numerous devices on a single sheet of acetate and the ease to dice these electrodes into any desired shape you may require.

3.3 Experimental Details

3.3.1 **Reagents**

3M black & white laser transparency film CG3300, Gold and Platinum materials were purchased from Pi-kem (UK), the silver was purchased from Umicore (UK), Ferric Chloride was purchased from Sigma - Aldrich (Dublin, Ireland), uric acid, tryptamine hydrochloride, dopamine (3-hydroxytyramine), epinephrine (1,2- benzene diol) and norepinephrine hydrochloride were purchased from Sigma - Aldrich (Dublin, Ireland). Deionised water (18.2 MΩ.cm) was obtained from a Milli-Q (Millipore, Bedford, MA) water purification system. All reagents were of analytical grade with highest purity. For the initial electrochemical testing the electrophoresis buffer contained 50 mM Phosphate solution, adjusted to pH 4 with 0.1 M Phosphoric acid. For the CE, the electrophoresis buffer contained 50 mM $Na_2B_4O_7 \cdot 10H_2O$ solution, adjusted to pH 9.5 with 1 M NaOH. All stock solutions were prepared before starting each set of experiments and stored under refrigeration away from the light. Diluted solutions were prepared just before use from the stock solutions. Buffers and samples were sonicated for 5 minutes before use. The capillary used was made of silica and was 50 cm long.

3.3.2 **Apparatus**

3.3.2.1 **Initial electrochemical testing**

The electrochemical experiments were performed with a CHi1040A electrochemical workstation (Shanghai, China). The micro-electrode used in this experiment contained a three electrode configuration with a gold (Au) working electrode, a Ag/AgCl reference electrode and a Pt counter electrode. Pads and connections have been done in gold material.

(A) (B)

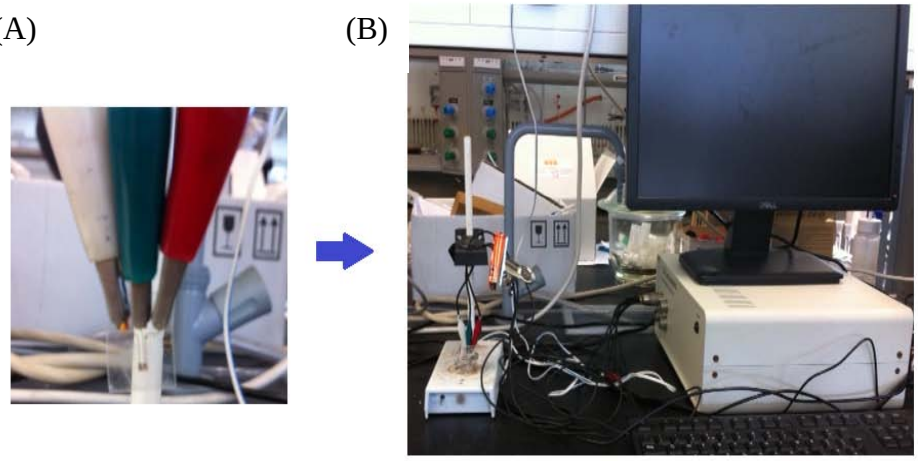

Figure 3.1: (A) Close-up view of microelectrode configuration connected to Chi 1040A. (B) View of experimental apparatus including Chi, monitor, microelectrode and connections.

3.3.2.2 **CE work**

The electrochemical experiments were performed with a CHI660C electrochemical workstation (Shanghai, China). The micro-electrode used in this experiment contained a three electrode configuration with a gold (Au) working electrode, a Ag/AgCl reference electrode and a Pt counter electrode. Pads and connections have been done in gold material.

3.4 Procedures

3.4.1 Fabrication of the Three Electrode System

3.4.1.1 Designing the Electrodes

A three electrode system was fabricated and consisted of gold (Au) as working electrode, platinum (Pt) as counter electrode and silver/silver chloride (Ag/AgCl) as reference electrode; as shown in Figure 3.2 (A). Design and fabrication of this electrode configuration was achieved using several steps including e-beam evaporation*. The electrodes dimensions are shown in Figure 3.2 (B).

(A) **(B)**

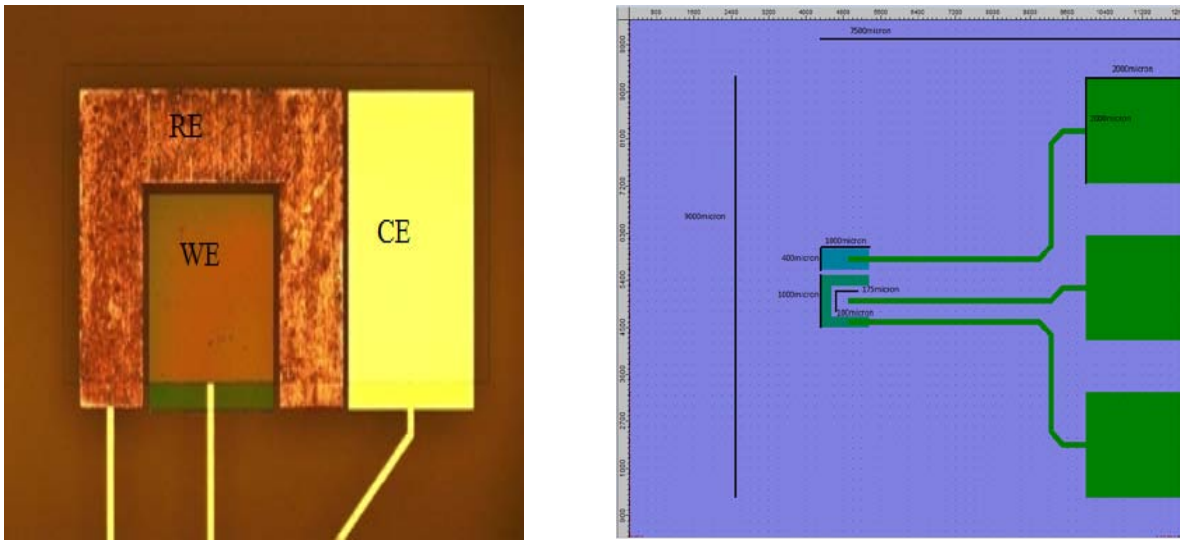

Figure 3.2: (A) Designs for the three electrode system and (B) dimensions of the electrodes (images are not in scale).

* Microchip was designed by Mr. R. Murphy and fabricated by Mr. D. O' Connell, Central fabrication, Tyndall National Institute.

3.4.1.2 **Steps involved in the fabrication of the microelectrodes**

Pattern for Au working electrode:

1. Acetate wafer was treated in O_2 asher for 2 mins at 50 W.

2. Acetate wafer was spin –coated with LOR3A lift-off resist at 3,000 rpm

3. Acetate wafer was hotplate-baked for 6 minutes at 115 °C.

4. Acetate wafer was spin-coated with Shipley S1805 imaging photoresist at 3,000 rpm.

5. Acetate wafer was hot-plate baked for 2 minutes at 115 °C.

6. Acetate wafers were aligned and exposed in KS MA1006 mask aligner with appropriate photomask (exposure dose = 40 mW/cm^2).

7. Acetate wafer was developed in Microposit MF319 developer for 1 minute and was rinsed with deionised water for 1 minute and blow dried with OFN
   .
8. Acetate wafer was oven-baked at 90 °C for 30 minutes.

9. Acetate wafer was loaded into Temescal FC2000 e-beam evaporator and pump down to $<5x10^{-7}$ T.

10. Acetate wafer was evaporated with Ti:Au (20 nm : 200 nm).

11. Acetate wafer had excess metal lifted off in baths of Microchem R1165 resist remover at 80 °C.

12. Acetate wafer was rinsed in running deionised water and blow dried with OFN.

Pattern for Pt counter electrode:

The wafer was patterned with the Pt counter electrode using the same lift-off process described in steps 1-12 above for the working electrode, using the appropriate photomask in step 6 and evaporating 100 nm of Pt instead of the Ti:Au in step 10.

Pattern for Ag/AgCl reference electrode:

Repeated steps 1-10 above. The method of electrochemical anodisation in HCl and chemical oxidation with aqueous $FeCl_3$ was much faster to perform and produced a uniform coating of AgCl. A 0.050 M solution of $FeCl_3$ was applied to the electroplated silver surface for 50 seconds at room temperature followed by rinsing with deionised water; dried with nitrogen and steps 11 and 12 above were then performed.

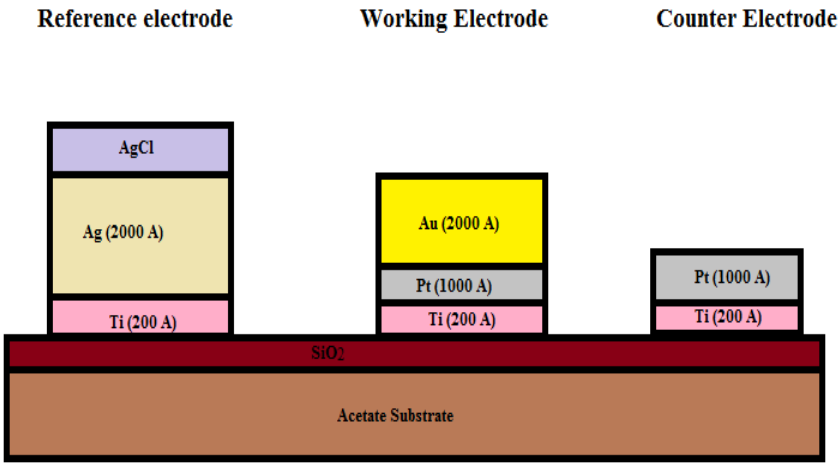

Figure 3.3 Schematic diagram of the different layers of the microchip

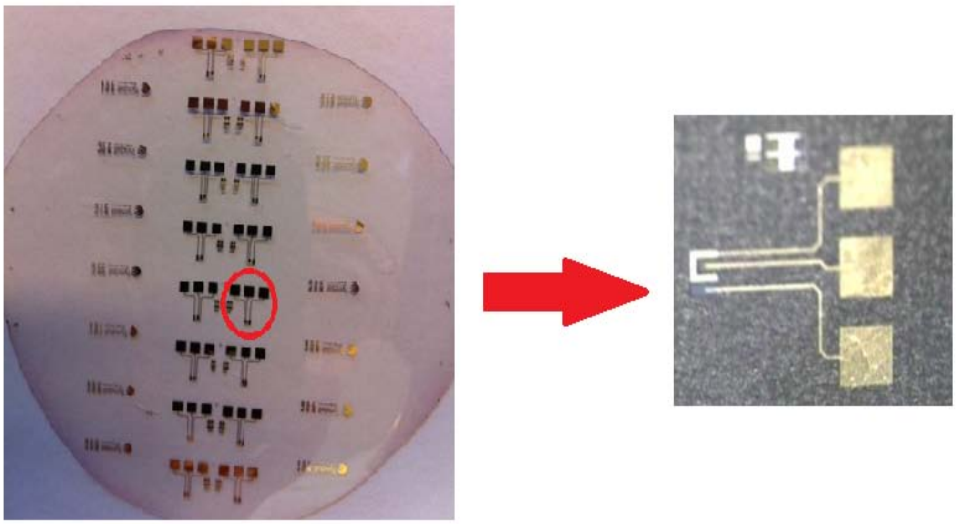

Figure 3.4 Acetate wafer and a close up view of an individual microelectrode

3.4.2 **Preparing electrode for CE**

3.4.2.1 **Acetate microelectrode with CE**

The microelectrode configuration was coupled with capillary electrophoresis to separate and detect a number of neurotransmitters including; tryptophan, dopamine, epinephrine and norepinephrine. The microelectrode was cut into a desirable shape and placed inside a vial cap to ensure it is held steady while the capillary is being aligned and throughout the CE run.

3.4.2.2 **Conventional 3-electrode system with CE**

The gold electrode was cleaned with wet silicon carbide paper, grid 1500 (Hand American Made Hardwood Products, South Plainfield, NJ), followed by polishing with 0.05 µM alumina slurry (Buehlar, Markham, ON, Canada) on velvet to a mirror finish. After 5 min of sonication in deionised water, the electrode was immersed in ethanol for 5 min sonication followed by another 5 min of sonication in deionised water once more. After these pre-treatments the electrode was allowed to dry at room temperature.

3.4.3 **Electrode system setup with Capillary Electrophoresis**

3.4.3.1 Conventional 3-electrode system

The capillary outlet was epoxy sealed into a pipette tip so that only ~1 cm protruded. The pipette tip was firmly attached vertically into a micromanipulator (HS6, World Precision Instruments, and Sarasota, FL, USA) with three-dimensional adjustment capabilities. A cylindrical cathodic /detection reservoir (2 cm diameter x 1 cm height) contained Pt wires (1 mm in diameter, 99.9 % purity), serving as the counter electrode for amperometric detection and the cathode for electrophoresis. An Ag/AgCl (3 M NaCl) reference electrode was placed vertically into the reservoir whereas the gold electrode was inserted upward from the reservoir's bottom and sealed with epoxy (the working reservoir volume was ~3 mL) (Figure 3.12). The micromanipulator and a laboratory jack (to which the reservoir was solidly mounted on) were attached to a solid breadboard to prevent movement during alignment. The capillary outlet was aligned to the detecting electrode using the micromanipulator with the aid of a surgical microscope (World Precision Instruments). The capillary outlet was adjusted until it touched the electrode surface (evident by a slight bend in the capillary observed by

microscopic inspection) and it was then backed off 25–30 μm using the micromanipulator's z-control. The gold electrode was connected to an electrochemical work station (CHI660C, CH Instruments, Austin, TX, USA) consisting also of a platinum wire (1 mm in diameter) as counter electrode and an Ag/AgCl (3 M NaCl) electrode as reference electrode. The gold electrode (1 mm in diameter), was purchased from Windsor Scientific (Slough, Berkshire, UK). The electrophoretic separation was conducted at -10 kV (reversed polarity) unless otherwise stated. A plastic cap with a central hole of ~1 mm was firmly attached to the surface of the gold electrode to reduce the active sensing area. The analyte sample was injected electrokinetically for 5 s at -10 kV. Peak identification was based on the migration time of a single standard with that of unknown peaks. The scheme of capillary electrophoresis system with conventional 3-electrode configuration for detection is shown in Figure 3.5.

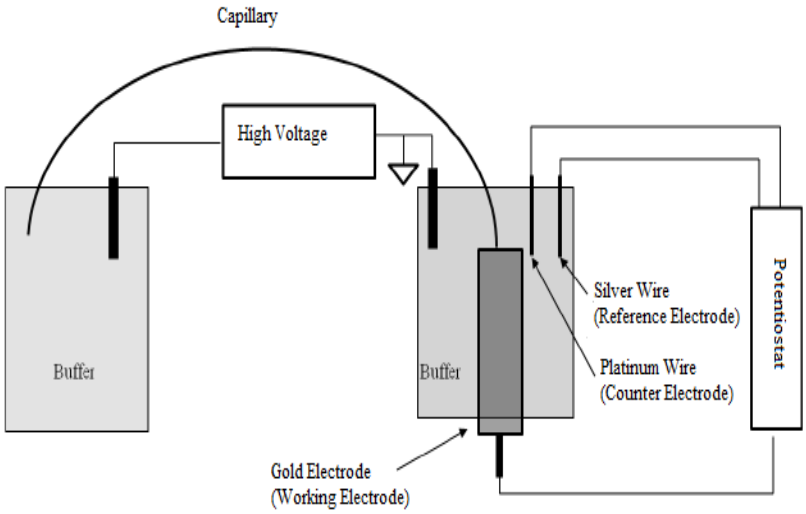

Figure 3.5: Scheme of the conventional 3-electrode system

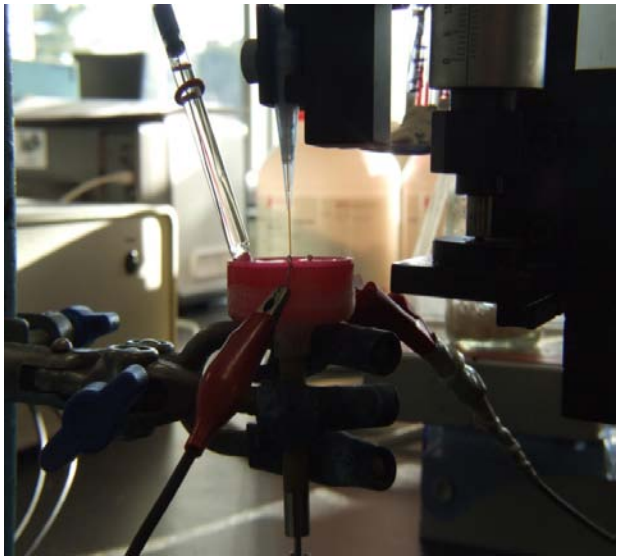

Figure 3.6: Setup of the conventional 3-electrode system which includes a Au working electrode, Ag/AgCl reference electrode and Pt wire for the counter electrode.

3.4.3.2 Acetate microelectrode

The capillary outlet was epoxy sealed into a pipette tip so that only ~1 cm protruded. The pipette tip was firmly attached vertically into a micromanipulator (HS6, World Precision Instruments, and Sarasota, FL, USA) with three-dimensional adjustment capabilities. A cylindrical cathodic /detection reservoir (1.5 cm diameter x 1 cm height) contained a Pt wire (1 mm in diameter, 99.9% purity), serving as the cathode for electrophoresis. The 3 microelectrode configuration consisted of Ag/AgCl reference electrode, gold working electrode and platinum counter electrode and was placed horizontally into the reservoir via a small slit that allowed it to fit into place and this slit was then sealed with epoxy (the reservoir volume was ~1 mL) (Figure 3.7). The micromanipulator and a laboratory jack (to which the reservoir was solidly mounted on) were attached to a solid breadboard to prevent movement during alignment. The capillary outlet was aligned to the detecting electrode using the micromanipulator with the aid of a surgical microscope (World Precision Instruments). The capillary outlet was adjusted until it touched the electrode surface (evident by a slight bend in the capillary observed by microscopic inspection) and it was then backed off 25–30 μm using the micromanipulator's z-control. The microelectrode configuration was then

connected to an electrochemical work station (CHI660C, CH Instruments, Austin, TX, USA). The electrophoretic separation was conducted at -10 kV (reversed polarity) unless otherwise stated. The analyte sample was injected electrokinetically for 5 s at -10 kV. Peak identification was based on the migration time of a single standard with that of unknown peaks.

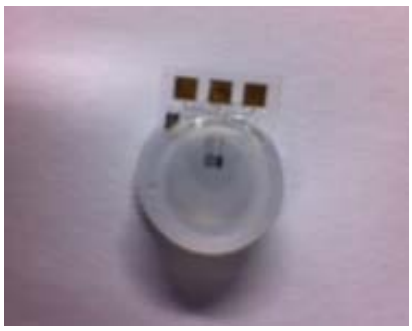

Figure 3.7: Setup of the microelectrode system

3.5 Results

3.5.1 **Initial Testing of microelectrodes**

3.5.1.1 **Electrochemical behaviour of UA at the microelectrode**

Cyclic voltammograms of 5.0 mM $Fe(CN)_6^{3-/4-}$ containing 0.1 M KCl were initially performed followed by CVs of 50 mM phosphate buffer pH 4 to investigate the electrochemical behaviour of UA with the electrode-configuration on acetate. First the microelectrode underwent CV in buffer only, then in buffer with 1.7 mM UA added. From overlaying the graphs, Figure 3.8, only one additional oxidation peak was observed in the buffer with UA at a potential of approximately 0.4 V, revealing that UA underwent an irreversible redox process on the microelectrode.

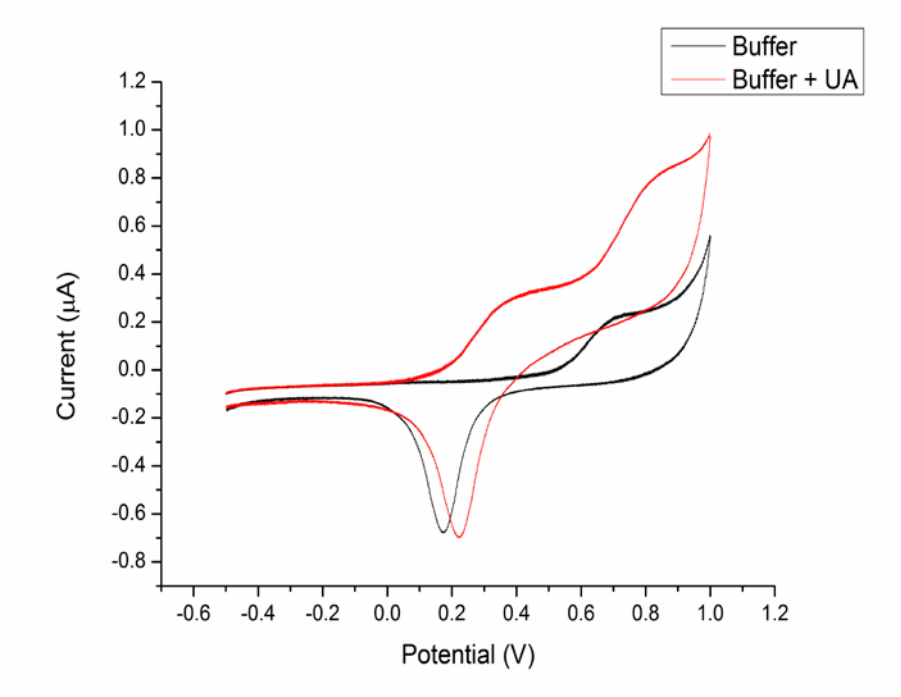

Figure 3.8: Cyclic voltammograms of acetate microelectrode configuration using a) 50 mM Phosphate buffer solution pH 4 and b) 50 mM Phosphate buffer solution pH 4 with 1.7 mM UA. Scan rate: 50 mV/s.

3.5.1.2 Effect of Scan Rate

The electrochemical behaviour of the acetate microelectrode was investigated using the redox couple: $[K_3Fe(CN)_6]$ / $[K_4Fe(CN)_6]$. It is clear that the redox peak currents of $[Fe(CN)_6]^{3-/4-}$ enhanced with increasing scan rate, suggesting quasi-reversible one-electron redox behaviour and can be seen in Figure 3.9. Both the anodic (Ipa) and cathodic (Ipc) were linearly proportional to the square root of the scan-rate ($V^{1/2}$) as can be seen in Figure 3.10. The linear regression equation for Ip_a (µA) = 0.3587X + 1.063, with a correlation coefficient of R^2 = 0.9998. The linear regression equation for Ip_c (µA) = -0.3463X – 0.8735, with a correlation coefficient of R^2 = 0.9999.) Since both Ipa and Ipc are linearly proportional, the peak current was controlled by the mass diffusion, showing a diffusion-controlled process in the solution.

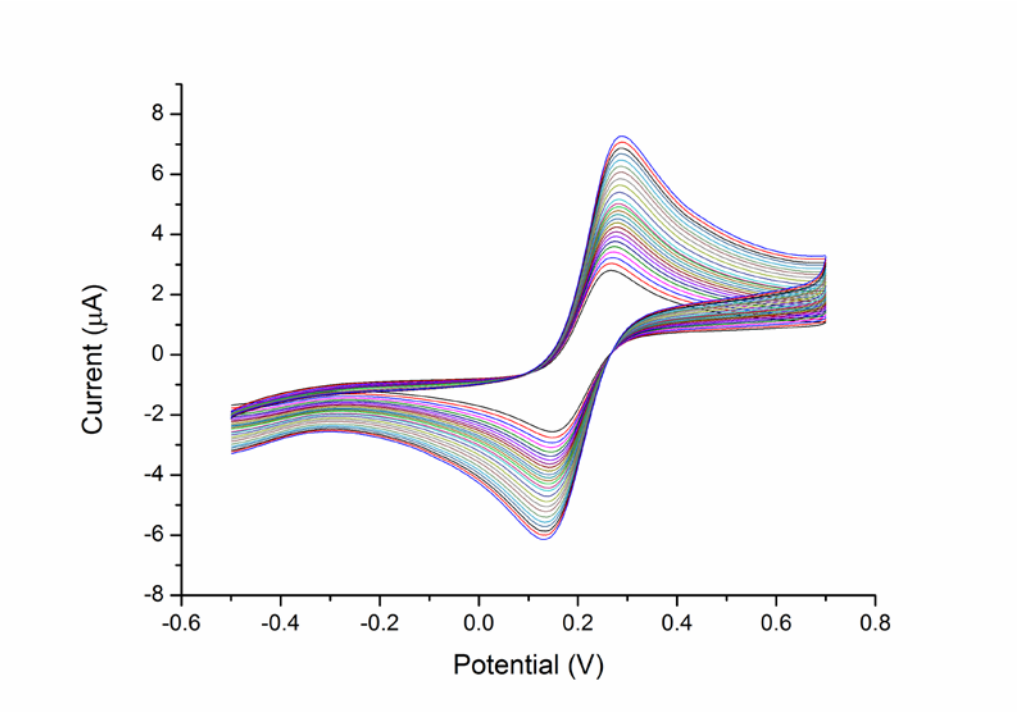

Figure 3.9: Cyclic voltammograms of acetate electrode in 5 mM $Fe(CN)_6^{3-/4-}$ containing 0.1 M KCl solution at scan rate from 50 to 400 mV/s.

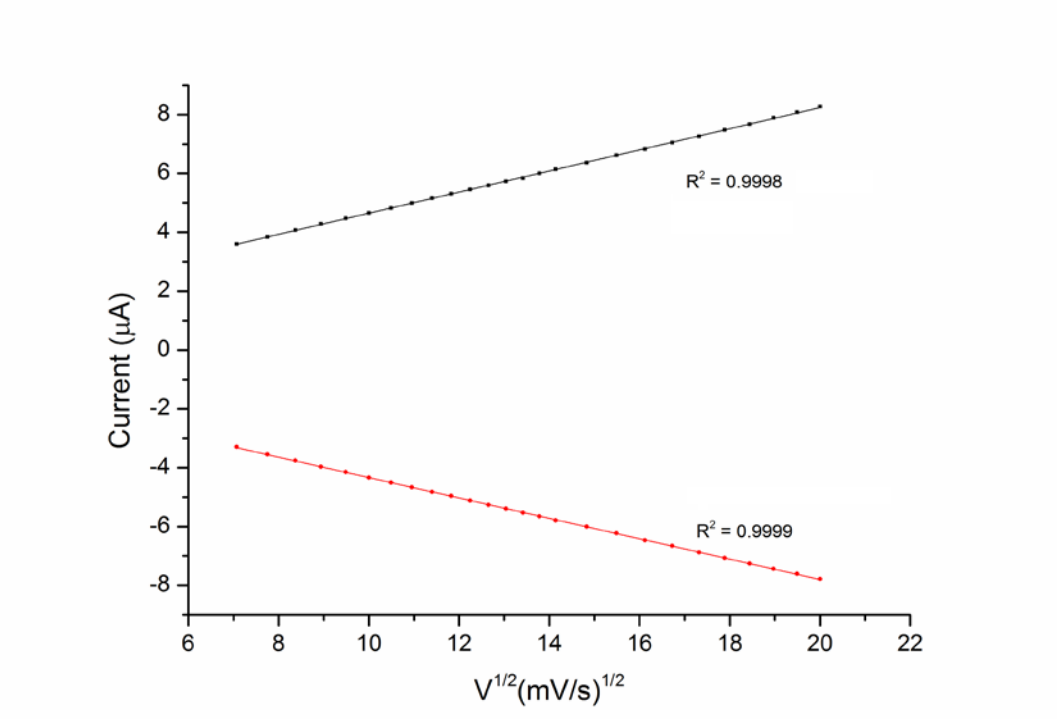

Figure 3.10: The plot of the anodic peak current versus square root of the scan rate.

3.5.1.3 Effect of solution pH

The effect of solution pH on the response of uric acid (UA) at the acetate gold electrode was investigated over the pH range of 3-7. Figure 3.11, shows that the anodic peak current increased up to pH 4 then began decreasing when the pH>4 and significantly decreased when the pH was above pH 6, thus the maximal current response of UA was observed at pH 4. The influence of solution pH on the peak potential (E_{pa}) and current response of UA at the acetate microelectrode in 50 mM Phosphate buffer solution was also investigated. The anodic peak potential of UA shifted negatively as pH increased, depicted in Figure 3.12, with the slope obtained from the linear behaviour between the applied potential and the pH for UA being 0.0576 V/pH, which is close to the anticipated Nernstian value (0.059 V/pH) for a two electons/two protons reaction.

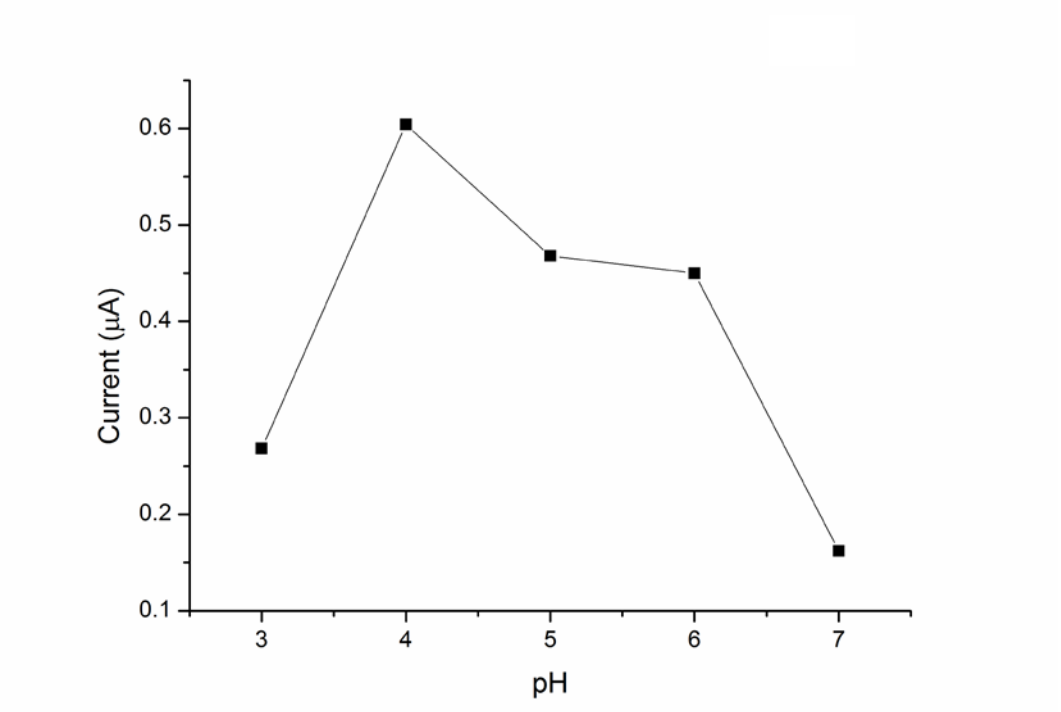

Figure 3.11: The plot of anodic current of UA versus pH values on cyclic voltammograms.

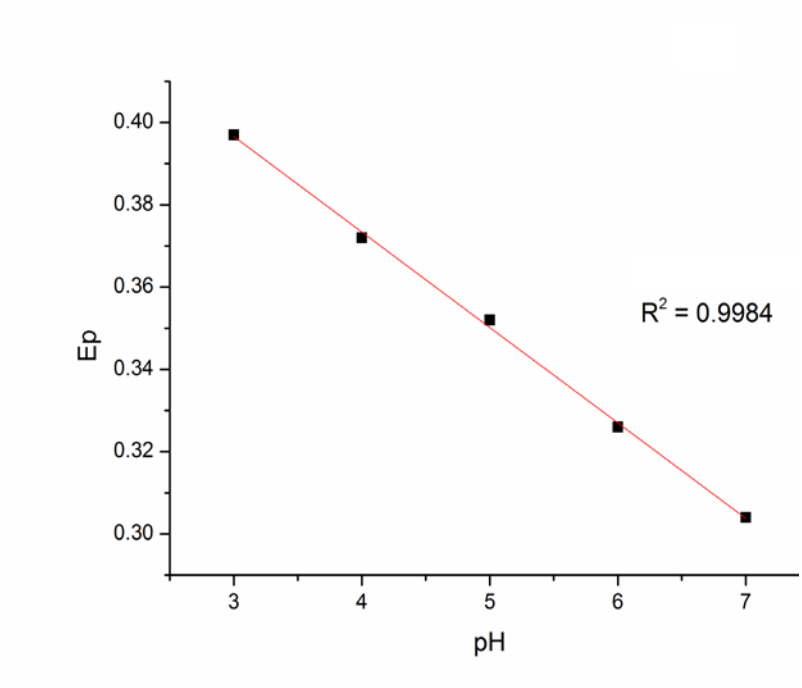

Figure 3.12: The linear relationship between the peak potential (EP) and solution pH of UA.

3.5.1.4 Determination of UA by Cyclic Voltammetry

The determination of UA concentration at the acetate microelectrode was performed with cyclic voltammetry. The oxidation peak current of UA was selected as the analytical signal. A six point calibration curve was prepared by analyzing a series of analyte standard solutions at different concentrations ranging from 1.7 x 10^{-3} M to 4.14 x 10^{-3} M, Figure 3.13. The linear regression equation was Ip$_a$ (µA) = 0.1024C – 0.8055, where Ip$_a$ (µA) is the peak current and C (µM) is the concentration of the analyte with a correlation coefficient of R^2 = 0.9992. The relative standard deviation of 5 successive scans was 3.06% for 2.73 x 10^{-3} M UA, indicating that the microelectrode on acetate substrate had good reproducibility. Under the optimum conditions, the detection limit (s/n = 3) for UA was calculated to be 59.8 x 10^{-6} M.

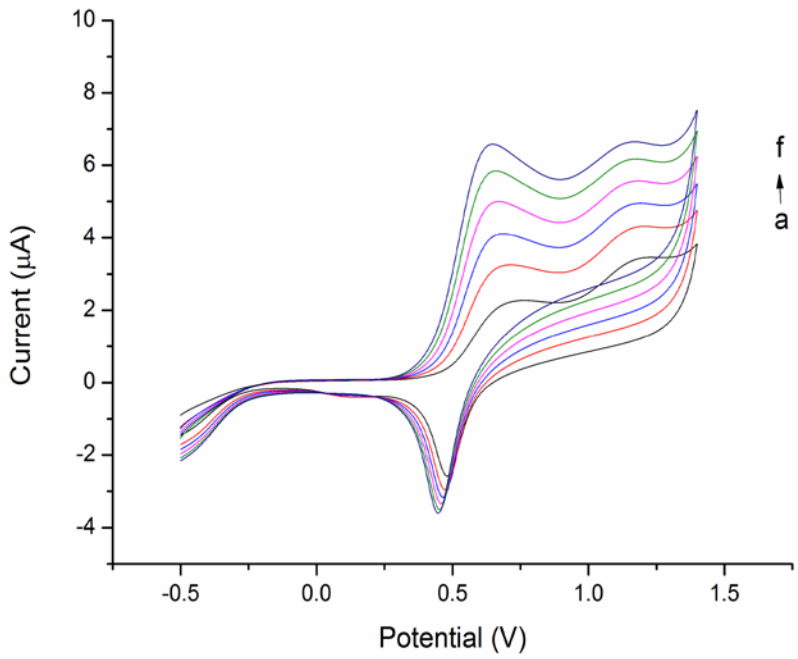

Figure 3.13: CVs of various UA concentrations (a-f); 1.7 x 10^{-3} M, 2.22 x 10^{-3} M, 2.73 x 10^{-3} M, 3.21 x 10^{-3} M, 3.68 x 10^{-3} M and 4.14 x 10^{-3} M at the acetate gold electrode in 0.05 mol L^{-1} PB solution in pH 4.0.

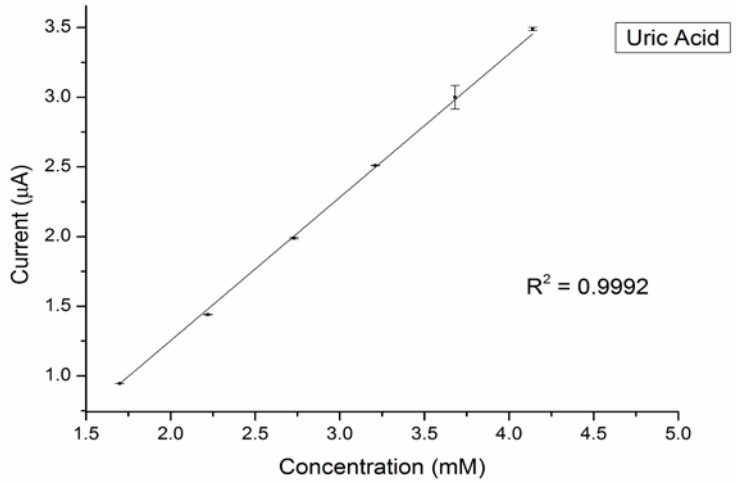

Figure 3.14: Calibration plot obtained from the CVs shown above.

3.5.1.5 Real sample analysis: determination of UA in human plasma serum

The human serum sample was diluted 5 times with phosphate buffer solution before the measurements to prevent the matrix effect of real samples. A certain value of standard solutions of UA was added into the corresponding plasma serum for testing recovery. The results obtained for UA in serum are listed in table 3.1. To ascertain the correctness of the result the serum sample was spiked with certain amounts of UA in about the same concentration as found in the samples.

Table 3.1: The recovery of UA in real-sample for the proposed method:

Analyte	Spiked (mM)	Found (mM)	Recovery (%)
UA	2.22	1.99	89.4±1.6
	2.73	2.53	92.67±2.3
	3.21	3.01	93.77±3.1

3.5.2 Coupling microelectrode with CE

3.5.2.1 $Na_2B_4O_7 \cdot 10H_2O$ solution, pH 9.5

The electrochemical responses of the acetate microelectrode and conventional 3-electrode system was characterised by cyclic voltammetry (CV) in 50 mM $Na_2B_4O_7 \cdot 10H_2O$ solution, pH 9.5 and can be seen in Figure 3.15. The background current of the conventional 3-electrode system is significantly higher as expected due to the much greater surface area of the conventional gold working electrode. The CV of the acetate electrode was very similar to that of the conventional which is typical of using a gold working electrode.

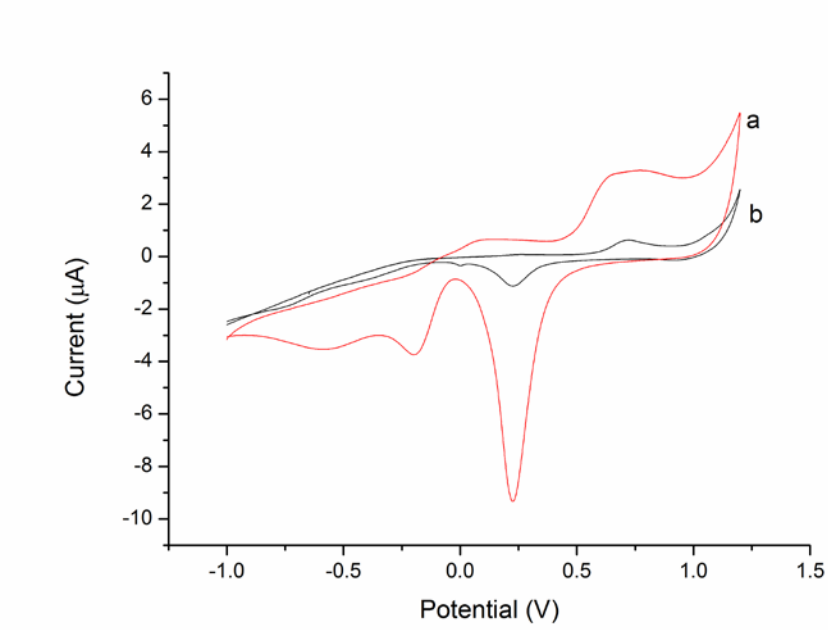

Figure 3.15 Cyclic voltammogram obtained at (a) the conventional 3-electrode system and (b) the acetate microelectrode in 50 mM $Na_2B_4O_7 \cdot 10H_2O$ solution, pH 9.5 at scan rate 100 mV/s.

3.5.2.2 Determination of analytes individually with the acetate microelectrode using cyclic voltammetry

The analytes were then individually determined using cyclic voltammetry and the results are shown in Fig 3.16.

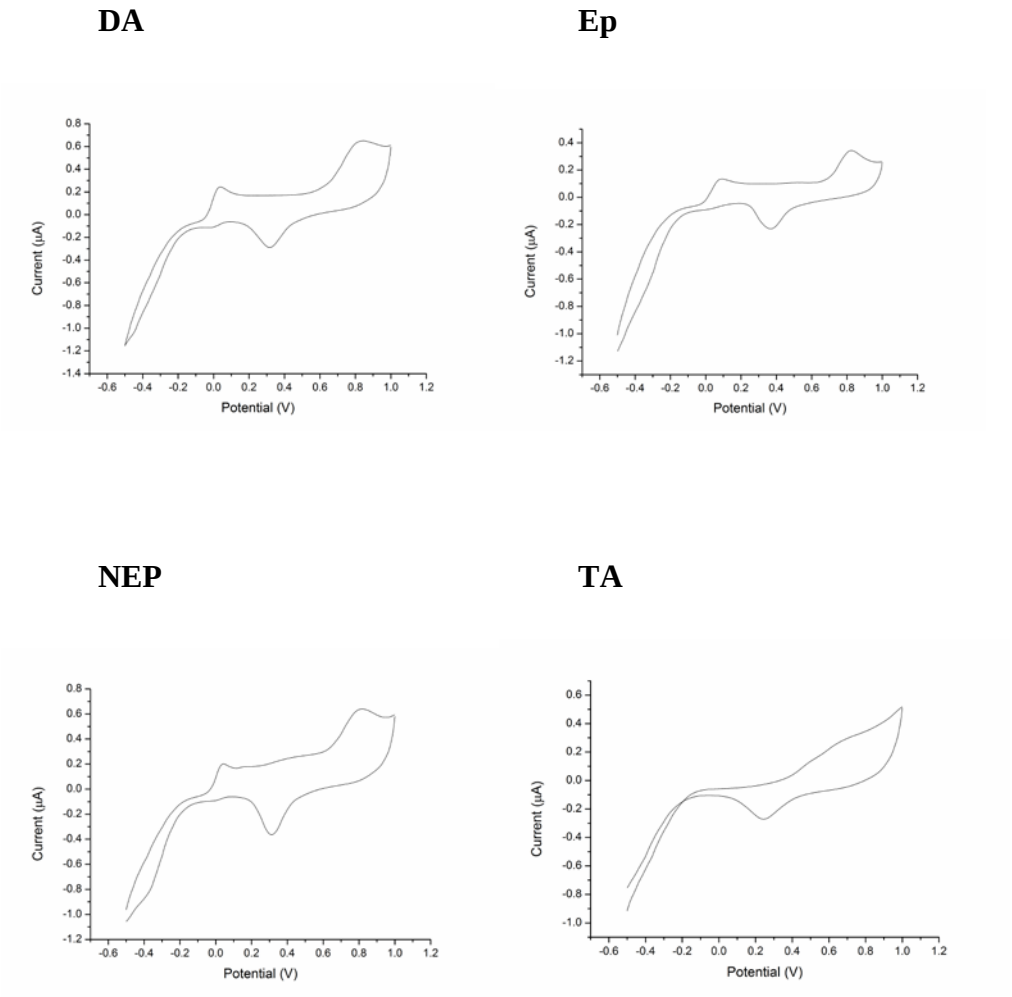

Figure 3.16: CVs obtained from the individual analytes using the acetate microelectrode in 50 mM $Na_2B_4O_7 \cdot 10H_2O$ solution, pH 9.5. All analyte concentrations are 100 µM.

3.5.2.3 Optimising conditions for acetate microelectrode coupled with CE

3.5.2.3.1 Effect of Injection time

Once the acetate microelectrode configuration was coupled with CE, the optimum conditions for the separation of the neurotransmitters were investigated. The injection time was first optimised and the results can be seen in Figure 3.17 below. With an injection time of 3 seconds the electropherogram obtained showed the first peak but the other three analytes were not well separated. Using an injection time of 7 seconds the electropherogram was not well resolved although there are 4 separated peaks. The five second injection time gave a good separation of all four analytes and was chosen as the optimum injection time.

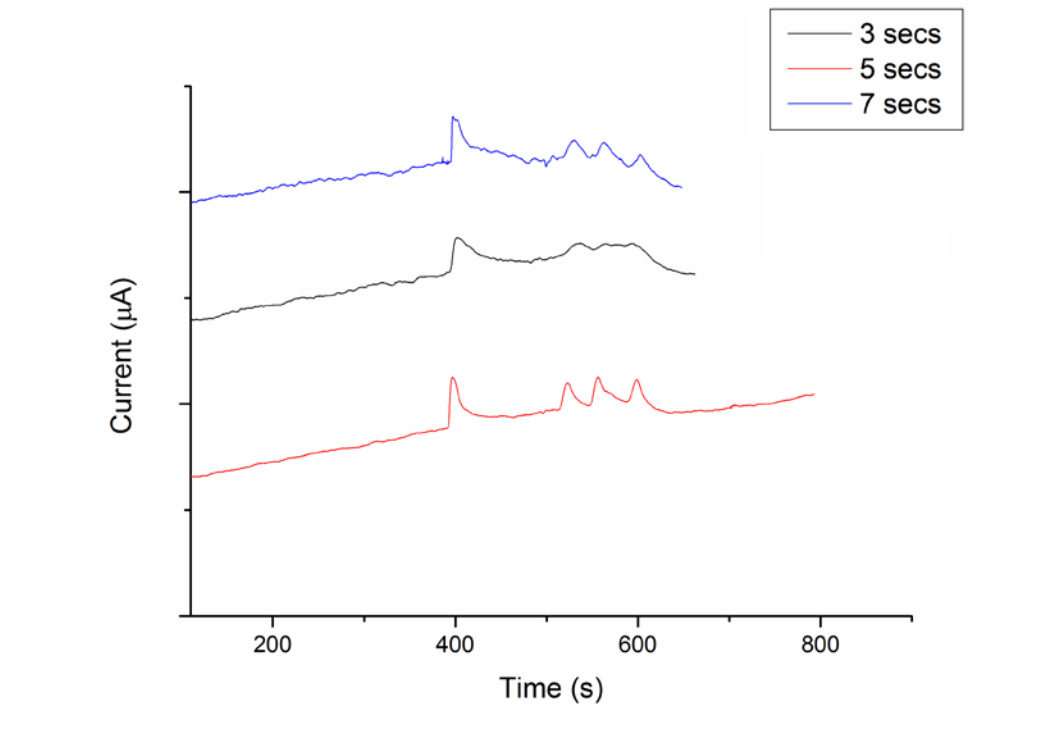

Figure 3.17: Electropherograms obtained from varying the injection time. Injection buffer: 50 mM $Na_2B_4O_7 \cdot 10H_2O$ solution, pH 9.5 and the running buffer was similar to the injection buffer. Acetate electrode poised at +0.9 V vs. Ag/AgCl. Concentration of analytes: 100 µM (each) TA, DA, Ep, NEP. Separation voltage: 10kV.

3.5.2.3.2 Effect of buffer pH

The effect of solution pH at the acetate gold electrode on the response of each of the four neurotransmitters was also investigated and can be seen in Figure 3.18. At pH 9 the peaks were all separated however they were in relatively close proximity to each other. At pH 10 the peaks did not seem to separate well however pH 9.5 gave an electropherogram with four well separated peaks and was chosen as the optimum pH.

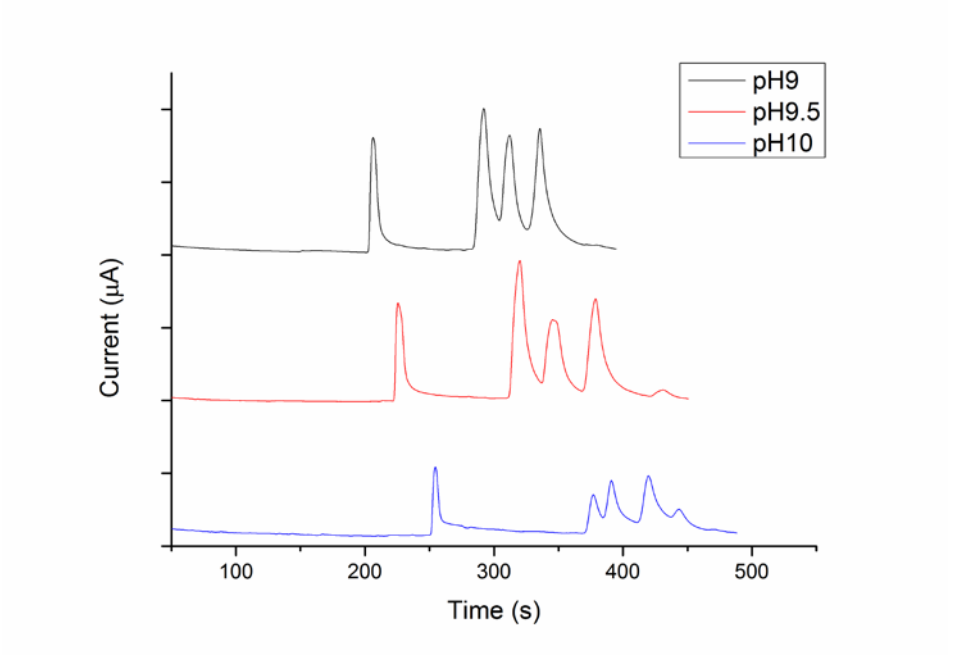

Figure 3.18: Electropherograms obtained from varying the buffer pH. Injection buffer: 25 mm $Na_2B_4O_7 \cdot 10H_2O$ solution, and the running buffer was similar to the injection buffer with an injection time of 5 s. Acetate electrode poised at +0.9 V vs. Ag/AgCl. Concentration of analytes: 600 µM (each) TA, DA, Ep, NEP. Separation voltage: 10 kV.

3.5.2.3.3 Effect of buffer concentration

The effect of the buffer concentration was also varied and the results are depicted in Figure 3.19. For all three variation of the buffer concentration, 15 mM, 25 mM and 50 mM all four analytes were separated. The main difference between the graphs was at 15 mM the analytes were all detected at an earlier time than the 25 mM and 50 mM. This was the same for the 25 mM buffer concentration with respect to the 50 mM. The 50 mM allowed all four peaks to be well separated from each other and this was chosen to be the optimal concentration.

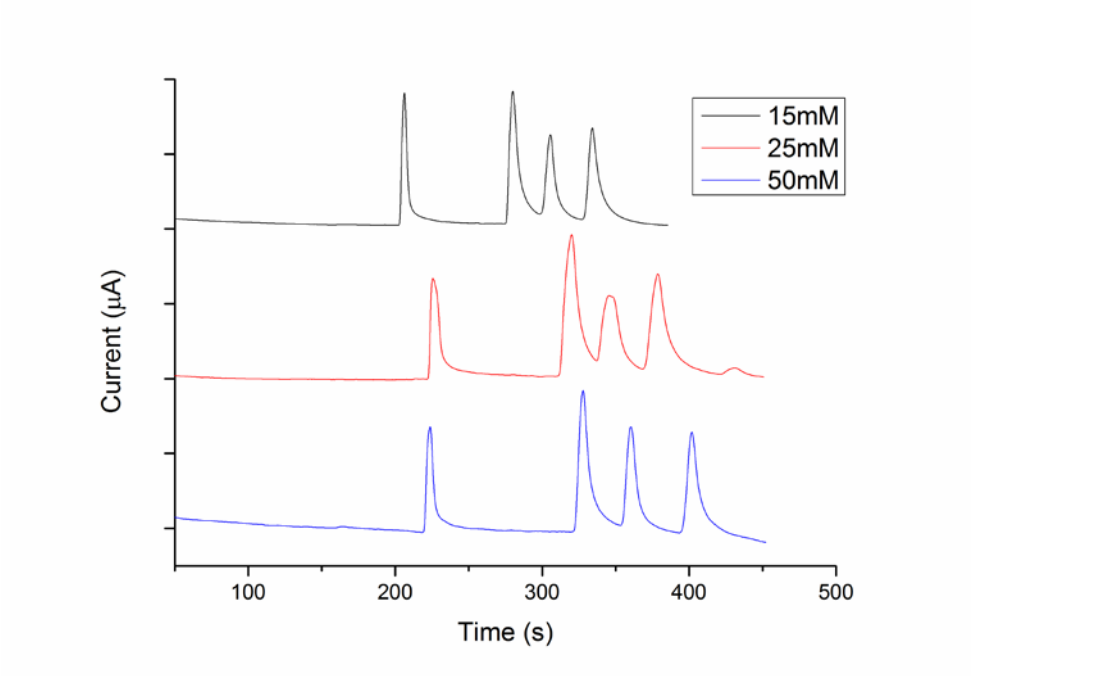

Figure 3.19: Electropherograms obtained from varying the buffer concentration. Injection buffer: varied concentration $Na_2B_4O_7 \cdot 10H_2O$ solution, pH 9.5, and the running buffer was similar to the injection buffer with an injection time of 5 s. Acetate electrode poised at +0.9 V vs. Ag/AgCl. Concentration of analytes: 600 µM (each) TA, DA, Ep, NEP. Separation voltage: 10kV.

3.5.2.4 Preparation of calibration curve of neurotransmitters using acetate microelectrode configuration

A calibration was carried out with aqueous standard solutions of 0.1, 0.2, 0.4, 0.6, 0.8, 1, 1.2 mmol (7 points). The curve of peak area versus concentration was found to be linear for this range. The following regression equations were obtained; TA: I(µM) = 0.202 C(µM) + 0.002; DA: I(µM) = 0.306 C(µM) – 0.002; Ep: I(µM) = 0.162 C(µM) – 0.008 and NEP: I(µM) = 0.205 C(µM) + 0.001. The corresponding correlation coefficient, R^2, was determined as 0.998 for tryptamine, 0.996 for dopamine, 0.994 for epinephrine and 0.985 for norepinephrine (n=3). The limits of detection (LOD, 3 x signal-to-noise) were; TA 40 µM; DA 12 µM; Ep 16 µM and NEP 30 µM (n=5). The results are summarized in Table 3.2.

Table 3.2 Linear ranges and detection limits of the analytes:

	Linear Range (mM)	Calibration Equation	R^2	Detection Limit (µM)	Recovery % 1 mM
TA	0.1-1.6	I(nA) = 0.202 C(µM) + 0.002	0.998	40	82.4
DA	0.1-1.6	I(nA) = 0.306 C(µM) - 0.002	0.996	12	90.0
Ep	0.1-1.2	I(nA) = 0.162 C(µM) - 0.008	0.994	16	87.8
NEP	0.1-1.2	I(nA) = 0.205 C(µM) + 0.001	0.985	30	84.3

3.5.2.5 Stability and Repeatability of the acetate microelectrode

The stability and repeatability of the acetate microelectrode was also studied. This was performed first by 5 replicates of the microelectrode to determine the relative standard deviation (RSD), which was found to be 4.45% for tryptamine, 1.81% for dopamine, 2.98% for epinephrine and 2.72% for norepinephrine. The microelectrode lost ca. 3.5% of its initial response after 2 days and could be used for at least 1 month, without significant loss of electrochemical signal.

3.5.2.6 Real sample analysis: determination of neurotransmitters in human plasma serum

A typical electropherogram of the half diluted plasma sample spiked with the same four neurotransmitters with a concentration of 1 mM each is shown in Figure 3.27. The % recovery of each of the neurotransmitters in the plasma are listed in table 3.2. Standard tryptamine, dopamine, epinephrine and norepinephrine were spiked into the plasma sample for peak identification. Dilution of the plasma sample also improved peak to peak separation and peak identification. All peaks were identified and the sequence was assigned as tryptamine, dopamine, epinephrine and norepinephrine. The blank sample gave a relatively stable baseline Figure 3.20.

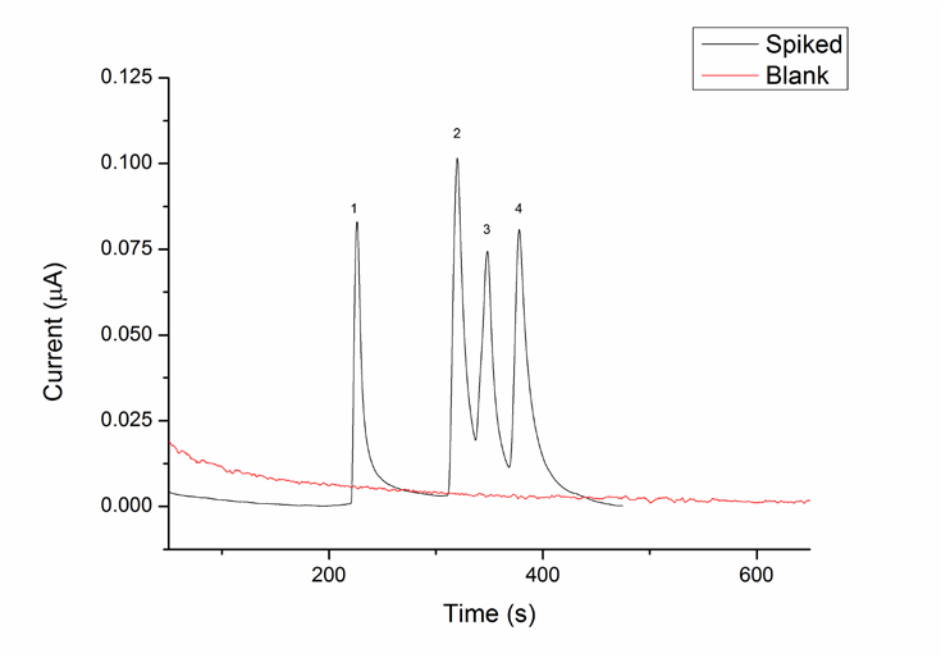

Figure 3.20: Electropherograms obtained from the plasma sample spiked with 1 mM TA, DA, Ep and NEP Injection buffer: 25 mM $Na_2B_4O_7 \cdot 10H_2O$ solution, pH 9.5, and the running buffer was similar to the injection buffer with an injection time of 5 s. Acetate electrode poised at +0.9 V vs. Ag/AgCl. Separation voltage: 10 kV. Order of elution; TA, DA, Ep and NEP.

3.5.2.7. Comparison of optimum microelectrode results with the conventional 3-electrode system

The acetate microelectrode's performance was then compared with the performance of the conventional 3-electrode system as shown in Figure 3.21 (A) and (B). The most notable difference between these 2 systems is the size of the working electrode's area. The area of the conventional Au electrode is 0.785 mm^2 and the acetate working electrode is 0.175 mm^2, so it is approximately 4.5 times smaller. The main difference between the Figures 3.21 (A) and (B) is the peak current which is approximately three times less for the acetate electrode however considering the size of the working electrode this is a satisfactory result.

(A)

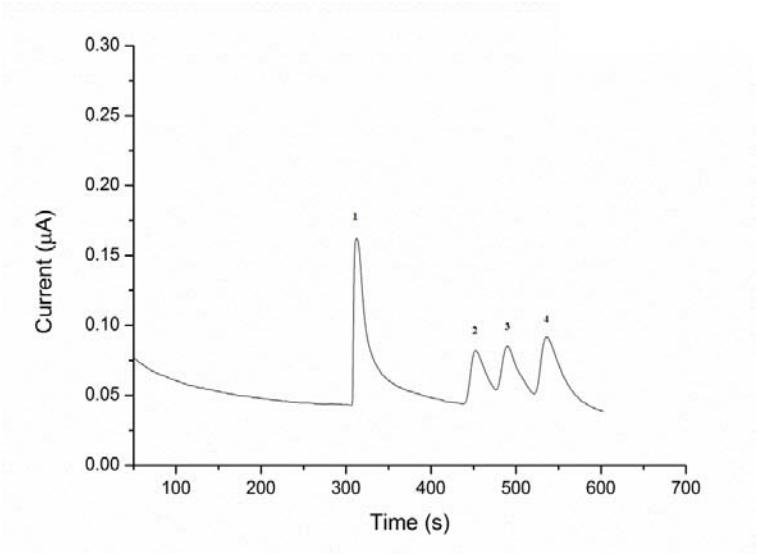

(B)

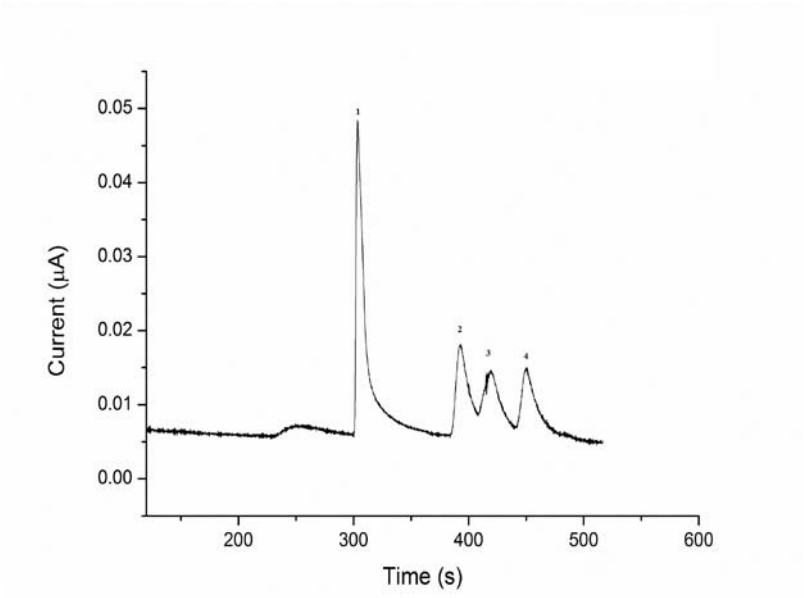

Figure 3.21: Electropherograms obtained from the separation of a standard sample (A) using the conventional 3-electrode system and (B) using the acetate microelectrode. Analyte concentrations are 500 µM TA and 200 µM DA, Ep and NEP. Injection buffer: 50 mM $Na_2B_4O_7 \cdot 10H_2O$ solution, pH 9.5, and the running buffer was similar to the injection buffer with an injection time of 5 s. Both electrodes poised at +0.9 V vs. Ag/AgCl. Separation voltage: 10 kV. Order of elution; TA, DA, Ep and NEP.

3.6 Conclusions and Future Work

In this chapter a novel microelectrode was fabricated onto inexpensive acetate substrate using photolithographic processes and etching techniques. The microelectrode configuration included a gold working electrode, platinum counter electrode and Ag/AgCl reference electrode. The fabrication was a success and the microelectrodes were then characterised and tested using electrochemical techniques. The microelectrode exhibited highly electrocatalytic activity to UA oxidation as well as excellent reproducibility and stability. The relative standard deviation between 5 successive scans was 3.06%. Successful attempts were made for the analysis of a real biological sample – serum, with the microelectrode giving an acceptable recovery value. Good reproducibility and recovery made itself attractive for further development in the field of electrochemical sensors. After the microelectrode's performance was characterised, it was then coupled with capillary electrophoresis. Once the conditions for the microelectrode were optimised, its performance was then compared with the conventional 3-electrode system. From these results it is clear that this novel microelectrode can be used to separate multiple neurotransmitters with very similar results to the more conventional three electrode system at a fraction of the cost.

Future work with this low-cost microdevice will include separating and detecting a number of different analytes including amino acids and chiral compounds.

3.7 Highlights

This chapter focused on fabricating a novel microelectrode configuration onto acetate substrate. This was made in Tyndall National Institute using several fabrication steps including e-beam evaporation.

Because the microelectrodes were on acetate substrate there was no requirement for a dicing step and the microelectrodes could be easily cut to a desired shape using a scissors.

The microelectrodes were first characterised to ensure good reproducibility and reliability. Once the initial testing of the microelectrodes was complete they were then coupled with capillary electrophoresis.

Several analytes were separated and detected and once the conditions were optimized the analytes were spiked into a real-sample, human plasma serum. The microelectrode gave good % recovery values as well as acceptable % RSD values.

The microelectrode configuration was then compared to the conventional 3-electrode system using the same materials as in the microelectrode - gold working electrode, platinum counter electrode and Ag/AgCl reference electrode.

3.8 References

[1] B. Bohl, R. Steger, R. Zengerle, P. Koltay, Journal of micromechanics and microengineering 15 (2005) 1125.

[2] R. Feng, R.J. Farris, Journal of micromechanics and microengineering 13 (2003) 80.

[3] M.J. Madou, Fundamentals of Microfabrication: The Science of Miniaturization, Second Edition, Taylor & Francis, 2002.

[4] W. Kern, Journal of the Electrochemical Society 137 (1990) 1887.

[5] M. Dineen, in, Oxford Instruments Plasma Technology, 2004.

[6] J.W. Jorgenson, K.D. Lukacs, Analytical Chemistry 53 (1981) 1298.

[7] J.W. Jorgenson, K.D. Lukacs, Journal of Chromatography A 218 (1981) 209.

[8] R.A. Wallingford, A.G. Ewing, Analytical Chemistry 59 (1987) 1762.

[9] J.C. Olsson, P.E. Andersson, B. Karlberg, A.-C. Nordström, Journal of Chromatography A 755 (1996) 289.

[10] F.D. Swanek, G. Chen, A.G. Ewing, Analytical Chemistry 68 (1996) 3912.

[11] M.-C. Chen, H.-J. Huang, Analytical Chemistry 67 (1995) 4010.

[12] F.-M. Matysik, A. Meister, G. Werner, Analytica chimica acta 305 (1995) 114.

[13] D. Müller, I. Jelínek, F. Opekar, K. Štulík, Electroanalysis 8 (1996) 722.

[14] H. Salimi-Moosavi, R. Cassidy, Analytical Chemistry 67 (1995) 1067.

[15] P.D. Voegel, W. Zhou, R.P. Baldwin, Analytical Chemistry 69 (1997) 951.

[16] W. Jin, W. Li, Q. Xu, Q. Dong, Electrophoresis 21 (2000) 1409.

[17] G.S. Owens, W.R. LaCourse, Journal of Chromatography B: Biomedical Sciences and Applications 695 (1997) 15.

[18] R.E. Roberts, D.C. Johnson, Electroanalysis 7 (1995) 1015.

[19] M. Zhong, S.M. Lunte, Analytical Chemistry 68 (1996) 2488.

[20] L.A. Colon, R. Dadoo, R.N. Zare, Analytical Chemistry 65 (1993) 476.

[21] H. Lin, D.-K. Xu, H.-Y. Chen, Journal of Chromatography A 760 (1997) 227.

[22] J. Ye, R.P. Baldwin, Analytical Chemistry 66 (1994) 2669.

[23] X. Fang, J. Ye, Y. Fang, Analytica Chimica Acta 329 (1996) 49.

[24] A.M. Fermier, L.A. Colón, Journal of High Resolution Chromatography 19 (1996) 613.

[25] Y. Li, X. Lin, Sensors and Actuators B: Chemical 115 (2006) 134.

[26] W.S. Waring, D.J. Webb, S.R.J. Maxwell, QJM 93 (2000) 707.

[27] W. Nyhan, Journal of autism and childhood schizophrenia 6 (1976) 235.

[28] V.W.R. H.A. Harper, P.A. Mayes, in Lange Medical Publication, 1979.

[29] S. Gjørup, H. Poulsen, E. Prætorius, Scandinavian Journal of Clinical & Laboratory Investigation 7 (1955) 201.

[30] H.M. Kalckar, Journal of Biological Chemistry 167 (1947) 429.

[31] E. Praetorius, Scandinavian Journal of Clinical & Laboratory Investigation 1 (1949) 222.

[32] W. Pudelkiewicz, M. Stutz, L. Matterson, Poultry Science 47 (1968) 1274.

[33] D.A. Mei, G.J. Gross, K. Nithipatikom, Analytical Biochemistry 238 (1996) 34.

[34] M.A. Ross, Journal of Chromatography B: Biomedical Sciences and Applications 657 (1994) 197.

[35] Y. Yue-dong, Biomedical Chromatography 12 (1998) 47.

[36] J. Ping, J. Wu, Y. Wang, Y. Ying, Biosensors and Bioelectronics 34 (2012) 70.

[37] E. Popa, Y. Kubota, D.A. Tryk, A. Fujishima, Analytical Chemistry 72 (2000) 1724.

[38] Z. yan, J.-R. Zhang, H.-Q. Fang, Analytical Letters 32 (1999) 223.

[39] J.-M. Zen, Analyst 123 (1998) 1345.

[40] J.-M. Zen, C.-T. Hsu, Talanta 46 (1998) 1363.

[41] D.A. Chambers, R.L. Cohen, R.L. Perlman, Neurochemistry International 22 (1993) 95.

[42] J. Bergquist, A. Ciubisz, A. Kaczor, J. Silberring, Journal of Neuroscience Methods 113 (2002) 1.

[43] K.A. Sagar, M.R. Smyth, Journal of Pharmaceutical and Biomedical Analysis 22 (2000) 613.

[44] T. Yoshitake, J. Kehr, S. Yoshitake, K. Fujino, H. Nohta, M. Yamaguchi, Journal of Chromatography B: Analytical Technologies in the Biomedical and Life Sciences 807 (2004) 177.

[45] X. Zhu, P.N. Shaw, D.A. Barrett, Analytica Chimica Acta 478 (2003) 259.

[46] E. Nalewajko, A. Wiszowata, A. Kojło, Journal of Pharmaceutical and Biomedical Analysis 43 (2007) 1673.

[47] M. Du, V. Flanigan, Y. Ma, Electrophoresis 25 (2004) 1496.

[48] J. Kang, X.B. Yin, X. Yang, E. Wang, Electrophoresis 26 (2005) 1732.

[49] J. Bergquist, J. Silberring, Rapid Communications in Mass Spectrometry 12 (1998) 683.

[50] M. Chicharro, A. Sánchez, A. Zapardiel, M.D. Rubianes, G. Rivas, Analytica Chimica Acta 523 (2004) 185.

[51] T.L. Paxon, P.R. Powell, H.G. Lee, K.A. Han, A.G. Ewing, Analytical Chemistry 77 (2005) 5349.

[52] L.K. Abdulrahman, A.M. Al-Abachi, M.H. Al-Qaissy, Analytica Chimica Acta 538 (2005) 331.

Chapter 4

Modification of Macro electrodes using metal nanoparticles and carbon monolith

4. SPE modified with metal nanoparticles and carbon monolith

4.1 Objectives

This chapter focuses on modifying screen printed electrodes (SPEs) to allow for simultaneous determinations of multiple analytes which is rarely reported as the SPEs are unable to discriminate between signals. There were two aims of this chapter. The first was to modify an in-house screen printed electrode (SPE) with metal nanoparticles, gold and palladium, electrodeposited onto it. The second was to modify the SPE with carbon monolith material and again metal nanoparticles electrodeposited onto the material.

4.2 Introduction

Screen-printed electrodes are planar devices with plastic substrates that are coated with layers of electroconductive and insulating inks at a controlled thickness. The advent of screen-printed (thick-film) technology has made it possible to mass-produce inexpensive disposable electrodes for use with electrochemical instruments [1-4]. In recent years, screen-printed electrodes (SPEs) have attracted considerable attention in electrochemical sensing due to the inexpensive, rapid and simple manufacturing process. However, the use of the SPEs for simultaneous determination of DA and UA has been rarely reported, since the unmodified SPEs are unable to discriminate the signals. There are reports of coating the SPEs with electrocatalytic films, such as polyacrylic acid–carbon nanotubes [5] and iridium oxide [6], for the selective determination of these compounds. However, sensitivity and reproducibility of these electrodes is poor and the fabrication process is complex.

The great versatility of screen-printed electrodes resides in their wide range of possible modifications. In fact, the composition of the inks used in the printing process can be modified by the addition of substances of a very different nature, such as metals, enzymes, polymers, complexing agents, etc. There are numerous methods describing the synthesis of metallic nanoparticles in solution as well as by deposition on solid surfaces. They include chemical synthesis by means of reduction with different reagents [7], UV light or electron-beam irradiation [8] and electrochemical methods[9-14]. The latter provides an easy and rapid alternative for the preparation of metallic nanoparticle electrodes within a short period

of time. The combination of electrodeposition and the screen-printing process is beginning to allow mass production of electrochemical sensors that possess various catalyst activities. The sensor strips fabricated by this process are promising tools with more sensitive detection rates that are now starting to come on stream.

Noble metal nano-structures like gold and palladium have attracted tremendous attention in recent decades, due to their excellent optical, electrochemical and electronic properties [15-17], which are different from those of bulk metal materials. Particularly, due to the unique properties of these metal nanoparticles, such as good conductivity, useful electrocatalytic and biocompatibility, several researchers utilized Au and Pd nanoparticles to fabricate electrochemical sensors and biosensors [18-22].

Dopamine (DA) is an important neurotransmitter in the mammalian central nervous system. Low levels of the neurotransmitter may be an indication of a neurological disorder, such as Parkinson's disease and schizophrenia [23]. DA is currently the subject of intense research focus to neuroscientists and chemists and it is essential to develop rapid and simple methods for its determination. The common instrumental techniques like high performance liquid chromatography (HPLC) have been widely used for the determination of DA [24]. However, such methods are often complicated and very expensive. The electrochemical oxidation of DA has been studied and the results show that the electrochemical oxidation is a two-electron process with transfer of two protons [[25]. The various inorganic and organic materials [26], Langmuir-Blodgett (LB) film [27], microfluidics system [28], sol-gel material based electrodes [[29]], enzymeless biosensor [30], enzyme amplification system [[31] and voltammetric electrodes [32] have all been reported for the oxidation of DA.

Ascorbic acid (AA) (vitamin C) is present in both animals and plants and is a vital component in the human diet. Among animal organs, the liver, leukocytes and anterior pituitary lobe show the highest concentrations of AA [23]. It is present in mammalian brains along with several neurotransmitter amines. AA has been utilised and used for the prevention and treatment of the common cold, mental illness, infertility, cancer and AIDS. It is also used in foods and drinks as an antioxidant. The Prussian blue [33], ruthenium (III) diphenyldithiocarbamate [34], polypyrrole/ferrocyanide [35], polyaniline [36], polyglycine [37], poly(*N*,*N*-dimethylaniline) [38], poly(*p*-aminobenzene sulfonic acid) [39] have been

used to fabricate modified electrode which can enhance the electron transfer rate and reduce the overpotential for the oxidation of AA.

Uric acid (UA) is the primary end product of purine metabolism. Several diseases such as gout, Lesch-Nyhan syndrome and hyperuricemia are believed to occur due to abnormal levels of UA in the body [40-41]. It is therefore essential to develop rapid methods, preferably simple and inexpensive, for the determination of UA in routine analysis. In general, electroactive UA can be irreversible oxidised in aqueous solution and the major product is allantoin [42]. Although there are several techniques available for the determination of UA including spectrophometry [43-46] and chromatography [47-49], electrochemical detection of UA has received much interest due to its biological importance and easy oxidation properties [50-53]. Electrochemical sensors also have the ability to be miniaturised for implanting. More information is provided on UA in Chapter 3 section 3.2.9.1.

In this chapter the SPE has been characterised and modified in situ with first electroplated gold (Au) nanoparticles and then palladium (Pd) nanoparticles. The new electrodes have been characterised using electrochemical methods such as cyclic voltammetry (CV), electrochemical impedance spectroscopy (EIS) and amperometric (I-t) curve. The surface topology has been studied using scanning electron microscopy (SEM). The SPE with metal nanoparticles exhibited far superior results compared to the unmodified SPE with respect to both sensitivity and selectivity.

This chapter also introduces a new class of carbonaceous nanomaterial that is carbon monolith, which has established itself as a new class of carbon materials. This new material is exhibiting very interesting physicochemical properties [54] and its high surface area makes it a potential material for sensors and biosensors. The SPE modified with CM has been characterised and modified in situ with first electroplated gold (Au) nanoparticles and then palladium (Pd) nanoparticles. The new electrodes were once again characterised using the electrochemical methods mentioned above. The surface topology has once again been studied using scanning electron microscopy (SEM). The SPE/CM with metal nanoparticles exhibited once again superior results compared to the SPE and SPE/CM. The use of the carbon monolith increased the surface area of the SPE surface and thus allowed for better results than the other modified electrodes with metal-nanoparticles respect to both sensitivity and

selectivity. This work modifies simple SPE in an inexpensive and fast fabrication process which then allows multiple analytes to be detected simultaneously.

4.3 Experimental

4.3.1 Reagents

All the chemicals used were of analytical grade with highest purity and aqueous solutions were prepared with deionised water (18.2 $M\Omega.cm^{-1}$) using a Milli-Q (Millipore, Bedford, MA) water purification system.NaH_2PO_4, Na_2HPO_4, H_3PO_4, $[Fe(CN)_6]^{3-/4-}$, HAuCl4.3$H_2$0, , K_2PdCl_4, uric acid and dopamine were purchased from Sigma - Aldrich (Dublin, Ireland).

Stock solution of DA (0.010 mol L^{-1}) (cat no: H8502) was prepared daily by dissolving a suitable amount of the reagent in water and was kept in the dark before use. UA (cat no: U0881) solution (0.05 mol L^{-1}) was prepared by first dissolving it in a small volume of 0.1 M NaOH solution and diluted with water. AA (cat no: A5960) solution (0.05 mol L^{-1}) was prepared daily by dissolving a suitable amount of the reagent in water.

Phosphate-buffers of desired pH values were prepared by mixing solutions of 0.1 M NaH_2PO_4 and 0.1 M Na_2HPO_4 at different ratios. The pH values were adjusted by H_3PO_4 solution. Buffers and samples were sonicated for 5 minutes before use.

4.3.2 Apparatus

The electrochemical experiments were performed with a CHI1040A electrochemical workstation, Figure 4.1, (set-up) at room temperature. A three electrode system consisting of a screen printed working electrode (16 mm^2), a Ag/AgCl (3M NaCl) reference electrode and a platinum wire counter electrode (Sigma-Aldrich, Dublin, Ireland). Magnetic stirring was performed during the amperometric determination of this experiment.

Figure 4.1: Experimental Apparatus which includes the Chi1040A with monitor attached to3-electrode system, SPE, Ag/AgCl electrode and platinum wire.

4.3.3 Procedures

4.3.3.1 Fabrication of the Screen-Printed Electrode

The SPE were prepared using Electrodag 423 SS carbon ink, Electrodag 477 SS silver ink for conductor paths, and a Matt Vinyl White MV27 (Apollo td., London, UK) for insulation layers. Screen-printer DEK 247 was used for printing. The squeegee velocity was set to 4. Each layer was left for one hour at 90 ºC in order to achieve compact and reproducible layers as well as to evaporate the solvent in order to obtain a dry path. After printing the last path, the electrodes were cured at 80ºC overnight. The electrode area was 4 x 4 mm, i.e. 16mm^2.The electrode should be washed before any measurements are carried out to remove any weakly bound carbon particles from the surface. Figure 4.2 illustrates the SPE design and layer development.

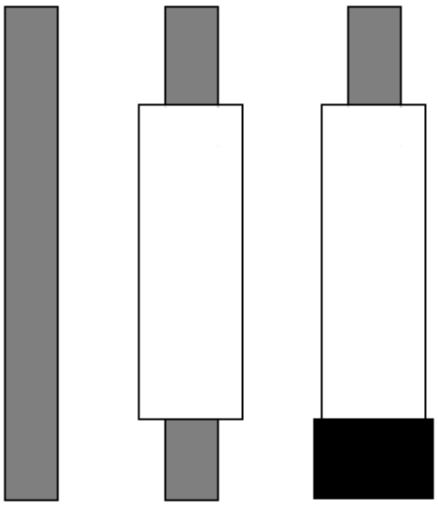

Figure 4.2: SPE design and layer development

4.3.3.2 Protocol for modifying the SPE with gold and palladium nanoparticles

The SPE has been electroplated with Au nanoparticles by applying a potential of -0.2 V (vs. Ag/AgCl) for a period of time under stirring in 0.5 M H_2SO_4 solution containing 0.2 mM Au nanoparticles for 40 seconds. The electrode was then rinsed with H_2O and introduced into phosphate buffer solution pH 4 and stabilised by applying a potential of -500 mV to 1000 mV with a scanrate of 500 mV/s using CV until a steady voltammogram was obtained. The same procedure was carried out using Pd nanoparticles again 0.2 mM Pd nanoparticles in 0.5 mM H_2SO_4.

4.3.3.3 Protocol for modifying the SPE with CM

This electrode has been coated with carbon monolith (CM) material that was obtained from Dublin City University, Dublin, Ireland. This new carbonaceous material is exhibiting very interesting physicochemical properties and characterisation results can be seen in a previous paper [54]. Briefly, a weight of 5mg CM was dispersed in 1 mL N,N-dimethyformamide

(DMF), then sonicated for 16 hours until a homogenous suspension was obtained. Then 5 µL of CM dispersion was carefully dropcast on the SPE and the solvent was allowed to evaporate off at room temperature. Once the solvent evaporated the SPE/CM was modified with the Au and Pd nanoparticles using the same procedure as 4.3.3.2.

4.3.3.4 Protocol for drop angle measurement

The measurement of the contact angle of the SPE, and the SPE/Au was conducted at the Tyndall National Institute, UCC, Cork. The contact angle analysis was performed using the sessile drop method on a Contact Angle System OCA 30, DataPhysics Instruments GmbH, Germany. The contact angle between a droplet of water and the surface of the SPEs was determined using the following procedure. The SPE was placed on a raised platform of the instrument which was monitored by a digital camera. This allowed for a magnified image of the water surface to be viewed on the computer screen. The height and position of the platform was adjusted as was the focus of the camera to ensure a clear image of the camera to ensure a clear image of the electrode in the correct position is obtained. The instrument holder with a syringe was positioned approximately 1 cm above the electrode's surface. A droplet of deionised water was dispensed automatically from the syringe onto the electrode surface at a rate of 5 µL at 0.5µL/s. Once the droplet was released onto the electrode's surface it assumed a position in relation to the properties of the surface of the electrode. The angle formed between the liquid/solid interface is the contact angle. A high resolution camera captured and analysed the contact angle for each of the SPE and the SPE/Au. Prior to each contact angle being measured, each electrode was cleaned by nitrogen gas to ensure a clean surface. The contact angle of the droplet of water with each of the electrodes was determined using the sessile drop method, which is an optical contact angle measurement. The sessile drop method involves the measurement of the contact angle between the baseline of the drop and the tangent at the drop boundary.

4.3.3.5 Protocol for Electrochemical Impedance Spectroscopy (EIS)

For the impedance measurement, a Frequency Response Analysis (FRA) is used to impose a small amplitude AC signal to the SPE. The impedance behaviour of the electrode is determined by analysing the AC voltage abd current response at frequencies ranging from 1 Hz to 1 kHz. Measurements were carried out in the presence of a 5 mM redox probe $[Fe(CN)_6]^{3-/4-}$ in 0.1 M KCl at an applied potential of +0.025V with amplitude of 0.1 V. All measurements were recorded at room temperature.

4.3.3.6 Studies on the influence of Scan Rate

In order to study the influence of the san rate, the SPE and the modified SPE were scanned between -1 V and +1 V in 5 mM $[Fe(CN)_6]^{3-/4-}$ in 0.1 M KCl. Measurements were carried out using different scan rates from 50 to 400 mV s^{-1} versus Ag/AgCl.

4.3.3.7 Cyclic Voltammetry (CV)

CV measurements were carried out with a Chi 1040A instrument.The measurements were all performed at room temperature with a scan rate of 50 mV s^{-1}.

4.4 Results

The results section will be broken up into two areas. The first set of results will be for the SPE with metal nanoparticles. The second set of results will be for the SPE with carbon monolith and metal nanoparticles. For both sections the results will include characterisation data, cyclic voltammogramms, EIS measurements and real sample analysis data.

4.4.1 SPE/Au nanoparticles

This section will be further broken up into two areas. The first set of results will be for the SPE with Au nanoparticles. The second set of results will be for the SPE with Pd nanoparticles.

4.4.1.1 Characterisation using SEM of the SPE with gold nanoparticles

The modified electrode's morphology was investigated using scanning electron microscopy (SEM). The SEM is a microscope that uses electrons instead of light to form an image. The SEM has a large depth of field, which allows more of a specimen to be in focus at one time. The SEM also has much higher resolution, so closely spaced specimens can be magnified at much higher levels. Because the SEM uses electromagnets rather than lenses, the researcher has much more control in the degree of magnification. All of these advantages, as well as the actual strikingly clear images, make the scanning electron microscope one of the most useful instruments in research today. The SEM model used in this research was an FEI FEG 650 scanning electron microscope.

The SEM image of the SPE can be seen in a Fig 4.3 (A). The imaging showed the bare surface of the SPE with Au nanoparticles Fig 4.3 (B) and Fig. 4.3 (C) shows the magnified image of the SPE with gold nanoparticles dispersed on the surface. The shiny clusters scattered around the SPE are the Au nanoparticles.

(A) **(B)** **(C)**

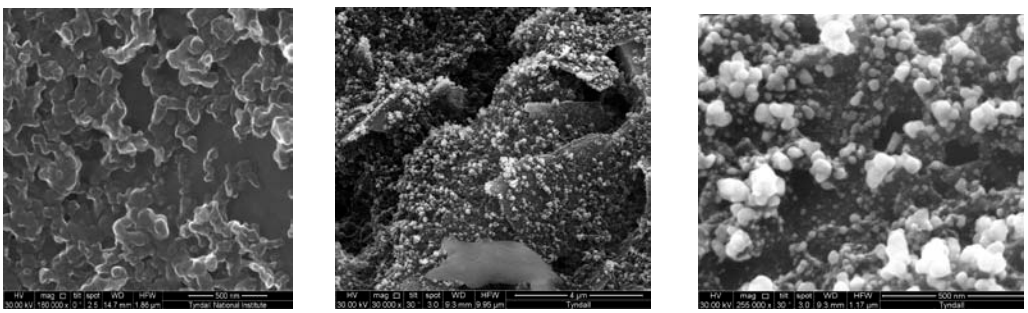

Figure 4.3: The SEM images (A) of the SPE, (B) of the bare surface with Au nanoparticles, (C) of the bare surface with Au nanoparticles magnified.

4.4.1.2 Contact-angle measurement of SPE and SPE/Au

The measurement of the contact angle of the SPE, and the SPE/Au was conducted at the Tyndall National Institute, UCC, Cork as discussed in section 4.3.3.4. The SPE has a contact angle of 118.7 º. Fig 4.4 (A) which suggests it has a relatively hydrophobic surface area. The SPE/Au has a contact angle of 95 º Fig 4.4 (B) which indicates that the Au caused the surface to become less hydrophobic.

(A) **(B)**

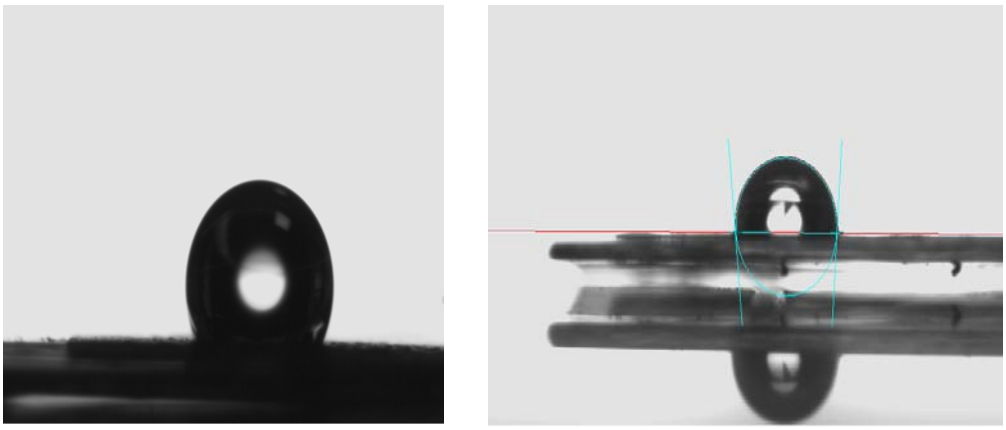

118.7º **95º**

Figure 4.4: Images of water droplet on surface of (A) SPE (CA = 118.7º) and (B) SPE/Au (CA = 95º)

4.4.1.3 Electrochemical behaviour of SPE and SPE/ Au

4.4.1.3.1 Compare Cyclic Voltammogramms

The electrochemical responses of a SPE, and a SPE/Au were characterised by cyclic voltammetry (CV) in phosphate buffer solution (PB) at pH 5 and can be seen in Fig. 4.5.The background current of the SPE/Au has increased, indicating that the bare electrode was modified efficiently with gold nanoparticles.

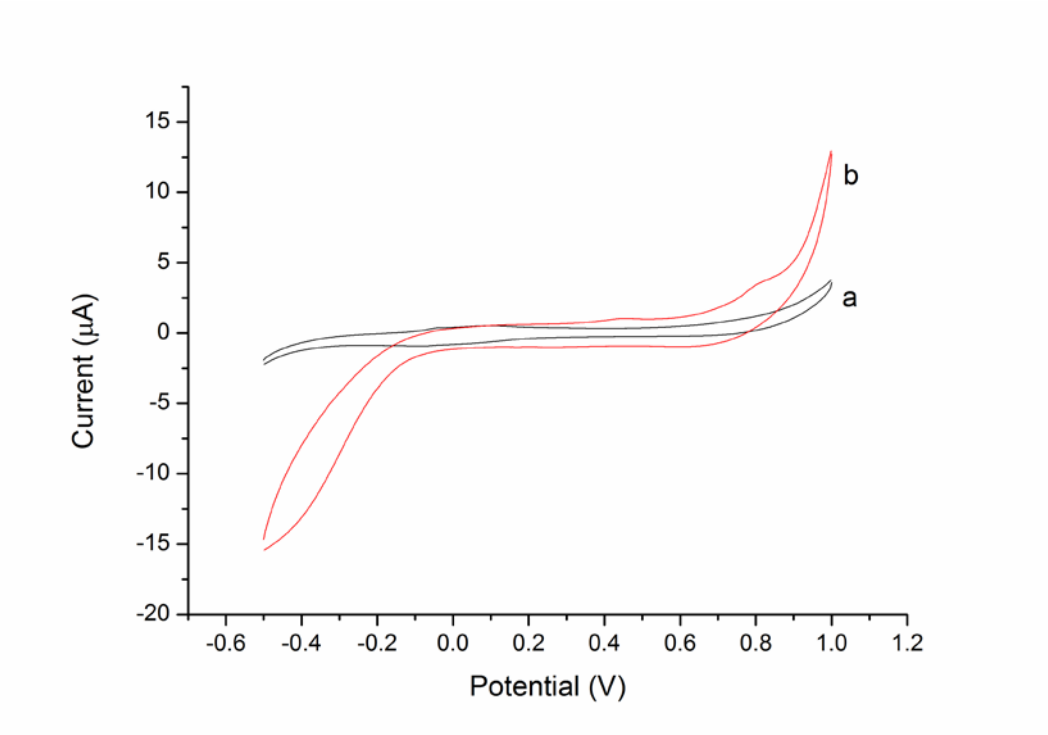

Fig. 4.5: Cyclic voltammograms obtained at the (A) SPE/Au and (B) SPE in 0.1 mol L^{-1} PB solution pH 5 at scan rate 100 mV/s.

4.4.1.3.2 Vary scan-rate

The electrochemical behaviour of the SPE and the SPE/Au was further investigated using the redox couple: $[K_3Fe(CN)_6]$ / $[K_4Fe(CN)_6]$. Fig 2.6 shows the cyclic voltammograms of a SPE (A), and a SPE/Au (B) in 5 mM $[Fe(CN)_6]^{3-/4-}$ in 0.1 M KCl with varying scan rate of 50 to 400 mV/s.

(A)

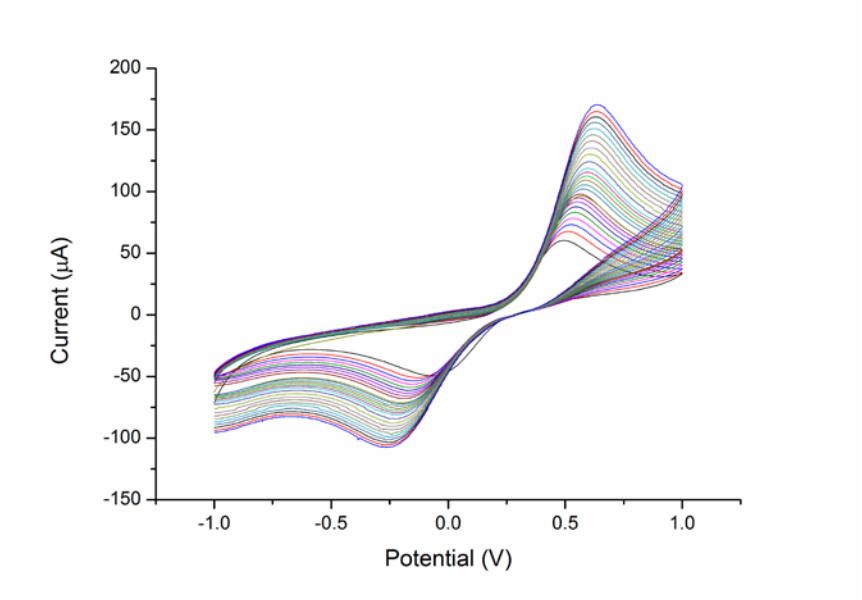
Current (µA)
Potential (V)
200
150
100
50
0
-50
-100
-150
-1.0
-0.5
0.0
0.5
1.0

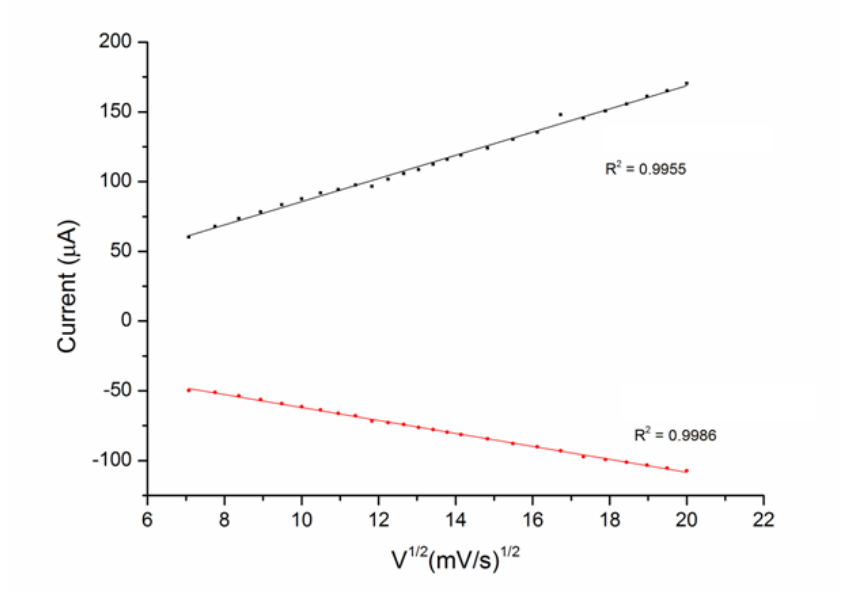
Current (µA)
V^1/2(mV/s)^1/2
R² = 0.9955
R² = 0.9986
200
150
100
50
0
-50
-100
6
8
10
12
14
16
18
20
22

(B)

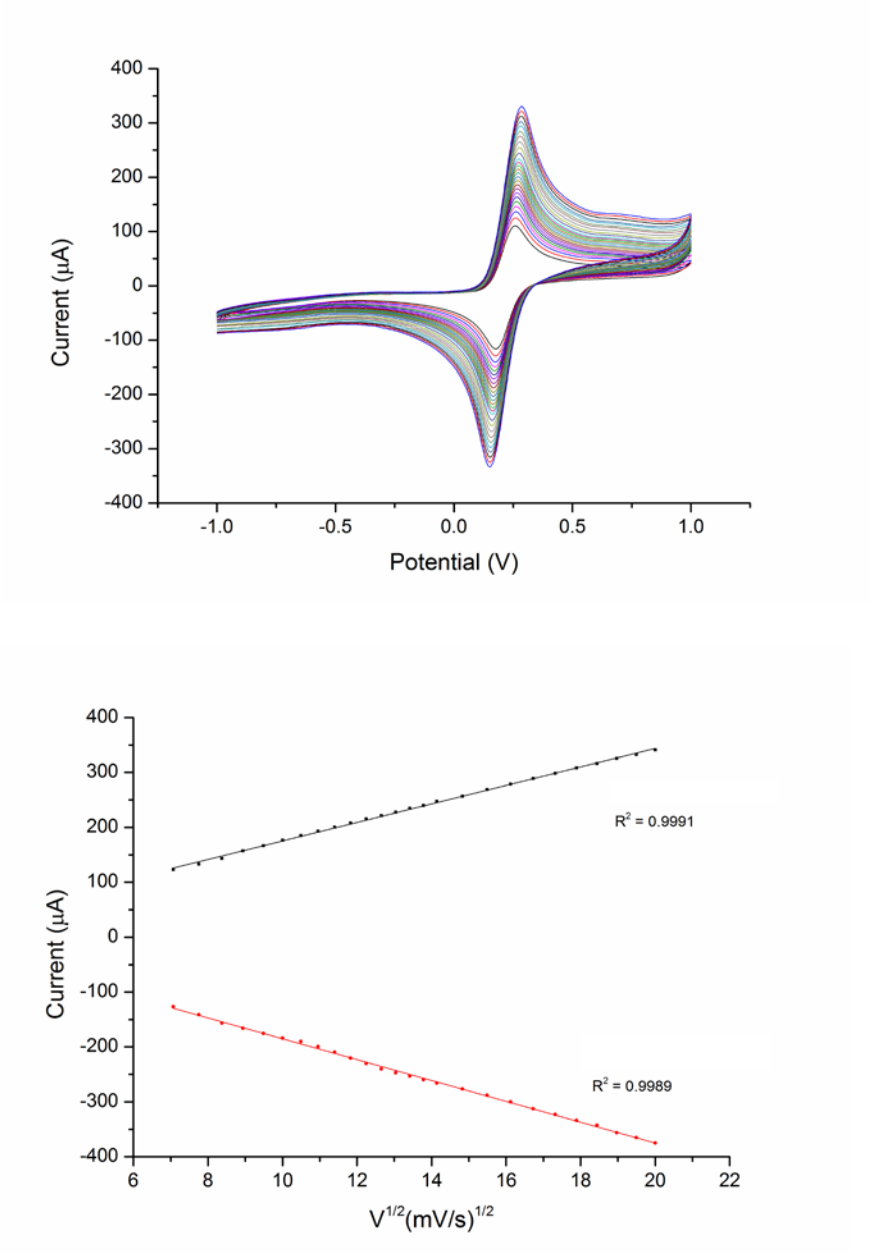

Figure 4.6: Cyclic voltammograms obtained at the (A) SPE and (B) the SPE/Au in 5 mM $[Fe(CN)_6]^{3-/4-}$ in 0.1M KCl solution at scan rate 50 to 400 mV/s. Below the scan rates: the plot of the redox peak currents versus square root of the scan rate.

It is clear that the redox peak currents of $[Fe(CN)_6]^{3-/4-}$ enhanced with increasing scan rate, suggesting quasi-reversible one-electron redox behaviour. Both the anodic (Ipa) and cathodic (Ipc) were linearly proportional to the square root of the scan-rate ($V^{1/2}$) and the data can be seen in Table 4.1.

Table 4.1: The anodic (Ipa) and catodic (Ipc) peak currents vesus the square root of the scan rate ($V^{1/2}$) for the SPE and SPE/Au. The testing was performed in 5 mM $[Fe(CN)_6]^{3-/4-}$ in 0.1 M KCl with varying scan rate of 50 to 400 mV/s.

Electrode	Linear regression equation	R^2
SPE	Ipa (µA) = 8.309X + 2.561	R^2 = 0.9955
	Ipc (µA) = -4.642X -15.551	R^2 = 0.9986
SPE/Au	Ipa (µA) = 16.849X + 6.714	R^2 = 0.9991
	Ipc (µA) = -18.991X + 4.656	R^2 = 0.9989

The results show a diffusion-controlled process taking place for both electrodes. The peak to peak separations are 390 mV for the SPE and 95 mV for the SPE/Au at 100 mV/s respectively. This shows that the SPE provides a slower electron transfer when compared to the SPE/ Au. This suggests that the Au nanoparticles played a role in the increasing of the electroactive surface area for the electron-transfer of $[Fe(CN)6]^{3-/4-}$.

4.4.1.4 EIS measurements

EIS is an important technique for studying the interface properties of the modified electrodes. The electron-transfer resistance at the electrode surface is equal to the semicircle diameter of EIS and this can be used to describe the interface properties of the electrode. The EIS measurements in this work were performed in a background solution of $[Fe(CN)_6]^{3-/4-}$. Fig 4.7 (A), shows the impedance graphs of (a) a SPE, and (b) a SPE/ Au. The SPE gave an impedance spectrum of a semicircle at a high ac modulation frequency and a line at low ac frequency indicating that the Warburg resistance was present as shown in Figure 4.7. This was related to the equivalent circuit which corresponds to the combination of the charge-transfer resistance (R_{ct}) representing the diffusion processes at the surface of the electrode. This reveals that the bare electrode process was controlled by electron transfer at the high frequency and by diffusion at low frequency. The EIS of the modified SPE demonstrated similar curves with a semicircle being displayed however with a much lower resistance. This is due to the electron-transfer resistance being significantly lower with the Au nanoparticles and might provide a higher electron conduction pathway.

(A) **(B)**

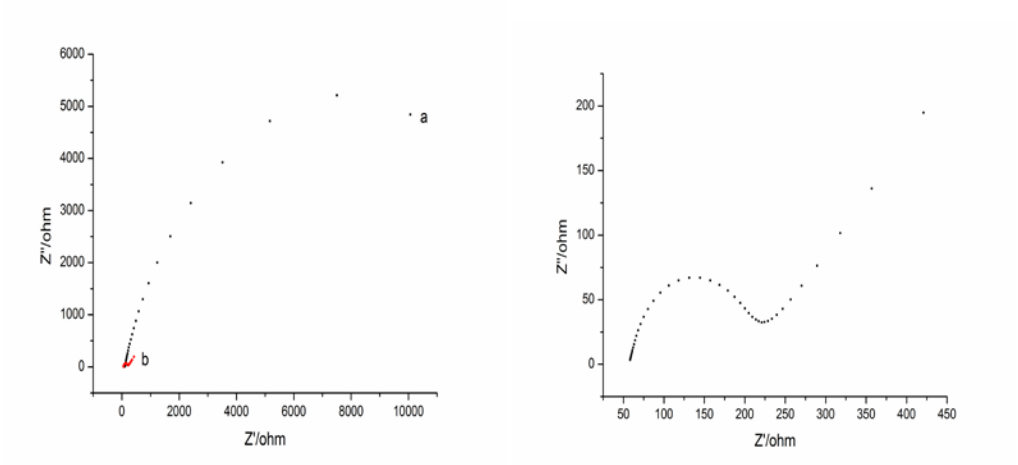

Figure 4.7: (A) Nyquist plots of $[Fe(CN)6]^{3-/4-}$ in 0.1 M KCl solution with (a) a SPE, and (b) a SPE/Au. **(B)** Nyquist plot of $[Fe(CN)6]^{3-/4-}$ in 0.1 M KCl solution a SPE/Au. The frequency range is from 1 Hz to 100 kHz.

4.4.1.5 Effect of pH on the oxidation of DA and UA in a mixture

The effect of solution pH on the response of DA and UA at the SPE/Au was investigated over the pH range of 2-7. Because proton takes part in the oxidation of UA and DA, the pH value of solution will greatly influence both the selectivity and sensitivity for the detection of DA and UA. The anodic peak potentials of both analytes shifted negatively as pH increased, depicted in Figure 4.9, with the slope obtained from the linear behaviour between the applied potential and the pH for DA and UA were found to be; 0.0627 and 0.0623 V/pH respectively, which are close to the anticipated Nernstian value (0.059 V/pH) for a two electons/two protons reaction. The pH value chosen to give the maximal separation of DA and UA was pH 5. The pH value chosen to give the maximal separation of DA and UA was pH 5.

(A) **(B)**

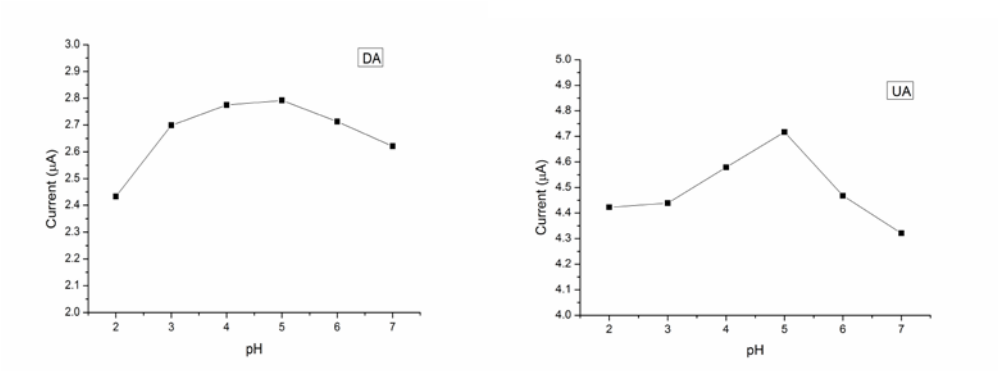

Figure 4.8: Effect of buffer pH on the peak current for the oxidation of (A) DA and (B) UA. Concentrations: DA, 0.08 mM; UA, 0.2 mM. Scan rate 50 mV/s.

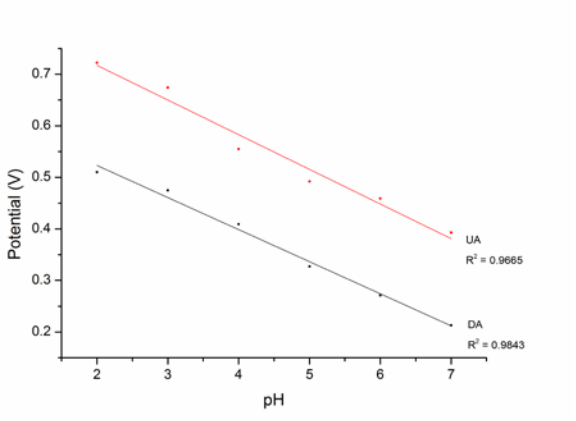

Figure 4.9: Effect of buffer pH on the peak oxidation potential for the oxidation of AA and UA. Concentrations: DA, 0.08 mM; UA, 0.2 mM. Scan rate 50 mV/s.

4.4.1.6 Effect of deposition time on the oxidation of DA and UA in a mixture

The effect of the electro-deposition time of the Au nanoparticles was also investigated and it was found that 40 seconds deposition time gave the maximum signal for both DA and UA based on Fig. 4.10. It can be seen that beyond the 50 seconds the Ip begins to drop due to the surface of the SPE becoming over-saturated.

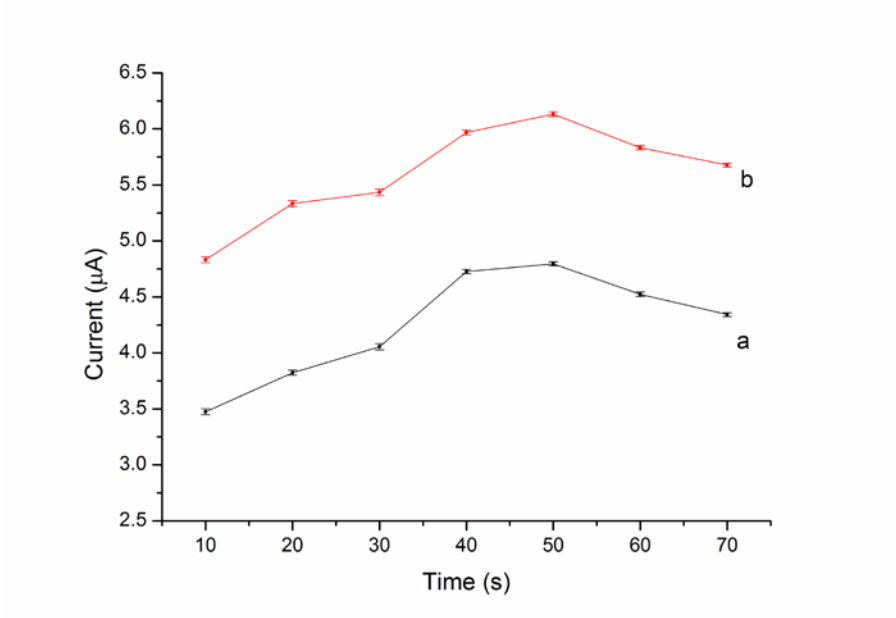

Figure 4.10: Effect of deposition time on the peak current for the oxidation of DA and UA. Concentrations: DA, 0.08 mM; UA 0.2 mM. Scan rate 50 mV/s.

4.4.1.7 Simultaneous determination of DA and UA

The determination of DA and UA concentrations at the SPE/Au was performed with cyclic voltammetry. The oxidation peak currents of DA and UA were selected as the analytical signals. A seven point calibration curve was prepared for both DA and UA by analyzing a series of analyte standard solutions at different concentrations. The DA concentration range was from 0.05 mM to 0.167 mM, and the UA concentration range was from 0.12 mM to 0.3 mM. Fig. 2.11 (B). The linear regression equation for DA was $I\mathrm{p_a}$ (µA) = 0.1875 + 34.453C with a correlation coefficient of R^2 = 0.9987. The linear regression equation for UA was $I\mathrm{p_a}$

(µA) = 1.435 + 21.022C with a correlation coefficient of R^2 = 0.9971. The linear range was 0.03 mM to 0.2 mM for DA and 0.1mM to 1.17 mM for UA.

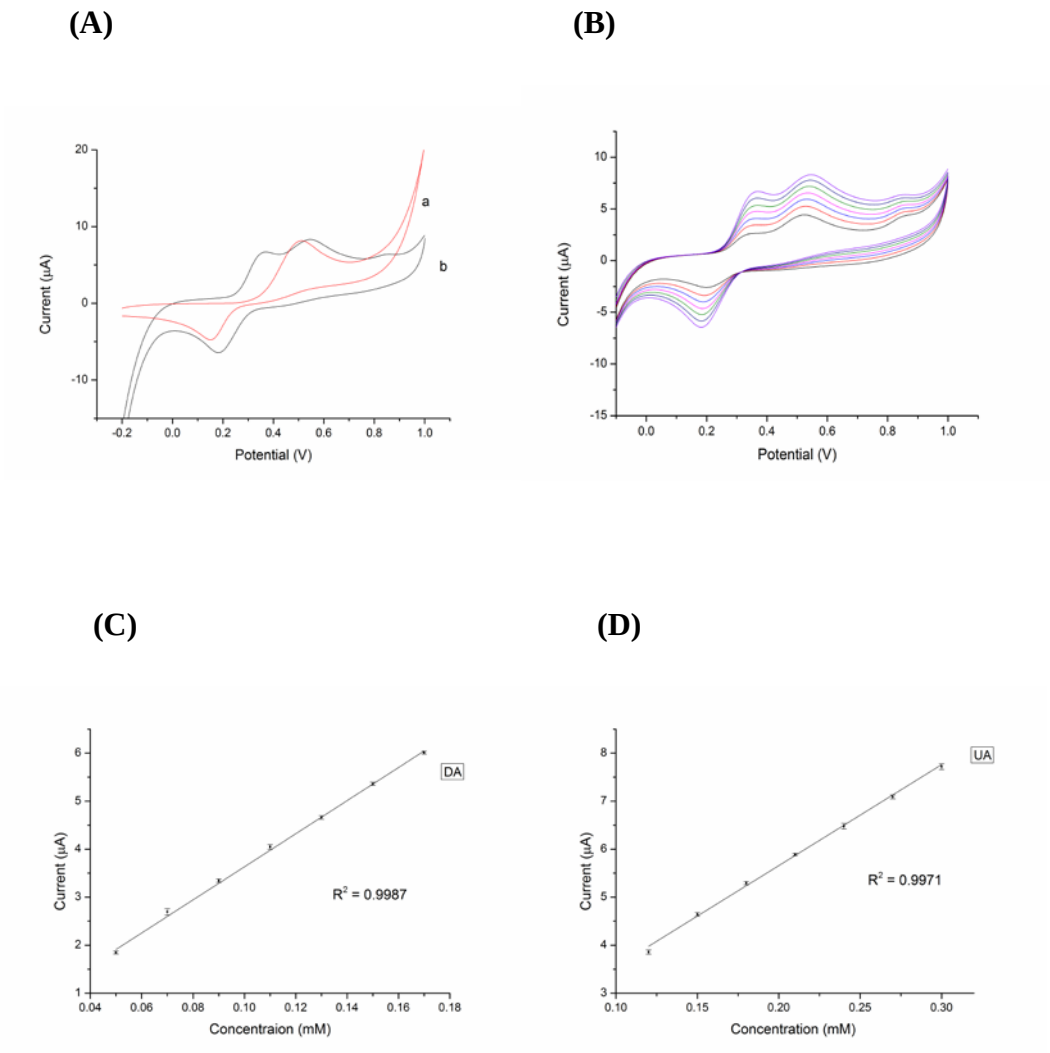

Figure 4.11: (A) CV of DA 0.17 mM and UA 0.3 mM at the (a) SPE and (b) SPE/Au in 0.1 M PB solution pH 5.0. (B) CVs of various DA and UA concentrations at the SPE/Au in 0.1 M PB solution pH 5.0. Concentrations of analytes (a-g); 0.05, 0.07, 0.09, 0.11, 0.13, 0.15 and 0.17 mM for DA and 0.12, 0.15, 0.18, 0.21, 0.24, 0.27 and 0.3 mM for UA. (C) Calibration plot for DA obtained from the CV's recording shown in (B). (D) Calibration plot for UA obtained from the CV's recording shown in (B). Scan rate: 50 mV/s.

4.4.1.8 Characterisation of the SPE/Au using amperometric (I-t) curve

Figure 4.12 shows the curves for the SPE/Au poised at +0.2 V in response to 4 µL DA (10 mM) (Fig.4.12(A)) and 4 µM UA (0.05M) (Fig.4.12(B)) at pH 5. Amperometric detection tests were performed separately for each of the two analytes with the aim of ensuring the electrode could detect increasing concentrations of the analytes at suitable increments of current. The detection potential was 200 mV at a 0.1 s scan rate.

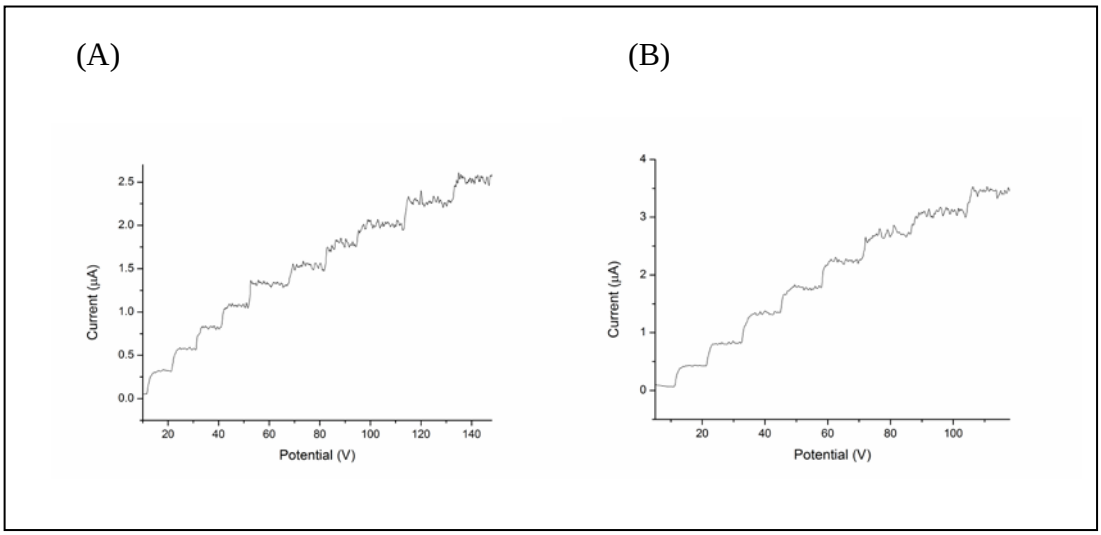

Figure 4.12: A typical current-time response of the SPE/CM/Au upon the successive additions of (A) 8 µM DA and (B) 40 µM UA in 0.1M PBS solution pH 5, E= 0.2 V.

Under the optimum conditions, the detection limit (s/n = 3) for DA was calculated to be 8 x 10^{-6} M and for UA the detection limit is 40 x 10^{-6} M.

4.4.1.9 Stability and repeatability of the SPE/Au

The stability and repeatability of the SPE/Au was also studied. This was performed first by 8 replicates of the SPE/Au to determine the relative standard deviation (RSD) for the oxidation peak of DA and UA for 0.07 mM for DA and 0.21 mM for UA, which were found to be 2.45% and 1.78%, respectively. The electrode with the Au nanoparticles adsorbed on the surface lost ca. 7% of its initial response after 2 days. The SPE/Au could be used for at least 1 week, without significant loss of electrochemical signal.

4.4.1.10 Real sample analysis: determination of DA and UA in human serum

The human serum sample was diluted 5 times with phosphate buffer solution before the measurements to prevent the matrix effect of real samples. A certain value of standard solutions of DA and UA was added into the corresponding plasma serum for testing recovery. The results obtained for DA and UA in serum are listed in Table 4.2. To ascertain the correctness of the result the serum sample was spiked with certain amounts of DA and UA in about the same concentration as found in the samples.

Table 4.2: The recovery of DA and UA for the proposed method: (n=3)

Analyte	Spiked	Found	Recovery %
DA	0.07	0.065	92.9±2.7
	0.09	0.087	96.7±1.5
	0.11	0.102	92.7±2.6
UA	0.15	0.131	87.3±1.8
	0.18	0.165	91.67±2.3
	0.21	0.185	88.01±3.1

4.4.2 SPE/ Pd nanoparticles

4.4.2.1 Characterisation using SEM of the SPE with palladium nanoparticles

The modified electrode's morphology was investigated using scanning electron microscopy (SEM) as mentioned in 4.4.1.1.

The SEM image of the SPE can be seen in a Fig 4.13 (A) and the image of the SPE with Pd nanoparticles dispersed on the surface is shown in Fig 4.13 (B). The shiny clusters scattered on the surface of the electrode are the palladium nanoparticles.

(A) **(B)**

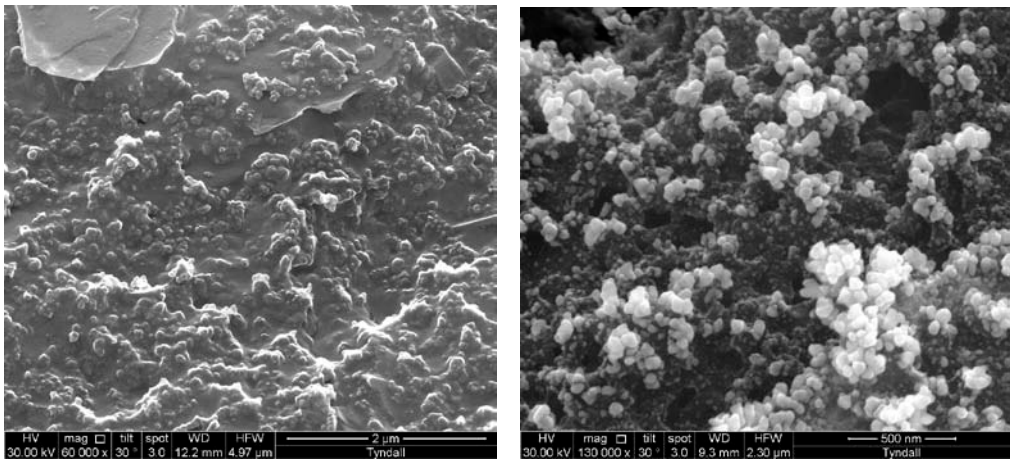

Figure 4.13: The SEM images (A) of the SPE and (B) of the SPE surface with Pd nanoparticles.

4.4.2.2 Contact-angle measurement of SPE and SPE/Pd

The measurement of the contact angle of the SPE and the SPE/Pd was conducted at the Tyndall National Institute, UCC, Cork, as described in 4.4.1.2. The SPE has a contact angle of 118.7 º Fig 2.14 (A) which suggests it has a relatively hydrophobic surface area. The SPE/Pd has a contact angle of 79 º Fig 2.14 (B) which indicates that the Pd caused the surface to become less hydrophobic.

(A) (B)

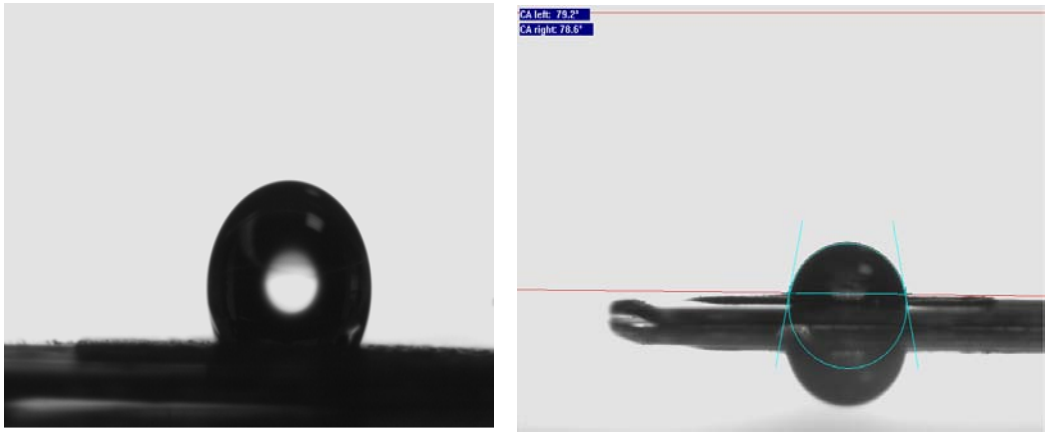

118.7º **79º**

Figure 4.14 Images of water droplet on surface of (A) SPE (CA = 118.7º) and (B) SPE/Pd (CA = 79º)

4.4.2.3 Electrochemical behaviour of SPE/CM and SPE/CM/Pd

4.4.2.3.1 Compare Cyclic Voltammogramms

The electrochemical responses of a SPE, and a SPE/Pd were characterised by CV in 5 mM $[Fe(CN)_6]^{3-/4-}$ in 0.1 M KCl and can be seen in Fig 4.15. The background current of the SPE/Pd increased significantly, indicating that the bare electrode was modified efficiently by the Pd nanoparticles.

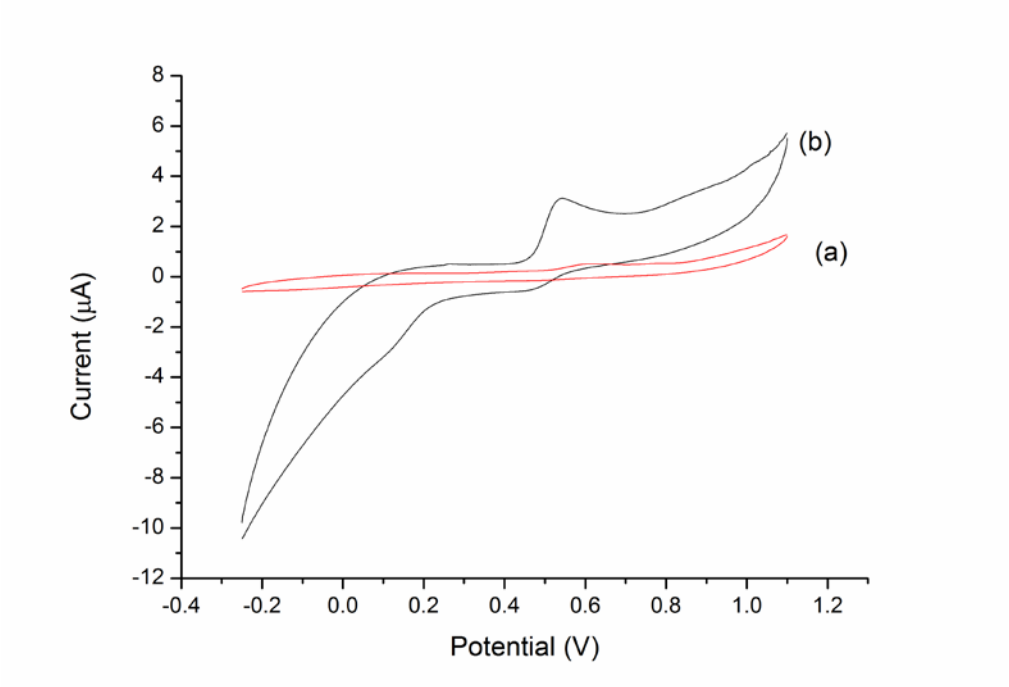

Figure 4.15: Cyclic voltammograms obtained at the (A) SPE and (B) SPE/Pd in 5 mM $[Fe(CN)_6]^{3-/4-}$ in 0.1 M KCl at scan rate 50 mV/s.

4.4.2.3.2 Vary scan-rate

This testing was carried out in section 4.4.1.3.2 for the bare screen-printed electrode. Below in Fig 4.16 are the results of the SPE/Pd.

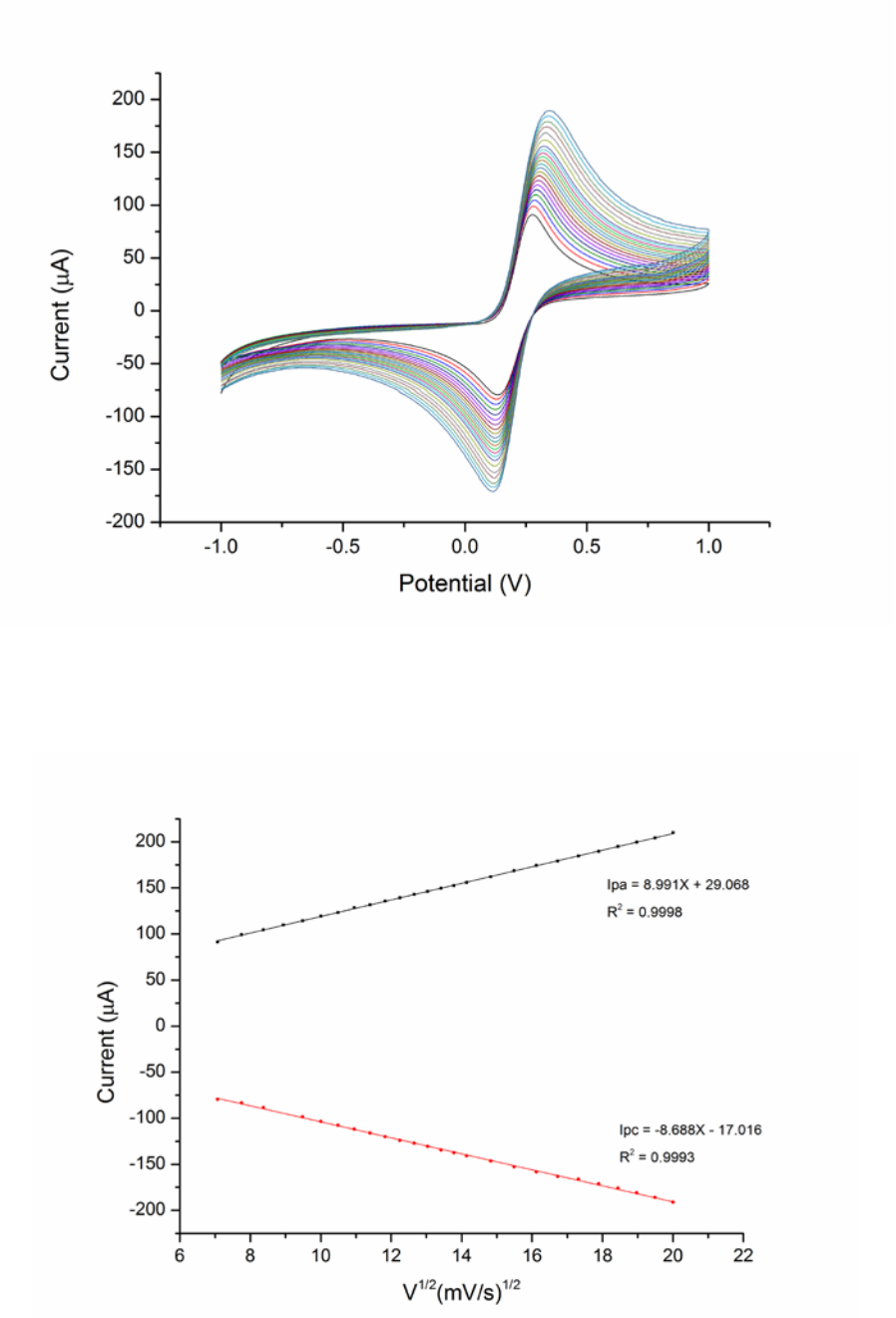

Figure 4.16: Cyclic voltammogram and the plot of the redox peak currents versus square root of the scan rate obtained at the SPE/Pd in 5 mM $[Fe(CN)_6]^{3-/4-}$ in 0.1M KCl solution at scan rate 50 to 400 mV/s.

Again it is clear that the redox peak currents of $[Fe(CN)_6]^{3-/4-}$ enhanced with increasing scan rate, suggesting quasi-reversible one-electron redox behaviour. Both the anodic (Ipa) and cathodic (Ipc) were linearly proportional to the square root of the scan-rate ($V^{1/2}$) and the data including the SPE data carried out in section 4.4.1.3.2 (A) can be seen in Table 4.3

Table 4.3: The anodic (Ipa) and catodic (Ipc) peak currents vesus the square root of the scan rate ($V^{1/2}$). The testing was performed in 5 mM $[Fe(CN)_6]^{3-/4-}$ in 0.1 M KCl with varying scan rate of 50 to 400 mV/s for the SPE and SPE/Pd.

Electrode	Linear regression equation	R^2
SPE	Ipa (μA) = 8.309X + 2.561	R^2 = 0.9955
	Ipc (μA) = -4.642X -15.551	R^2 = 0.9986
SPE/Pd	Ipa (μA) = 8.991X + 29.068	R^2 = 0.9998
	Ipc (μA) = -8.688X + 17.016	R^2 = 0.9993

4.4.2.3.3 EIS measurements

The EIS measurements in this work were performed in a similar way to that described in section 4.4.1.4, in a background solution of $[Fe(CN)_6]^{3-/4-}$. Fig. 4.16 (A) shows the impedance graphs of (a) a SPE and (b) a SPE /Pd. The SPE gave an impedance spectrum of a semicircle at a high ac modulation frequency and a line at low ac frequency indicating that the Warburg resistance was present as shown in Figure 4.17. This was related to the equivalent circuit which corresponds to the combination of the charge-transfer resistance (R_{ct}) representing the diffusion processes at the surface of the electrode. This reveals that the electrode process was controlled by electron transfer at the high frequency and by diffusion at low frequency. The EIS of the modified SPE demonstrated a similar curve but at much lower resistance values,

which demonstrates that with the Pd nanoparticles the SPE might provide a higher electron conduction pathway.

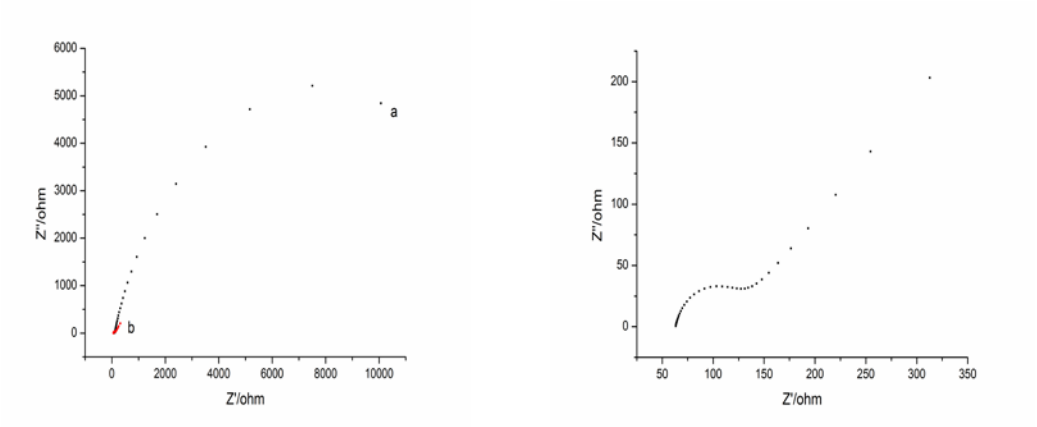

Figure 4.17: (A) Nyquist plots of $[Fe(CN)6]^{3-/4-}$ in 0.1 M KCl solution with (a) a SPE, and (b) a SPE/Pd. **(B)** Nyquist plot of $[Fe(CN)6]^{3-/4-}$ in 0.1 M KCl solution a SPE/Pd. The frequency range is from 1 Hz to 100 kHz.

4.4.2.3.4 Effect of pH on the oxidation of AA and UA in a mixture

The effect of solution pH on the response of AA and UA at the SPE/Pd was investigated over the pH range of 3-7. Because proton takes part in the oxidation of AA and UA, the pH value of solution will greatly influence both the selectivity and sensitivity for the detection of AA and AA. The anodic peak potentials of both analytes shifted negatively as pH increased, depicted in Figure 4.19, with the slope obtained from the linear behaviour between the applied potential and the pH for AA and UA were found to be; 0.052 and 0.0599 V/pH respectively, which are close to the anticipated Nernstian value (0.059 V/pH) for a two electons/two protons reaction. The pH value chosen to give the maximal separation of AA and UA was pH 4.

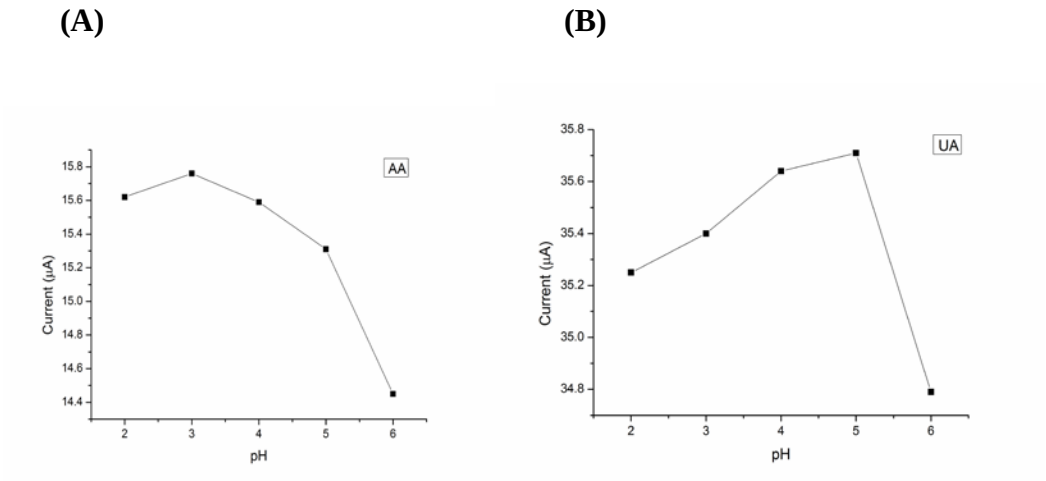

Figure 4.18: Effect of buffer pH on the peak current for the oxidation of (A) AA and (B) UA. Concentrations: AA, 0.5 mM; UA, 0.5 mM. Scan rate 50 mV/s.

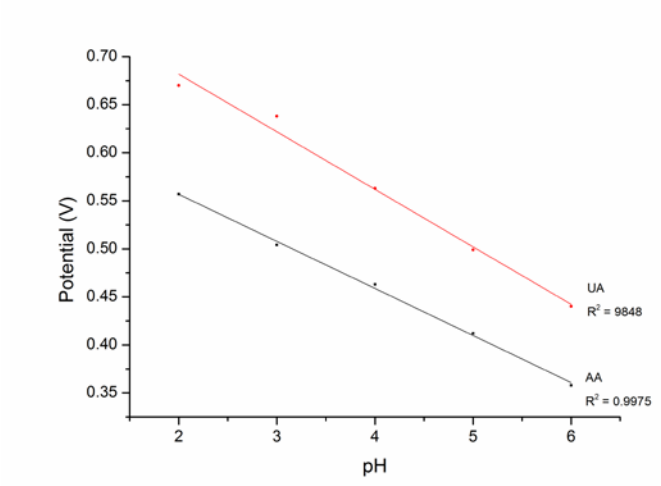

Figure 4.19: Effect of buffer pH on the peak oxidation potential for the oxidation of AA and UA. Concentrations: AA, 0.5 mM; UA, 0.5 mM. Scan rate 50 mV/s.

4.4.2.3.5 Effect of deposition time on the oxidation of AA and UA in a mixture

The effect of the electro-deposition time of the Pd nanoparticles was also investigated and it was found that 40 seconds deposition time gave the maximum signal for AA (Fig 4.20 (A)) and 50 seconds for UA (Fig 4.20 (B)). It can be seen that beyond the 50 seconds the Ip begins to drop for both analytes due to the surface of the SPE becoming over-saturated. The optimum deposition time chosen was 40 seconds.

(A) **(B)**

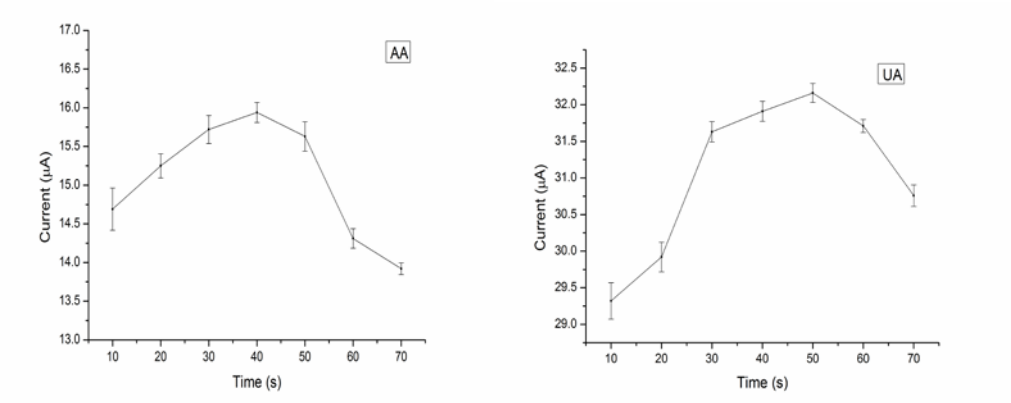

Figure 4.20: Effect of deposition time on the peak current for the oxidation of (A) AA and (B) UA. Concentrations: AA, 0.5 mM; UA, 0.5 mM. Scan rate 50 mV/s.

4.4.2.3.6 Simultaneous determination of AA and UA

The determination of AA and UA concentrations at the SPE/Pd was performed with cyclic voltammetry. The oxidation peak currents of AA and UA were selected as the analytical signals. A seven point calibration curve was prepared for both AA and UA by analyzing a series of analyte standard solutions at different concentrations. The AA concentration range was from 0.03 mM to 0.21 mM, and the UA concentration range was also from 0.03 mM to 0.21 mM. The linear regression equation for UA was Ip_a (µA) = 0.3311C + 0.4835 with a correlation coefficient of R^2 = 0.9984. The linear regression equation for UA was Ip_a (µA) = 0.7876C + 0.5011 with a correlation coefficient of R^2 = 0.9958. The linear range was 0.03 mM to 0.3 mM for AA and 0.03 mM to 0.52 mM for UA.

(A)

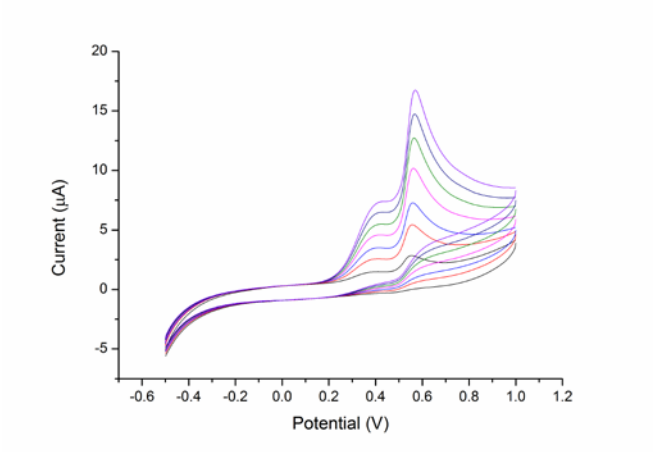

(B) (C)

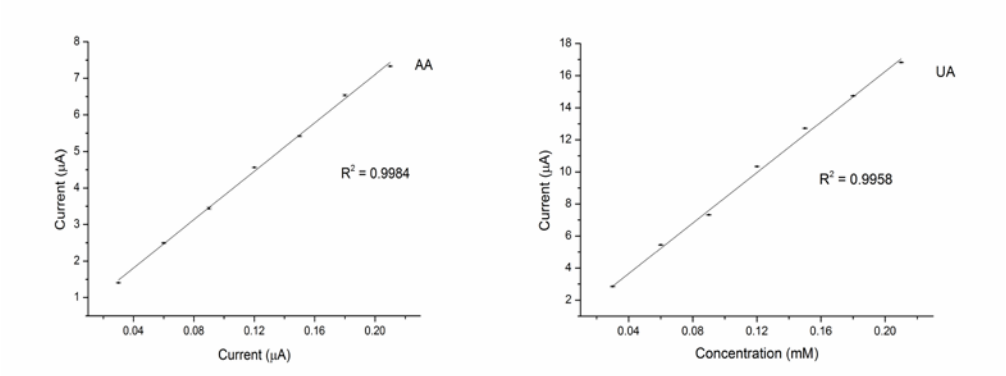

Figure 4.21: (A) CVs of various AA and UA concentrations at the SPE/Pd in 0.1 M PB solution pH 4.0. Concentration of analytes; 0.03, 0.06, 0.09, 0.12, 0.15, 0.18 and 0.21 mM for both AA and UA. (B) Calibration plot for AA obtained from the CV's shown in (A). (C) Calibration plot for UA obtained from the CV's shown in (A). Scan rate: 50 mV/s.

4.4.2.3.7 Characterisation of the SPE/Pd using amperometric (I-t) curve

Figure 4.22 shows the curves for the SPE/Pd poised at +0.2 V in response to 2 µM AA (0.05 M) ((Fig 4.21(A)) and 3 µM UA (0.05 M) (Fig 4.21(B)) at pH 4. Amperometric detection tests were performed separately for each of the two analytes with the aim of ensuring the electrode could detect increasing concentrations of the analytes at suitable increments of current. The detection potential was 200 mV at a 0.1 s scan rate.

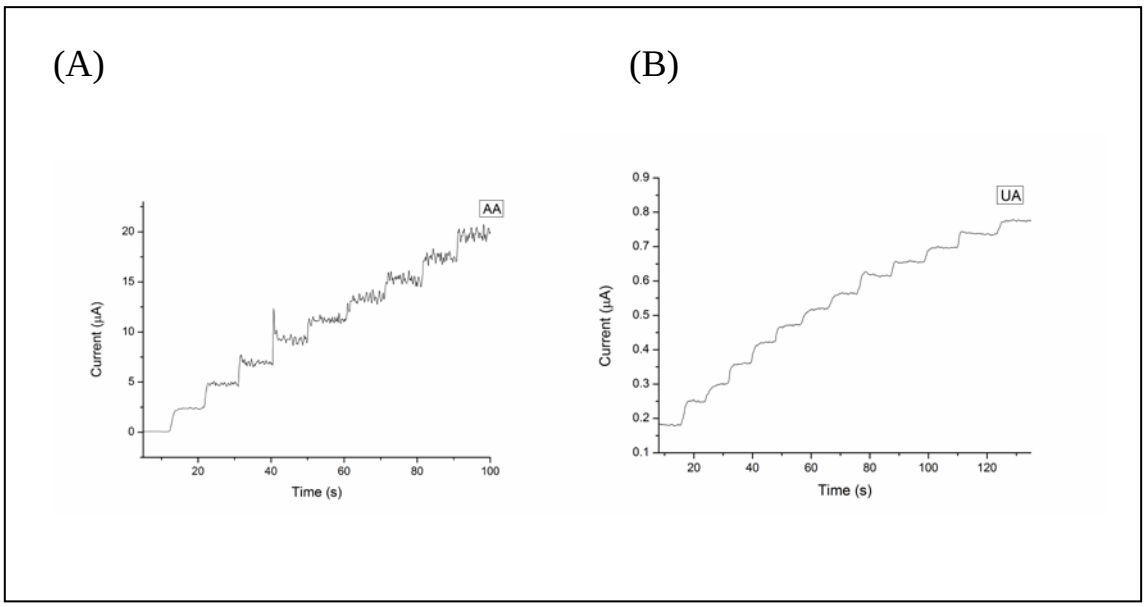

Figure 4.22: A typical current-time response of the SPE/Pd upon the successive additions of (A) 20 µM AA and (B) 30 µM UA in 0.1M PB solution pH 4, E= 0.2V.

Under the optimum conditions, the detection limit (s/n = 3) for AA was calculated to be 20 x 10^{-6} M and for UA the detection limit is 30 x 10^{-6} M.

4.4.2.3.8 Stability and repeatability of the SPE/Pd

The stability and repeatability of the SPE/Pd was also studied. This was performed first by 8 replicates of the SPE/Pd to determine the relative standard deviation (RSD) for the oxidation peak of AA and UA for 0.12 mM for AA and 0.12 mM for UA which was found to be 2.89 % and 2.44 %, respectively. The electrode with CM adsorbed on the surface lost ca. 6 % of its initial response after 2 days. The SPE/Pd could be used for at least 1 week, without significant loss of electrochemical signal.

4.4.2.3.9 Real sample analysis: determination of AA and UA in human serum

The human serum sample was diluted 5 times with phosphate buffer solution before the measurements to prevent the matrix effect of real samples. A certain value of standard solutions of AA and UA was added into the corresponding plasma serum for testing recovery. The results obtained for AA and UA in serum are listed in Table 4.4. To ascertain the correctness of the result the serum sample was spiked with certain amounts of AA and UA in about the same concentration as found in the samples.

Table 4.4: The recovery of AA and UA for the proposed method: (n=3)

Analyte	Spiked (mM)	Found (mM)	Recovery (%)
AA	0.06	0.0573	95.5±1.3
	0.09	0.0805	89.4±2.87
	0.12	0.114	95.0±1.29
UA	0.06	0.061	101.7±3.53
	0.09	0.089	98.8±2.19
	0.12	0.114	95.1±1.54

4.4.3 SPE/ CM/Au nanoparticles

This section will be further broken up into two areas. The first set of results will be for the SPE modified with CM and Au nanoparticles. The second set of results will be for the SPE modified with CM and Pd nanoparticles.

4.4.3.1 Characterisation using SEM of the SPE/CM with gold nanoparticles

The modified electrode's morphology was investigated using SEM as discussed in section 4.4.1.1.

The SEM image of the SPE can be seen in a Fig 4.23 (A). The imaging showed the porous nature and irregular shapes of carbon monoliths in Fig 4.23 (B) and confirms that the CM is well dispersed in DMF. This porous structure could significantly increase the electrode's surface as well as the electron transfer pathway. Fig 4.23 (C) shows an area of the CM surface at a higher magnitude while Fig 4.23 (D) shows the magnified CM area with gold nanoparticles dispersed on the surface.

(A) **(B)**

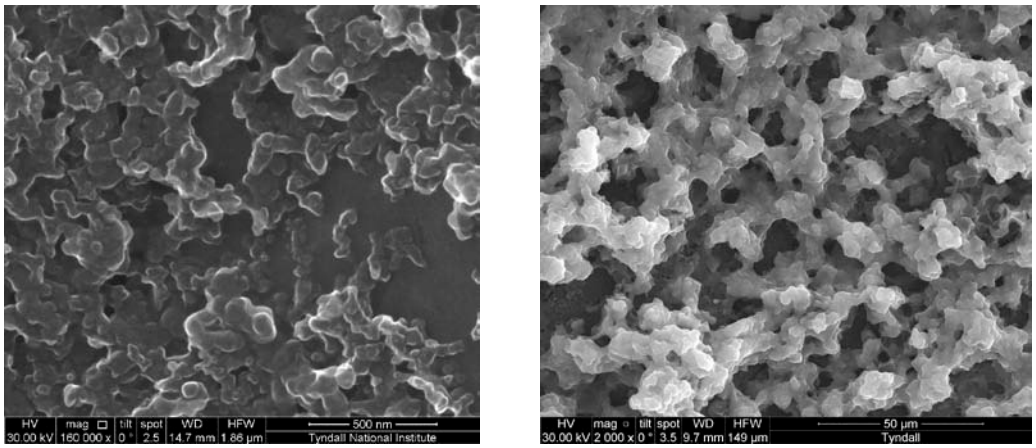

(C) **(D)**

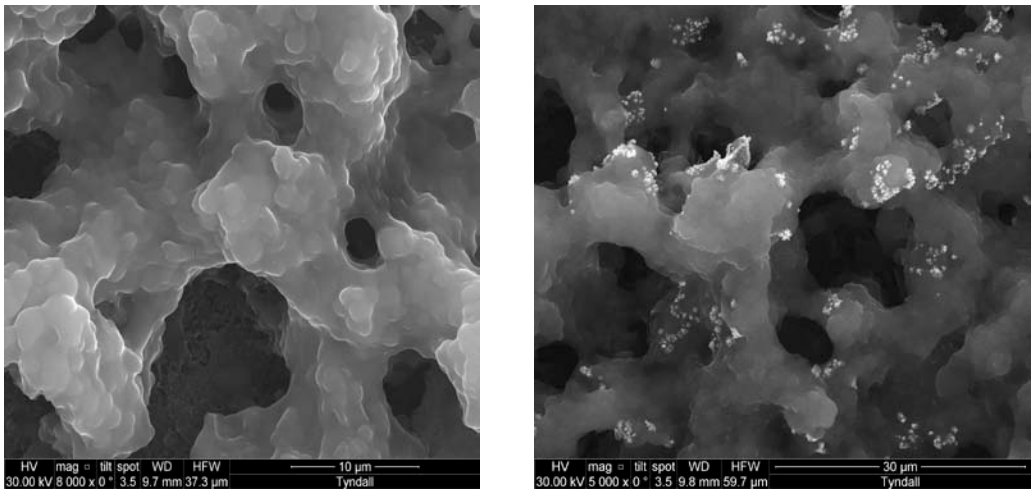

Figure 4.23: The SEM images (A) of the SPE, (B) of the CM surface, (C) of the magnified CM surface and (D) of the magnified CM with Au nanoparticles.

4.4.3.2 Contact-angle measurement of SPE, SPE/CM and SPE/CM/Au

The measurement of the contact angle of the SPE and the SPE/CM and SPE/CM/Au was conducted at the Tyndall National Institute, UCC, Cork, as described in 4.4.1.2. . The SPE has a contact angle of 118.7 º Fig 4.24 (A) which indicates it has a relatively hydrophobic surface area. The SPE/CM has a contact angle of 132.8 º Fig 4.24 (B) which means the surface area has become more hydrophobic with the CM and since carbon is hydrophobic this result is expected. The SPE/CM/Au gave a contact angle of 106.5 º Fig 4.24 (C) indicating that the Au caused the surface to become less hydrophobic.

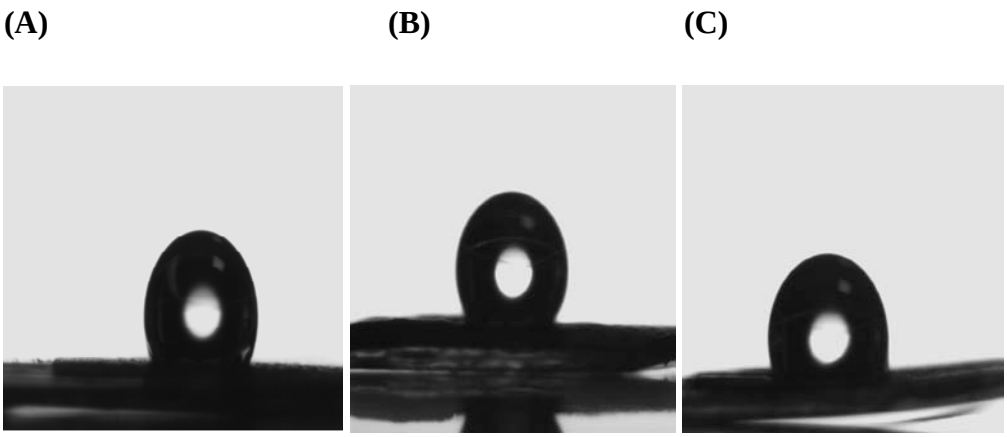

Figure 4.24: Images of water droplet on surface of (A) SPE (CA = 118.7º), (B) SPE/CM (CA = 132.8º) and (C) SPE/CM/Au (CA = 106.5º).

4.4.3.3 Electrochemical behaviour of SPE/CM and SPE/CM/Au

4.4.3.3.1 Compare Cyclic Voltammograms

The electrochemical responses of a SPE, a SPE/CM/Au were characterised by cyclic voltammetry (CV) in phosphate buffer (PB) solution at pH 5 and can be seen in Figure 4.25. The background current of the SPE/CM/Au increased greatly, indicating that the bare electrode was modified efficiently by carbon monolith with gold nanoparticles.

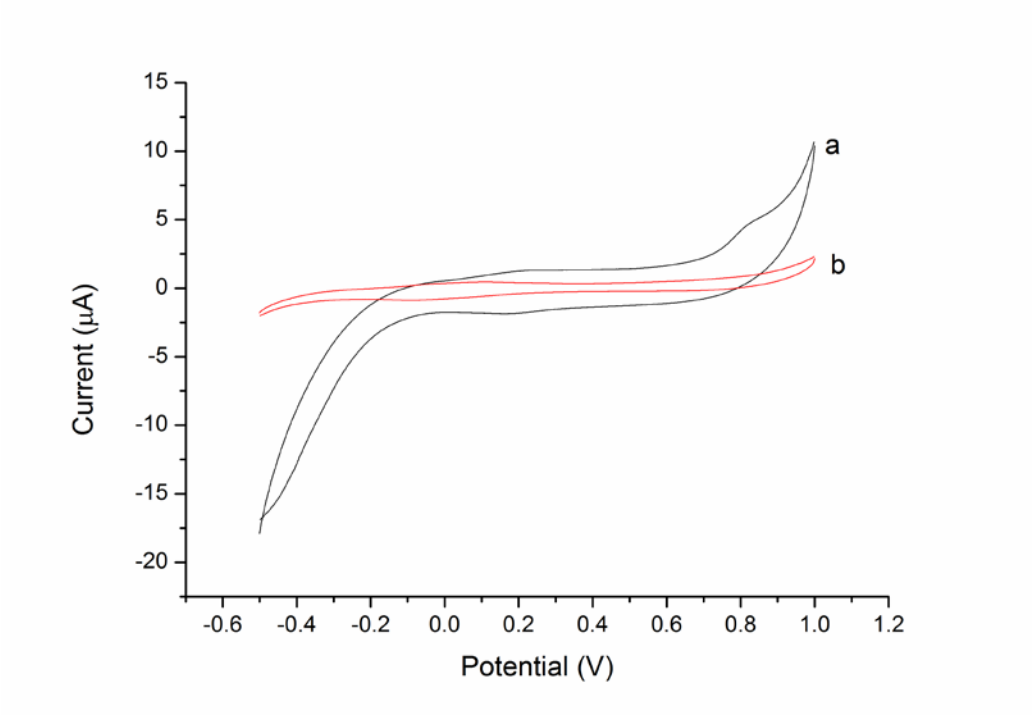

Figure 4.25: Cyclic voltammograms obtained at the (A) SPE, and (B) SPE/CM/Au in 0.1 mol L^{-1} PB solution pH 5 at scan rate 50 mV/s.

4.4.3.3.2 Vary scan-rate

The electrochemical behaviour of the SPE/CM/Au was further investigated using the redox couple: $[K_3Fe(CN)_6]$ / $[K_4Fe(CN)_6]$. Figure 4.26 shows the cyclic voltammograms of a SPE/CM/Au in 5 mM $[Fe(CN)_6]^{3-/4-}$ in 0.1 M KCl with varying scan rate of 50 to 400 mV/s.

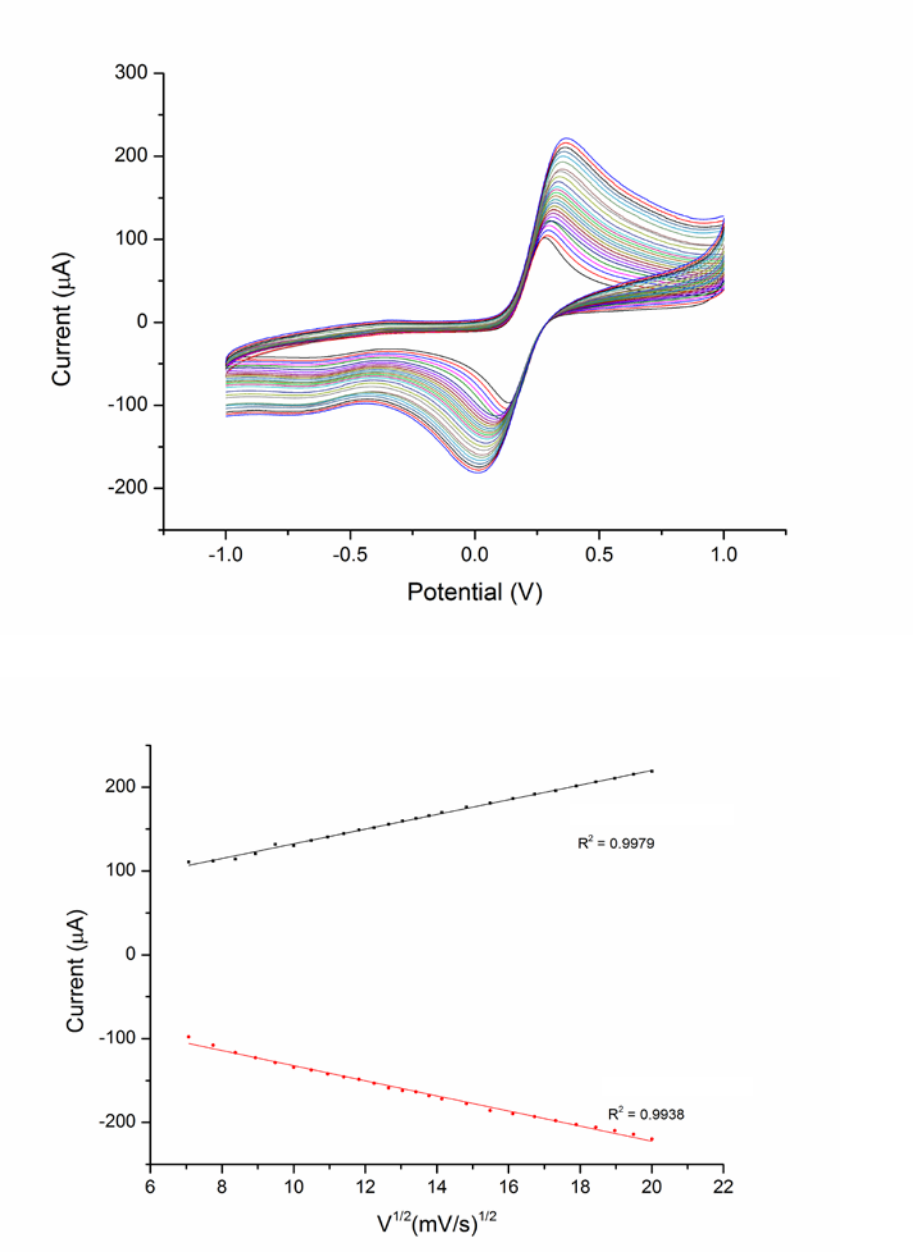

Figure 4.26: Cyclic voltammograms and the plot of the redox peak currents versus square root of the scan rate obtained at the (A) SPE and (B) SPE/CM/Au in 5 mM $[Fe(CN)_6]^{3-/4-}$ in 0.1M KCl solution at scan rate 50 to 400 mV/s.

It is clear that the redox peak currents of $[Fe(CN)_6]^{3-/4-}$ enhanced with increasing scan rate, suggesting quasi-reversible one-electron redox behaviour. Both the anodic (Ipa) and cathodic (Ipc) were linearly proportional to the square root of the scan-rate ($V^{1/2}$) and the data can be seen in Table 4.5 along with the data of the SPE as performed in section 4.4.1.3.2.

Table 4.5: The anodic (Ipa) and catodic (Ipc) peak currents vesus the square root of the scan rate ($V^{1/2}$). The testing was performed in 5 mM $[Fe(CN)_6]^{3-/4-}$ in 0.1 M KCl with varying scan rate of 50 to 400 mV/s.

Electrode	Linear regression equation	R^2
SPE	Ipa (µA) = 8.309X + 2.561 Ipc (µA) = -4.642X - 15.551	R^2 = 0.9955 R^2 = 0.9986
SPE/CM/Au	Ipa (µA) = 8.748X + 44.939 Ipc (µA) = -9.01X + 42.144	R^2 = 0.9979 R^2 = 0.9938

The results show a diffusion-controlled process taking place for both electrodes. The peak to peak separations are 390 mV for the SPE and 223 mV for the SPE/CM/Au at 100 mV/s, respectively. This shows that the SPE provides a slower electron transfer when compared to the SPE/CM/Au. This suggests that the Au nanoparticles played a role in the increasing of the electroactive surface area for the electron-transfer of $[Fe(CN)6]^{3-/4-}$.

4.4.3.3.3 EIS measurements

The EIS measurements in this work were performed in a similar way to that described in section 4.4.1.4, in a background solution of $[Fe(CN)_6]^{3-/4-}$. Figure 4.27 (A) shows the impedance graphs of (a) a SPE, (b) a SPE/CM and (c) a SPE/CM/Au. The SPE gave an

impedance spectrum of a semicircle at a high ac modulation frequency and a line at low ac frequency indicating that the Warburg resistance was present as shown in Figure 4.27. This was related to the equivalent circuit which corresponds to the combination of the charge-transfer resistance (R_{ct}) representing the diffusion processes at the surface of the electrode. This reveals that the electrode process was controlled by electron transfer at the high frequency and by diffusion at low frequency. The EIS of the modified SPES demonstrated different curves with no semicircle being displayed. This is due to the electron-transfer resistance being significantly lower with the CM. The SPE/CM/Au seen in Figure 4.27 (B) gave much lower resistance values than the SPE/CM which demonstrates that with the Au nanoparticles the SPE might provide a higher electron conduction pathway.

(A) **(B)**

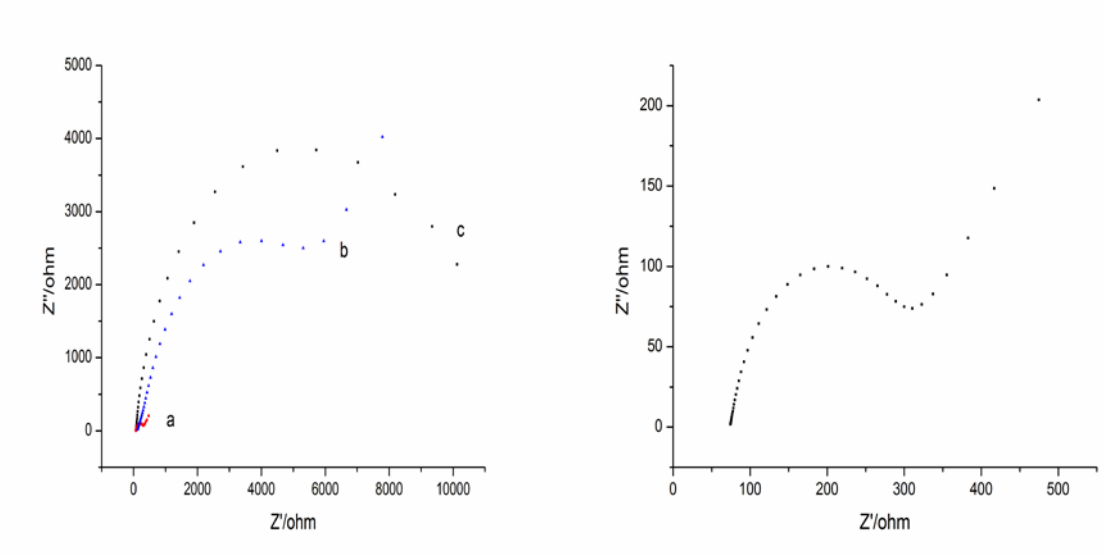

Figure 4.27: (A) Nyquist plots of $[Fe(CN)6]^{3-/4-}$ in 0.1 M KCl solution with (a) a SPE, (b) a SPE/CM, and (c) a SPE/CM/Au. The frequency range is from 1 Hz to 100 kHz. **(B)** Nyquist plot of $[Fe(CN)6]^{3-/4-}$ in 0.1 M KCl solution with a SPE/CM/Au.

4.4.3.3.4 Effect of pH on the oxidation of DA and UA

The effect of solution pH on the response of DA and UA at the SPE/CM/Au was investigated over the pH range of 2-7. Because proton takes part in the oxidation of UA and DA, the pH value of solution will greatly influence both the selectivity and sensitivity for the detection of DA and UA. The anodic peak potentials of both analytes shifted negatively as pH increased, depicted in Figure 4.29, with the slope obtained from the linear behaviour between the applied potential and the pH for DA and UA were found to be; 0.0587 and 0.0562 V/pH respectively, which are close to the anticipated Nernstian value (0.059 V/pH) for a two electons/two protons reaction. The pH value chosen to give the maximal separation of DA and UA was pH 5.

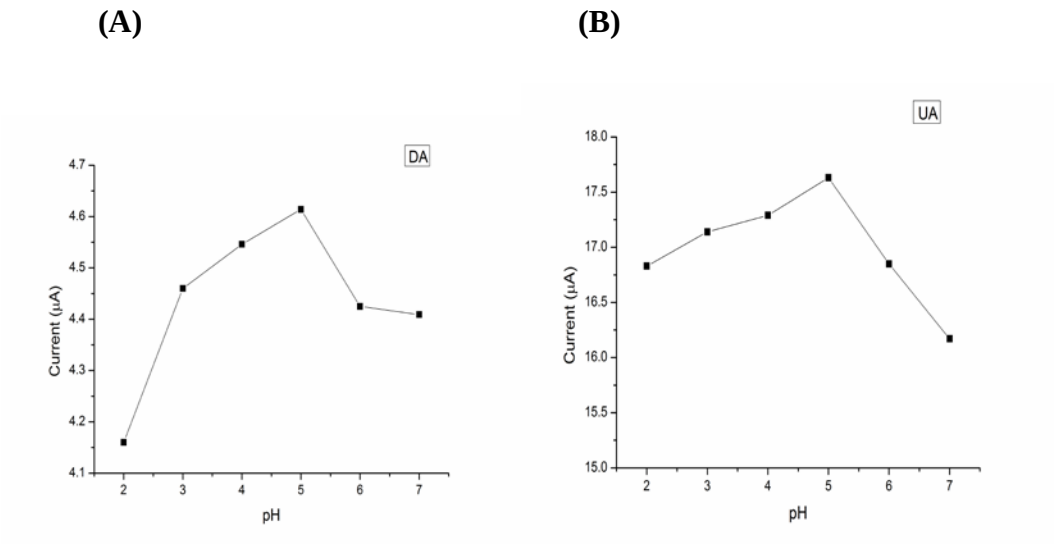

Figure 4.28: Effect of buffer pH on the peak current for the oxidation of (A) DA and (B) UA. Concentrations: DA, 0.128 mM; UA, 0.64 mM. Scan rate 50 mV/s.

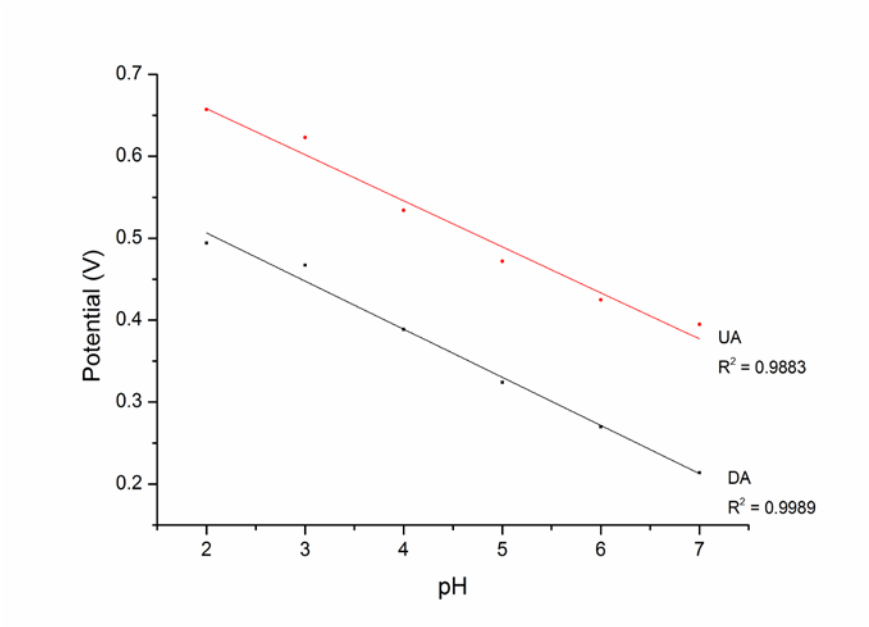

Figure 4.29: Effect of buffer pH on the peak oxidation potential for the oxidation of (A) DA and (B) UA. Concentrations: DA, 0.128 mM; UA, 0.64 mM. Scan rate 50 mV/s.

4.4.3.3.5 Effect of deposition time on the oxidation of DA and UA

The effect of the electro-deposition time of the Au nanoparticles was also investigated and it was found that 40 seconds deposition time gave the maximum signal for both DA and UA. This result is shown in Fig. 4.30. It can be seen that beyond the 50 seconds the Ip begins to drop due to the surface of the SPE becoming over-saturated.

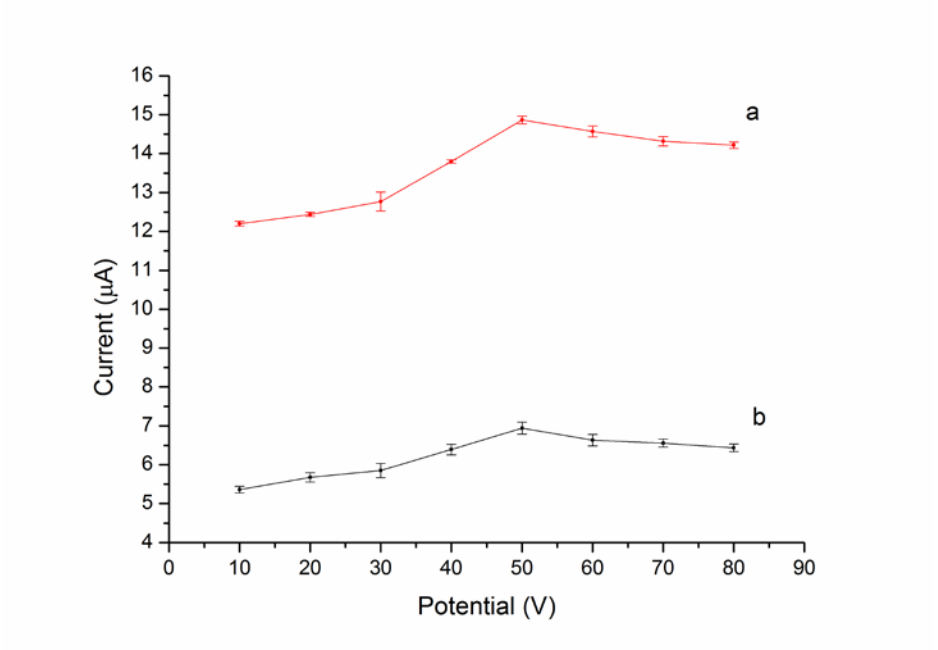

Figure 4.30: Effect of deposition time on the peak current for the oxidation of (a) UA and (b) DA. Concentrations: UA, 0.64 mM; DA, 0.128 mM. Scan rate 50 mV/s.

4.4.3.3.6 Simultaneous determination of DA and UA

The determination of DA and UA concentrations at the Au-CM SPE was performed with cyclic voltammetry. The oxidation peak currents of DA and UA were selected as the analytical signals. A six point calibration curve was prepared for both DA and UA by analyzing a series of analyte standard solutions at different concentrations. The DA concentration range was from 0.03 mM to 0.18 mM, and the UA concentration range was from 0.298 mM to 1.028 mM. The linear regression equation for DA was Ip_a (µA) = 25.3719 + 0.4977C with a correlation coefficient of R^2 = 0.9997. The linear regression equation for

UA was Ip_a (µA) = -2.249 + 0.1616C with a correlation coefficient of R^2 = 0.9941. The linear range was 0.196 mM to 1.67 mM for DA and 1.15mM to 5 mM for UA.

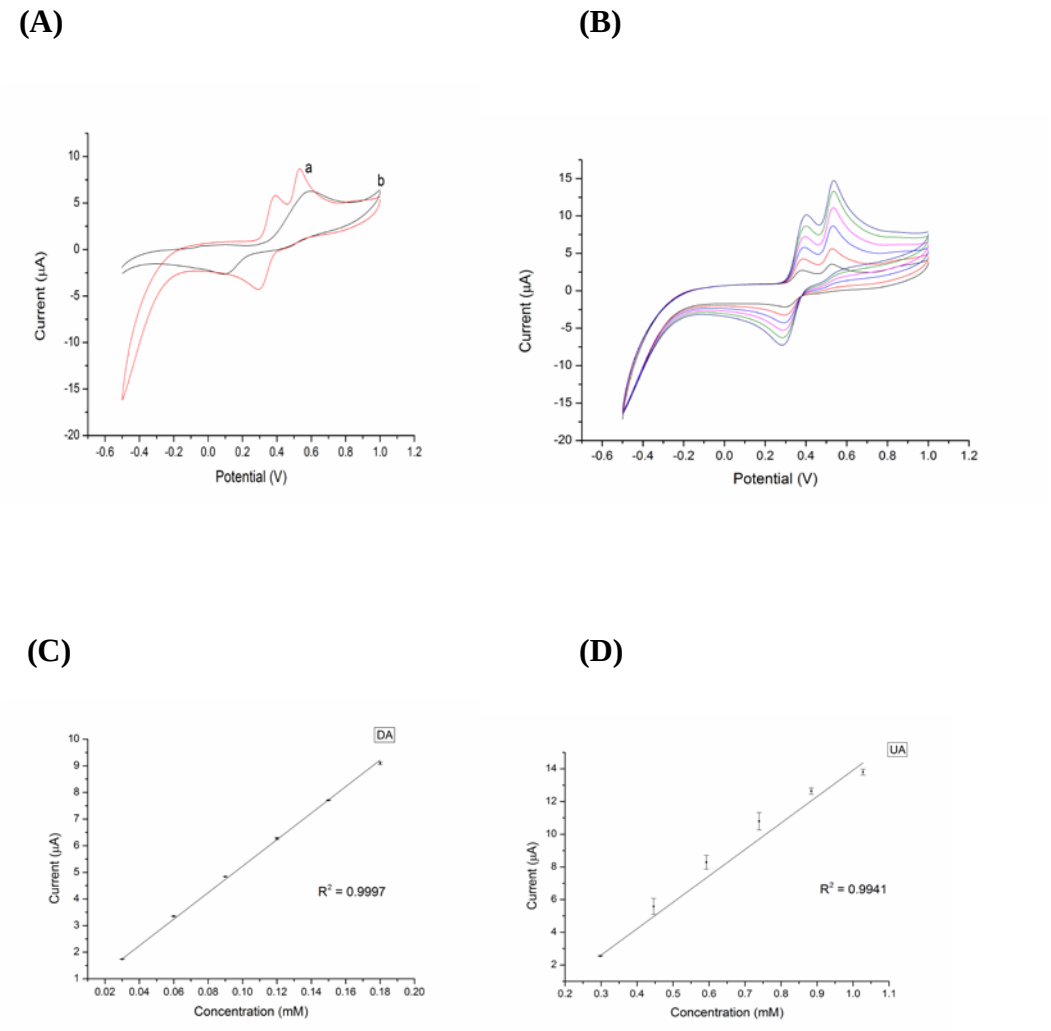

Figure 4.31: (A) CV of DA 0.06 mM and UA 0.593 mM at the (a) SPE and (b) SPE/CM/Au in 0.1 M PBS solution pH 5.0. (B) CVs of various DA and UA concentrations at the SPE/CM/Au in 0.1 M PB solution pH 5.0. Concentrations of analytes (a-e); 0.03, 0.06, 0.09, 0.12, 0.15 and 0.18 mM for DA and 0.298, 0.446, 0.593, 0.739, 0.884, and 1.028 mM for UA. (C) Calibration plot for DA obtained from the CV's shown in (B). (D) Calibration plot for UA obtained from the CV's shown in (B). Scan rate: 50 mV/s.

4.4.3.3.7 Characterisation of the SPE/CM/Au using amperometric (I-t) curve

Figure 4.32 shows the curves for the SPE/CM/Au poised at +0.2 V in response to 3 µL DA (0.01 M) (Fig. 6A) and 3 µL UA (0.05 M) at pH 5. Amperometric detection tests were performed separately for each of the two analytes with the aim of ensuring the electrode could detect increasing concentrations of the analytes at suitable increments of current. The detection potential was 200 mV at a 0.1 s scan rate.

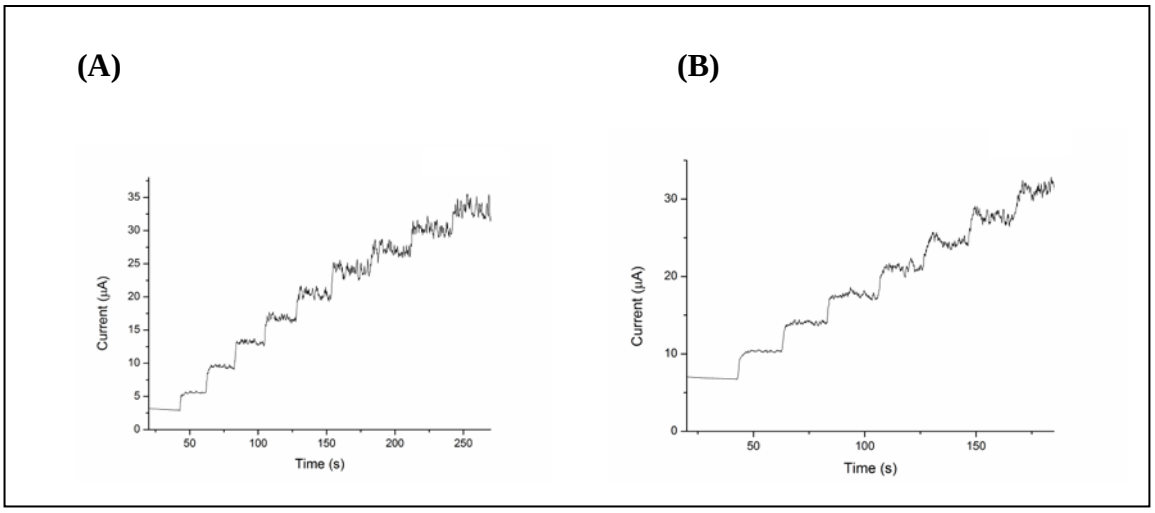

Figure 4.32: A typical current-time response of the SPE/CM/Au upon the successive additions of (A) 6 µM DA and (B) 30 µM UA in 0.1M PBS solution pH 5, E= 0.2V.

Under the optimum conditions, the detection limit (s/n = 3) for DA was calculated to be 6 x 10^{-6} M and for UA the detection limit is 30 x 10^{-6} M.

4.4.3.3.8 Stability and Repeatability of the SPE/CM/Au

The stability and repeatability of the SPE/CM/Au was also studied. This was performed first by 8 replicates of the SPE/CM/Au to determine the relative standard deviation (RSD) for the oxidation peak of DA and UA for 0.09 mM for DA and 0.593 mM for UA, which was found to be 0.52% and 5.03%, respectively. The electrode with CM adsorbed on the surface lost ca. 4% of its initial response after 2 days. The SPE/CM/Au could be used for at least 1 month, without significant loss of electrochemical signal.

4.4.3.3.9 Real sample analysis: determination of DA and UA in human serum

The human serum sample was diluted 5 times with phosphate buffer solution before the measurements to prevent the matrix effect of real samples. A certain value of standard solutions of DA and UA was added into the corresponding plasma serum for testing recovery. The results obtained for DA and UA in serum are listed in Table 4.6. To ascertain the correctness of the result the serum sample was spiked with certain amounts of DA and UA in about the same concentration as found in the samples.

Table 4.6: The recovery of DA and UA for the proposed method: (n=3)

Analyte	Spiked (mM)	Found (mM)	Recovery (%)
DA	0.06	0.055	91.6±1.7
	0.09	0.084	93.3±3.5
	0.12	0.114	95.1±2.8
UA	0.446	0.432	96.9±1.9
	0.593	0.553	93.3±2.8
	0.739	0.701	94.9±3.3

4.4.4 SPE/CM/ Pd nanoparticles

4.4.4.1 Characterisation using SEM of the SPE with palladium nanoparticles

The modified electrode's morphology was investigated using scanning electron microscopy (SEM) as mentioned in 4.4.1.1. The SEM image of the SPE can be seen in a Figure 4.33 (A). The imaging showed the porous nature and irregular shapes of carbon monoliths in Figure 4.33 (B) and confirms that the CM is well dispersed in DMF. This porous structure could significantly increase the electrode's surface as well as the electron transfer pathway. Figure 4.33 (C) shows the CM surface with Pd nanoparticles dispersed on the surface while Figure 4.33 (D) shows the magnified CM area with palladium nanoparticles. The Pd nanoparticles are the shiny clusters seen scattered around the SPE.

(A) **(B)**

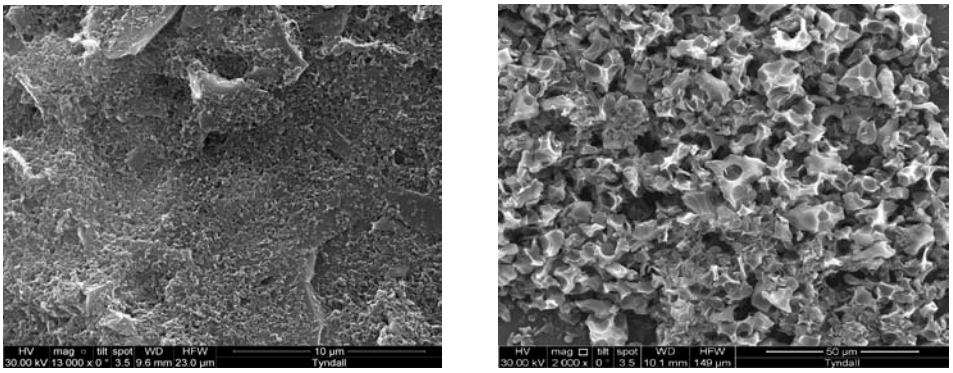

(C) **(D)**

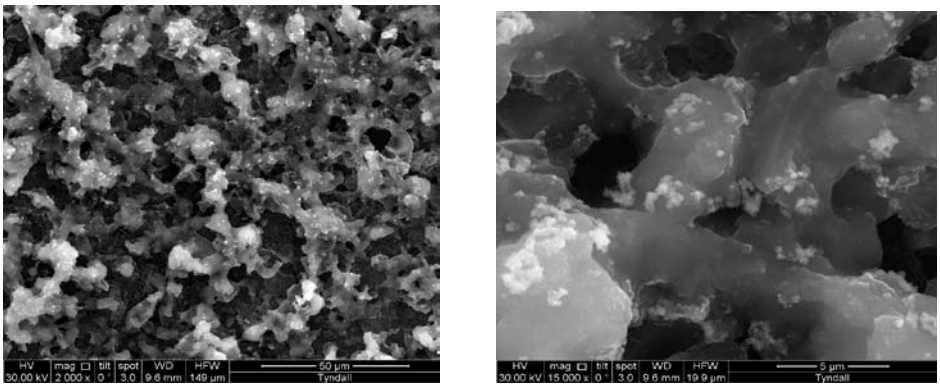

Figure 4.33: The SEM images (A) of the SPE, (B) of the CM surface, (C) of the CM surface with Pd nanoparticles and (D) of the magnified CM with Pd nanoparticles.

4.4.4.2 Contact-angle measurement of SPE, SPE/CM and SPE/CM/Pd

The measurement of the contact angle of the SPE, SPE/CM and the SPE/CM/Pd was conducted at the Tyndall National Institute, UCC, Cork as described in 4.4.1.2. The previous results in this section gave the contact angle of the bare screen-printed electrode being 118.7 º (in section 4.4.1.2) and the SPE/CM having a contact angle of 132.8º (in section 4.4.3.2). The SPE/CM/Pd had to be measured and it was found to give a contact angle measurement of 116.7 º, as shown below in Figure 4.34 (C). This result again indicates that the Pd caused the SPE modified with CM to become less hydrophobic.

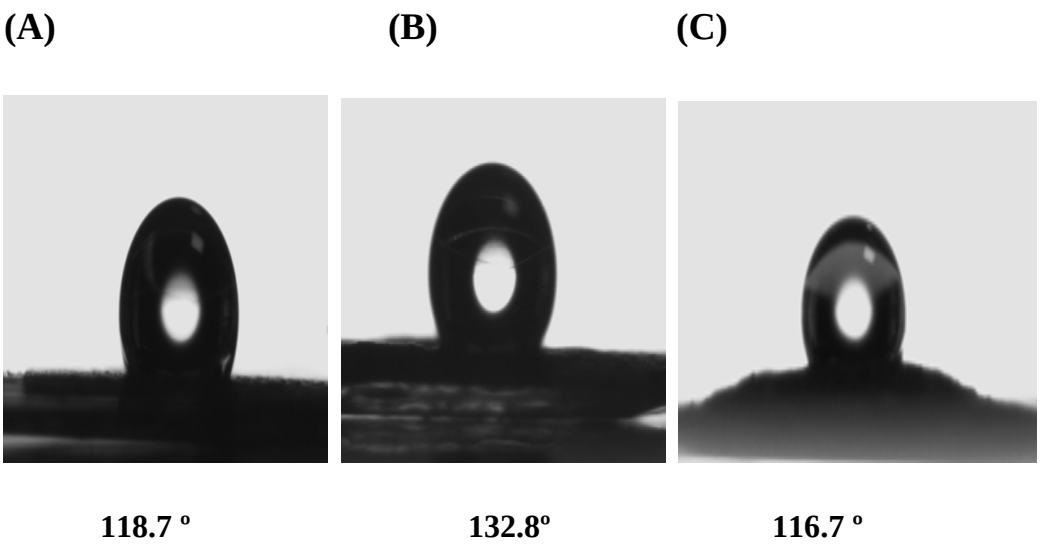

Figure 4.34: Images of water droplet on surface of (A) SPE (CA = 118.7º), (B) SPE/CM (CA = 132.8º) and (C) SPE/CM/Au (CA = 116.7º).

4.4.4.3 Electrochemical behaviour of SPE and SPE/CM/Pd

4.4.4.3.1 Compare Cyclic Voltammograms

The electrochemical responses of a SPE and a SPE/CM/Pd were characterised by cyclic voltammetry (CV) in phosphate buffer (PB) solution at pH 4 and can be seen in Figure 4.35. There were no redox peaks in the SPE and clearly there is one present in the SPE/CM/Pd. The background current of the SPE/CM/Pd increased greatly, indicating that the bare electrode was modified efficiently by CM with Pd nanoparticles.

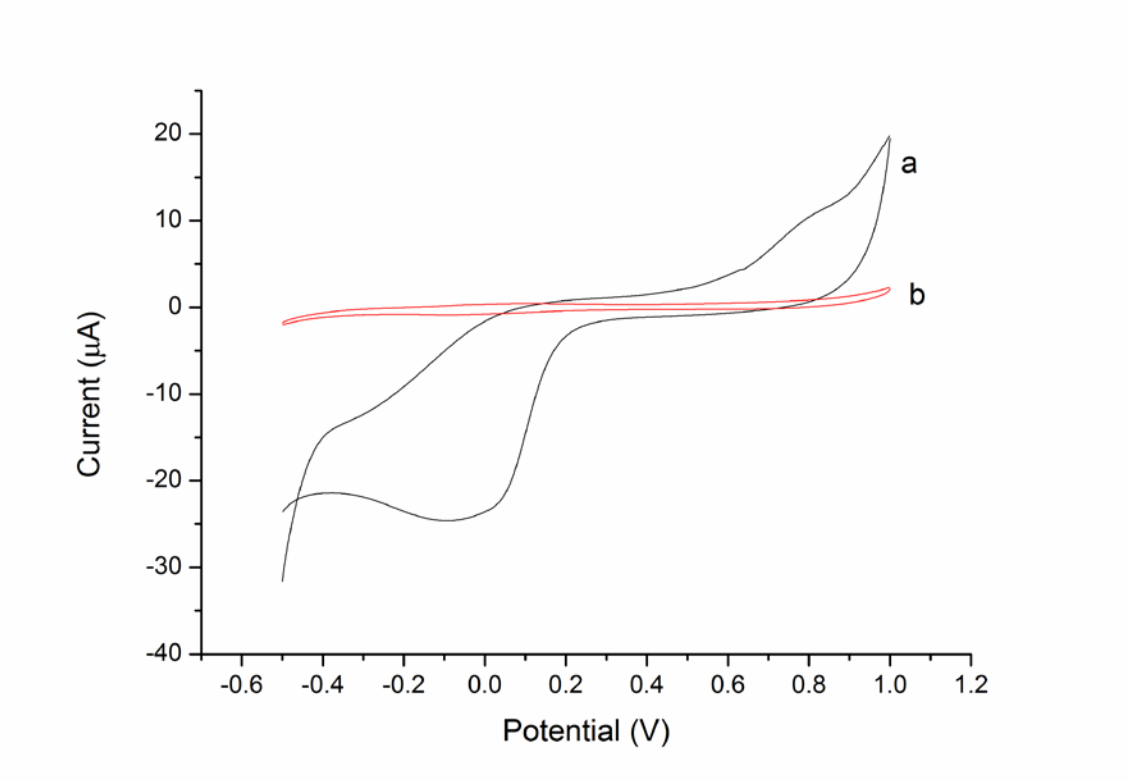

Figure 4.35 Cyclic voltammograms obtained at the (A) SPE and (B) SPE/CM/Pd in 0.1 mol L^{-1} PB solution pH 4 at scan rate 50 mV/s.

4.4.4.3.2 Vary scan-rate

This testing was carried out in section 4.4.1.3.2 for the bare screen-printed electrode. Below in Figure 4.36 is the results of the SPE/CM/Pd.

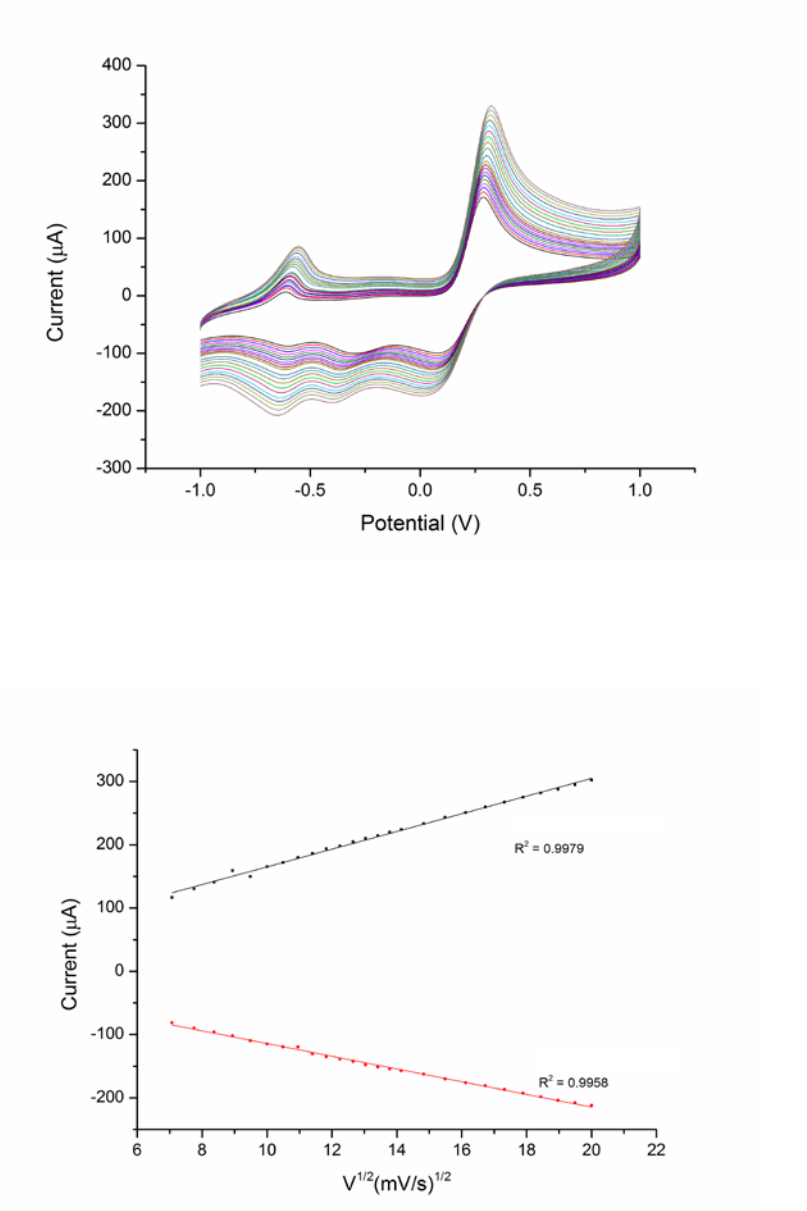

Figure 4.36: Cyclic voltammogram and the plot of the redox peak currents versus square root of the scan rate obtained at the SPE/CM/Pd in 5 mM $[Fe(CN)_6]^{3-/4-}$ in 0.1M KCl solution at scan rate 10 to 100 mV/s.

Again it is clear that the redox peak currents of $[Fe(CN)_6]^{3-/4-}$ enhanced with increasing scan rate, suggesting quasi-reversible one-electron redox behaviour. Both the anodic (Ipa) and cathodic (Ipc) were linearly proportional to the square root of the scan-rate ($V^{1/2}$) and the data can be seen in Table 4.7.

Table 4.7: The anodic (Ipa) and catodic (Ipc) peak currents vesus the square root of the scan rate ($V^{1/2}$). The testing was performed in 5 mM $[Fe(CN)_6]^{3-/4-}$ in 0.1 M KCl with varying scan rate of 50 to 400 mV/s for the SPE and the SPE/CM/Pd.

Electrode	Linear regression equation	R^2
SPE	Ipa (µA) = 8.309X + 2.561	R^2 = 0.9955
	Ipc (µA) = -4.642X - 15.551	R^2 = 0.9986
SPE/CM/Pd	Ipa (µA) = 2.71X + 32.424	R^2 = 0.9827
	Ipc (µA) = -0.45X – 5.79	R^2 = 0.9454

4.4.4.3.3 EIS measurements

The EIS measurements in this work were performed in a similar way to that described in section 4.4.1.4, in a background solution of $[Fe(CN)_6]^{3-/4-}$. Figure 4.37 (A) shows the impedance graphs of (a) a SPE, (b) a SPE/CM and (c) a SPE/CM/Pd. The SPE gave an impedance spectrum of a semicircle at a high ac modulation frequency and a line at low ac frequency indicating that the Warburg resistance was present as shown in Figure 4.37. This was related to the equivalent circuit which corresponds to the combination of the charge-transfer resistance (R_{ct}) representing the diffusion processes at the surface of the electrode. This reveals that the electrode process was controlled by electron transfer at the high

frequency and by diffusion at low frequency. The EIS of the modified SPES demonstrated different curves with no semicircle being displayed. This is due to the electron-transfer resistance being significantly lower with the CM. The SPE/CM/Pd seen in Figure 4.37 (B) gave much lower resistance values than the SPE/CM which demonstrates that with the Au nanoparticles the SPE might provide a higher electron conduction pathway.

(A) **(B)**

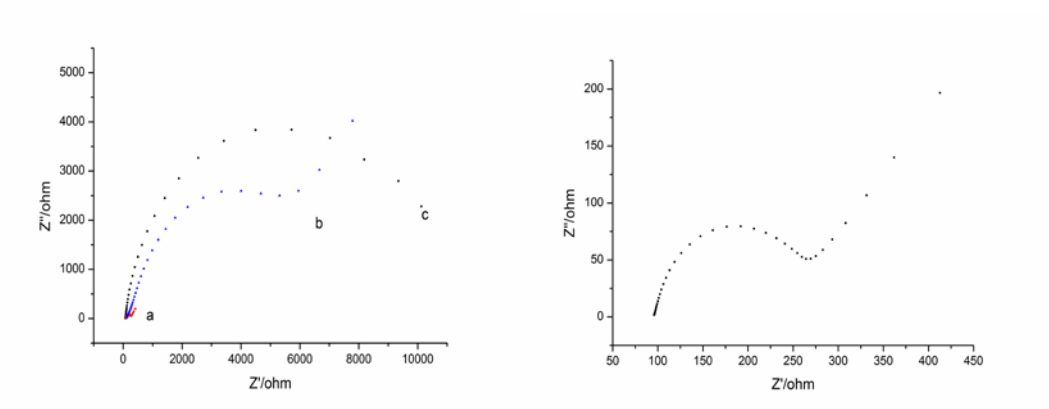

Figure 4.37: Nyquist plots of $[Fe(CN)6]^{3-/4-}$ in 0.1 M KCl solution with a SPE, a SPE/CM, and a SPE/CM/Pd. The frequency range is from 1 Hz to 100 kHz.

4.4.4.3.4 Effect of pH on the oxidation of AA and UA

The effect of solution pH on the response of AA and UA at the SPE/CM/Pd was investigated over the pH range of 2-7. Because proton takes part in the oxidation of UA and AA, the pH value of solution will greatly influence both the selectivity and sensitivity for the detection of AA and UA. The anodic peak potentials of both analytes shifted negatively as pH increased, depicted in Figure 4.38, with the slope obtained from the linear behaviour between the applied potential and the pH for AA and UA were found to be; 0.0513 and 0.0589 V/pH respectively, which are close to the anticipated Nernstian value (0.059 V/pH) for a two electons/two protons reaction. The pH value chosen to give the maximal separation of AA and UA was pH 4.

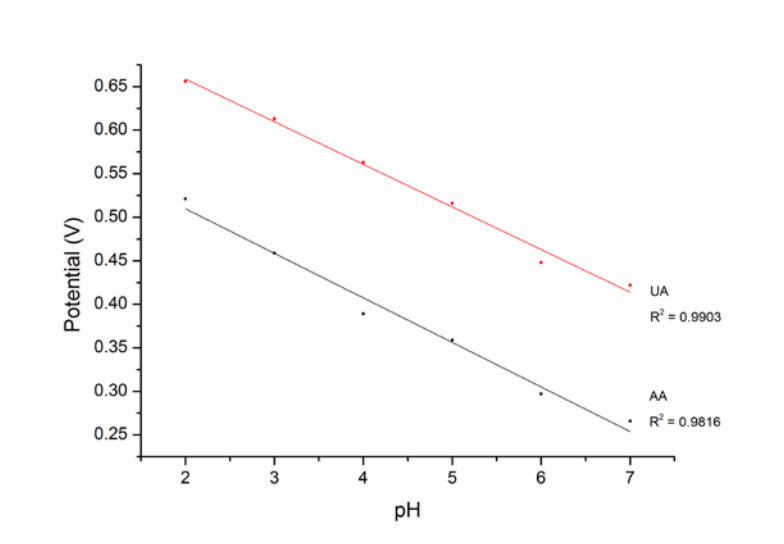

Figure 4.38: Effect of buffer pH on the peak oxidation potential for the oxidation of AA and UA. Concentrations: AA, 0.787 mM; UA, 1.27 mM. Scan rate 50 mV/s.

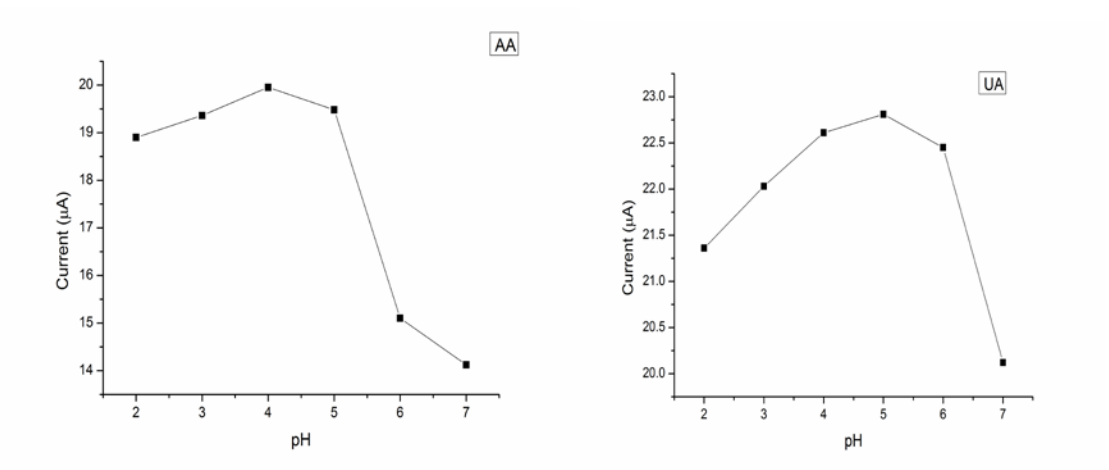

Figure 4.39: Effect of buffer pH on the peak current for the oxidation of AA and UA. Concentrations: AA, 0.787 mM; UA, 1.27 mM. Scan rate 50 mV/s.

4.4.4.3.5 Effect of deposition time on the oxidation of AA and UA

The effect of the electro-deposition time of the Pd nanoparticles was also investigated (n=3) and it was found that 40 seconds deposition time gave the maximum signal for both AA and UA. This result is shown below in Figure 4.40 and it can be seen that beyond the 40 seconds the Ip begins to drop due to the surface of the SPE becoming over-saturated.

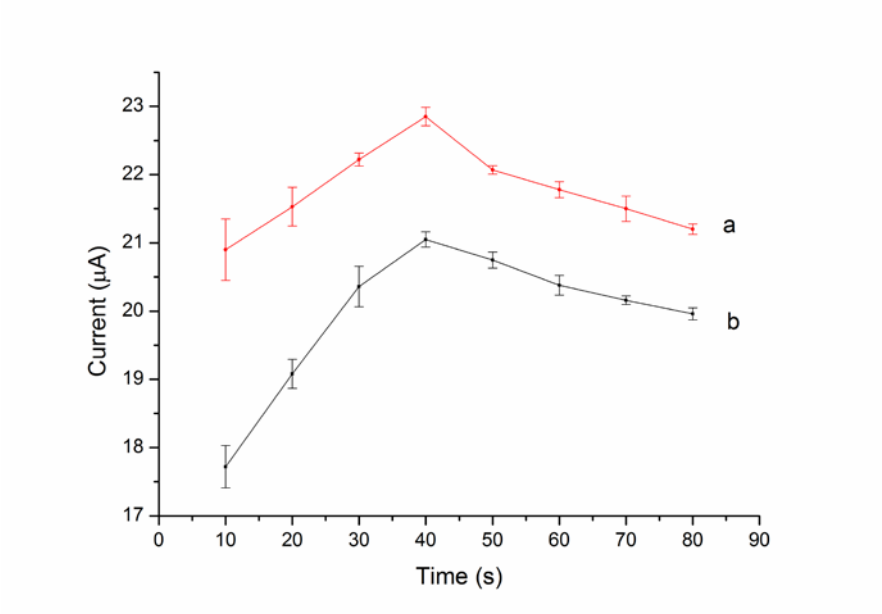

Figure 4.40: Effect of deposition time on the peak current for the oxidation of AA and UA. Concentrations: AA, 0.787 mM; UA, 1.27 mM. Scan rate 50 mV/s.

4.4.4.3.6 Simultaneous determination of AA and UA

The determination of AA and UA concentrations at the Pd-CM SPE was performed with cyclic voltammetry. The oxidation peak currents of AA and UA were selected as the analytical signals. A seven point calibration curve was prepared for both AA and UA by analyzing a series of analyte standard solutions at different concentrations. The AA concentration range was from 0.1 mM to 0.586 mM, and the UA concentration range was from 0.3 mM to 1.7 mM. The linear regression equation for UA was $I\text{p}_a$ (µA) = 3.042 + 0.2284C with a correlation coefficient of R^2 = 0.9976. The linear regression equation for UA was $I\text{p}_a$ (µA) = 4.418 + 0.2223C with a correlation coefficient of R^2 = 0.9901. The linear range was 0.2 mM to 2.38 mM for AA and 0.4 mM to 2.56 mM for UA.

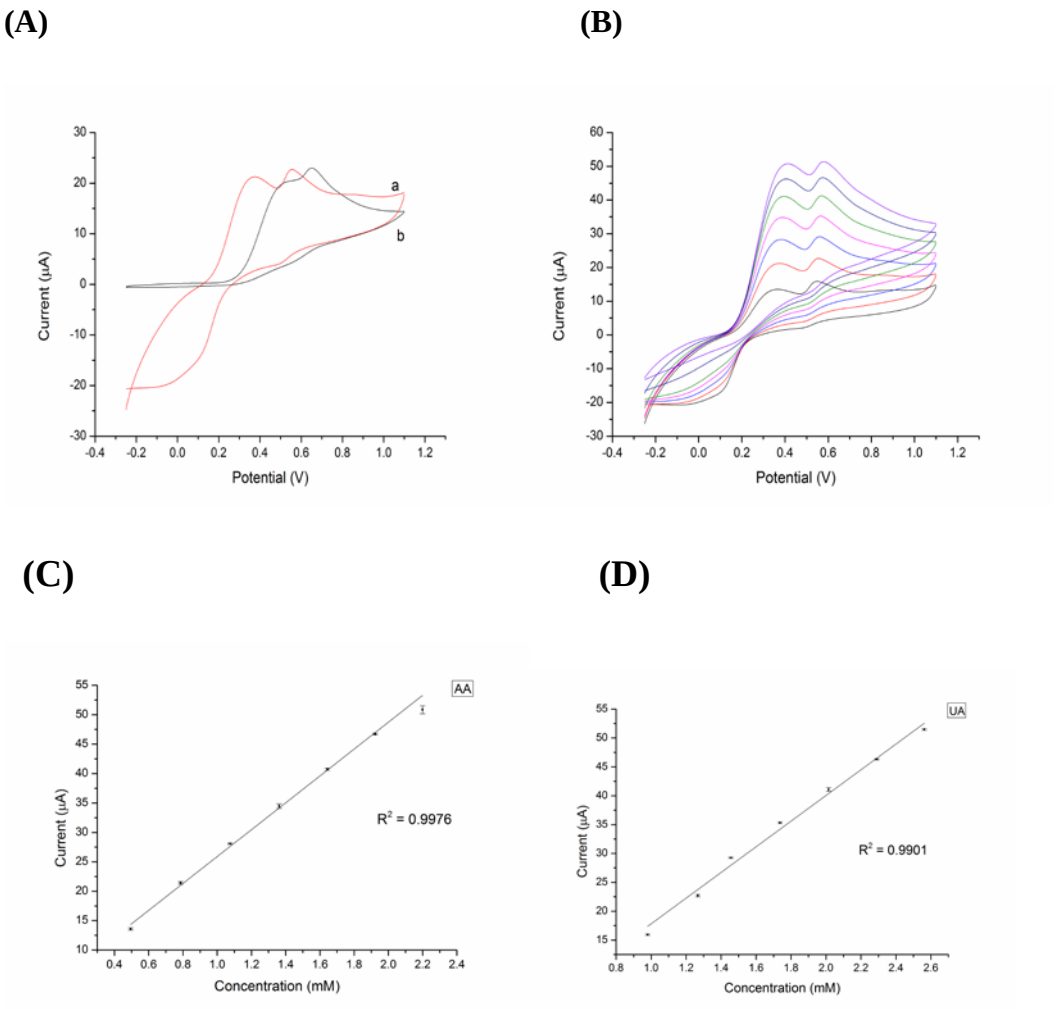

Figure 4.41: (A) CV of AA 0.787 mM and UA 1.27 mM at the (a) SPE/CM/Pd and (b) SPE in 0.1 M PB solution pH 4.0. (B) CVs of various AA and UA concentrations at the SPE/CM/Pd in 0.1 M PB solution pH 4.0. Concentrations of analytes (a-e); 0.495, 0.787, 1.076, 1.362, 1.644, 1.923 and 2.199 mM for AA and 0.98, 1.267, 1.456, 1.737, 2.015, 2.29 and 12.562 mM for UA. (C) Calibration plot for AA obtained from the CV's recording shown in (B). (D) Calibration plot for UA obtained from the CV's recording shown in (B). Scan rate: 50 mV/s.

4.4.4.3.7 Characterisation of the SPE/CM/Au using cyclic amperometric detection

Figure 4.42 shows the curves for the SPE/CM/Au poised at +0.2 V in response to 5 µL AA (0.05 M) (Fig.A) and 7 µL (0.05 M) UA at pH 4. Amperometric detection tests were performed separately for each of the two analytes with the aim of ensuring the electrode could detect increasing concentrations of the analytes at suitable increments of current. The detection potential was 200 mV at a 0.1 s scan rate.

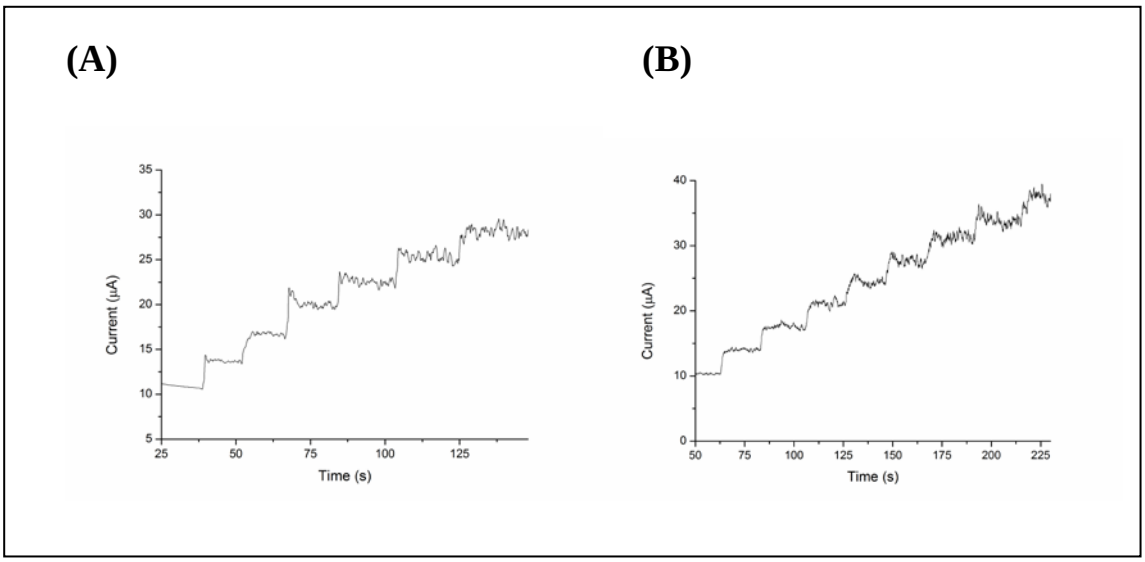

Figure 4.42: A typical current-time response of the SPE/CM/Pd upon the successive additions of (A) 50 µM AA and (B) 70 µM UA in 0.1M PBS solution pH 4, E= 0.2V.

Under the optimum conditions, the detection limit (s/n = 3) for AA was calculated to be 50 x 10^{-6} M and for UA the detection limit is 70 x 10^{-6} M.

4.4.4.3.8 Stability and repeatability of the SPE/CM/Pd

The stability and repeatability of the SPE/CM/Pd was also studied. This was performed first by 8 replicates of the SPE/CM/Pd to determine the relative standard deviation (RSD) for the oxidation peak of AA and UA for 0.52 mM for AA and 1.92 mM for UA, which was found to be 1.08 % and 1.80 %, respectively. The electrode with CM adsorbed on the surface lost ca. 3.7 % of its initial response after 2 days. The SPE/CM/Pd could be used for at least 1 month, without significant loss of electrochemical signal.

4.4.4.3.9 Real sample analysis: determination of AA and UA in human serum

The human serum sample was diluted 5 times with phosphate buffer solution before the measurements to prevent the matrix effect of real samples. A certain value of standard solutions of AA and UA was added into the corresponding plasma serum for testing recovery. The results obtained for AA and UA in serum are listed in Table 4.8. To ascertain the correctness of the result the serum sample was spiked with certain amounts of AA and UA in about the same concentration as found in the samples.

Table 4.8: The recovery of DA and UA for the proposed method: (n=3)

Analyte	Spiked (mM)	Found	Recovery %
AA	0.787	0.742	94.28±2.1
	1.076	1.019	94.44±2.5
	1.362	1.256	92.22±2.8
UA	1.267	1.108	87.45±2.7
	1.456	1.328	91.21±2.3
	1.737	1.558	89.69±2.9

4.5 Discussion & Future Work

This chapter discussed the method development of modifying in-house SPE's by two simple fabrication methods. The first method was using metal nanoparticles to enhance the SPE's sensitivity. The metal nanoparticles were attached to the SPE via electrodeposition.

Both the SPE/Au and the SPE/Pd were able to perform simultaneous determinations of multiple analytes which the SPE was unable to achieve by itself as it was unable to discriminate the signals. The SPE/Au was able to provide better sensitivity than the SPE/Pd due to the excellent electrochemical properties of gold.

The second method was using a new class of carbonaceous material known as carbon monolith again with metal nanoparticles. Again, both of the modified SPEs were able to perform simultaneous determinations, with the SPE/CM/Au again achieving better sensitivity than the SPE/CM/Pd. The main difference between the SPE/Au and the SPE/CM/Au was the electrodes ability to have a larger linear range with the CM due to the larger surface area it provides. This larger linear range allowed for more defined separations between the analytes and thus an overall better electrode performance. This is the same for the SPE/Pd and the SPE/CM/Pd. The surface topology of all four modifications were studied using SEM and the CM gives the SPE a much different surface than the SPE with far more sites for the metal nanoparticles to attach themselves onto compared to the SPE.

Screen-printed electrodes (SPEs) have attracted considerable attention in electrochemical sensing due to the inexpensive, rapid and simple manufacturing process. However, the use of the SPEs for simultaneous determination of multiple analytes including DA and UA, and AA and UA, has been rarely reported, since the unmodified SPEs are unable to discriminate the signals. Although other modified SPE's exist for multiple determinations. Their fabrication procedure is relatively complex for disposable devices. This work has allowed SPE's to be modified by a number of different methods quickly and efficiently at a very low cost.

Future work will look at the effect of ascorbic acid and other interfering compounds on simultaneous determination of DA and UA as well as coupling these modified electrodes with other electrochemical techniques such as capillary electrophoresis to see if these electrodes have the capabilities to separate and detect multiple analytes. Other future work

will also include modifying the SPE with carbon nanotubes as well as carbon nanotubes and metal nanoparticles to compare with the electrodes studies in this chapter.

4.6 Highlights

This chapter focused on the method development of modifying in-house SPE's by two simple fabrication methods. The first method was using metal nanoparticles to enhance the SPE's sensitivity. There were two types of metals used. The first modifications were carried out using gold nanoparticles. Following on from this palladium nanoparticles were attached to the SPE via electrodeposition.

The second method modifies the SPE with first carbon monolith material and then with metal nanoparticles. Bare SPE's were unable to simultaneously determine multiple analytes however all four modified electrodes were capable of performing simultaneous determinations.

4.7 References

[1] D. Desmond, B. Lane, J. Alderman, M. Hill, D.W.M. Arrigan, J.D. Glennon, Sensors and Actuators B: Chemical 48 (1998) 409.

[2] M. Jasinski, P. Gründler, G.U. Flechsig, J. Wang, Electroanalysis 13 (2001) 34.

[3] P. Ugo, L.M. Moretto, P. Bertoncello, J. Wang, Electroanalysis 10 (1998) 1017.

[4] J. Wang, J. Lu, B. Tian, C. Yarnitzky, Journal of Electroanalytical Chemistry 361 (1993) 77.

[5] S.H. Huang, H.H. Liao, D.H. Chen, Biosensors and Bioelectronics 25 (2010) 2351.

[6] A. Salimi, V. Alizadeh, R.G. Compton, Analytical Sciences 21 (2005) 1275.

[7] L. Sun, Z. Zhang, H. Dang, Materials Letters 57 (2003) 3874.

[8] M. Fukushima, H. Yanagi, S. Hayashi, N. Suganuma, Y. Taniguchi, Thin Solid Films 438 (2003) 39.

[9] M. Chikae, K. Idegami, K. Kerman, N. Nagatani, M. Ishikawa, Y. Takamura, E. Tamiya, Electrochemistry Communications 8 (2006) 1375.

[10] X. Dai, O. Nekraseova, M.E. Hyde, R.G. Compton, Analytical chemistry 76 (2004) 5924.

[11] M.S. El-Deab, T. Okajima, T. Ohsaka, Journal of the Electrochemical Society 150 (2003) A851.

[12] E. Majid, S. Hrapovic, Y. Liu, K.B. Male, J.H.T. Luong, Analytical chemistry 78 (2006) 762.

[13] C.M. Welch, C.E. Banks, A.O. Simm, R.G. Compton, Analytical and Bioanalytical Chemistry 382 (2005) 12.

[14] Z. Tang, S. Liu, S. Dong, E. Wang, Journal of Electroanalytical Chemistry 502 (2001) 146.

[15] C. Demaille, M. Brust, M. Tsionsky, A.J. Bard, Analytical chemistry 69 (1997) 2323.

[16] F.L. Leibowitz, W. Zheng, M.M. Maye, C.-J. Zhong, Analytical chemistry 71 (1999) 5076.

[17] A.C. Templeton, J.J. Pietron, R.W. Murray, P. Mulvaney, The Journal of Physical Chemistry B 104 (2000) 564.

[18] M.-C. Daniel, D. Astruc, Chemical reviews 104 (2004) 293.

[19] J. Huang, Y. Liu, H. Hou, T. You, Biosensors and Bioelectronics 24 (2008) 632.

[20] S.H. Lim, J. Wei, J. Lin, Q. Li, J. KuaYou, Biosensors and Bioelectronics 20 (2005) 2341.

[21] L.-P. Lu, S.-Q. Wang, X.-Q. Lin, Analytica chimica acta 519 (2004) 161.

[22] S. Zhang, N. Wang, H. Yu, Y. Niu, C. Sun, Bioelectrochemistry 67 (2005) 15.

[23] S. Thiagarajan, S.-M. Chen, Talanta 74 (2007) 212.

[24] R.P.H. Nikolajsen, Å.M. Hansen, Analytica chimica acta 449 (2001) 1.

[25] H.R. Zare, N. Rajabzadeh, N. Nasirizadeh, M. Mazloum Ardakani, Journal of Electroanalytical Chemistry 589 (2006) 60.

[26] G.-P Jin, X-Q. Lin, J.-M. Gong, Journal of Electroanalytical Chemistry 562 (2004) 135.

[27] M. Ferreira, L.R. Dinelli, K. Wohnrath, A.A. Batista, O.N. Oliveira Jr, Thin Solid Films 446 (2004) 301.

[28] K. Hayashi, Y. Iwasaki, R. Kurita, K. Sunagawa, O. Niwa, Electrochemistry Communications 5 (2003) 1037.

[29] R.D Shankaran, N. Uehara, T. Kato, Analytica chimica acta 478 (2003) 321

[30] M.D Pilar, T. Sotomayor, A.A. Tanaka, L.T. Kubota, Analytica chimica acta 455 (2002) 215.

[31] F. Lisdat, U. Wollenberger, A. Makower, H. Hörtnagl, D. Pfeiffer, F.W. Scheller, Biosensors and Bioelectronics 12 (1997) 1199.

[32] M.A. Dayton, A.G. Ewing, R.M. Wightman, Journal of Electroanalytical Chemistry 146 (1983) 189.

[33] S. Hrapovic, Y. Liu, K.B. Male, J.H.T. Luong, Analytical chemistry 76 (2004) 1083.

[34] B. Nalini, S. Sriman Narayanan, Analytica chimica acta 405 (2000) 93.

[35] S.S.L. Castro, V.R. Balbo, P.J.S. Barbeira, N.R. Stradiotto, Talanta 55 (2001) 249.

[36] I.G. Casello, M.R. Guascito, Electroanalysis 9 (1997) 1381.

[37] A.M. Yu, H.L. Zhang, H.Y. Chen, Electroanalysis 9 (1997) 788.

[38] P.R. Roy, T. Okajima, T. Ohsaka, Bioelectrochemistry 59 (2003) 11.

[39] Z. Gao, K.S. Siow, A. Ng, Y. Zhang, Analytica chimica acta 343 (1997) 49.

[40] W. Nyhan, Journal of autism and childhood schizophrenia 6 (1976) 235.

[41] V.W.R. H.A. Harper, P.A. Mayes, in Lange Medical Publication, 1979.

[42] L. Zhang, X. Lin, Analyst 126 (2001) 367.

[43] S. Gjørup, H. Poulsen, E. Prætorius, Scandinavian Journal of Clinical & Laboratory Investigation 7 (1955) 201.

[44] H.M. Kalckar, Journal of Biological Chemistry 167 (1947) 429.

[45] E. Praetorius, Scandinavian Journal of Clinical & Laboratory Investigation 1 (1949) 222.

[46] W. Pudelkiewicz, M. Stutz, L. Matterson, Poultry Science 47 (1968) 1274.

[47] D.A. Mei, G.J. Gross, K. Nithipatikom, Analytical Biochemistry 238 (1996) 34.

[48] M.A. Ross, Journal of Chromatography B: Biomedical Sciences and Applications 657 (1994) 197.

[49] Y. Yue-dong, Biomedical Chromatography 12 (1998) 47.

[50] E. Popa, Y. Kubota, D.A. Tryk, A. Fujishima, Analytical Chemistry 72 (2000) 1724.

[51] Z. yan, J.-R. Zhang, H.-Q. Fang, Analytical Letters 32 (1999) 223.

[52] J.-M. Zen, Analyst 123 (1998) 1345.

[53] J.-M. Zen, C.-T. Hsu, Talanta 46 (1998) 1363.

[54] X. He, L. Zhou, E.P. Nesterenko, P.N. Nesterenko, B. Paull, J.O. Omamogho, J.D. Glennon, J.H. Luong, Analytical chemistry 84 (2012) 2351.

Chapter 5

Conclusions & Future Work

5.1 Introduction

Electroanalytical techniques, which are concerned with the interplay between electrical quantities such as current, potential or charge, have found widespread use in a vast range of applications, including industrial quality control, environmental monitoring and biomedical advances. From its discovery over 200 years ago by Galvani, overwhelming advances (many of which have been described in Chapter 1) have been made in the field. Advances in recent decades such as the development of micro- and ultramicro-electrodes, progress in the methods of electrode modification, the coupling of biological components and electrochemical transducers, the development of ultratrace voltammetric techniques and high resolution scanning probe microscopies have led to a substantial increase in the popularity of electroanalysis. Its popularity can also be attributed to its attractive advantages, such as selectivity and sensitivity, inexpensive equipment, ample choice of working electrode materials and ability to attain real-time measurements.

However, despite these obvious advantages, there seems to be a lack in the use of such techniques in certain analytical laboratories in which routine analysis is performed. The main applications in pharmaceutical companies in which electrochemistry plays a role in the laboratory are in conventional pH probes, conductivity detectors and coulometric Karl Fischer titrations. One of the primary reasons for this is surely the incorrect perception that such procedures are difficult to perform. Another reason lies in the properties of the most commonly employed electrode materials such as platinum, gold, glassy carbon and mercury. The limitations of the former three are primarily the necessity for electrode maintenance.

In order to encourage the use of electroanalytical techniques in industries such as the pharmaceutical industry, it seems much work is required to promote the advantages associated with such methods and to adequately train analysts in the understanding of electroanalytical theory and use of electroanalytical instrumentation. More importantly, it is necessary to develop electroanalytical procedures that are simple to perform and employ convenient, easy to maintain and non-toxic electrode materials. The work in this thesis describes simple analytical procedures using inexpensive sensors and separation devices for health applications.

5.2 Chapter 2

The first separation device that was fabricated and investigated was the toner-based microchip. This inexpensive device was coupled with chemiluminescence detection and two potential applications were tested. The first application was the separation and detection of four amino acids which gave all gave limits of detection below 1 µM as well as giving a good % recovery when spiked in human serum. The second application was the separation of chiral compounds, which again gave very low limits of detection, again below 1 µM. The separations of both applications can be achieved in less than 1 minute. The issue with this device is not the sensitivity that can be achieved but rather the % RSD which is a disappointing 34%. This high value can be explained due to the fabrication process. Currently each device is individually made by hand and thus no two microchips can be deemed to be identical however these devices should be used for qualitative analysis rather than quantitative analysis until the % RSD is greatly reduced. Future work on these devices will aim to lower this % RSD by using masks when fabricating these devicesto ensure better reproducibility between them.

5.3 Chapter 3

The aim of the research presented in Chapter 3 was to fabricate and develop a novel microelectrode configuration onto acetate substrate for the effective separation and quantification of biologically important neurotransmitters. This microelectrode consisted of a gold working electrode, platinum counter electrode and silver/silver chloride reference electrode. There has been much work in the area of microelectrodes in the literature over the last number of years due to their distinct advantages over the conventional macroelectrodes. These advantages include faster mass transport, decreased capacitance and reduced signal to noise ratio as well as reduced ohmic effects. The acetate microelectrode was initially tested using cyclic voltammetry and uric acid to ensure good reproducibility and reliability. The microelectrode gave excellent stability and repeatability results including a correlation coefficient of R^2 = 0.999 with increasing concentrations of uric acid. Once the microelectrodes reliability was verified, it was then coupled with capillary electrophoresis (CE) to separate and detect biologically important neurotransmitters. The microelectrode was

able to detect all four neurotransmitters as well as being able to carry out quantitative analysis effectively. The limit of detection for all four analytes was under 40 µM with a correlation coefficient of R^2 = 0.9 for each neurotransmitter. The novelty of this microelectrode lies in the fact that it is fabricated onto inexpensive, flexible acetate offering the advantage of being able to exclude any dicing step and allowing the microelectrodes to be easily cut and tailored to fit any required shape needed. The final test in this chapter was to compare the performance of the microelectrode with a convention 3-electrode system using the same electrode materials. The results were as expected with both electropherograms giving very similar results with regards to migration times and peak shape. The main difference between these graphs was the current obtained using the microelectrode was approximately 3times less than the conventional system. This is a good result considering the area of the working electrode in the acetate microelectrode is over 4.5times smaller than the conventional working electrode. Future work will involve using the microelectrode coupled with CE to perform a number of other applications including separating and detecting amino acids, other neurotransmitters as well as chiral compounds. This microelectrode will also be coupled with the toner-based microdevice to allow for electrochemical detection, both in-channel and end-channel detection.

5.4 Chapter 4

The final area of my research focused on modifying in-house fabricated screen-printed macroelectrodes (SPEs). In recent years, SPEs have attracted considerable attention in electrochemical sensing due to the inexpensive, rapid and simple manufacturing process. The use of the SPEs for simultaneous determinations of analytes has however, rarely been reported, since the unmodified SPEs are unable to discriminate the signals. There are reports of modifying these SPEs with electrocatalytic films however this fabrication process is complex and time-consuming for electrodes that are intended to be disposable, cheap and simple to manufacture. There were four modifications made to the SPEs in this chapter, firstly the SPEs were modified with gold nanoparticles via electrodeposition. The second modification involves a similar procedure except with palladium nanoparticles. Both modifications allowed for simultaneous determinations of analytes; however the gold nanoparticles enhanced the sensitivity of the SPE about 4-5 times more than the palladium

nanoparticles due to the excellent electrochemical properties of gold. The third modification involved drop-casting carbon monolith material onto the SPE and then electrodepositing gold nanoparticles onto it. The fourth modification was similar to the third except using palladium nanoparticles instead of gold. There were significant differences to these types of modified electrodes in particular to the linear range of the analytes tested due to the increased surface are of the SPE from the carbon monolith material. The cyclic voltammograms obtained using the third and fourth modifications showed much clearer separated peaks than when the SPEs were only modified with nanoparticles as it was possible to use higher concentrations of analytes. All four modifications allowed for simultaneous determinations with excellent reproducibility and stability with all four modified SPEs have a % RSD below 5%. Future work with these SPEs will involve modifying the SPE with multi-walled carbon nanotubes and subsequently electrodepositing metal nanoparticles to these and comparing these results with the data in this work. Other noble metal nanoparticles will also be tested and compared to the performance of the gold and palladium nanoparticles.

5.5 Conclusions

On successful completion of the work described in this thesis, it is envisaged that the proposed sensors and separation devices could be used in the determination of a wide variety of analytes allowing for multiple health applications. The sensors and separations devices are easy to fabricate and modify and involve the use of relatively inexpensive equipment when compared to instrumental techniques such as ICP-MC or AAS. It is hoped that this work and others in the same vein will lead to the further promotion of the advantages of electroanalytical techniques and result in their increase use in analytical laboratories carrying out both routine analysis and research.

Chapter 6

Appendix

6. Appendix

6.1 List of Journal Publications, Oral and Poster Presentations

6.1.1 List of Journal Publications

1. Una Crowley, Francesco Dicorato, Jeremy D. Glennon, Eric Moore.
'Microchip capillary electrophoresis system with amperometric detection: A review of the theory, recent developments and future evolutions', Research Trends; Current topics in analytical chemistry; Volume 9, pgs 77-86, 2012.

2. Una B. Crowley, Walter Messina, Miloslav Pravda, Jeremy D. Glennon, Eric Moore. 'Electrochemical property of screen printed electrode modified with gold nanoparticles for the simultaneous determination of Dopamine and Uric acid', accepted and in press, Journal of Electroanalytical Chemistry.

3. Una B. Crowley, Siriboon Mukdasai, Walter Messina, Xiaoyun He, Supalax Sriharanai, Ekaterina P. Nesterenko, Pavel N. Nesterenko , Brett Paull, Miloslav Pravda, Jeremy D. Glennon, Eric Moore.
'Electrochemical properties of carbon monolith with gold nanoparticles modified screen printed electrode for the simultaneous determination of Dopamine and Uric acid'. Submitted to Electroanalysis.

4. Una B. Crowley, Jeremy D. Glennon, Eric Moore.
'Novel microelectrodes fabricated on acetate substrate used for electrochemical determination of uric acid', - in preparation.

5. Una B. Crowley, Jeremy D. Glennon, Eric Moore.
'Novel microelectrodes fabricated on acetate substrate coupled with capillary electrophoresis to separate and detect multiple neurotransmitters', - in preparation.

6. Walter Messina, Una Crowley, Michelle Fitzgerald, Eric Moore
'Fabrication of gold nanopillars on gold interdigitated impedance electrodes for biological applications', Submitted to ICST 2014 conference proceedings

6.1.2 List of Oral Presentations

1. Una Crowley, Mark Nussbaum, Jeremy D Glennon, Eric Moore
'Separation of Biomarkers by Micro-Electrophoresis with Chemiluminescence Detection in Toner-Based Microchips', The 11th Asia Pacific Symposium on Microscale Separations and Analysis (*APCE 2011*), Hobart, Tasmania, November 27-30 2011.

2. Una Crowley, Jeremy D Glennon, Eric Moore
'Toner-based microchips coupled with luminol chemiluminescence detection and in-channel amperometric detection', ISSC review meeting, Dublin City University, Dublin, Ireland, June 26-27 2012.

3. Una Crowley, Mila Pravda, Eric Moore, Jeremy D Glennon
'Toner-based microchips coupled with luminol chemiluminescence detection and in-channel amperometric detection', NanoBio Europe, Varesse, Italy, July 18-20 2012.

4. Una Crowley, Jeremy D Glennon, Eric Moore
'Detection of analytes using toner-based microchips, electrodes fabricated onto acetate and enhanced capabilities of screen-printed electrodes', 8th Conference on Analytical Sciences Ireland (Casi), University College Cork, Cork, July 1-2 2013.

5. Una Crowley, Jeremy D Glennon, Eric Moore
'Detection of analytes using toner-based microchips, electrodes fabricated onto acetate and enhanced capabilities of screen-printed electrodes', Postgraduate Research Day, Department of Chemistry, University College Cork, Cork, Ireland, August 14th 2013.

6.1.3 List of Poster Presentations

1. Una Crowley, Mila Pravda, Eric Moore, Jeremy D. Glennon.
'Method of development for toner-based microchips', ISSC review meeting, Clarion Hotel, Cork, December 6-7 2010.

2. Una Crowley, Mila Pravda, Eric Moore, Jeremy D. Glennon.
'Method of development for toner-based microchips', 6th Conference on Analytical Sciences Ireland (Casi), Dublin City University, Dublin, Ireland, February 21-22 2011.

3. Una Crowley, Mila Pravda, Eric Moore, Jeremy D. Glennon.
'Method of development for toner-based microchips', 37th International Symposium on High performance liquid Separations and related techniques, Budapest, June 19-23 2011.

4. Una Crowley, Mila Pravda, Jeremy D Glennon, Eric Moore.
'Toner-based microchips coupled with luminol chemiluminescence detection and in-channel amperometric detection', NanoBio Europe, Varesse, Italy, July 18-20 2012.

5. Una Crowley, Jeremy D Glennon, Eric Moore.
'Separation of Biomarkers by Micro-electrophoresis with Chemiluminescence and Electrochemical detection in Toner-based microchips', 29th international Symposium on Chromatography, Torun, Poland, September 9-13th 2012.

6. Una Crowley, Jeremy D Glennon, Eric Moore.
'Separation of Biomarkers by Micro-electrophoresis with Chemiluminescence and Electrochemical detection in Toner-based microchips', Institute of Chemistry of Ireland Congress 2012, University College Cork, Cork, Ireland, November 26 2012.

7. Una Crowley, Jeremy D Glennon, Eric Moore.
'Novel acetate electrode and increased sensitivity of screen printed electrodes using metal nano-particles for electrochemical detection', Tyndall Internal Conference, Tyndall, Cork, Ireland, 25th May 2013.

8. Una Crowley, Jeremy D Glennon, Eric Moore.
'Detection of analytes using toner-based microchips, electrodes fabricated onto acetate and enhanced capabilities of screen-printed electrodes", PACCON 2014, Khon Kaen, Thailand January 8-10th January 2014.

6.1.4 List of Awards

1. Awarded the "The Best Overall Student", at the NanoBio Europe conference in Varesse Italy, June 20th 2012.

2. Awarded the 'Outstanding Poster Presentation', at PACCON 2014, Khon Kaen, Thailand January 8-10th January 2014